

# Metabolomic analyses of the malaria parasite after inhibition of polyamine biosynthesis

By

Shaun Bernard Reeksting

Submitted in partial fulfilment of the requirements for the degree

*Magister Scientiae*

in the Faculty of Natural and Agricultural Sciences

Department of Biochemistry

University of Pretoria

March 2009

## Declaration

I, Shaun Bernard Reeksting, declare that this thesis/dissertation, which I hereby submit for the degree *Magister Scientiae* at the University of Pretoria, is my own work and has not previously been submitted by me for a degree at this or any other tertiary institution.

Signature: .....

Date: .....

## Plagiarism Declaration

**UNIVERSITY OF PRETORIA**  
**FACULTY OF NATURAL AND AGRICULTURAL SCIENCES**  
**DEPARTMENT OF BIOCHEMISTRY**

Full name: \_\_\_\_\_ Student number: \_\_\_\_\_

Title of the work: \_\_\_\_\_

### Declaration

1. I understand what plagiarism entails and am aware of the University's policy in this regard.
2. I declare that this \_\_\_\_\_ (e.g. essay, report, project, assignment, dissertation, thesis etc) is my own, original work. Where someone else's work was used (whether from a printed source, the internet or any other source) due acknowledgement was given and reference was made according to departmental requirements.
3. I did not make use of another student's previous work and submit it as my own.
4. I did not allow and will not allow anyone to copy my work with the intention of presenting it as his or her own work.

Signature \_\_\_\_\_

Date \_\_\_\_\_

## **Acknowledgements**

My supervisors Dr. L. Birkholtz and Prof. A. I. Louw from the University of Pretoria, Department of Biochemistry, for their wealth of knowledge, encouragement, guidance, and most of all, patience.

Dr. I. B. Müller, Dr. C. Wrenger, and Prof. R. D. Walter at the Bernard-Nocht Institute (BNI) for Tropical Medicine, in Hamburg, Germany for providing laboratory support and technical guidance.

Dr. A. C van Brummelen for help in experimental design, and Dr. P. B. Burger for providing novel inhibitors that facilitated a research visit to Germany.

My parents, Bernard and Pearl, for their emotional and financial support.

My loving and caring girlfriend, Bianca, for offering kind words of motivation.

The South African Malaria Initiative (SAMI) for sponsoring a student bursary and financing an international research visit to the BNI.

## Summary

Malaria, a disease transmitted by female mosquitoes, has plagued the world for many centuries. The disease is associated with high mortality rates, severe poverty, and economic burden. These are factors which hamper effective eradication of the disease. Drug resistant forms of the parasite have caused increasing concerns and questioned the longevity of current effective antimalarials. Efforts are therefore aimed at the identification and exploitation of essential parasite proteins as potential drug targets. The polyamine pathway of *Plasmodium falciparum* is an exploitable pathway which contains two distinct, chemically validated drug targets; a bifunctional *PfAdoMetDC-ODC* protein and *PfSpdSyn*. These enzymes ensure intricate regulation of polyamine production and the pathway contains various distinctive features which could be selectively targetable from the mammalian counterpart pathways. However, inhibition of polyamine production through the use of specific enzyme inhibitors has revealed various compensatory responses that negate the efficacy of these inhibitors. An account is given of the metabolomic fluctuations in the parasite during inhibition of polyamine biosynthesis. From co-inhibited *P. falciparum* extracts, it could be demonstrated that the characteristic growth-arrest coincided with the depletion in spermidine, the metabolic product of *PfSpdSyn*. The co-inhibition strategy therefore emphasised the importance of spermidine biosynthesis by *PfSpdSyn*. Moreover, adenosyl-related metabolite levels were not disrupted during polyamine depletion, supporting the notion that these metabolites are intricately recycled within the parasites. The identified metabolic compensatory mechanisms have further potential for exploitation, and can strategically be combined with polyamine biosynthesis inhibition to ensure parasitic attenuation. In addition, several novel inhibitors were previously computationally identified, based on a dynamic receptor-based pharmacophore model of *PfSpdSyn*. The *in vitro* inhibiting activity of these compounds was determined against *PfSpdSyn*. Results from the *in vitro* experiments supported the *in silico* predictions, and emphasized the supportive role of pharmacophore modelling has for the identification of novel inhibitors. The research contributed in understanding parasitic polyamine metabolite regulation, and will aid in the future optimization of therapeutic strategies, aimed at exploitation of the polyamine pathway as a potential antimalarial drug target.

## Contents

<b>Declaration</b> .....	ii
<b>Plagiarism declaration</b> .....	iii
<b>Acknowledgements</b> .....	iv
<b>Summary</b> .....	v
<b>List of Figures</b> .....	ix
<b>List of Tables</b> .....	x
<b>Abbreviations</b> .....	xi

### Chapter 1: Malaria and prevention strategies

1.1. An introduction to malaria.....	1
1.2. <i>Plasmodium falciparum</i> and malaria.....	2
1.2.1. <i>P. falciparum</i> life-cycle in the mosquito and human hosts.....	2
1.2.2. Parasite cytoadherence.....	4
1.2.3. Clinical conditions of severe malaria.....	5
1.3. Treatment strategies.....	6
1.3.1. Vaccine based approaches.....	6
1.3.2. Insecticide spraying.....	7
1.3.3. Antimalarial therapeutics and drug resistance.....	7
1.3.3.1. Quinoline therapeutics.....	7
1.3.3.2. Folate metabolism and the antifolates.....	9
1.3.3.3. Artemisinin.....	11
1.4. Newer strategies, novel therapeutics and new drug targets.....	13
1.4.1. Combination therapeutic administration.....	13
1.4.2. Drug target and lead identification.....	13
1.5. Polyamine biosynthesis and its potential for drug development.....	14
1.5.1. Polyamines in biological tissues.....	14
1.5.2. Essential polyamine metabolism in <i>P. falciparum</i> .....	15
1.5.3. The polyamine biosynthetic pathway of <i>P. falciparum</i> .....	16
1.6. ODC enzymes and putrescine production.....	18
1.6.1. General features.....	18
1.6.2. Direct enzyme inhibitors.....	20
1.7. The relationship between SAM homeostasis and polyamine biosynthesis.....	22
1.7.1. SAM recycling and adenosyl related metabolite regulation in <i>P. falciparum</i> .....	22

1.7.2.	General characteristics and AdoMetDC architecture.....	22
1.7.3.	Direct enzyme inhibitors.....	24
1.8.	Aims.....	26

## Chapter 2: Metabolite profiling during *Pf*ODC-AdoMetDC inhibition

2.1.	Polyamine and other related metabolites in <i>P. falciparum</i> .....	27
2.1.1.	Metabolomics and the polyamines.....	27
2.1.2.	Implication and metabolic effects of ODC enzyme inhibition.	27
2.1.3.	Implications and metabolic consequence of AdoMetDC inhibition.....	29
2.2.	Methods.....	30
2.2.1.	Quantification of polyamine and adenosyl-related metabolites.....	30
2.2.1.1.	Estimation of limit of detection (LOD) and limit of quantification (LOQt) of benzoylation.....	30
2.2.1.2.	Estimation of LOD and LOQt of adenosyl-related standards.....	31
2.2.2.	Metabolomic profiling of polyamine co-inhibited <i>P. falciparum</i> .....	31
2.2.2.1.	Culturing of <i>P. falciparum</i> .....	32
2.2.2.2.	Co-inhibition of <i>P. falciparum</i> using polyamine enzyme inhibitors.....	33
2.2.2.3.	Polyamine and adenosyl-containing metabolite extraction.....	33
2.2.2.4.	Polyamine derivatization and HPLC separation of benzoylated derivatives.....	34
2.2.2.5.	HPLC detection of adenosyl compounds extracted from <i>P. falciparum</i> .....	35
2.3.	Results and Discussion.....	35
2.3.1.	Detection and quantification of polyamine and adenosyl-related metabolites.....	35
2.3.1.1.	Benzoylation polyamine derivatization .....	35
2.3.1.2.	HPLC quantification of adenosyl containing compounds.....	41
2.3.2.	Polyamine and adenosyl-related metabolites quantified from <i>P. falciparum</i> .....	44

2.3.2.1. Polyamine levels during erythrocytic maturation of <i>P. falciparum</i> .....	44
2.3.2.2. Adenosyl-related metabolite fluctuations during the IDC of <i>P. falciparum</i> .....	49
2.3.3. Polyamine and adenosyl-related metabolite fluctuations during <i>PfA/O</i> co-inhibition.....	53
2.3.3.1. Co-inhibition of <i>P. falciparum</i> and reflecting polyamine levels .....	53
2.3.3.2. SAM homeostasis during co-inhibition of <i>P. falciparum</i> polyamine enzymes.....	58
2.4. Conclusion.....	63

### **Chapter 3: Evaluation of newly identified *PfSpdSyn* inhibitors *in vitro***

3.1. Introduction to <i>PfSpdSyn</i> .....	65
3.1.1. The functional importance of spermidine.....	65
3.1.2. General characteristics.....	65
3.1.3. Active site properties.....	66
3.1.4. Direct enzyme inhibitors.....	68
3.1.5. Implications of inhibition.....	71
3.1.6. Pharmacophore modelling of <i>PfSpdSyn</i> .....	71
3.2. Methods.....	76
3.2.1. Expression of spermidine synthase.....	76
3.2.1.1. Heat shock transformation of <i>E. coli</i> .....	76
3.2.1.2. Protein expression.....	76
3.2.1.3. Protein isolation .....	76
3.2.1.4. Protein concentration determination.....	77
3.2.1.5. Polyacrylamide gel electrophoresis.....	77
3.2.2. Kinetic determinations.....	78
3.2.2.1. 100 $\mu$ M inhibitor assays .....	78
3.2.2.2. Dissociation constant ( $K_i$ ) determinations.....	78
3.2.2.3. TLC separation of polyamines formed in <i>SpdSyn</i> reaction.....	79
3.3. Results and Discussion.....	79
3.3.1. <i>PfSpdSyn</i> protein expression and isolation.....	79
3.3.2. Evaluation of inhibitors at 100 $\mu$ M.....	81
3.3.3. Kinetics of compound 7 .....	87



3.4. Conclusions.....	91
<b>Chapter 4: Concluding Discussion.....</b>	<b>93</b>
<b>Appendix.....</b>	<b>95</b>
<b>References.....</b>	<b>106</b>

## List of Figures

Figure 1.1: The life-cycle of <i>P. falciparum</i> .....	3
Figure 1.2: Quinolines.....	8
Figure 1.3: Antifolates.....	11
Figure 1.4: Artemisinins.....	12
Figure 1.5: The ongoing process of antimalarial drug design.....	14
Figure 1.6: Polyamine levels established for asexual phase parasite stages...	15
Figure 1.7: The polyamine pathway of <i>P. falciparum</i> .....	17
Figure 1.8: ODC proteins of <i>Trypanosoma brucei</i> and <i>P. falciparum</i> .....	19
Figure 1.9: ODC reaction mechanism.....	20
Figure 1.10: Mechanism of SAM decarboxylation in human AdoMetDC.....	23
Figure 1.11: Monofunctional <i>PfAdoMetDC</i> .....	24
Figure 2.1: Benzoylation of polyamines.....	37
Figure 2.2: Separated benzoylated polyamines.....	38
Figure 2.3: Benzoylated polyamine regression line.....	39
Figure 2.4: Adenosyl standards separated during Ion pairing-RP HPLC.....	42
Figure 2.5: Linear regression of adenosyl containing standards during ion-pairing RP HPLC.....	43
Figure 2.6: Chromatogram representing benzoylated polyamines extracted from mid-trophozoite parasites.....	46
Figure 2.7: Polyamine concentrations during the IDC of <i>P. falciparum</i> . ....	47
Figure 2.8: A chromatogram representing adenosyl-containing metabolites identified from late trophozoite iRBC.....	51
Figure 2.9: Polyamine concentrations measured in treated (T) and untreated (UT) trophozoites.....	55
Figure 2.10: The ratio of putrescine compared to spermidine production.....	57
Figure 2.11: Adenosyl metabolites extracted from <i>P. falciparum</i> T and UT trophozoites.....	60
Figure 2.12: The methylation potential of DFMO / MDL73811 co-inhibited <i>P. falciparum</i> .....	61
Figure 2.13: MDL73811 inhibitory action.....	62
Figure 3.1: <i>PfSpdSyn</i> dimer in complex with dcSAM and <i>trans</i> -4-methylcyclohexylamine (4MCHA).....	66
Figure 3.2: Interactions of <i>PfSpdSyn</i> with dcSAM and 4MCHA.....	67
Figure 3.3: The catalytic interacting residues of <i>PfSpdSyn</i> active sites....	68
Figure 3.4: The DPM cavities of <i>PfSpdSyn</i> .....	73
Figure 3.5: <i>PfSpdSyn</i> protein expression and TLC kinetic analysis.....	80
Figure 3.6: 100 $\mu$ M inhibitor assay of 4MCHA and APA against <i>PfSpdSyn</i> .....	82

Figure 3.7:	The inhibition of <i>PfSpdSyn</i> DPM1 active site using 100 $\mu$ M of compounds 1, 5, and 8.....	83
Figure 3.8:	The activity of inhibitors targeted at the DPM 2 cavity of <i>PfSpdSyn</i> at 100 $\mu$ M.....	85
Figure 3.9:	<i>In silico</i> docked compound 7 in <i>PfSpdSyn</i> (PDBid 2PT9)...	85
Figure 3.10:	Compounds proposed to bind in the DPM3 active site tested against <i>PfSpdSyn</i> at 100 $\mu$ M concentrations.....	86
Figure 3.11:	Compound 4 was predicted to bind in the large DPM4 cavity of <i>PfSpdSyn</i> at 100 $\mu$ M concentrations.....	87
Figure 3.12:	Michaelis-Menten enzyme kinetics of <i>PfSpdSyn</i> .....	89
Figure 3.13:	Lineweaver-Burk enzyme kinetics of <i>PfSpdSyn</i> .....	90
Figure 3.14:	Secondary plot of <i>PfSpdSyn</i> inhibited by compound 7.....	91

## List of Tables

Table 1.1:	Comparison of ODC residues from <i>T. brucei</i> , <i>P. falciparum</i> , <i>Homo sapiens</i> and <i>Mus musculus</i> .....	19
Table 1.2:	<i>Pf</i> ODC inhibitors.....	21
Table 1.3:	Inhibitors of <i>P. falciparum</i> AdoMetDC.....	25
Table 2.1:	LOD and LOQt for benzoylated polyamines.....	40
Table 2.2:	Summary of adenosyl-compound HPLC LOD and LOQt determinations from standard linear lines.....	43
Table 2.3:	Polyamine levels in <i>P. falciparum</i> iRBC as determined by Das Gupta <i>et al.</i> [1].....	45
Table 2.4:	Adenosyl metabolism in normal and iRBC.....	52
Table 3.1:	Inhibitors of <i>PfSpdSyn</i> .....	70
Table 3.2:	Pharmacophore identified inhibitors of <i>PfSpdSyn</i> .....	74

## Abbreviations

APA	3-aminooxy-1-propanamine
4MCHA	4-Methylcyclohexylamine
ABA	4-aminooxy-1-butanamine
ACT	Artemisinin-based combinational therapy
AdoDATO	S-adenosyl-1,8-diamino-3-thiooctane
AdoMetDC	S-adenosyl-L-methionine decarboxylase
ADP	Adenosine diphosphate
AMP	Adenosine monophosphate
APE	5-amino-1-pentene
ATP	Adenosine triphosphate
AU	Absorbance units
B&MGF	Bill & Melinda Gates foundation
CCM	Complete culture media
CCM	Complete culture media
CHA	Cyclohexylamine
CM	Cerebral malaria
CQ	Chloroquine
CR1	Complement receptor 1
CSP	Circumsporozoite protein
DBL	Duffy binding ligand domains
DCA	Dichloroacetate
dcSAM	Decarboxylated S-adenosyl-L-methionine
DDT	Dichloro-diphenyl-trichloroethane
DFMO	DL- $\alpha$ -difluoromethylornithine
DNA	Deoxyribonucleic acid
DPM	dynamic receptor-based pharmacophore model
DTT	Dithiotreitol
EDTA	Ethylenediaminetetraacetic acid
eIF5a	eukaryotic translation initiation factor 5a
EMP	Erythrocyte membrane protein
EPI	Enhanced product ion
EPM	Erythrocyte plasma membrane
GPI	Glycosylphosphatidylinositol
h	Hour(s)
HbS	Hemoglobin S
Hcy	Homocysteine
HEPES	4-(2-hydroxyethyl)-1-piperazineethanesulfonic acid
HFBA	Heptafluorobutyric acid
HPI	Hours post invasion
HPLC	High pressure liquid chromatography
<i>Hs</i> ODC	<i>Homo sapiens</i> ODC
HTS	High throughput screening
I.S	Internal standard
I.S.	Internal standard
IC	Inhibitory concentration
ICAM-1	Inter-cellular adhesion molecule 1

IDC	Intra-erythrocytic developmental cycle
IPTG	Isopropyl $\beta$ -D-1-thiogalactopyranoside
iRBC	Infected red blood cells
IRS	Indoor residual spraying
ITN	Insecticide treated net
Ki	Dissociation constant
LB	Luria-Bertani
LDH	Lactate dehydrogenase
LOD	Limit of detection
LOQt	Limit of quantification
MAA	5'-(methylamino)-5'-deoxyadenosine
MAT	Methionine adenosyltransferase
MDL73811	5'-((Z)-4-amino-2-butenyl)methylamino)-5'-deoxyadenosine
MDR	Multi-drug resistance
MeOH	Methanol
MGBG	methylglyoxal bis(gaunylhydrazone)
min	Minute(s)
MQ	Mefloquine
MRM	Multiple reaction monitoring
MS	Mass spectrometry
MSP	Merozoite surface protein
MTA	5'-Deoxy-5'-(methylthio)adenosine, methylthioadenosine
NAC	N-(3-aminopropyl)-cyclohexylamine
NAD	Nicotinamide adenine dinucleotide
NaN	Sodium azide
Ni-NTA	Nickel-nitrilo triacetic acid
NPP	New permeability pathways
ODC	Ornithine decarboxylase
Orn	Ornithine
OSA	Octanesulfonic acid
PAGE	Polyacrylamide gel electrophoresis
PAPT	Putrescine aminopropyltransferase
PCA	Perchloric acid
PDC	Pyruvate dehydrogenase multienzyme complex
<i>PfA/O</i>	<i>P. falciparum</i> AdoMetDC-ODC
<i>PfAdoMetDC</i>	<i>P. falciparum</i> AdoMetDC
<i>PfCRT</i>	<i>P. falciparum</i> chloroquine resistance transporter
<i>PfCSP</i>	<i>P. falciparum</i> circumsporozoite protein
<i>PfLDC</i>	<i>P. falciparum</i> lysine decarboxylase
<i>PfMDR</i>	<i>P. falciparum</i> multidrug resistant protein
<i>PfODC</i>	<i>P. falciparum</i> ODC
Pgh1	P-glycoprotein homologue 1
PLP	Pyridoxal-5'-phosphate
PMP	Pyridoxamine-5'-phosphate
PMSF	Phenylmethane sulphonylfluoride
PPM	Parasite plasma membrane
PS	Pyrimethamine-sulfadoxine
Put	Putrescine

PV	Parasitophorous vacuole
PVM	Parasitophorous vacuolar membrane
<i>R</i>	<i>rectus</i> (stereochemical description)
RBM	Roll Back Malaria
RNA	Ribonucleic acid
RP	Reverse phase
rpm	revolutions per minute
<i>RS</i>	Racemic mixture of enantiomers
RT	Room temperature
<i>S</i>	<i>sinister</i> (stereochemical description)
S/N	Signal-to-noise
SAH	S-adenosyl-L-homocysteine
SAHH	S-adenosyl-l-homocysteine hydrolyase
SAM	S-adenosyl-L-methionine
SAMe	S-adenosylmethionine
SAMS	SAM synthetase
SAPT	Spermine aminopropyltransferase
SBDD	Structure based drug design
SD	Standard deviation
SDS	Sodium dodecyl sulphate
sec	Second(s)
SEM	Standard error of the mean
SERCA	Sarcoplasmic endoplasmic calcium ATPase
Spd	Spermidine
SpdSyn	Spermidine synthase
Spm	Spermine
SpmSyn	Spermine synthase
T	Treated
TCA	Trichloroacetic acid
TEMED	Tetramethyl ethylenediamine
THF	Tetrahydrofolate
TIM	Triosephosphate isomerase
TRAP	Thrombospondin related anonymous protein
TWC	Total wavelength chromatogram
unRBC	Uninfected red blood cells
UT	Untreated
WHO	World health organization

## **Chapter 1: Malaria and prevention strategies**

### **1.1. An introduction to malaria**

Malaria predominates in sub-tropical and sub-Saharan areas and influences the daily lives of approximately 40% of the world population [2]. The disease, principally transmitted by mosquitoes, has left a scar on the African continent. The ongoing epidemic of malaria is still the major cause of poverty in many developing African countries, causing social devastation and crippling economic progression [3]. The disease is also one of the oldest known parasitic infections still in existence, and its continental perseverance is testament to the cunning evasive mechanisms of the parasite. The emergence of drug resistant parasites is decreasing effectiveness of current antimalarial therapeutics, and adds to the list of circumstances that makes eradication of the disease difficult.

Malaria infects some 250 million people each year, of which ~1 million infections are fatal [4, 5]. On the African continent alone, it is proposed that 84% of the population is at risk of contracting malaria, and the mortality due to severe malaria accounts for 90% of global fatal malaria incidence [5]. Moreover, in Africa, 25% of the fatalities occur in Nigeria, and currently the number of reported cases is increasing [5]. South-East Asian countries are also heavily burdened by the disease, and within the high population density of an estimated 1.7 billion people, two out of three are thought to be at risk of contracting malaria [5]. South Africa had approximately 32 thousand reported cases of malaria in 2006, which resulted in 146 fatalities, however, the overall infection rate is decreasing steadily [5]. The World Health Organization (WHO) has focussed on providing endemic countries with insecticide treated nets (ITNs), artemisinin-based combinational therapies (ACTs), and indoor residual spraying (IRS) of insecticides is practiced stringently. The relentless campaign of the WHO has significantly impacted on the number of ITNs per household in endemic malaria areas, and further aims to make these preventative nets more readily available [5]. The number of reported fatal malaria incidences has not decreased in the last two years, necessitating the introduction of more effective preventative and treatment strategies.

Malaria is a disease of poverty stricken third world countries, and further burdens the potential economic growth in these countries. The WHO estimates that malaria can cost some countries up to 1.3% of potential economic growth each year [6]. Malaria is thought to impact the economy in terms of local household income and work output, as well is in broader terms, with respect to trade and tourism, which is diminished in endemic countries [3].

Campaigns aimed at combating malaria include the Roll Back Malaria (RBM) program and the Bill & Melinda Gates foundation Global Health Program (B&MGF). The RBM partnership includes the WHO, the United Nations Children's Fund, the United Nations Development Programme and the World Bank. One of the RBM Partnership's goals is also to reduce global malaria deaths up to 75% by the year 2015, however based on increasing annual death reports some speculate this proposition is unrealistic [7]. The RBM's strategy includes providing

effective malaria preventatives in areas of high parasite transmission, and aims to ensure elimination of the parasites in countries that have low transmission and incidence rates [8]. The B&MGF funds research focussed on malaria vaccine development and antimalarial drug discovery. Funds are also donated to impoverished countries and aids in the distribution of antimalarials and preventative ITN's. The Global Fund, which also supports the fight against AIDS and tuberculosis, has contributed approximately US\$ 2.6 billion to aid the fight against malaria. The Global Fund is the largest financier of ITN around the world, and has distributed around 70 million ITN's [9]. These campaigns aimed at reducing the transmission of the malaria parasite have, however, according to a recent WHO World Malaria Report, not made a significant impact in the number of fatal malaria incidences that occur at the epidemic epicentre in East-Africa [5]. Newer, more effective preventative and treatment strategies are still required to aid the global fight against malaria.

## **1.2. *Plasmodium falciparum* and malaria**

Members of the *Apicomplexa* phylum include *Theileria*, *Toxoplasma*, *Babesia* and *Plasmodium*. The term „apicomplexa“ refers to the complexity of organelles, located on the apical ends of invasive forms, of members from this phylum [10]. *Plasmodium* species which infect humans include *P. falciparum*, *P. vivax*, *P. ovale*, and *P. malariae*. Two species of *Plasmodium* are predominantly found; *P. falciparum* and *P. vivax*, the former is limited to tropical and sub-tropical areas, and found mostly in sub-Saharan Africa. It is estimated that more than 90% of reported incidents that result in death are caused by *P. falciparum* [4].

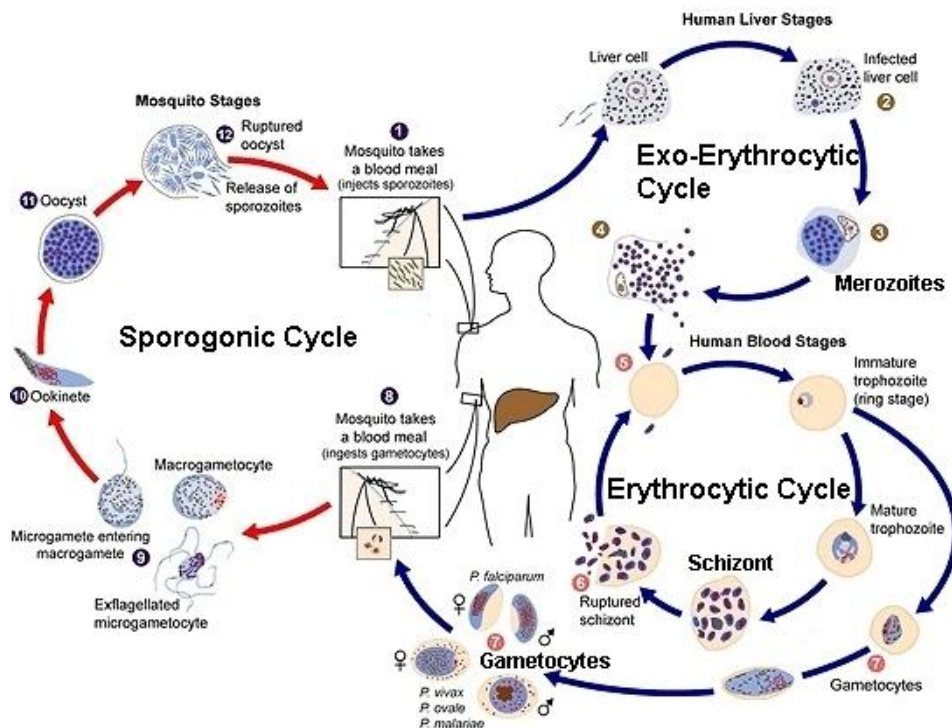
### **1.2.1. *P. falciparum* life-cycle in the mosquito and human hosts**

*Plasmodium* parasites are transmitted to human hosts by infected female mosquitoes of the *Anopheles* genus. It is believed that an infected mosquito has altered biting habits which results in more frequent transmission events [11]. Moreover, the life-span of the infected mosquito, partly compromised by harboring *P. falciparum*, determines the number of biting events and can therefore be ascribed as another critical factor determining the rate of transmission [11]. Mature *P. falciparum* sporozoite forms of the parasite are located within the salivary glands of the mosquito, and can remain active for weeks until transmission occurs. During a blood meal taken by the mosquito, the sporozoites are injected into the human skin and start their voyage through the host tissues. Reports suggest that the event of sporozoite invasion can be quite rapid and only a single sporozoite is required to establish an infection within the host [12].

Sporozoitic forms of the parasite possess gliding motility that enables their progression through dermal and other tissues. Sporozoite motility is facilitated by specialized parasite organelles including rhoptries, micronemes, and dense granules situated at the apical site of the sporozoite [13]. These organelles contain various proteases and adhesion proteins required to move through the dermal tissue and also, later during liver cell invasion, to establish a parasitophorous vacuole (PV) around the parasites [13]. Circumsporozoite protein (CSP), located on the surface of the sporozoites, also facilitates gliding and is characteristically shed during passage through the host

tissue [10]. Once sporozoites enter the blood, the parasites are carried towards the liver where these cross the liver sinusoidal vein, as shown in Fig 1.1 [14]. The endothelial tissues in the sinusoidal veins are also proposed to be highly specialized, and selective attachment of sporozoites is thought to be facilitated by CSP and thrombospondin related anonymous protein (TRAP) [15]. Sporozoite differentiation and maturation occurs within the hepatocytes.

Mature infected hepatocytes rupture to release newly formed merozoites, which enter the blood stream to invade erythrocytes, marking the initiation of the intra-erythrocytic developmental cycle (IDC) or asexual blood-stage cycle (Fig 1.1) [16]. Parasite merozoite invasion is facilitated by the dominantly expressed merozoite surface protein-1 (MSP-1) of the parasites [17]. This glycosylphosphatidylinositol (GPI) anchored surface protein also has N-terminal domains which facilitate initial attachment to the erythrocyte membranes [16]. Merozoite invasion follows the process of proteolytic MSP-1 shedding, and results in the formation of the parasitophorous vacuole (PV) [17].



**Figure 1.1: The life cycle of *P. falciparum*.** The parasite life-cycle can be divided into the sporogonic, exo-erythrocytic and erythrocytic cycles. The sporogonic cycle involves sexual development in which the parasites are harbored in mosquitoes. The exo- and erythrocytic phases are associated with the invasion of human host tissues, more specifically hepatocytes and erythrocytes, respectively. Figure taken from [18].

Erythrocytic maturation results in the sequential formation of ring, trophozoite and schizont parasite forms. Each distinctive stage is proposed to have a definitive role in the erythrocytic cycle of the parasite. Transcriptomic profiling of *P. falciparum* has revealed that functionally related genes families are transcribed at the distinctive erythrocyte phases during erythrocytic maturation [19]. Ring stage parasites, with ring-like morphological characteristics, occupy the erythrocyte for the first 18 hours post merozoite invasion (HPI). This stage is proposed to reflect a nutrient acquisition stage of the parasite and transcripts corresponding to glycolysis and protein translation have been shown to peak during this time [19]. Protein and RNA synthesis



prominently occurs in the trophozoite stages of the parasites [20]. Late-trophozoite stages additionally reflect a stage in which DNA replication components are upregulated [19].

The final schizont parasite phases show prominent transcript production of parasite invasion proteins, like *PfMSP-1* [19]. The maturation of schizonts is marked by the release of ten to thirty newly formed merozoite parasites. These can either re-enter uninfected red blood cells (unRBC) to continue in the IDC, or undergo sexual development into parasite gametocyte forms (Fig 1.1). The mechanism of gametocyte formation is still speculative in *P. falciparum*. Some suggest under asexual proliferation pressure, schizonts enter a committed sexual stage in which gametocytes are formed instead of normal merozoite formation [21]. Gametocytogenesis occurs within the human host, and results in the formation of either male or female gametocytes [21]. Gametocytes are transferred to the mosquito vector during a blood meal, and these forms subsequently undergo maturation into oocysts. Rupture of oocysts result in the release of sporozoitic parasite forms which reinvade the salivary glands of the mosquito and re-initiate the parasitic life cycle.

### 1.2.2. Parasite cytoadherence

Parasite infected red blood cells (iRBC) are modified in many different aspects during the maturation of *P. falciparum* parasites, and this includes decoration of the erythrocyte membrane with parasite derived proteins. The *P. falciparum* erythrocyte membrane protein (*PfEMP1*) is a dominant protein of the iRBC membrane, and is thought to be involved host immune evasion and parasite cytoadherence [22-24]. Parasite cytoadherence has been suggested to be a contributing virulence factor, more prominent in falciparum malaria, and facilitates evasion of host immune responses [25]. Mature trophozoite and schizont parasites are able to adhere to endothelial cells that line the blood vessels, and can result in parasite sequestering within the peripheral circulatory network [26]. Sequestering allows the mature forms of the parasite to evade clearance by the spleen [26]. Diagnostic blood smear analyses of infected individuals also reflect this and reveal less prominent trophozoite and schizonts forms compared to ring stage-parasite forms [23]. Rosetting is another form of parasite cytoadherence in which infected cells associate with unRBC. Sequestering and rosetting may contribute to cerebral microvascular obstruction leading to the clinical condition of cerebral malaria (CM). The higher mortality rates associated with *P. falciparum* are therefore related to the cytoadhering ability of the parasites [24].

*PfEMP1* is a membrane protein with prominent surface expression during the late-ring and early-trophozoite parasite stages [22, 23]. The protein plays a definite role in immune evasion of the parasites through antigenic variation in extracellular Duffy binding ligand domains (DBL) [23]. The protein is encoded by 60 members of the *var* gene family, and these facilitate the generation of the polymorphic extracellular DBL of *PfEMP1* [23]. *PfEMP1* was proposed to bind to an array of different host receptors including complement receptor 1 (CR1), inter-cellular adhesion molecule 1 (ICAM-1) and CD36 expressed in erythrocytes and host endothelial cells [23]. CR1 is also thought to be involved during rosetting, and polymorphisms which result in low cellular expression of CR1 have been linked with the reduced onset of severe malaria [25].

The distribution of red blood cell polymorphisms is known to be greater in areas of endemic malaria transmission. This is related to the host's ability to avoid parasitic cytoadherence, and hence the onset of severe malaria [25, 27]. Traits such as sickle cell anemia, also known as Hemoglobin S (HbS), are strongly correlated with the geographic incidence of malaria [25]. Sickle cell anemia has been shown to confer 90% protection against the onset of fatal malaria [28]. Other hemoglobinopathies, which refer to the condition of altered hemoglobin production, like thalassemia, or altered structural forms of hemoglobin, such as HbC and HbS, are known to confer resistance against the parasites [25]. The mechanisms of host cell resistance are however not always well understood. Furthermore, the impaired erythrocyte function associated with these hemoglobinopathies, and the propagation of these mutations, is determined by the degree of parasite resistance gained. The resistance can be both reduced onset of severe malaria or lowered infection and reinfection rates.

### 1.2.3. Clinical conditions of severe malaria

The clinical conditions associated with severe malaria manifests as cerebral malaria (CM) and severe anaemia. Acidosis is a common denominator associated with both these clinical manifestations, and is readily associated with high mortality rates [24]. CM is caused when cerebral vessels are blocked by iRBC that cytoadhere to endothelial host tissues [23, 24]. Cytoadherence of the parasites, sequestering and rosetting, results in cerebral microvascular obstruction, blockage of functional capillaries, and leads to convulsions and coma [23, 24, 29]. Severe malarial anaemia, caused through excessive, synchronized rupture of erythrocytes, also results in the activation of host inflammatory responses. Severe anaemia is responsible for fewer deaths as opposed to CM, and this rare clinical condition is associated with hemoglobin levels below  $5 \text{ g.dl}^{-1}$ , where normal individuals have ranges between  $12\text{-}18 \text{ g.dl}^{-1}$  ( $7.5\text{-}11.2 \text{ mmol.l}^{-1}$ ) [30]. It was postulated that severe malaria represents a myriad array of physiological mishaps and the process of acidosis was also thought to contribute to eventual death [29]. Hyperventilation and deep breathing, a characteristic clinical symptom in severe malaria patients, is also thought to be caused by acidosis [29].

The onset of acidosis occurs due to accumulation of lactic acid and other ketoacids [29]. Diminished erythrocyte levels contribute to decreased oxygen carrying capacity of the blood, resulting in lowered oxygen transport to muscles. Anaerobic muscular function is associated with the formation of lactic acid from pyruvate through the reversible action of lactate dehydrogenases (LDH) [31]. This reaction restores depleted nicotinamide adenine dinucleotide ( $\text{NAD}^+$ ), an essential cofactor for the continuation of glycolysis and cell survival. Hyperlactatemia can, however, effectively be treated through the administration of dichloroacetate (DCA) to patients with severe malaria [29, 32]. DCA has been proposed to maintain the activity of pyruvate dehydrogenase multienzyme complex (PDC), which is the first reaction of the tricarboxylic acid cycle [31]. DCA, normally orally administered, is very rapidly absorbed, and found within most tissues within minutes, maintaining low cellular levels of lactic acid [32]. Other symptoms including fever, vomiting, and diarrhoea are also proposed to contribute to fluid loss. This results in hypovolaemic shock and is observed as diminished blood plasma levels. Hypovolaemia is also

associated with acidosis, eventual systemic organ failure, and ultimately death [29]. Aggressive fluid resuscitation has also been suggested for treatment of hypovolaemic shock during severe malaria; however the procedure has not yet been clinically validated [33].

### 1.3. Treatment strategies

Malaria disease prevention has been most successful with the employment of chemoprophylactics and chemical therapeutics [34, 35]. The employment of quinolones, antifolates, and artemisinins and the underlying mechanisms of toxicity have greatly aided understanding of parasite biology. However, ensuing drug-resistance forms of the parasite have required new drug target selection and treatment strategies to be implemented. There is potential for vaccines in the eradication of malaria, however this approach has not been successful yet. Insecticide spraying has also reduced the habitual environments of malaria mosquito vectors, and the deployment of ITNs is also becoming increasingly effective for the prevention of malaria.

#### 1.3.1. Vaccine based approaches

Vaccine-based strategies are thought to hold potential for the eradication of malaria. The most significant motivation is that vaccine implementation would require less frequent administration compared to antimalarial prophylactics [36]. This could therefore help eliminate the occurrence and transmission of the parasites. Vaccine development has mainly focused on the pre-erythrocytic stages of the parasites that occur in the human host. The initial discovery that irradiated sporozoitic forms of the parasites could confer a degree of protection, prompted vaccine development to focus more intently on these pre-erythrocytic parasitic stages [37]. Low levels of sporozoites, together with the asymptomatic clinical conditions, were factors proposed to make pre-erythrocytic vaccines more favorable compared to erythrocytic based vaccines [15].

The *P. falciparum* circumsporozoite protein (*PfCSP*), located on the surface of sporozoite, was later identified as the immune recognized antigen in the attenuated sporozoite vaccines. The generation of attenuated vaccines was, however, not feasible due to large scale culturing requirements [37]. CSP was suggested, apart from assisting parasite gliding motility, to facilitate the invasion of liver cells through cellular adhesion onto hepatocytes [37]. Some degree of mechanistic conservation, and hence protein homology, was expected for CSP, and this was thought to be exploitable in vaccine design. The CSP proteins contain a central domain consisting of amino acid repeats. The number of repeats have been shown to differ amongst the various *P. falciparum* isolates, making vaccine design challenging [37]. However, a part of the central repeat region is thought to be recognized by host antibodies, and recently a subunit vaccine, „RTS,S“, consisting of C-terminal and repeat domains of CSP has shown promise in Phase III clinical trials [38, 39]. The vaccine was proposed to confer 40% protection against the challenge of sporozoite infection, however the immunity was short-lived, lasting about 6 months [15, 39].

Other vaccine design approaches include targeting of the asexual erythrocytic stage parasites, these aim to reduce parasite numbers rather than to prevent infection [39]. Parasites have evolved

mechanisms of immune evasion, which may predominantly be active during circulation in the blood. Current vaccine candidates include *PfMSP-1* and *PfEMP1*; however these proteins contain highly variable domains involved in antigenic variation, and an effective vaccine has not yet been developed [39]. Gametocyte vaccines, targeting the sexual phase of the parasite within the human, are aimed at preventing transmission of the parasites. These, however, would require large-scale implementation to significantly affect transmission in an endemic malaria area [15].

### **1.3.2. Insecticide spraying**

Global efforts in eradication *P. falciparum* carriers, mosquitoes of the *Anophele* family, have been met with success in some parts of the world, including the USA. These efforts have had little impact on the raging epidemic found in poverty stricken West- and Central-Africa. People living in poverty stricken areas are bitten several hundred times per night, however, the employment of ITNs has greatly impacted on this number [4]. Distribution of ITNs, impregnated with long residual acting pyrethroids, has been part of the WHO campaign to eradicate malaria. The ITNs are proposed to have both physical and chemical protective functions [40].

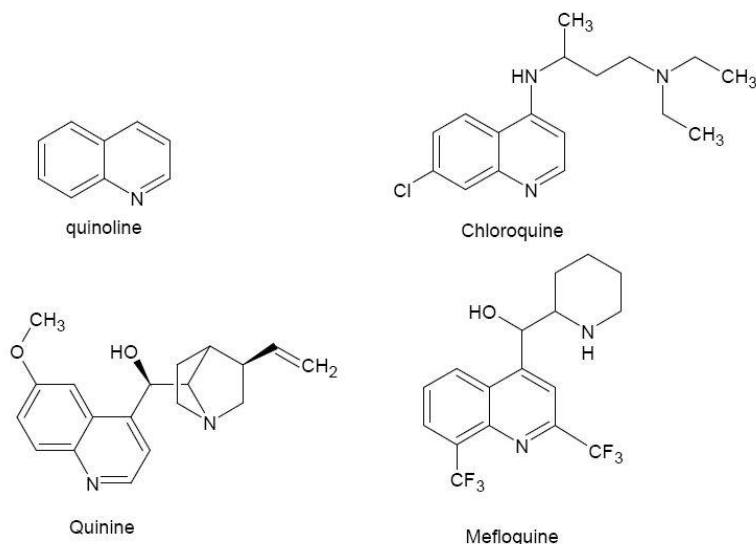
Aggressive insecticide spraying regimes using dichloro-diphenyl-trichloroethane (DDT) in most parts of the USA has most definitely helped reduce the incidence of malarial infection to almost zero [15]. DDT's success was attributed to the long residual activity span, and a single indoor residual spraying event was proposed to have insecticidal effectiveness for up to 6 months [40]. The broad-spectrum insecticidal action of DDT also ensured that mosquito stages, both larval and adult, were effectively controlled [40]. DDT is a comparatively cheap insecticide, and this was a determining factor that could have resulted in its over-use. The insecticide is restricted due to reports of environmental accumulation and potential toxic effects [41]. After DDT, the use of insecticides with lowered vertebrate toxicity, like pyrethroids introduced in the 1970s, became more widespread. Since 1990 the distribution of ITNs in endemic malaria areas has been combined with indoor residual spraying (IRS) regimes [42]. Fear of potential mosquito tolerance and resistance to currently employed insecticides remains, and newer strategies are aimed at the creation of novel, effective, and long lasting insecticides [42].

### **1.3.3. Antimalarial therapeutics and drug resistance**

#### **1.3.3.1. Quinoline therapeutics**

The quinoline group of compounds has had an appreciable level of success in the treatment of malaria in the last century. Compounds of this group include quinine, chloroquine (CQ, Resochin) and mefloquine (MQ) (Fig 1.2). Quinine, isolated from the bark of the South American cinchona tree, was one of the first quinolines employed in the early treatment of malarial infections [43]. The compound has been used since the middle 1600s and the first isolated form of the alkaloid was used as early as 1820 [44]. The first incidence of resistance was only reported in 1910, suggesting that the quinoline enjoyed a lengthy two-hundred year period of success [44]. The compound is, however, currently only used in combination with other effective antimalarials

and reserved for patients with severe malaria due to its toxic side-effects [44-46]. Chloroquine, a 4-aminoquinoline, was first synthesized in 1934 as alternative, however only became notably used during the 1950s and early 1960s. It is widely established that the success of chloroquine was attributed to the low cost of the treatment [43, 47]. The drug also had mild side-effects compared to other quinolines [45]. Mefloquine (Larium<sup>®</sup>, Roche [48], Mefliam<sup>®</sup>, Cipla Medpro [48]), an aryl amino alcohol derivative of quinine, was initially employed in areas of quinine-resistance, but soon after its introduction parasite resistance was also reported, and this was partly attributed to the similarity between resistance mechanisms against these two quinoline compounds [43, 49].



**Figure 1.2: Quinolines.** These have been widely used in the treatment of *P. falciparum*, and the basic quinoline scaffold has been maintained. The compounds have been found to inhibit parasite hemozoin formation. Figure generated using Advanced Chemistry Development, Inc. (ACD/Labs) software [50].

The efficacy of quinolines could be attributed to the fact that these interfere with the parasite heme-detoxification process [51]. Hemoglobin, which makes up a staggering 95% of the total protein complement of erythrocytes, is a large, but incomplete, source of amino acids for the parasites [34, 51, 52]. Hemoglobin catabolism takes place within the acidic food vacuoles of *P. falciparum* through the action of specialized digestive proteins; plasmepsins, falcipains, falcilysin, and other proteases [34, 51, 53]. Free heme molecules released during hemoglobin digestion are toxic, and also result in free hydroxyl radical formation and oxidative stress [52]. Heme detoxification therefore plays an important role during immobilization of toxic free heme, and forms a central part of parasite survival in the erythrocyte [52].

Heme detoxification in *P. falciparum* is facilitated through the formation of hemozoin, also referred to as  $\beta$ -haematin. It is believed that 95% of released heme is sequestered into this solid, compact, inert hemozoin form [34, 51]. Hemozoin is composed of multiple dimeric heme units, linked through iron III-carboxylate bonds, which further associate by hydrogen bonding [52]. These units form a brick-like, non-polymeric, crystalline structure, characteristically visible in parasite vacuoles [51, 52]. Hemozoin crystals are quite large, and also have magnetic character due to the presence of oxidized ferric ions, exploitable during the purification of iRBC from uninfected cells [52]. The mechanism of parasitic hemozoin formation was disputed for some

time and various protein facilitators were thought to be involved. Recently it was proposed that crystal formation is autocatalytic, and cell-free crystal growth has been observed under scanning light microscopy [51]. Evidence exists which suggests that lipid encapsulation of the hemozoin in the food vacuoles is paramount to the process [51].

CQ is known to inhibit hemozoin formation and cause toxic side-effects in the parasites, a similar mode of action is also postulated for other quinolines [51, 54]. It is also suggested that CQ is accumulated in parasite food vacuoles due to the weak basic character of the compound [52]. Questions still exist as to the exact mechanism of quinoline toxicity, and it is not known whether aqueous-soluble hemozoin dimers, drug-hemozoin complexes, or free heme results in the toxic effects [52, 54].

Emerging CQ drug resistance was suggested to have spread from Thailand to Southeast Asia in the 1960s [44]. Parasites from South America were found to have different determinant alleles which conferred CQ resistance during the same time [54]. CQ resistance gradually spread to Africa, and during the late 1970s markedly decreased efficacy of CQ became problematic [43, 49, 55]. Various transporters are known to be involved in quinoline resistance [54]. One transporter involved is the *P. falciparum* chloroquine resistance transporter (*PfCRT*). The *PfCRT* protein is situated on parasite digestive food vacuole membranes. CQ resistance has been shown to be related to mutations in the *pfert* gene, and a corresponding K<sub>76</sub> to T<sub>76</sub> mutation was found to be associated with African and Asian CQ resistant strains [44, 56]. Moreover, a definite efflux or influx function of the transporter has not yet been established [54]. It is therefore not known whether mutations in *pfert* promote efflux of CQ or decrease the influx of the quinoline into the food vacuoles.

The protein product of *pfmdr1*, P-glycoprotein homologue 1 (Pgh1), was found to be a parasite vacuolar membrane protein and a member of the ATP-binding cassette (ABC) transporter superfamily [54]. Pgh1 is thought to be involved in the efflux of quinoline compounds from the parasite food vacuoles. CQ resistance mechanisms were identified as *pfmdr1* gene over-expression [54, 56]. Moreover, mutation of an D<sub>86</sub> residue to Y<sub>86</sub> in Pgh1 has been reported to confer both CQ and mefloquine resistance [44, 56]. The *P. falciparum* multidrug resistant protein (*PfMDR1*) is yet another transport protein predicted to occur on the parasite food vacuole membrane and is associated with CQ and quinine resistance [54].

### **1.3.3.2. Folate metabolism and the antifolates**

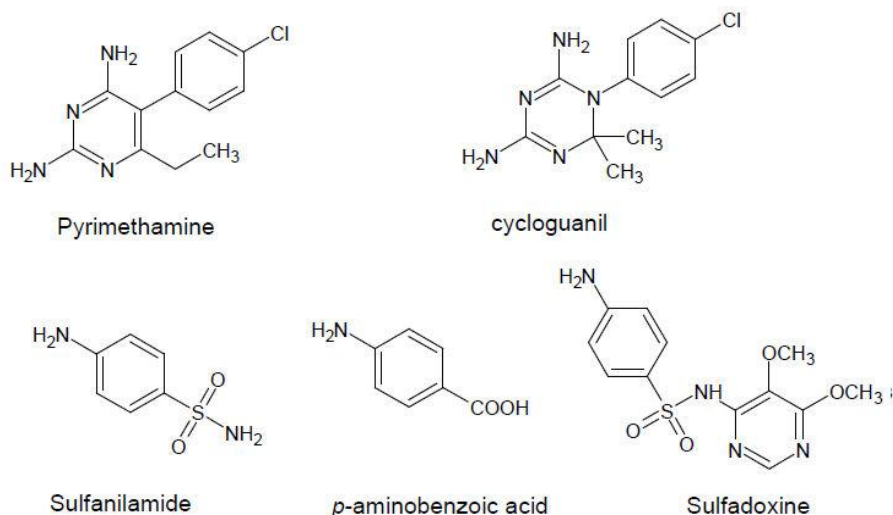
The folate biosynthesis in *P. falciparum* has been exploited, and resulted in the development of several effective therapeutics. Pyrimethamine (Daraprim<sup>®</sup>), cycloguanil, and sulfadoxine were introduced in the early 1950s and were found to be effective against CQ-resistant forms of the parasite [43]. The compounds were proposed to interfere with parasite folate biosynthesis. Folate biosynthesis entails the formation of a tetrahydrofolate cofactor (THF), which is an essential carbon (C<sub>1</sub>) substrate for methyl transfer reactions in most living cells [31]. In humans, folate is salvaged from the diet and converted to THF through an enzymatic reduction reaction catalyzed

by dihydrofolate reductase (DHFR, E.C. 1.5.1.3) [57]. The situation in *P. falciparum* is markedly different, where *de novo* synthesis of THF precursors occurs. The formation of THF involves the *en route* synthesis of 7,8-dihydropteroate from *p*-aminobenzoic acid (Fig 1.3) and dihydropterin, a folate-like precursor, through the action of dihydropteroate synthase (DHPS, E.C.2.5.1.15) [57]. Later downstream reactions involve the reduction of the 7,8-dihydropteroate precursor through the action of a parasite equivalent *Pf*DHFR, and Thymidylate synthase (TS) maintains active forms of 7,8-dihydropteroate through recycling of consumed THF forms [57].

Pyrimethamine was found to be a potent, parasite selective, DHFR inhibitor, and was proposed to disrupt DNA synthesis within the parasites (Fig 1.3). This characteristically resulted in death of schizont developmental stages [43]. Cycloguanil (Fig 1.3), a structural analogue of pyrimethamine, with correlating 2,4-*meta* amino benzene substituents, was an effective therapeutic administered in pro-drug form: proguanil (Paludrine<sup>®</sup>) [57]. Proguanil was postulated to target DHFR [35, 57]. During this period sulfonamide antibiotics, which share structural similarity with the *p*-aminobenzoic acid substrate of DHPS, also became available. The success of the sulfonamides, like sulfadoxine (Fig 1.3), has been correlated to effective inhibition of the DHPS, leading to disruption of DNA synthesis in the parasites [43]. Sulfadoxine, like pyrimethamine, also showed potent schizonticide activity against *P. falciparum* [43].

These compounds, however, had a relatively short period of success, and parasitic resistance was reported during the late 1950s [43, 57]. From introduction, pyrimethamine is believed to have had a five year life-span before the parasite-resistance development required doses above the therapeutic threshold for effective treatment [57]. Also compared to the quinolines, which are effective against ring stage forms of the parasite, the late schizontocidal activity of the antifolate inhibitors was an unwanted effect when treating severe malarial infections. This late therapeutic action meant that cytoadherence of the trophozoites and schizonts was still possible, and could complicate patient conditions before an improvement was observed [43].

With some incidence of resistance reported for pyrimethamine, a combination of pyrimethamine-sulfadoxine (PS) (Fansidar<sup>®</sup>, Roche [57]) became more widely used. The combination therapy was also testament to the success of a synergistic combination therapy focused on a particular parasitic pathway [44]. The advantage of the combination therapy was slower resistance development, compared to monotherapeutic administration, and also faster schizontocidal efficacy [43]. Other effective combinations also included Proguanil administered with atovaquone (Malarone<sup>®</sup>, GSK [57]).



**Figure 1.3: Antifolates.** Pyrimethamine and Cycloguanil are examples of DHFR inhibitors found to be effective against *P. falciparum*. Sulfonamide therapeutics, which resemble the DHPS substrate *p*-aminobenzoic acid, was proven to work well in combination with other antifolate inhibitors against *P. falciparum*.

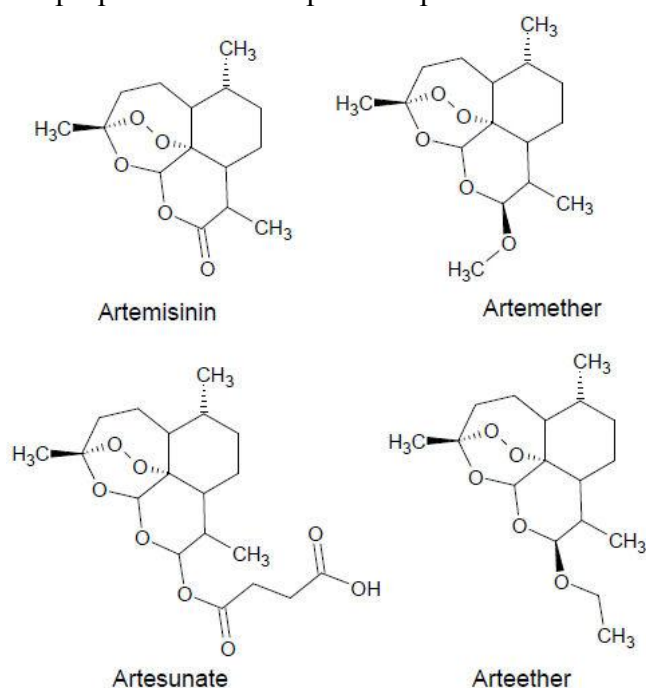
Spread of PS parasite resistance is well documented and was first observed at the Thai-Cambodian border in the late 1960s [44, 49]. Allelic mutants of *pfldhfr*, which confer pyrimethamine resistance, were also proposed to have spread from Southeast Asia to Africa [49]. During the late 1980s East African parasite isolates were increasingly desensitized against PS, and this was proposed to have spread to West Africa [44]. The molecular basis of pyrimethamine and sulfadoxine resistance was attributed to amino acid mutations in the folate biosynthetic enzymes; DHFR and DHPS, respectively [43, 57]. Pyrimethamine resistance was associated with a serine to alanine (S108A) mutation in DHFR, which resulted in reduced inhibitor affinity [44]. The most common substitutions in the DHPS enzyme associated with resistance were the lysine to glutamic acid (K540E) and alanine to glycine (A437G) mutations [44]. Fortunately, resistance development in DHFR is well understood, and various crystal structures of the *P. falciparum* protein and mutant forms are available [58]. DHFR is an established drug target, and future developments are already focused on improved inhibitor design [57].

### 1.3.3.3. Artemisinin

Artemisinin was first extracted from the annual shrub *Artemisia annua* by Chinese scientists in the early 1970s, and subsequently, in 1979 the compound was reported to have antimalarial activity [59]. The compound has been used extensively in China and southeast Asia, however the introduction of the compound in other parts of the world only occurred in the early 1990s [59]. Later, in 2004, the WHO recommended that drug resistant *P. falciparum* forms should be treated with artemisinin combinational therapeutics (ACTs) [60]. ACT's included an artemether and lumefantrine combination (Coartem<sup>®</sup>, Novartis [48]), and artemisinin and pyrimethamine-sulfadoxine combinations [59]. The former, lumefantrine, is thought to have a similar mode of action as compared to the quinolines, and in combination with artemether, was shown to be well tolerated and effective against multi-drug resistant *P. falciparum* [61].



Artemisinin and derivatives, as shown in Fig 1.4, have a sesquiterpene lactone structure with an endoperoxide bridge [59]. Artemether is an oil-based derivative which can be administered intramuscularly, compared to artesunate which is water-soluble and can be administered intravenously [60]. Intramuscular artesunate is also a preferred route of administration due to rapid absorption [33]. The artemisinin compounds have a short-half life, and once administered are eliminated within 8 hours (h) [59]. The efficacy of the artemisinin and ACTs was attributed to its fast action and ability to kill all asexual blood-stage forms of *P. falciparum* [62]. Elimination of early stage ring forms was suggested to reduce the risk of parasitic cytoadherence and sequestering, and therefore reduce possible clinical complications during treatment [33]. The compounds were proven to be effective gametocidals, this was proposed to reduce the transmission of the parasites [62]. The relatively short half-life of the compounds, together with gametocidal activity, was proposed to reduce possible parasite resistance development [44, 59].



**Figure 1.4: Artemisinins.** These molecules are currently the prescribed regimen for treatment of malaria by the WHO. Various modifications to the basic artemisinin structure have allowed adsorption through different administration routes.

The molecular basis of inhibitory action of artemisinin was attributed to selective inhibition of *PfATP6*, a sarcoplasmic endoplasmic calcium ATPase (SERCA), identified in *P. falciparum* [62]. The inhibitory effects of artemisinin were therefore related to disruption of  $\text{Ca}^{2+}$  ion concentrations in the parasite [62]. Decreased sensitivity was associated with point mutations in *PfATP6*, and has been observed in some resistant parasite isolates [62]. Resistance against artemisinins has been reported in western Cambodia, and this was partly attributed to previous monotherapeutic administration in the region for the last thirty years [63]. Some propose that the ABC transporter *PfMDR1*, located on the vacuolar membrane of the parasites, had increased *pfmdr1* gene copy number, which was correlated with artemisinin resistance [62]. This was also a parasite resistance mechanism to quinolines, as previously mentioned. With various incidence of parasitic resistance, strict adherence to combinational therapeutic administration is required.

Aside from mild side effects, artemisinin compounds have been proven safe and can be administered as a prophylactic, as well as for treatment of patients with severe malaria [33].

#### **1.4. Newer strategies, novel therapeutics and new drug targets**

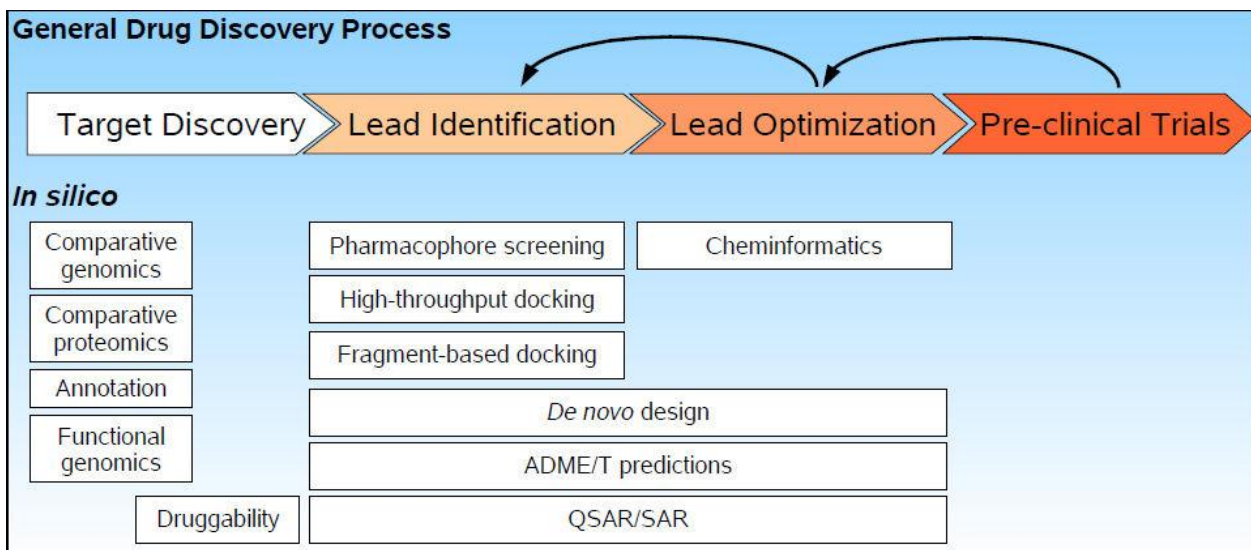
Antimalarial drug discovery is an ongoing process, and the emergence of drug resistant parasites necessitates the need for newer, inexpensive therapies [47, 64]. Malaria is primarily a third world disease, and these countries are many times severely economically burdened. This has led some researchers to stipulate that cheap, single-dose, orally available therapies would be best suited for effective treatment [47]. The previous successes of CQ and PS therapies are attributed to their low cost, and hence widespread availability [55]. Low marketability is also associated with these cheap antimalarial drugs, and the economic viability is a daunting consideration for large pharmaceutical companies. The contribution of academic research has greatly outnumbered commercial endeavors and has improved our understanding of the fascinatingly complex parasite.

##### **1.4.1. Combination therapeutic administration**

The employment of a combination of effective therapeutics is proposed to have various advantages in *P. falciparum*. Firstly, a combination therapy may decrease the probability of parasite drug resistance development [64]. The combinations ideally result in a very low parasite recrudescence rates and hence also a lower possibility of resistance development [53]. The second advantage of co-inhibition would be the lowered required doses of the compounds, and therefore potentially lower therapeutic side effects. For therapeutics of which the parasitic drug target, and associated cellular function, is well defined, a cocktail therapy can be designed which reduces compensatory parasitic responses. This could also promote synergistic action of the therapeutics, requiring even lower dosing concentrations [47, 53].

##### **1.4.2. Drug target and lead identification**

A recent review by de Beer *et al.* ([65], unpublished) describes the processes involved in drug discovery and the contribution of various *in silico* approaches throughout this process (Fig 1.5) [65]. In their paper they emphasized the usefulness of *in silico* structure-based drug design (SBDD) during lead identification, which exploits the structural qualities of a drug target to determine hypothetical ligand scaffolds [65]. Virtual screening can be performed through extraction of receptor-based pharmacophores, and the identification of complementary virtual docking ligands from large chemical libraries [66]. Other methods for the identification of novel therapeutics include the large scale shotgun approach of high throughput screening (HTS). HTS involves the automated *in vitro* screening of large chemical libraries against whole parasites and essential parasite proteins [66]. Upon identification of active compounds, further investigations pursue the possible drug targets and therapeutic candidates. HTS is, unfortunately, a costly route for lead identification and has been more popular in large pharmaceutical companies.



**Figure 1.5: The ongoing process of antimalarial drug discovery.** The usefulness of *in silico* approaches during drug design strategies has been demonstrated by de Beer *et al.* (unpublished) Figure taken from [65].

In terms of identifying possible drug targets, ongoing efforts are aimed at the identification of indispensable parasite proteins. Various approaches including mRNA expression profiling, proteome elucidation, and metabolome analysis have been suggested to greatly help identify such essential proteins [67-69]. With the aid of *in vitro* culturing, various knock-out *P. falciparum* cell-lines have further complemented validation of these targets. Specifically, understanding the interconnectivity of transcriptomics, proteomics, and metabolomics in the parasites will aid in drug target selection, and in the creation of effective combination treatments and help rationalize parasite resistance development [69, 70].

## 1.5. Polyamine biosynthesis and its potential for drug development

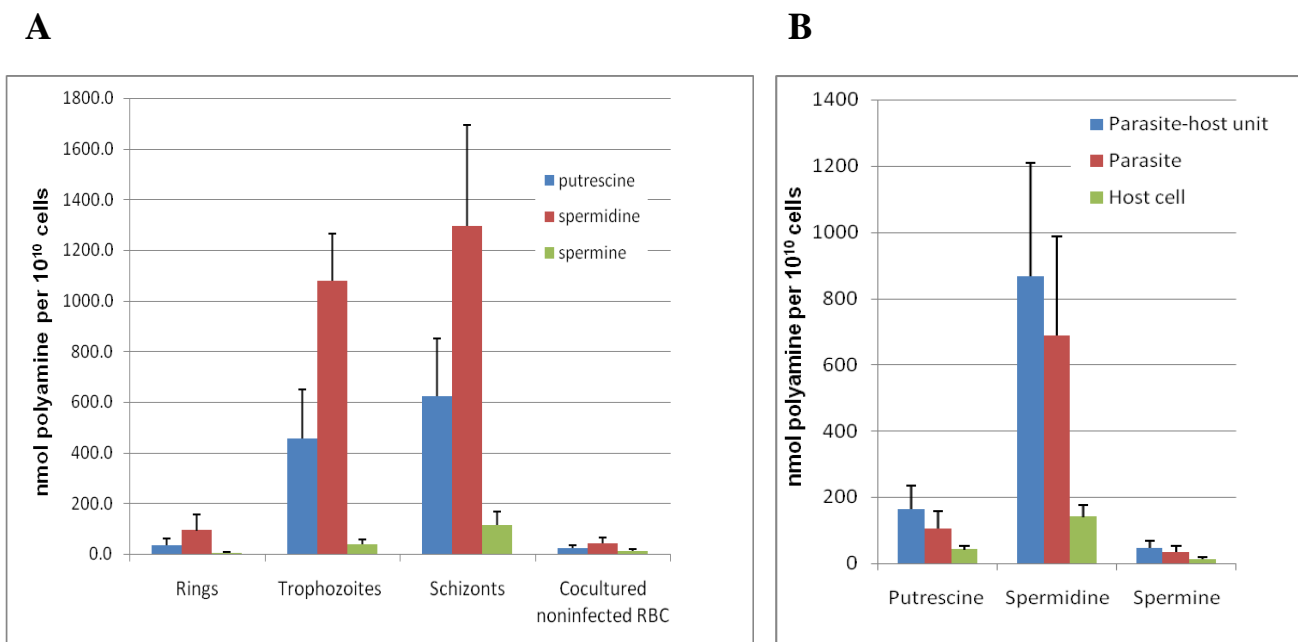
### 1.5.1. Polyamines in biological tissues

The polyamines; putrescine, spermidine and spermine, are essential, integral components found in all living organism, with the exception to some Archaea, Halobacteriales, and Methanobacteriales [71]. The polyamines are di- and poly-cationic molecules, which can interact with anionic cellular components and are essential for cellular differentiation and proliferation. These small molecules are predominantly involved in stabilization of anionic cellular components, including interactions with DNA [72, 73], RNA [71], phospholipids [71], and membrane transporters [74]. Most notably, polyamines are postulated to play a role in regulation of gene expression and have various direct and indirect mechanisms, ranging from interactions with histone proteins [75], to direct binding within DNA major and minor grooves [72, 73, 76]. Apart from the roles in maintaining cellular homeostasis, these molecules are also implicated in apoptotic processes [77, 78]. The polyamine levels have been shown to increase during cellular growth, often during the transition from the G<sub>1</sub> to the S phase, a period which is characterized by rapid DNA synthesis. Depletion of cellular polyamine concentrations by the use of polyamine-specific enzyme inhibitors often leads to the arrest of cellular growth and the inhibitory effect is

most pronounced at the G<sub>1</sub> to S phase transition [76]. An interesting fact is the presence of low levels of polyamines in mature human erythrocytes, which supports the notion that polyamines are linked to stabilization of nucleic acids.

### 1.5.2. Essential polyamine metabolism in *P. falciparum*

The majority of studies relating to polyamines in *P. falciparum* have established that these small molecules are essential in the asexual erythrocytic maturation of the parasites [79-81]. unRBC have been shown to contain trace levels of polyamines, and upon infection with the malaria parasite, these levels markedly increase [1, 79]. Assaraf *et al.* [82] provided experimental evidence that suggested ring stage forms of the parasite contain the least amount of polyamines, and these are concomitant with erythrocytic maturation, with schizont stages containing the highest levels. Das Gupta *et al.* [1] demonstrated the concomitant increase of polyamines during the parasite IDC (Fig 1.6). Moreover, a recent report by Teng *et al.* confirmed that the polyamines are major metabolic constituents of the parasite and concentrations were measured to be even greater than previously reported by Assaraf *et al.*, within millimolar concentrations ranges [81].



**Figure 1.6: Polyamine levels established for asexual phase parasite stages. A)** Das Gupta *et al.* verified that the polyamine levels increase with maturation of the parasite in the iRBC. **B)** The majority of polyamines were shown through compartmental analysis, by Das Gypta *et al.*, to be associated with the parasites, rather than the erythrocyte host cells. The figures were generated from data listed in [1].

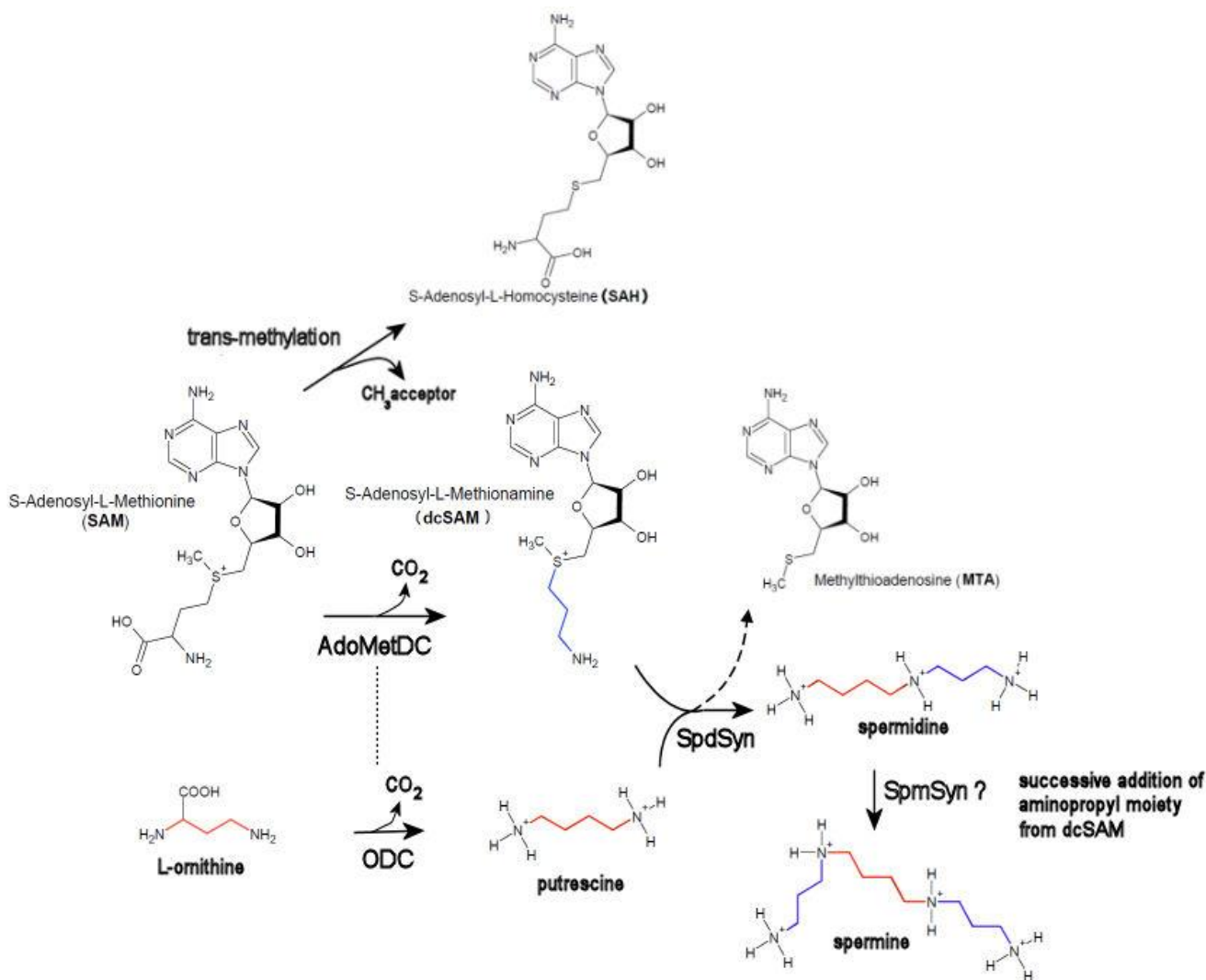
Additional compartmental analysis also revealed that the majority of putrescine and spermidine is located within the parasite, and minor levels are present within the erythrocytic compartments (Fig 1.6) [1]. Some reports also suggested that unRBC had pre-existing mechanisms for low level putrescine and spermidine uptake [83]. This was found more so for iRBC, which have dramatically altered patterns of polyamine uptake [84]. Facilitated influx of spermine has not yet been identified in either red blood cells or *P. falciparum* parasitized red blood cells [83, 85].

### 1.5.3. The polyamine biosynthetic pathway of *P. falciparum*

Although relatively little is known as to the function of polyamines, apart from stabilization of nucleic material, their dramatic increase during the IDC of *P. falciparum* has underscored the metabolic importance of their biosynthesis [82]. Initial biosynthesis of the polyamines utilizes substrate molecules; L-ornithine and S-adenosyl-L-methionine (SAM) (Fig 1.7). The formation of putrescine occurs through the decarboxylation of L-ornithine molecules, a reaction catalyzed by L-ornithine decarboxylase (ODC, E.C 4.1.1.17). Decarboxylated S-adenosyl-L-methionine (dcSAM) is the essential aminopropyl donor for the sequential formation of the true polyamines, spermidine and spermine, and is formed from SAM in a reaction catalyzed by S-adenosyl-L-methionine decarboxylase (AdoMetDC, E.C 4.1.1.50) (Fig 1.7).

The remaining polyamines; spermidine and spermine, are formed through the additional covalent linkage of the aminopropyl moiety to the primary amino groups of the putrescine molecule (Fig 1.7). Spermidine synthase (SpdSyn), also known as putrescine aminopropyltransferase (PAPT) (E.C 2.5.1.16), is able to catalyze the transfer of the aminopropyl group from the dcSAM substrate onto the putrescine moiety. In a similar type of reaction, spermine can be formed from spermidine through the additional linkage of an aminopropyl moiety, where spermine synthases (SpmSyn, E.C. 2.5.1.22) catalyzes this reaction (Fig 1.7). A enzyme of this nature has not been identified in *P. falciparum*, however, it was found that the *PfSpdSyn* has extended substrate accommodative properties, allowing additional formation of low levels of spermine from spermidine [86].

In most mammalian tissues AdoMetDC and ODC occur as separate proteins, however, quite strikingly, and often functionally questioned, is the nature of AdoMetDC and ODC proteins found in *P. falciparum*. Remarkably, the AdoMetDC and ODC domains are encoded on a single polypeptide forming a large 330 kDa bifunctional protein [87]. The expression of the *PfAdoMetDC-ODC* (*PfA/O*) bifunctional protein was also found to peak in trophozoite parasite stages corresponding to the requirement of greater polyamine production during this stage [87]. The advantage gained during the domain fusion event is still speculative, however, it has been demonstrated that the individual enzyme activities are functionally related to the presence of the opposing enzyme domains [88]. The cellular need for polyamine production requires increased activity of both ODC and AdoMetDC, and hence the regulation of a single mRNA, and protein fragment, may achieve this more efficiently. The bifunctional *PfA/O* of *P. falciparum* has been shown to have a central regulatory function in maintaining polyamine homeostasis within the parasite [87-89]. Compared to homologous proteins from other organisms, the individual parasitic ODC and AdoMetDC proteins have conserved features and inhibition appears to occur through similar mechanisms. However, the unique bifunctional nature of these proteins in the parasites may facilitate more efficient regulation of polyamines through mechanisms not yet understood.



**Figure 1.7: The polyamine pathway of *P. falciparum*.** Synthesis of polyamines occurs through the decarboxylation of L-ornithine and SAM to form putrescine and decarboxylated S-adenosyl-L-methionine (dcSAM), respectively. Additional linkage of aminopropyl groups, derived from dcSAM, onto the putrescine moiety results in the production of spermidine and with another successive addition, in the formation of spermine. The dashed line indicates the bifunctional nature of ODC and AdoMetDC enzymes in *P. falciparum*.

The pathway is distinctly different from that of the human host, and is thought to have selective targetability. For one, the mammalian pathway contains enzymes that are involved in the back-conversion of polyamines [90]. This feature effectively allows, for example, the spermidine polyamine to be formed through either SpdSyn or through the back-conversion from the spermine metabolite [91]. The lack of any identifiable back-conversion enzymes in the parasitic polyamine pathway could suggest that either, this regulatory feature is incorporated and polyamine production is efficiently regulated to this degree in the parasites. Peculiar regulation mechanisms have been revealed through the use of polyamine enzyme specific inhibitors, and some specific functional roles have been assigned to individual polyamines [89]. Results from previous investigations suggest that polyamine metabolism is controlled by the parasites through regulation of *PfA/O* production [89].

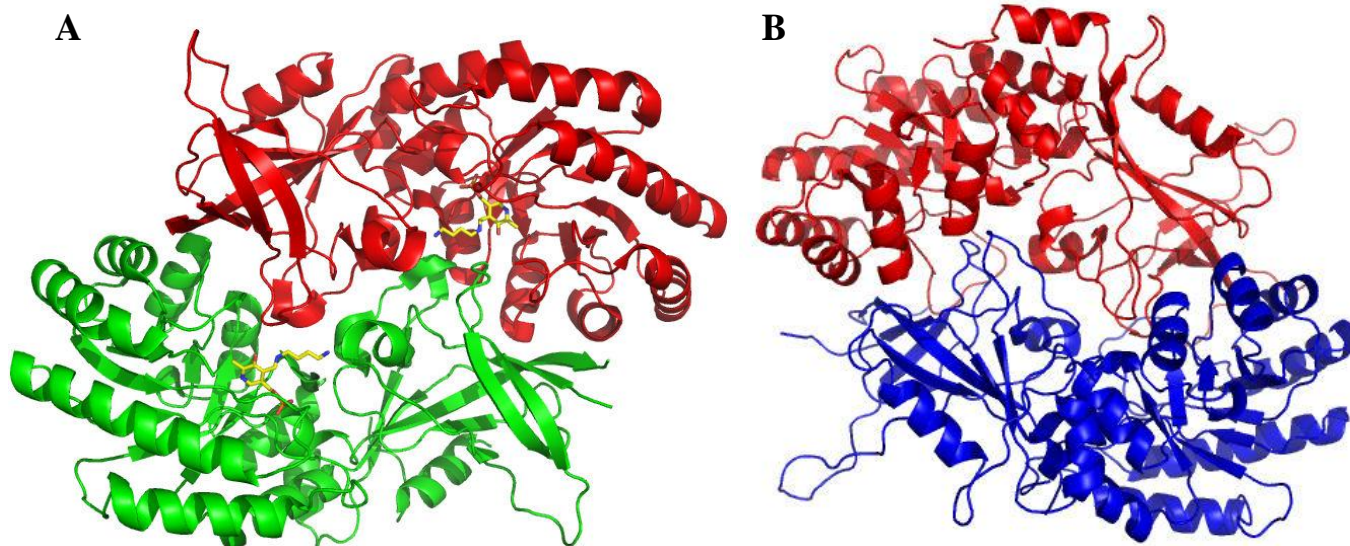
Polyamine biosynthetic enzymes are potential parasitic drug targets. The ODC enzyme specific inhibitor, DL- $\alpha$ -difluoromethylornithine (DFMO, Eflornithine<sup>®</sup>, Ornidyl<sup>®</sup>), is used to treat human African sleeping sickness caused by the apicomplexan *Trypanosoma brucei gambiense* [92]. The safety of the drug has been established and the compound is also thought to have potential for the treatment of tumors [92]. The effect of the drug was previously studied to determine its potential as malarial prophylactic or antimalarial therapeutic. The results revealed the drug caused cytostasis *in vitro*, however, underlying compensatory features are thought to negate the intended effect of the polyamine-enzyme inhibitor [80]. For one, the parasites were shown to have polyamine salvage mechanisms allowing parasites to evade polyamine depletion, and underscores the importance of the polyamines in the parasite [84]. These underlying compensatory mechanisms were studied at metabolome level to determine factors involved in circumventing the metabolic effect of polyamine depletion, for the purpose of exploitation during antimalarial drug design.

## 1.6. ODC enzymes and putrescine production

### 1.6.1. General features

Ornithine decarboxylases (ODC) are part of the larger pyridoxal-5'-phosphate (PLP) or vitamin B<sub>6</sub> superfamily [93]. Enzymes of this family utilize either PLP or pyridoxamine-5'-phosphate (PMP), which serve to resonance stabilize intermediates formed during a catalytic reaction [94]. PLP is also considered as one of the most versatile co-factors involved in both non-enzymatic and enzymatic catalysis [94, 95]. The B<sub>6</sub>-enzymes are involved in a range of different reactions including  $\alpha$ -decarboxylation, transamination, racemisation, retro-aldol cleavage and deamination [96, 97].

Eukaryotic ODCs fall into the Type III fold vit. B<sub>6</sub> family, and is said to have divergent evolutionary fold owing to their ( $\beta/\alpha$ )<sub>8</sub> barrel or Triosephosphate isomerase (TIM) characteristic [95, 97]. Proteins of this fold share structural similarity to alanine racemases (AR), which are, with exception, obligate or intimate homodimers, with N-terminal TIM barrel and C-terminal  $\beta$ -class monomeric domains [97]. The *P. falciparum* ODC (*Pf*ODC) has characteristics of a Type IV fold vit. B<sub>6</sub> dependent enzyme, and has two putative domains, a N-terminal  $\alpha/\beta$  TIM barrel fold and a modified C-terminal Greek key  $\beta$ -barrel (Fig 1.8 B) [98]. *Pf*ODC forms a homodimer, in which monomeric forms of the protein assemble in a head-to-tail orientation, with the N-terminal residues embedding in the C-terminal of the opposite monomer [98]. The lack of any crystal structure of this protein makes rationalizing inhibitor kinetics difficult, however generation of a homology model of the *Plasmodium* protein has revealed active site amino acid arrangement that compare well to other ODC homologs, like that of *T. brucei* (Fig 1.8 A, Table 1.1) [98].



**Figure 1.8: ODC proteins of *Trypanosoma brucei* and *P. falciparum*.** A) *T. brucei* ODC dimer with individual coloured domains, revealing formation of two active sites, with PLP - Put adducts shown in yellow (1F3T). B) The homology model generated for *P. falciparum* ODC domain of bifunctional PfA/O, shown with individual monomeric proteins coloured in red and blue, reveal the characteristic N-terminal  $\alpha/\beta$  Triosephosphate isomerase (TIM) barrel fold, and a modified C-terminal Greek key  $\beta$ -barrel component [98].

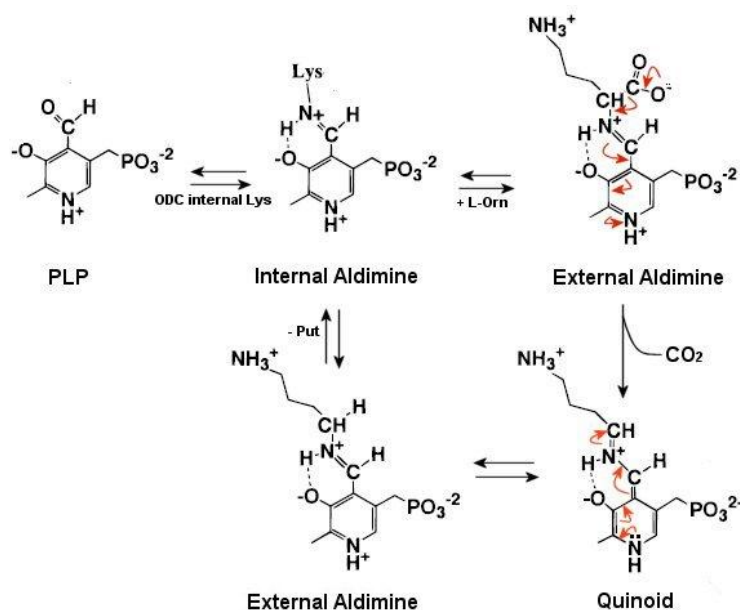
The ODC active site is acidic to accommodate both the cationic L-ornithine and putrescine substrates and products, respectively. The acidic active site arrangement is essentially conserved among the genera, as shown in Table 1.1. Both acidic acid residues, as well as a C-residue, are almost fully conserved and play an important part in PLP and substrate cofactor docking and stabilization (Table 1.1). General features of the ODC active site include the internal K-residue, involved in internal docking of the PLP co-factor, and a region of conserved acidic residues proposed to aid in substrate docking and stabilization of the substrate and product. Other entities of the active site include a C-residue strictly involved in determining the specific decarboxylation outcome of the docked intermediate molecules. These distinguishing features of the ODC active site are important considerations when inhibitor binding is rationalized.

**Table 1.1: Comparison of ODC residues from *T. brucei*, *P. falciparum*, *Homo sapiens* and *Mus musculus* [99, 100].**

Active site <i>Trypanosoma brucei</i> ODC residues [101, 102]	Corresponding residues in PfODC model and sequence [98]	Location in human ODC [100] ( <i>H. sapiens</i> )	Location in murine ODC [96] ( <i>M. musculus</i> )
Lys <sub>69</sub>	Lys <sub>868</sub>	Lys <sub>57</sub>	Lys <sub>69</sub>
Asp <sub>88</sub>	Asp <sub>887</sub>	Asp <sub>88</sub>	Asp <sub>88</sub>
Glu <sub>94</sub>	Glu <sub>893</sub>	Glu <sub>94</sub>	Glu <sub>94</sub>
Asp <sub>233</sub>	Asn <sub>1034</sub>	Asp <sub>233</sub>	Asp <sub>233</sub>
Glu <sub>274</sub>	Glu <sub>1114</sub>	Glu <sub>274</sub>	Glu <sub>274</sub>
Asp <sub>332</sub>	Asp <sub>1320</sub>	Asp <sub>332</sub>	Asp <sub>332</sub>
Cys <sub>360</sub>	Cys <sub>1355</sub>	Cys <sub>360</sub>	Cys <sub>360</sub>
Asp <sub>361</sub>	Asp <sub>1356</sub>	Asp <sub>361</sub>	Asp <sub>361</sub>



All PLP dependent enzymes contain an internal K-residue which forms a covalent imine bond with the PLP co-factor, also referred to as an internal aldimine (Fig 1.9). This residue plays an important part in docking, and localizing PLP for association and dissociation of the substrate and product molecules. Initial binding of L-ornithine in ODC enzymes entails a reversible imine reaction of the  $\alpha$ -amino group of the substrate with the PLP cofactor, during which the internal Lys Schiff-base is displaced (Fig 1.9). Irreversible decarboxylation of L-ornithine occurs when the  $\alpha$ -carbonyl group dissociates, forming a quinoid in the process (Fig 1.9). The carbanion intermediate is resonance stabilized by the pyridine component of the PLP co-factor and the cofactor therefore acts as an electron sink [101]. Of the various intermediate steps occurring during decarboxylation, the final reprotonation of the putrescine carbanion and hydrolysis of the putrescine-PLP bond is considered to be rate-limiting [101].



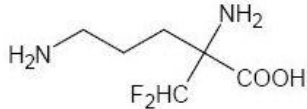
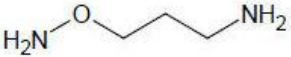
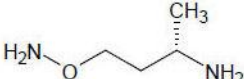
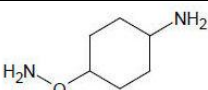
**Figure 1.9: ODC reaction mechanism.** An internal lysine residue is located with the ODC active site which binds a PLP co-factor. When in quinoid form, the cofactor is able to stabilize the L-ornithine carbanionic. Reprotonation on the  $\alpha$ -carbon on the already putrescine intermediate completes the enzymatic catalysis, and this is followed by dissociation of putrescine and the reformation of the internal aldimine.

### 1.6.2. Direct enzyme inhibitors

Two classes of ODC inhibitors have shown to have appreciable efficacy, these are; fluorinated substrate analogues, which are similar to L-ornithine, and aminoxy compounds which are proposed to act as competitive inhibitors. During the late 1970s, through deductions made using L-ornithine analogues, Bey *et al.* [103] could accurately conclude the requirement for an effective ODC inhibitor was molecules containing a uncomplexed primary terminal amino groups ( $\delta$ -NH<sub>2</sub>) [103]. During this time, Bey *et al.* [103] also found that the substrate analogue (+)- $\alpha$ -methyl ornithine had the greatest inhibitory effect on rat liver ODC, with a inhibitory constant ( $K_i$ ) of 20  $\mu$ M [103, 104]. In a separate publication, Metcalf and Bey *et al.* [105], reported the synthesis and evaluation of irreversible inhibitors of ODC, including the most famous polyamine inhibitor; DFMO (Table 1.2). Metcalf *et al.* proposed a mechanism of irreversible inactivation of ODC, and

this involved the conserved active site C-residue nucleophile, which forms a covalent bond with the DFMO substrate [105]. DFMO has been shown to inhibit *Pf*ODC and with corresponding active site residues predicted in the *Pf*ODC model (Table 1.2), a similar mechanism of DFMO-cysteine (*Pf*C<sub>1355</sub>) adduct formation is thought to be possible.

**Table 1.2: *Pf*ODC inhibitors.** Inhibitors of *Pf*ODC indicated with specific inhibitory activity against purified ODC ( $K_i$ ) and cultured parasites ( $IC_{50}$ ) [1].

Inhibitor	Chemical structure	$K_i$ ( $\mu$ M)	$IC_{50}$ ( $\mu$ M)	Mechanism and transport
DFMO		87.60	1250	Covalent adduct to internal C-residue, results in irreversible inhibition.
APA		0.0027	1.0	Aminooxy compounds covalently bind to PLP co-factor, results in irreversible type inhibition. Recent evidence suggests no aldimine is formed [106]
CGP 54169A		0.0079	2.0	
CGP 52622A		0.0020	2.7	

Other ODC inhibitors include 3-aminooxy-1-propanamine (APA, also called 1-aminooxy-3-aminopropane) and CGP54169A (3-aminooxy-1-methylpropanamine), as shown in Table 1.2. APA was originally synthesized in 1960 by McKay *et al.* [107], and it was found to be a potent competitive inhibitor against mouse kidney ODC [108]. The application of this inhibitor against the malarial ODC counterparts revealed that the inhibitor had remarkably low  $K_i$  values of 2.7 nM compared to DFMO with  $K_i = 87.6 \mu$ M [1]. APA was thought to be a non-specific inhibitor that inactivates the PLP co-factors, rather than influence L-ornithine active site binding. APA inhibition was originally shown to be independent of the presence of PLP, and it was proposed that APA directly interacts with ODC active site residues [108, 109]. Khumotov *et al.* could also show that APA had specific activity towards ODC, and minimal effect on other PLP-dependent enzymes [108]. It was later concluded that the highly selective inhibitory action of APA towards ODC may involve the formation of the PLP-oxime specifically within the ODC active site, resulting in an reversible type blockage [1]. Dufe and Persson *et al.* could show that APA occupies a position similar to the L-Ornithine substrate in *Homo sapien* ODC (*Hs*ODC); however the inhibitor maintains interactions with enzyme active site tyrosine residues, and the aminooxy groups were hydrogen bonded to the PLP-O4 oxygen atom [106]. This therefore indicated PLP was not inactivated as previously thought.

Other amino-oxy compounds include CGP52622A and CGP54169A (Table 1.2) [110]. CGP 54169A, resembling the APA aminooxy inhibitor with an additional methyl substituent on the primary amine, also had potent *Pf*ODC inhibitory activity [1, 111]. The slightly lowered activity compared to APA, at  $K_i = 7.9$  nM, did suggest that bulky groups on the amine ( $\delta$ -carbon) terminal negatively influence active site binding. CGP52622A was also shown to have low nanomolar efficacy with  $K_i$  values around 20.4 nM. This may lead one to suggest the large cyclohexyl ring components may have less favourable interactions compared to uncomplexed alkane chains.

## 1.7. The relationship between SAM homeostasis and polyamine biosynthesis

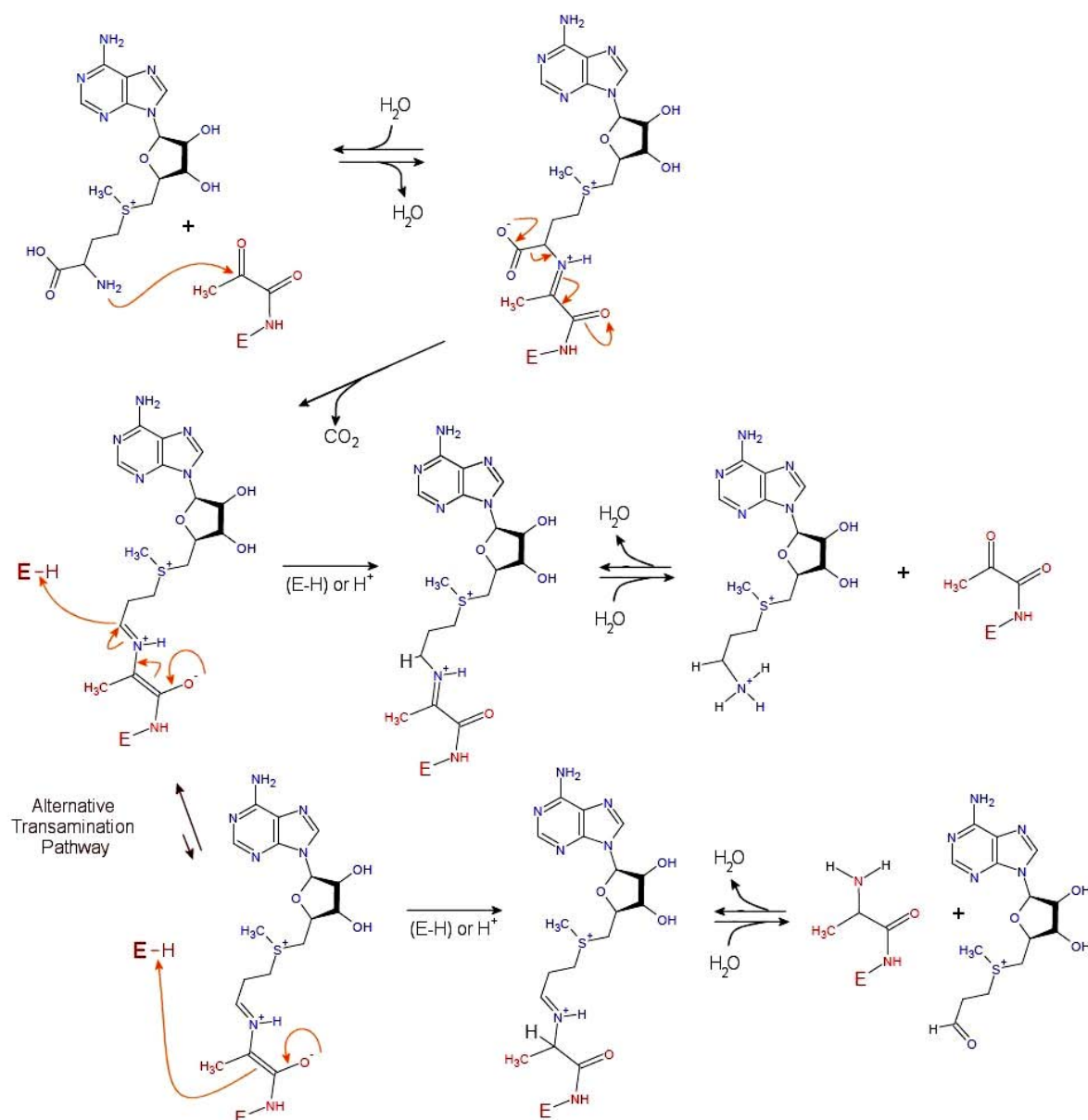
### 1.7.1. SAM recycling and adenosyl related metabolite regulation in *P. falciparum*

S-adenosyl-L-methionine (SAM), also known as AdoMet, is an essential metabolite involved in an array of biochemical pathways. Some speculate that SAM is the second most utilised substrate, ATP being the most abundantly used [112]. AdoMetDC catalyzes the decarboxylation of SAM, and dcSAM is subsequently utilised for transfer of aminopropyl groups to receiving polyamine molecules in the polyamine pathway, as already mentioned. Apart for its function in the polyamine pathway SAM also plays a vital role as methyl donor in methylation reactions occurring on a array of different substrates including nucleic acids, proteins, lipids, and other small molecules [113]. In some mammalian cells it is proposed that 95% of the total cellular available SAM is utilised in methylation reactions [114]. Considering this ubiquitous necessity of SAM, the importance of SAM flux diversion specifically through the polyamine pathway could have been previously underestimated.

### 1.7.2. General characteristics and AdoMetDC architecture

AdoMetDC is a SAM-binding protein, forming part of the larger SAM-binding protein family, which contains up to 15 different folds [115]. When compared to the larger family of Rossmann-like SAM methyltransferases, having a singly centered  $\beta$ -sheet topology with flanking  $\alpha$ -helical arrangement, AdoMetDC protein architecture reveals a unique  $\alpha\beta\beta\alpha$  sandwich fold. The human enzyme has two central  $\beta$ -sheets, individually composed of eight antiparallel strands, each sheet flanked by several amphipathic  $3_{10}$  and  $\alpha$ -helices. Sequence comparison between bacterial and eukaryotic AdoMetDC also suggested that the larger eukaryotic enzyme has been formed through a domain duplication event, as components of bacterial AdoMetDC are found in the larger eukaryotic sequence [115-117]. Eukaryotic AdoMetDC proteins are known to form homodimers, compared to plant and bacterial enzymes which remain dissociated monomers [118].

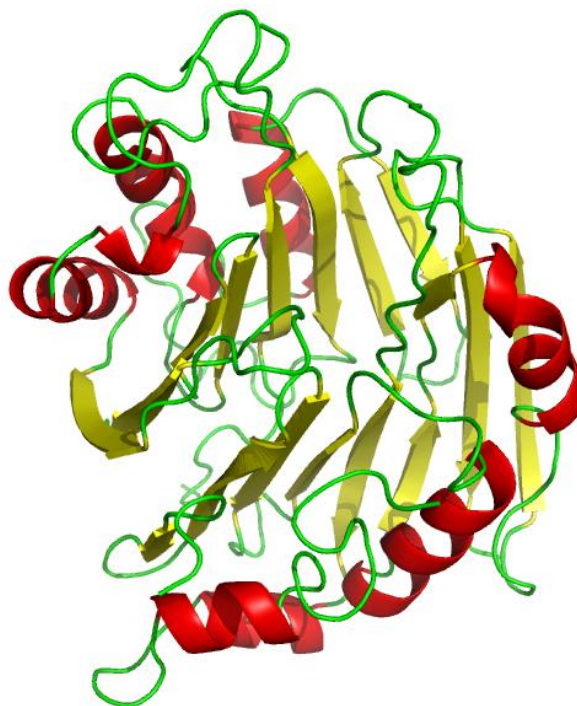
All known AdoMetDC paralogues are pyruvoyl-dependent decarboxylases, generally formed as proenzymes and require post-translational processing for enzymatic activation. The event of autocatalytic processing occurs when the hydroxyl groups of internal serine residues attack a preceding amino acid carbonyl group. This is often referred to as non-hydrolytic serinolysis and results in the formation of a pyruvoyl moiety [116]. Pyruvoyl formation also leads to internal protein cleavage, resulting in a larger C-terminal  $\alpha$ -subunit which contains the pyruvoyl group, with proximal association of smaller N-terminal  $\beta$ -subunits [118]. The resulting pyruvoyl group forms the catalytic center and act as a Schiff-base. The initial steps of the catalytic mechanism involve reversible imine formation with the active site pyruvoyl moiety. SAM molecules are covalently bound to this group through imine formation, and like the PLP cofactor, the pyruvoyl group stabilizes intermediate negative potential generated on transition state forms [118]. The process of decarboxylation is depicted in Fig 1.10.



**Figure 1.10: Mechanism of SAM decarboxylation in human AdoMetDC** [116, 119]. The pyruvate moiety formed from a Ser residue in the N-terminal of the  $\alpha$ -chain is able to form an imine with the SAM molecule. The formation of the carbocation during spontaneous dissociation of the  $\alpha$ -carbonyl group is resonance stabilized across the pyruvoyl moiety. An active site Cysteine residue plays an important part in re-protonation of the carbocation, and determines the specificity of the reaction. An alternative transamination pathway is thought to exist, in which the pyruvoyl enamine is the protonated product, and this subsequently results in inactivation of the enzyme [119].

The decarboxylation reaction mechanisms proceed as irreversible dissociation of the carbonyl group from the substrate and results in the formation of a carbocation, which is resonance stabilized through the pyruvoyl moiety (Fig 1.10). Re-protonation of the  $\alpha$ -carbon on the aminopropyl chain of the decarboxylated intermediate follows, and this process is thought to involve a conserved active site cysteine, discussed in more detail below. Reversible hydrolytic cleavage allows dissociation of the decarboxylated product and also regenerates the pyruvoyl group for subsequent decarboxylations reactions [116].

The monofunctional AdoMetDC protein of *P. falciparum* was modelled, and is postulated to form an  $\alpha\beta\alpha$  like protein, with a central associated  $\beta$ -sheet region flanked by several peripheral  $\alpha$ -helical moieties (Fig 1.11) [120]. The *PfAdoMetDC* protein is proposed, like its mammalian counterpart, to dimerize thereby forming a heterotetrameric protein. However, the *PfAdoMetDC* has greater resemblance to plant homologs, and the process of autocatalytic activation of *PfAdoMetDC* is also a unique feature where the allosteric presence of putrescine is not required [120, 121]. The post-translational event of autocatalytic cleavage occurs between Glu<sub>72</sub> (*PfD*<sub>72</sub>) and Ser<sub>73</sub> (*PfS*<sub>73</sub>) residues, and results in the formation of a heterodimeric enzyme, consisting of smaller N-terminal  $\beta$ -chain (9 kDa) and a larger C-terminal  $\alpha$ -chain (70 kDa) [121].



**Figure 1.11: Monofunctional *PfAdoMetDC*.** A homology model of the *PfAdoMetDC* domain of bifunctional *PfA/O* was constructed by Wells *et al.* [120].

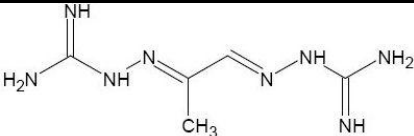
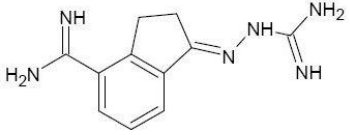
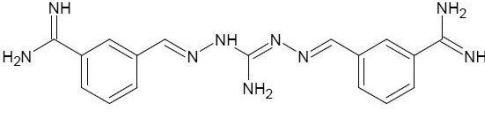
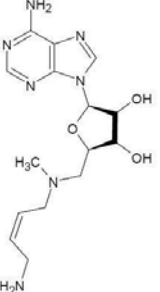
An important feature in human AdoMetDC enzymes is the possible irreversible inactivation during decarboxylation. As shown in Figure 1.10, re-protonation can either occur on the  $\alpha$ -carbon of dcSAM, or alternatively this can also occur on the pyruvate moiety, the latter resulting in complete inactivation of the enzyme [119, 122]. The *PfAdoMetDC* active site contains various corresponding residues and important residues are *PfF*<sub>5/415</sub>, and these are postulated to interact with the adenine ring of SAM. *PfD*<sub>438</sub> is also proposed to specifically hydrogen bond with the ribose hydroxyl groups of the SAM substrate [120]. A C-residue (*PfC*<sub>87</sub>) has also been modeled in the *PfAdoMetDC* active site, and is thought to be involved in reprotonation of the reaction intermediates. The mechanism of enzyme inactivation is therefore also thought to occur in the malarial proteins.

### 1.7.3. Direct enzyme inhibitors

Inhibitors of AdoMetDC enzymes mostly resemble the substrate molecule, dcSAM, and various rational chemical modifications have resulted in an arsenal of AdoMetDC inhibitors of both

competitive and irreversible type. Competitive type inhibitors include the Ciba-Geigy synthesized CGP40215A compound which share structural similarity to methylglyoxal bis(gaunylhydrazone) (MGBG), and 5'-((Z)-4-amino-2-butenyl)methylamino)-5'-deoxyadenosine (MDL73811) proposed to specifically bind to pyruvoyl groups of the AdoMetDC protein [122] (Table 1.3).

**Table 1.3: Inhibitors of *P. falciparum* AdoMetDC.** These are shown with enzyme specific activity ( $K_i$ ) and *in vitro* determined growth inhibitory efficiency ( $IC_{50}$ ) [1].

Inhibitor	Chemical structure	$K_i$ ( $\mu$ M)	$IC_{50}$ ( $\mu$ M)	Mechanism and transport
MGBG		-	-	-
CGP48664A (SAM 486A)		3.0	8.8	Competitive inhibition, alternative transport proposed. May however have multiple targets [1].
CGP40215A		1.3	1.8	Reported not to effect PA levels in parasite, yet is AdoMetDC inhibitor [1].
MDL73811 (AdoAbe)		1.6	3.0	Adenosine substituent might allow transport through purine salvage pathway [1].

Some of the most potent inhibitors against AdoMetDC resemble MGBG, one of the first AdoMetDC inhibitors identified in the late 70's (Table 1.3). MGBG was shown to bind competitively within the human AdoMetDC active site, specifically interacting with F-residues involved in hydrophobic aromatic stabilization of the SAM substrate [123]. Various studies indicated that MGBG lack specificity or albeit had additional side-effects. The compound was shown to have profound cytotoxicity, causing depletion of mitochondrial pyruvate oxidation and reduction of mitochondrial DNA [124, 125].

In search of greater specificity Stanek *et al.* was the first to synthesized additional aryl and cyclic MGBG analogues, these compounds having reduced toxicity with greater therapeutic efficiency against AdoMetDC compared to MGBG [126]. CGP48664A is one of these MGBG analogues that have received some attention in the last decade (Table 1.3). CGP48664A, also sometimes named SAM486A, is one of the most promising competitive-type AdoMetDC inhibitors, and is

even implicated for the treatment of solid tumours [124, 127]. The drug is also currently undergoing Phase II clinical trials [127]. In light of this, questions still remain as to the specificity of the MGBG analogue, and some evidence has accumulated supporting the notion that this inhibitor has other non-polyamine related side-effects [128]. When compared to MDL73811, an irreversible AdoMetDC inhibitor, CGP48664A also has additional inhibitory action. At equivalent  $IC_{50}$  doses both AdoMetDC inhibitors have similar cytostatic effects on L1210 cells, effectively decreasing enzymatic activity and depleting spermidine and spermine. The MGBG analogue however had additional cytotoxic effects at higher doses, and this was not always reflected in fluctuations of polyamines [128].

Das Gupta *et al.* reported antimalarial activity for CGP48664 ( $IC_{50} = 8.8 \mu\text{M}$ ,  $Pf\text{AdoMetDC } K_i = 3.0 \mu\text{M}$ ), but a relatively low efficacy compared to the situation in mammalian cells, may be due to underlying differences in transport of the compound [1]. This lowered inhibitory action demonstrates that selective attenuation of *PfAdoMetDC* may not be achieved; however pharmacokinetic optimization might reveal this compound as valuable a competitive inhibitor. Specifically relating to *P. falciparum* the compound, CGP 40214A, was shown to be currently the most potent AdoMetDC inhibitor *in vitro* with an  $IC_{50} = 1.8 \mu\text{M}$  (Table 1.3). CGP40215A, however, did not disrupt the polyamine distributions, even at  $2 \times IC_{50}$  concentration, yet ambiguously had an  $K_i = 1.3 \mu\text{M } Pf\text{AdoMetDC}$  reported in kinetic assays, suggesting possible off-target effects [1].

MDL73811, also called AbeAdo, is an example of a rationally designed inhibitor specific to AdoMetDC (Table 1.3). Originally synthesized at the Merrell Dow Research Institute in Strasbourg France, the inhibitor is currently one of the most promising compounds for the abrogation of the decarboxylases [122]. The compound was rationally designed with an amino group replacing the sulphur of SAM, also with an additional aminobutenyl group instead of the aminopropyl chain [122]. Various studies have indicated that the inhibitor binds, as the natural substrate SAM, to the pyruvoyl entity in the active site of AdoMetDC. It was therefore speculated that the inhibitor binds irreversibly in the AdoMetDC active site [122].

## 1.8. Aims

The objective of this study was to investigate the metabolomic responses of the malaria parasite after inhibition of its endogenous polyamine biosynthesis. This would aid in understanding of polyamine metabolism in this parasite such that it can be promoted as antimalarial target. In Chapter 2, a limited metabolomic investigation was performed on *P. falciparum* parasite after inhibition of the bifunctional drug target *PfA/O*. In Chapter 3, the efficacy of targeting *PfSpdSyn* as drug target was investigated following the identification of novel inhibitors originating from a rational SBDD strategy. Results indicated significant inhibition by one novel chemical compound.

## Chapter 2: Metabolite profiling during *Pf*ODC-AdoMetDC inhibition

### 2.1. Polyamine and other related metabolites in *P. falciparum*

#### 2.1.1. Metabolomics and the polyamines

The Central Dogma of Molecular biology, originally coined by Francis Crick in 1958, proposed a sequential, systemic pathway of how proteins are formed within most living organisms [129]. The classical „DNA to RNA to protein“ polymeric transfer process however is being reshaped with newer discoveries revealing that complex regulatory features and feedback loops are hidden within the dogma at each defined stage. The tail end of the dogma, the metabolome, reflects the collection of metabolites determined by the active proteome within a cell, at any given state [130]. Regulation of metabolite concentrations within the cell could therefore be considered to be most subject to the regulatory features imparted as a function of the transcriptome and proteome. The metabolome is also subject to a supply-demand chain and regulated by the availability of substrates, feedback loops of products, allosteric effectors and other protein partners [131]. Therefore the metabolome of an organism may be most reflective of long term, short term and immediate changes experienced within a changing environment. Entering the post genomic-era, new correlations and conclusions are necessary between the transcriptome, the proteome, and the metabolome [130]. These elucidations aim to achieve a global understanding of the complex workings within an organism.

Limited metabolomic investigations have, however, been performed on *P. falciparum*. This study had a focused metabolomic investigation approach, also termed „Target Analysis“, in which the polyamine metabolites and related adenosyl containing compounds of *P. falciparum* were studied [130]. Various research efforts have been focused on testing of effective inhibitors against polyamine enzymes, and in doing so have also reported the levels of polyamine fluctuations during inhibition. These studies have also collected data to suggest that some peculiarities exist when polyamine enzymes of *P. falciparum* are inhibited, and the metabolic implications are also further discussed.

#### 2.1.2. Implication and metabolic effects of ODC enzyme inhibition.

*In vitro* addition of DFMO to *P. falciparum* results in cytostasis [82, 85, 132]. Following treatment with DFMO, *Pf*ODC is irreversibly inhibited with a  $K_i = 87 \mu\text{M}$ , and *in vitro* experiments where DFMO was used against the malaria parasites showed a corresponding decline in putrescine [111]. The cellular reduction of putrescine also results in the reduction in spermidine levels, and the degree of observed growth reduction was shown to correlate with the degree of cellular depletion of spermidine [79, 80]. However, spermine levels in parasites treated with DFMO were found to either remain unchanged or increased [80, 82, 132]. At an effective dose of 5 mM DFMO (1.3 mM reported by [1, 79, 133, 134]) *in vitro*, the cytostatic effect of polyamine depletion was attributed to inhibition of DNA replication and protein synthesis, however this was easily reversed by the exogenous addition of putrescine [80, 82, 85], or spermidine [79, 85, 133] in some cases even spermine [79, 133], however the latter was not



always reproducible. In *P. falciparum* DFMO inhibits erythrocytic schizogony, arresting growth at the trophozoite stages, and due to the depletion of polyamines, exogenous salvage of putrescine, and less significantly spermidine, was also reported to increase [1, 84, 85, 133]. The rapid upregulation of these exogenous salvaging mechanisms is also testament to the cellular requirement of polyamines [84]. DFMO treated *P. falciparum* have marginal increased spermine levels, and this might be a compensatory mechanism due to the rapid decline in available putrescine, resulting in dcSAM accumulation [80, 82]. A spermine aminopropyltransferase (SAPT, SpmSyn) has not yet been identified in *P. falciparum*, and the formation of the spermine metabolite was therefore attributed to *PfSpdSyn*, which has been shown to have extended substrate binding capability [86]. A substantial increase in dcSAM, predicted in DFMO-treated cultures, is thought to drive this reaction and lead to accumulation of spermine.

The metabolic effect of APA on the parasites has also been studied by Das Gupta *et al.* to reveal that the compound is a prominent inhibitor of ODC.  $K_i$  values were reported in the low nanomolar range (Table 1.2) [1]. The effect on the polyamine levels was pronounced by a significant depletion in putrescine and spermidine within the first 24h after treatment corresponding to middle stage trophozoites. The extent of spermine accumulation, compared to DFMO-treated parasites, was not so prominent [1]. However, APA was also demonstrated to inhibit *PfSpdSyn* albeit at lower concentrations, and this could therefore account for the lack of significant increases in spermine [86]. This therefore further supported the fact that accumulation of dcSAM does play a role in the formation of spermine.

Studies using rodents infected with *Plasmodium berghei*, the closest relative of *P. falciparum*, it was shown that DFMO effectively blocks exoerythrocytic schizogony *in vitro* [135] and *in vivo* [136]. This illustrated that the liver-schizont forms of the parasite are susceptible to DFMO and maturation into merozoites requires polyamines. DFMO was also an effective antiplasmodial agent against blood stages or erythrocytic schizonts, decreasing *P. berghei* parasitemia *in vivo*, yet not able to rescue mice from death [79].

The efficacy of polyamine inhibitors is not doubted, as shown during *in vitro* addition of other ODC competitive inhibitors like APA, CGP54169A and CGP52622A (Table 2.2) to *P. falciparum* results in rapid reduction of putrescine and spermidine in the parasites, and results in growth arrest at the trophozoite developmental state [1]. DFMO treated parasites can be rescued using an exogenous source of putrescine, and this was also observed for APA-treated parasites [1].

DFMO has been successfully used in the treatment of African sleeping sickness caused by *Trypanosoma brucei gambiense* [92, 137]. The efficacy of DFMO, shown in *T. brucei gambiense*, was proposed due to depletion of parasitic polyamine levels, which in turn depletes the availability of dihydrotrypanothione ( $N^1$ ,  $N^8$ - bis(glutathionyl) spermidine), an essential spermidine-containing molecule required to maintain the intraparasitic glutathione thiol-redox balance [137, 138]. DFMO treatment was also shown to dramatically increase SAM levels, and this was partly attributed to the lack of metabolite feedback regulation in the *T. brucei* SAM

synthetase enzyme [139]. The lack of putrescine resulted in accumulation of both dcSAM and SAM, where the latter increased almost 50-fold [140]. It is therefore speculated that the increases in the essential methyl-donor SAM level, during DFMO treatment, correspond to a hypermethylated state, and this in turn could result in a trypanocidal effect [140, 141].

### 2.1.3 Implications and metabolic consequence of AdoMetDC inhibition

Generally the inhibition of AdoMetDC results in the accumulation of putrescine, and the levels of spermidine and spermine are also often observed to decrease [1, 133, 142]. The elegance of the mammalian dcSAM regulatory system is demonstrated, in which additional putrescine would result in increased catalytic activation of AdoMetDC, with resulting increases in dcSAM. Also depending on the organism, SAM levels have shown to fluctuate under conditions of low dcSAM, indicating that metabolic flux through the polyamine pathway is an important diversion in SAM metabolism [143].

A model situation exists that elegantly demonstrates disruption of SAM metabolism through the use of AdoMetDC inhibitors. In *T. brucei*, administration of MDL73811 increased SAM concentrations by 20-fold, which also resulted in effective clearance of the parasite from rats within 4h of treatment [140]. The trypanosome SAM synthetase (SAMS) proteins were believed not to be regulated through product feedback inhibition, and resulted this resulted in dramatic increased SAM levels [140]. With the inter-pathway relationship of the SAM substrate, the dramatic flux accumulation was proposed to cause greater inhibitor effect, also resulting in a state of hypermethylation [140]. Ultimately this suggests accumulation of SAM has detrimental effects, and this makes AdoMetDC, which diverts SAM metabolic flux, an important drug target.

MDL73811 inhibited *PfAdoMetDC* with  $K_i = 1.6 \mu\text{M}$  [127]. The compound is one of the most effective *P. falciparum* AdoMetDC inhibitors, and a dose of 3 - 5  $\mu\text{M}$  administered *in vitro* resulted in reduced spermidine and spermine levels typical of AdoMetDC inhibition. Some authors also report irreversible inhibition of the decarboxylase, and the addition of spermidine and spermine is said to antagonize the effects of MDL73811 [133] (this could be reproduced using only spermidine [1]). MDL73811 arrested growth at trophozoite developmental stages of *P. falciparum* and addition of adenine could not elevate the growth inhibition. Analogues of MDL73811 were also shown to be effective in the micro-molar concentrations, but it was clearly evident that a *cis*-configuration across the aminobutenyl chain, and the N-methyl substituent on the AdoAde molecule increased the potency [133]. This promising compound is also reported to have additive effects in *P. falciparum*, in combination with APA [1].

The efficacy of AdoMetDC inhibitors has been demonstrated in *P. falciparum in vitro*, and correlates with decreased levels of spermidine [1, 133]. AdoMetDC inhibitors are, however, only effective in depleting spermidine and spermine, and the lack of putrescine depletion in the parasites may overcome these effects [1]. Also, it is proposed that polyamine inhibitor combinations against *PfODC* and *PfAdoMetDC* could potentiate the depletion of all three polyamines and may have greater therapeutic action.

The effect of *PfA/O* co-inhibition, and the underlying fluctuations in polyamine-limited metabolites was studied in this dissertation. The importance of establishing the polyamine metabolite levels during *PfA/O* co-inhibition has been underscored in a recent publication by van Brummelen *et al.* [89]. The authors reported that the parasites circumvent polyamine depletion through remodelling of various transcript and protein levels. SAM synthesis was proposed to decrease during *PfA/O* inhibition and this mechanism was proposed to circumvent adenosyl-related flux. A metabolomic investigation further questioned the underlying perturbations in adenosyl-related metabolism during *PfA/O* co-inhibition.

## 2.2. Methods

### 2.2.1. Quantification of polyamines and adenosyl-related compounds

#### 2.2.1.1. Estimation of LOD and LOQt of benzylation

All reagents were of the highest purity grade; benzoyl chloride (Sigma-Aldrich, St. Louis, USA), sodium hydroxide (NaOH) (Fluka, Steinheim, Germany), cadaverine dihydrochloride (Fluka, Steinheim, Germany), 1,4-diaminobutane dihydrochloride (Putrescine) (Fluka, Steinheim, Germany), 1,7-diaminoheptane (Sigma-Aldrich, St. Louis, USA), spermidine trihydrochloride (Fluka, Steinheim, Germany) and spermine tetrahydrochloride (Fluka, Steinheim, Germany) were provided by Sigma-Aldrich. Methanol (MeOH) of HPLC grade was purchased from Sigma-Aldrich (St. Louis, USA) and Merck (Darmstadt, Germany). Chloroform (99.9%) from both Sigma-Aldrich and Merck, was also used throughout the procedure. Seventy percent v/v perchloric acid (PCA) was purchased from Fluka. SABAX Sterile H<sub>2</sub>O (Adcock-Ingram Ltd, SA) and Millipore triple distilled H<sub>2</sub>O (dddH<sub>2</sub>O) were sources of pyrogen-free water.

A modified benzylation procedure from Taibi *et al.* and Schenkel *et al.* [144, 145] was used to benzylate polyamine standards and *P. falciparum* extracted polyamines. The method included an overnight alkaline washing procedure to remove benzylation by-products. The limits of detection (LOD) and limits of quantification (LOQt) of the optimized benzylation procedure were determined from three experiments, performed on three separate days, and therefore accounted for the intra-day variation of the procedure. A 4 mM polyamine stock cocktail was prepared by adding equal parts of each 20 mM individual polyamine stocks previously prepared in 5% PCA. The cocktail consisted of 1,4-diaminobutane dihydrochloride, cadaverine dihydrochloride, spermidine trihydrochloride, spermine tetrahydrochloride and 1,7-diaminoheptane. The polyamine cocktail range was serially diluted using 5% PCA to obtain polyamine concentrations ranging from 2.5 – 40  $\mu$ M. One hundred and fifty microliters of each individual concentration polyamine cocktail was subjected to the benzylation derivatization.

Benzylation was performed by adding 1mL of 1M NaOH to the polyamine standard containing tubes. Five microliters of benzoyl chloride was added, and after vigorous vortexing, the tubes were incubated at 37°C for 20 min to allow completion of benzylation. One milliliter of chloroform was added, samples were vortexed, and centrifuged at 1000 x g for 10 min (Medifuge, Heraeus, Sepatech, Germany) to allow clear separation of aqueous and organic layers.

Aqueous layers were removed and washed in another 1 mL chloroform and centrifuged at 1000 x g for 10 min. Chloroform layers were pooled and evaporated under N<sub>2</sub>(g). 1 mL of 0.1 M NaOH (Fluka, Steinheim, Germany) was added to the tubes. The tubes were vigorously vortexed and left overnight at room temperature (RT). The following day 1 mL of chloroform was added to the tubes, and after centrifugation at 1000 x g for 10 min the lower chloroform layers were collected, and evaporated under N<sub>2</sub>(g). The final benzoylated polyamine residues were re-suspended in 0.5 mL 60% MeOH: H<sub>2</sub>O to give 0.75 – 12 μM concentrations. During HPLC separation according to “HPLC separation of benzoylated polyamines” section, duplicate 40 μL injections were made to obtain a range corresponding to 30 – 480 pmol benzoylated polyamines. Regression analysis was performed using GraphPad Prism Software (GraphPad Software Inc., Version 5.00 - trial version, San Diego, California, USA). The LOD and LOQt were calculated using the following formula;

$$LOD = \frac{3.3\sigma}{Slope} \qquad LOQt = \frac{10\sigma}{Slope}$$

The slope value is calculated from linear regression lines determined by plotting peak areas (μV\*sec) generated from benzoylated polyamines against the standard, fixed polyamine concentrations. The standard deviation, σ, is calculated through interpretation of the S<sub>y,x</sub> value. The S<sub>y,x</sub> value represents the sum of the standard deviations of the residuals, or Y-data points, in the benzoylated polyamine regression line. This value accounts for the error in consecutive peak area measurement at each distinct polyamine concentration.

#### 2.2.1.2. Estimation of LOD and LOQt of adenosyl-related standards

Standards consisted of S-adenosyl-L-methionine chloride (Sigma-Aldrich, St. Louis, USA), S-adenosyl-L-homocysteine (SAH) (Sigma-Aldrich, St. Louis, USA), and methylthioadenosine (MTA) (Sigma-Aldrich, St. Louis, USA). dcSAM was kindly provided by Keiji Samejima (Josai University, Japan). MDL73811 was obtained from Sanofi-Aventis (Paris, France). The standards were dissolved in 5% v/v perchloric acid (PCA, Fluka, Steinheim, Germany) at 1 mM concentrations. SAM standards which are known to be unstable were stored at -70°C, and fresh stocks were prepared for each separate HPLC procedure. SAH, MTA, dcSAM and MDL73811 were found to be stable if stored at -20°C in 5% PCA conditions.

A standard series containing SAH, SAM, MTA, dcSAM, and MDL73811 was prepared by using equal amounts of each 1 mM stock standard. This solution was diluted to 100 μM, 10 μM, 5 μM, 1 μM and 0.5 μM concentrations using 5% PCA. The combination standards were filtered by using 0.2 μm HPLC certified polypropylene filters, Minisart RC4 (Sartorius, Goettingen, Germany). One hundred microliter injections of these combination standards were performed in triplicate during HPLC separation, and represented 10 nmol - 0.05 nmol of each adenosyl-containing standard. HPLC separation of adenosyl-containing compounds was performed as mentioned in section 2.2.2.5. The LOD and LOQt of the HPLC procedure was calculated using the formula as given in section 2.2.1.1.

## 2.2.2. Metabolomic profiling of polyamine co-inhibited *P. falciparum*

### 2.2.2.1. Culturing of *P. falciparum*

*Plasmodium falciparum* (3D7) asexual blood phase parasites were maintained in synchronous continuous culture using established methods as previously reported by Trager *et al.* [146]. Parasites were cultured in RPMI-1640 (Sigma-Aldrich, St. Louis, USA) media. The media was additionally supplemented with 25 mM 4-(2-hydroxyethyl)-1-piperazineethanesulfonic acid (HEPES) (Sigma-Aldrich, St. Louis, USA), 22 mM D-Glucose (Sigma-Aldrich, St. Louis, USA) and 25 mM sodium bicarbonate (NaHCO<sub>3</sub>, Sigma-Aldrich, St. Louis, USA). Additionally 0.36mM hypoxanthine (50 mg/L) (Sigma-Aldrich, St. Louis, USA) and 48 mg/L Gentamicin (Sigma-Aldrich, St. Louis, USA) was also added to the media. The media was sterilized through filtration using Millipore™ filtration system (Millipore, Massachusetts, USA) and 0.22 µm acetate filters (Sartorius, Goettingen, Germany). The final RPMI-1640 media containing the above supplements (wash media), was stored at 4°C. Additionally 0.5% Albumax II (Invitrogen, Germany) was added as serum substitute to form complete culture media (CCM). During culturing, 5% hematocrit was maintained using RPMI washed O+ Type blood collected in EDTA Vacutainer® blood collection tubes (BD Biosciences, California, USA). Cultures were stored in atmospheric conditions comprising of a custom gas mixture of 90% N<sub>2</sub>, 5% O<sub>2</sub> and 5% CO<sub>2</sub> (Afrox, Pretoria, South Africa) and incubated at 37°C.

Parasitemia was assessed using Giemsa-stained blood smears. Stock Giemsa stain was prepared by adding 0.76 g Giemsa's Azur eosin methylene blue dye mixture (Merck, Darmstadt, Germany) to 50 mL glycerol (Merck, Darmstadt, Germany) and 50 mL MeOH (Merck, Darmstadt, Germany). The stock staining solution was left to stand for 5 days, with occasional shaking. The solution was passed through Whatman No. 1 filters (Voigt Global distribution Inc., Kansas, USA) and stored at RT. Microscope slides from parasite infected cultures were fixed by submerging the slides in 100% MeOH (Merck, Darmstadt, Germany). Phosphate buffered saline (PBS) was prepared using 136 mM NaCl, 2.6 mM KCl, 10 mM Na<sub>2</sub>HPO<sub>4</sub> and 1.7 mM KH<sub>2</sub>PO<sub>4</sub>, with the pH adjusted to pH 7.0 using 0.1 N HCl. PBS was used to prepare a Giemsa-staining solution. Four volumes of PBS was mixed with 1 volume stock Giemsa stain, and this freshly prepared Giemsa solution was applied to the fixed slide for approximately 4 min. The slides were washed with H<sub>2</sub>O, dried, viewed by oil emersion microscopy using a Nikon Labophot microscope (Nikon, Tokyo, Japan) with 100x magnification. Parasitemia was assessed by counting at least 1000 cells, the percentage of infected RBC compared to the total cell count was a reflection of the parasitemia.

Parasite cultures were synchronized using a modification of the original method as described by Lambros *et al.* [147]. A 20 mL sample of parasitized culture was centrifuged at 2500 x g (Hermle, Labortechnik, Germany) for 5min, after which the supernatant was removed. Four milliliters of preheated (37°C) sterilized 15% D-sorbitol (Sigma-Aldrich, St. Louis, USA) was added and the cells were incubated at 37°C for 5min. An additional 8 mL sterilized 0.1% D-Glucose (Sigma-Aldrich, St. Louis, USA) was added, with 5 min incubation at 37°C and centrifugation 2500 x g for 5 min. Upon removal of the supernatant, 37°C preheated complete

culture media (CCM) was added and the hematocrit was adjusted to 5% using washed erythrocytes. The synchronized parasites were gassed as previously mentioned and incubated at 37°C.

#### **2.2.2.2. Co-inhibition of *P. falciparum* using polyamine enzyme inhibitors**

DFMO was kindly provided by Pat Woster (Wayne State University, MI, USA). MDL73811 was obtained from Sanofi-Aventis (Paris, France). For co-inhibition purposes 800 mM DFMO and 800  $\mu$ M MDL73811 stock solutions were prepared in phosphate buffered saline (PBS). Synchronized *P. falciparum* cultures, at approximately 3 – 4% parasitemia, were used for co-inhibition experimentation. Inhibitor treatment occurred 3h pre-invasion, and a 12 - 14% parasitemia was observed for the following invasion cycle. DFMO and MDL73811 were added to parasite cultures at 5 mM and 5  $\mu$ M final concentrations, respectively. The solutions were filter sterilized using 0.22  $\mu$ m cellulose-acetate filters (Sartorius, Gottingen Germany) and preheated to 37°C prior to parasite treatment. Co-inhibition was performed by replacing the parasite culture media with 160 mL CCM, containing DFMO and MDL73811. Media in the untreated control samples was replaced with only CCM. Both treated (T) and untreated (UT) cultures were gassed for at least 2 min using a mixture of 90 % N<sub>2</sub>, 5% O<sub>2</sub> and 5% CO<sub>2</sub> and incubated at 37°C. At approximately 12HPI parasite culture media was again replaced with CCM containing 5 mM DFMO and 5  $\mu$ M MDL73811 in T iRBC cultures, and only CCM for UT iRBC cultures.

#### **2.2.2.3. Polyamine and adenosyl-containing metabolite extraction**

Selected intervals corresponding to early- (19HPI), mid- (27 HPI) and late- (35HPI) trophozoite parasite stages were selected for polyamine extraction. Duplicate samples of 20 mL parasite culture were removed from culture flasks, pelleted by centrifugation at 2500 x g for 5 min (Hermle, Labortechnik, Germany) and re-suspended in at least four times pellet volume 1 x PBS. The centrifugation process was repeated, and the pellets were washed four times in total. One milliliter of the washed packed cell pellet was accurately transferred to 2 mL microcentrifuge tube.

For cell counting purpose; 10  $\mu$ L of the packed cells were diluted in 990  $\mu$ L cell counting buffer, which was composed of 4% w/v D-glucose and 10% w/v formaldehyde in saline buffer, consisting of 10 mM Tris, 150 mM NaCl, 10 mM sodium azide (NaN<sub>3</sub>), adjusted to pH 7.3. Alternatively, 10  $\mu$ L of packed cells was added to 990  $\mu$ L PBS and cells were counted within one day from this time. Cell counting was performed in an improved Neubauer Cell counting chamber (Weber, England) with 1/400 mm<sup>2</sup> chamber volume. Cells were counted by adding 10  $\mu$ L of diluted cells to each chamber, and counts were performed in duplicate in each chamber. The final cell count was converted, considering the dilution during cell counting, to allow the count to be expressed as 10<sup>10</sup> cells per mL packed cell pellet.

The 1 mL PBS-washed pellets were further subjected to protein precipitation or deproteinized using final 5% v/v PCA. One milliliter of 10% PCA was added to the 1 mL cell pellet, the

solution was vigorously vortexed, and incubated at 4°C, overnight. The following day the rust coloured PCA extracts were centrifuged at 16000 x g for 10 min at 4°C (Eppendorf, Hamburg, Germany), and the pellets were discarded. The supernatant solutions were filtered through 0.2 µm Minisart RC4, certified-HPLC filters (Sartorius, Goettingen, Germany), and if necessary, stored at -70°C.

#### 2.2.2.4. Polyamine derivatization and HPLC separation of benzoylated derivatives

Benzoylation was performed as previously reported by Taibi *et al.* and Verkoelen *et al.* with slight modification [144, 148]. Five hundred microliters of 5% PCA extract or 500 µL polyamine standard was added to a glass tube. A negative control, or blank, consisted of only 5% PCA solution. An internal standard (I.S.) of known amount was included in *P. falciparum* extracts in order to normalize for the efficiency of benzoylation. Five nanomol of 1,7-diaminoheptane (Sigma-Aldrich, St. Louis, USA) was added to each reaction tube. One and a half milliliters of 2.0 M NaOH (Fluka, Steinheim, Germany) was added to each tube. The reaction mixtures were briefly vortexed, after which 5 µL of benzoyl chloride (Sigma-Aldrich, St. Louis, USA) was added to the tubes. The tubes were incubated at 37°C for 30 min. One milliliter of chloroform (<99%) (Merck, Darmstadt, Germany) was added to stop the reaction and allow the separation of organic derivatized molecules. The tubes were centrifuged at 1500 x g (Medifuge, Sepatech, Germany) for 10 min to allow clear visual separation of the separate organic and aqueous phases. The aqueous phases were removed to a new glass tube containing additional 1.0 mL chloroform. After another centrifugation process, as above, the chloroform layers were pooled and evaporated under N<sub>2</sub> (g). One milliliter 0.1 M NaOH (Fluka, Steinheim, Germany) was added to the white precipitate containing tubes, and these were incubated overnight at RT.

The following day, 1.0 mL chloroform was added to the aqueous phases, and the tubes were centrifuged at 1500 x g for 10 min (Medifuge, Sepatech) after which the chloroform phases was removed and evaporated under N<sub>2</sub> (g). Five hundred microliters of 60% MeOH (Merck, Darmstadt, Germany) was used to redissolve benzoylated products. The methanol solutions were passed through 0.2 µm HPLC-certified filters, Minisart RC4 (Sartorius, Goettingen, Germany).

HPLC separation of benzoylated polyamines was performed using WATERS System (Waters Corporation, Massachusetts, USA). Separation of the polyamines occurred either on 125 mm x 4.0 mm or 250 mm x 4.0 mm Luna C18 (2) 5 µm reverse-phase (RP) columns (Phenomenex, Chesire, United-Kingdom). A Guard-Pak™ Precolumn steel housing (Waters Corporation, Massachusetts, USA) with µBondapak C18 HPLC pre-column inserts (Waters Corporation, Massachusetts, USA) was connected in-line. Isocratic solvent conditions were maintained using 60% MeOH (Merck, Darmstadt, Germany): dddH<sub>2</sub>O at flow rate of 1 mL/min. All solvents were filtered using 0.2 µm cellulose acetate filters (Sartorius, Goettingen, Germany) in Millipore™ housing system (Millipore, Massachusetts, USA) and degassed prior to use. The HPLC pump system consisted of a WATERS 600 Controller (Waters Corporation, Massachusetts, USA) with a 600 Series WATERS Pump (Waters Corporation, Massachusetts, USA) and a WATERS 712 WISP Autosampler. UV absorbance was measured at 229 nm using a WATERS 996 Photodiode

array (PDA) (Waters Corporation, Massachusetts, USA). Peak integration was performed using the Empower 2 Software Edition (2006, Waters Corporation, Massachusetts, USA) with Apex™ Trac functionality.

#### **2.2.2.5. HPLC separation of adenosyl-containing compounds**

HPLC mobile phase solvents were prepared as follows; “Buffer A” consisted of 8 mM octanesulfonic acid (Fluka, Steinheim, Germany) in 50 mM phosphate buffer at pH 3.0 (6.00 g/L NaH<sub>2</sub>PO<sub>4</sub> (Fluka, Steinheim, Germany)). The pH was adjusted using concentrated phosphoric acid, H<sub>3</sub>PO<sub>4</sub> (Fluka, Steinheim, Germany). “Buffer B” consisted of 100% methanol (Merck, Darmstadt, Germany) and “Buffer C” consisted of triple distilled water (dddH<sub>2</sub>O) and was used to wash the HPLC system. The buffers were filtered using 0.2 µm filters (Sartorius, Goettingen, Germany) and degassed prior to use. An average HPLC run was 45 min with initial gradient conditions at 80% Buffer A: 20% Buffer B for the first 8 min. The mobile phase condition was changed to 60% Buffer A: 40% Buffer B at time 8.5 min and maintained until 21 min. The original 80% Buffer A: 20% Buffer B equilibration was re-established at 21.5 min and maintained until the end of the run at 45 min.

Chromatographic separation of adenosyl containing compounds was achieved using a 250 mm x 4.0 mm Luna C18 (2) 5 µm RP column (Phenomenex, Chesire, United-Kingdom). A Guard-Pak™ precolumn steel housing with µBondapak C18 HPLC pre-column inserts was used in line, the same as mentioned in section 2.2.2.4. The same WATERS HPLC system used for the detection of benzoylated polyamines, as mentioned in section 2.2.2.4, was used for HPLC separation. UV absorbance was monitored at 254 nm.

### **2.3. Results and Discussion**

#### **2.3.1. Detection and quantification of polyamines and adenosyl-related metabolites.**

##### **2.3.1.1. Benzoylation polyamine derivatization**

The chemical detection and quantification of polyamines has seen the development of numerous chromatographic procedures. Separation techniques range from capillary electrophoresis (CE), HPLC, thin-layer chromatography (TLC), and gas chromatography (GC) [149]. The detection of polyamines, however, with only primary and secondary aliphatic amine groups which has little native exploitable spectral characteristics, has limited quantification during separation. Most routine analyses have relied on derivatization agents targeted to the amine groups of these molecules to allow detection. These methods are readily employed before (pre-column) or after (post-column) chromatographic separation. Some successful UV based-adsorption derivatization agents include benzoyl chloride [148, 150, 151], *p*-toluene sulphonyl chloride [152] and 2,4-dinitrofluorobenzene (FDNB) [153]. Fluorescent pre-column derivatization has been the favoured method for detection of polyamines. Compounds like 5-dimethylamino naphthalene-1-sulphonyl chloride (dansyl chloride) [154], *o*-phthalaldehyde (with 2-mercaptoethanol) and fluorescamine

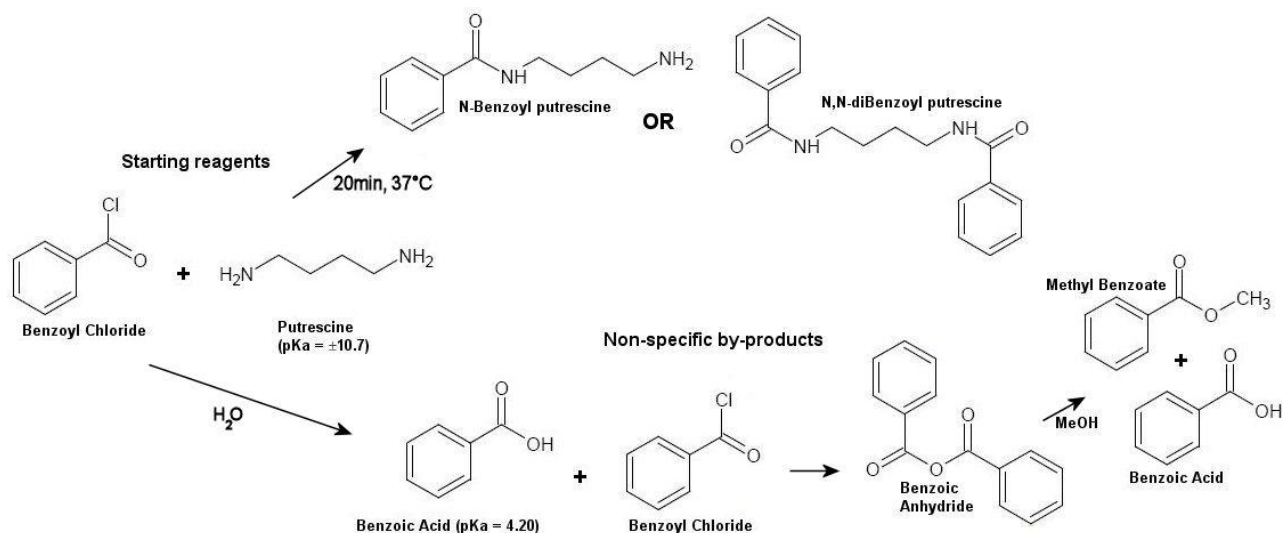


have successfully been used. The major advantage of fluorescent conjugation is higher sensitivity, with detection limits of these emitting molecules ranging in the low picomolar concentrations. In some cases, using fluorescein isothiocyanate (FITC), amine containing compounds could be detected in zepto molar ( $10^{-21}$ ) concentrations using CE separation [155].

Benzoyl chloride, and the process of benzoylation in alkaline conditions, has proved to be an effective UV absorbent derivatization technique for the detection of polyamines [148, 150, 151]. Benzoyl derivatives can be detected in the low picomolar concentrations, and the procedure has less intensive reaction by-product clean-up steps compared to dansylation [151, 153]. Advantages include relatively short derivatization times, and increased retention times which also allow better separation of benzoylated polyamines [156]. The process of polyamine benzoylation is illustrated in Fig 2.1. Here, an account is given on the benzoylation procedure followed to detect polyamine standards, and an optimized procedure is also proposed that eliminates some pitfalls associated with the derivatization technique. This section explains the methodology of benzoylation, and describes a suitable method which is later used during the quantification of polyamines from *P. falciparum*.

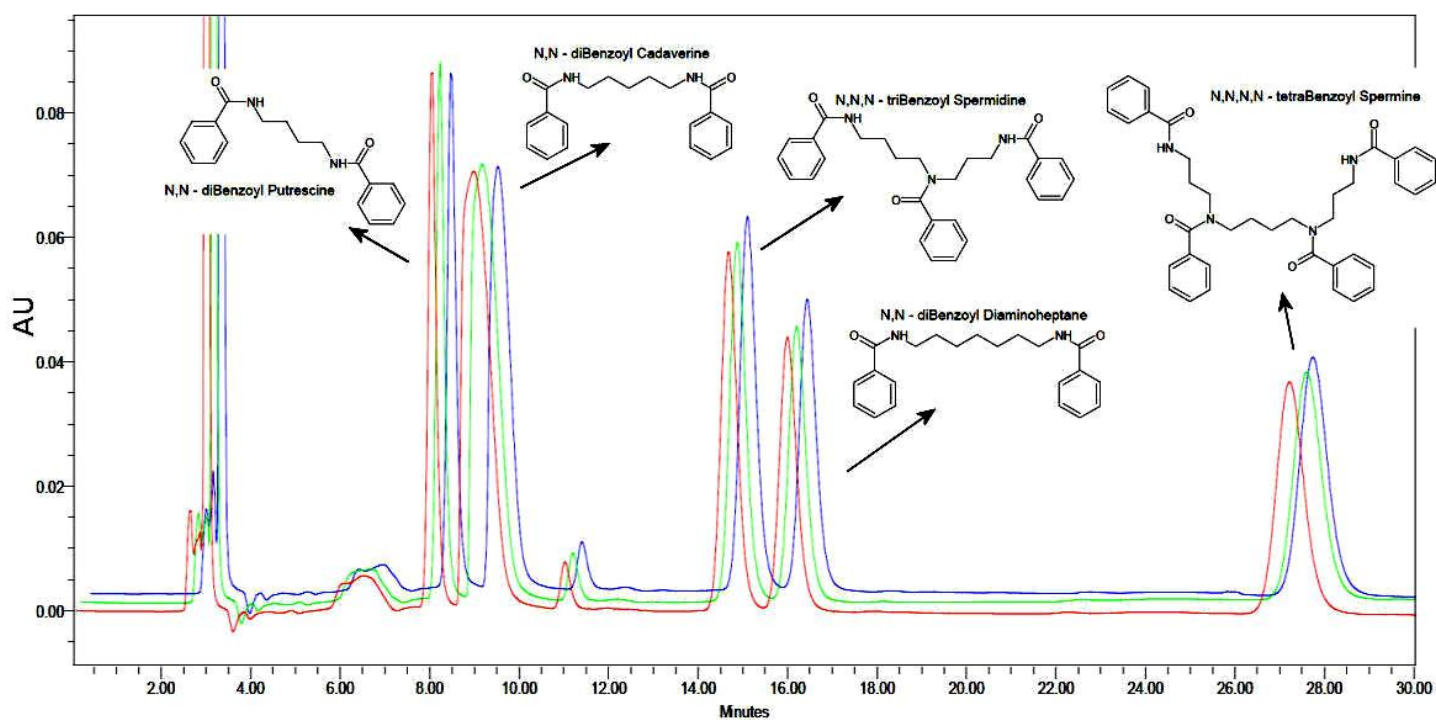
The benzoylation procedure, as mentioned, has fewer reaction by-products compared to dansylation, however, these can interfere in the accurate quantification of polyamine concentrations. Unreacted benzoyl chloride, as well as benzoic acid, formed during the hydroxylation of benzoyl chloride in the alkaline environment, is usually present in benzoylation reactions (Fig 2.1). Additionally, benzoic anhydride can also be formed when benzoic acid and benzoyl chloride molecules condense (Fig 2.1). The retention times of both benzoyl chloride and benzoic acid have been determined, and reflecting their polarity, these are eluted early during RP separation [148]. Fortunately, these compounds do not readily overlap with peak retention times of benzoylated polyamines and are therefore of little concern. However, the condensation product, benzoic anhydride, was shown to have similar retention times to benzoylated spermine [145]. Benzoic anhydride is therefore a major by-product of benzoylation. Several authors have reported optimized methods for the removal of various interfering by-products [144, 145, 148, 157]. Two procedures in particular, by Schenkel *et al.* [145] and Taibi *et al.* [144], have revealed conditions that favour the elimination of benzoic anhydride.

Schenkel *et al.* suggested that extensive washing of the final benzoylation reaction products overnight in 60% v/v methanol mobile phase resulted in effective removal of benzoic acid. The degradation of benzoic anhydride was shown to be time-dependent [145]. Taibi *et al.* revealed that washing of the reaction products in alkaline conditions, rather than in a methanol mixture, resulted in reduced levels of benzoic anhydride, also in lowered formation of methyl benzoate interfering products [144]. Both of these washing procedures were shown not to affect the stability of the benzoylated polyamines. A combined method of by-product elimination, incorporating both alkaline washing conditions, and an extended period of incubation in these conditions, was not attempted, and therefore studied here.



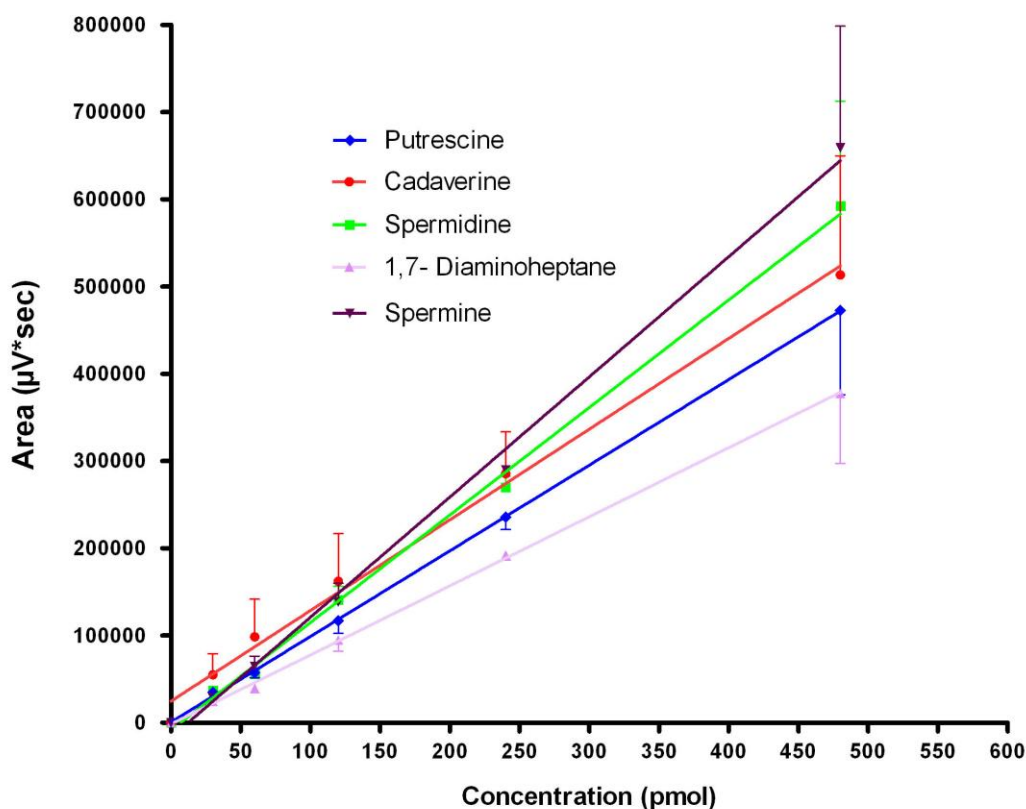
**Figure 2.1: Benzoylation of polyamines.** Benzoylation of putrescine is illustrated, and results in the conjugation of a UV absorbing benzoyl groups to terminal amine groups of the molecule. Benzoyl chloride can also undergo hydration upon interaction with H<sub>2</sub>O forming benzoic acid. Other benzoylation reaction by-products are formed when the benzoic acid reacts with excess benzoyl chloride. Methyl benzoate has also been shown to form in the presence of methanol [145].

In this study, polyamine standards were benzoylated according to a combined method, originally proposed by Schenkel *et al.* and Taibi *et al.* [144, 145]. Initially, four different benzoylation experiments were set-up, and combined various initial reaction conditions, with different post-reaction washing procedures. An optimized benzoylation procedure was established which showed less prominent methyl benzoate and benzoic anhydride peaks in chromatograms (results not shown). A typical chromatogram of benzoylated polyamine standards is shown in Fig 2.2. The final optimized procedure incorporated initial reaction conditions as proposed by Schenkel *et al.* [145], and utilised reaction clean-up washing steps according to Taibi *et al.* [144]. HPLC-RP separation of the benzoylated polyamines in 60% MeOH mobile phase conditions revealed well resolved peaks. The benzoylated cadaverine standard, which eluted at 9.0min, was often shown to co-elute with an unknown interfering substance (Fig 2.2). As discussed below, this affected cadaverine peak quantification, and often resulted in poor linear regression, making the estimation of cadaverine concentrations from extract samples inaccurate. The source of the contaminating peaks could not be identified.



**Figure 2.2: Separated benzoylated polyamines.** An overlay chromatogram of three consecutive 100  $\mu\text{L}$  injections, representing of 1 nmol of each putrescine, cadaverine, spermidine, 1,7-diaminoheptane and spermine. (This figure was modified with an imaging program, only the peak labels were removed for presentation purposes, detector response is given in absorbance units (AU) with values of  $\mu\text{V}\cdot\text{sec}$ ).

The LOD and LOQ<sub>t</sub> of the newly proposed benzoylation procedure was determined to establish the lower limits at which polyamines could be accurately detected and quantified. Two independent experiments were performed on separate occasions with a standard range of 30 - 480 pmol of each polyamine. The polyamines were benzoylated through the initial introduction of only benzoyl chloride, and the reaction products were washed overnight in alkaline conditions. Peak integration was performed using the Empower 2 Software package, and the established peak areas were plotted against the concentration of polyamine standard (Fig 2.3). Regression analysis of the peak areas ( $\mu\text{V}\cdot\text{sec}$ ) compared to fixed polyamine concentrations suggested a linear relationship, with the  $R^2$ -values, also called correlation coefficients, of the respective benzoylated polyamines all above 0.95 (Table 2.1). This suggested that a representative linear line could be generated that accounted for more than 95% of the standard deviation in benzoylated polyamine peak areas. Using these respective linear lines, generated for each individual polyamine standard, the concentration of a polyamine in an unknown sample could therefore be determined to a greater than 95% degree certainty. Cadaverine peaks areas were quantified, however, with the presence of contaminating peaks, linear lines constructed for increasing concentrations of benzoylated cadaverine often did not have  $R^2 > 0.95$  and suffered from positive y-axis intercept values in the absence of cadaverine standards (Fig 2.3).



**Figure 2.3: Benzoylated polyamine regression line.** Linear regression analysis of polyamine standard peak areas ( $\mu\text{V}\cdot\text{sec}$ ) plotted against the concentration for each respective polyamine. The graph represents data generated during the establishment of the LOD and LOQt of the benzoylation procedure. Error bars represent the standard deviation (SD) of two consecutive performed injections. The  $R^2$ -value of the individual lines was shown to be above 0.95 (Table 2.1).

The LOD and LOQt of benzoylation was determined from the polyamine standard linear lines, according to “EU Guidelines – Validation of analytical procedures” [158]. This entailed determining the residual standard deviations of the respective linear lines, and was performed using the GraphPad® Prism Software package. The residual standard deviation, or  $S_{y,x}$  value, represented the sum of the standard deviations in the observed y-value peak areas for each polyamine standard. The  $S_{y,x}$  parameter was calculated from the each respective polyamine linear line, and together with the slope, and are given in Table 2.1. The LOD and LOQt could be calculated using the slope and the  $S_{y,x}$  values in the formula as given in the method section, according to the EU Guidelines [158].

The average LOD was found to range from 43 pmol to 58 pmol, depending on the polyamine standard. The LOQt-values were found to range from 62 to 175 pmol (Table 2.1). These values were marginally higher compared to that reported in the literature. Hockl *et al.* suggested that the LOD for benzoylated polyamines were around 5 – 10 pmol [159]. Schenkel *et al.* calculated the LOD and LOQt as the amount of benzoylated polyamine that gave a peak height corresponding to three, and ten times the baseline, respectively. The author reports the LOD and LOQt of benzoylated polyamines to range from 2 – 12.5 pmol and 1.5 – 40 pmol, respectively [145]. The marginally higher LOD and LOQt calculated from this study could have been related to lowered UV detector sensitivity. The formula used to calculate the LOD and LOQt incorporates the

standard deviation of the peak areas generated for each respective benzoylated polyamines. Inclusion of this parameter scrutinizes the reproducibility of peak areas, compared to measuring the peak height values, which could be more prone to manipulation. The established LOQt parameter was used during polyamine determinations in unknown samples, and established the lower limit of accurate quantification.

**Table 2.1: LOD and LOQt for benzoylated polyamines.** Data generated from the linear regression analysis of two independent benzoylation reactions performed on separate days. Polyamine standards, ranging from 30 – 480 pmol, were benzoylated according to the optimized benzoylation procedure. The slope, LOD and LOQt values are given as average values, together with the standard deviation.

Experiment		Putrescine	Cadaverine	Spermidine	1,7- Diaminoheptane	Spermine
1	Slope $\pm$ SD	692.7 $\pm$ 16.99	684.9 $\pm$ 30.98	818.8 $\pm$ 44.70	492.6 $\pm$ 37.67	983.4 $\pm$ 26.96
	R <sup>2</sup>	0.9982	0.9939	0.9911	0.9828	0.9978
	S <sub>y,x</sub>	6622	12070	17420	14680	10510
	LOD (pmol)	32	58	70	98	35
	LOQt (pmol)	96	176	213	298	107
2	Slope $\pm$ SD	981.8 $\pm$ 6.773	1040 $\pm$ 41.78	1233 $\pm$ 31.04	792.1 $\pm$ 10.26	1378 $\pm$ 42.75
	R <sup>2</sup>	0.9998	0.9936	0.9975	0.9993	0.9962
	S <sub>y,x</sub>	2732	16850	12520	4139	17250
	LOD (pmol)	9	54	34	17	41
	LOQt (pmol)	28	162	102	52	125
<b>Average LOD (pmol)</b>		20 $\pm$ 16	56 $\pm$ 3	52 $\pm$ 26	58 $\pm$ 57	38 $\pm$ 4
<b>Average LOQt (pmol)</b>		62 $\pm$ 48	169 $\pm$ 10	157 $\pm$ 79	175 $\pm$ 174	116 $\pm$ 13

During the course of LOD and LOQt establishment, a considerable variation for the benzoylation procedure was observed, and this was reflected as large standard deviations in the average LOD and LOQt values listed in Table 2.1. This variation suggested that the polyamine peak areas differ in each experiment for a specific concentration of polyamine, and could have been related to the benzoylation efficiency. These experiments were also performed on separate occasions, and the differences of temperature and solvent preparation, which were controlled as far as possible, could have introduced some variation. However, an excellent linear correlation could be demonstrated for the polyamine linear lines in each experiment, observed as R<sup>2</sup> values above 0.95 (Table 2.1). This suggested that this experimental variation could be neglected if an external standard calibration curve is included within each unknown sample set analysis. Also, during benzoylation of polyamines in unknown samples, a known amount of I.S. is included to correct for the differences in benzoylation efficiency.

In conclusion, an optimized method of benzoylation, not dramatically different from Schenkel *et al.* [145] and Taibi *et al.* [144], was established. The procedure employed solely benzoyl chloride, with overnight washing in alkaline conditions. The procedure is proposed to result in less by-product formation and the LOD and LOQt were estimated for accurate polyamine detection and quantification. This method was applied for the determination of polyamine metabolites in *P. falciparum*. Previous accounts of polyamine measurements in the parasite performed by Das Gupta *et al.* [1] and Assaraf *et al.* [82] utilised dansylation derivatization techniques. Dansylation adds additional fluorescent character to the polyamines and allows more

sensitive detection of these strongly emitting molecules. Due to instrumental limitations in our laboratory an UV-based detection method of polyamine benzoylation was established. This method offers accurate detection of polyamines in low picomolar concentrations.

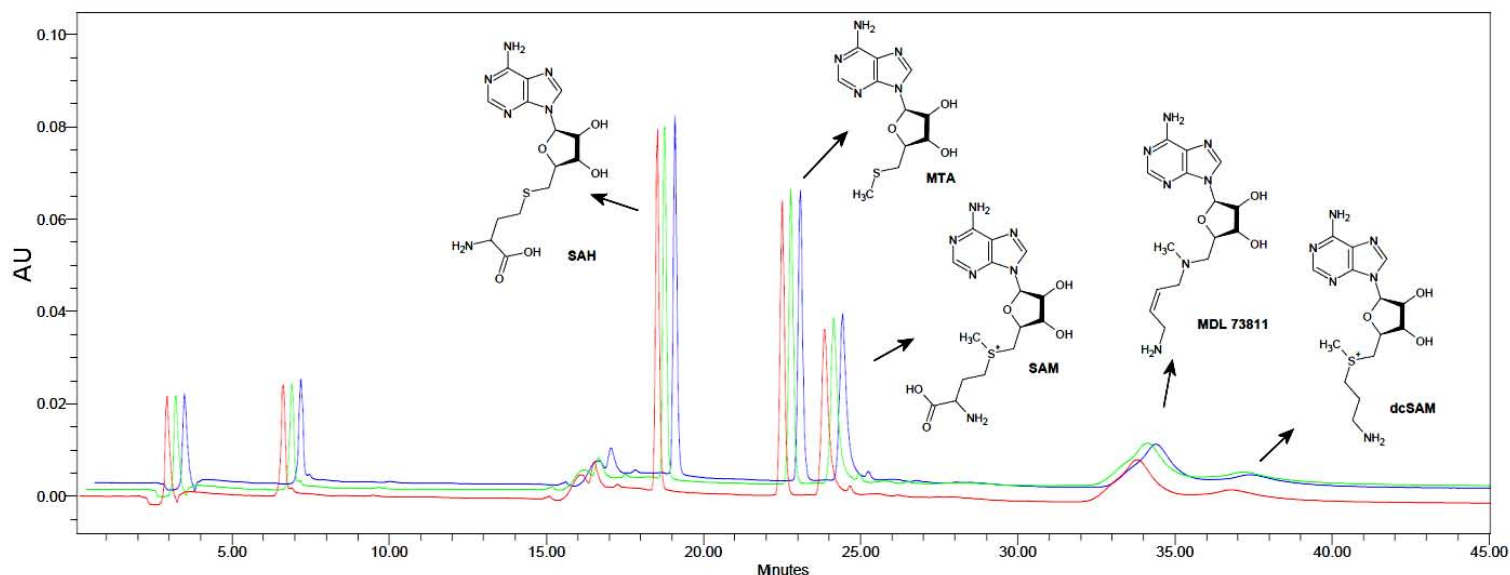
### 2.3.1.2. HPLC quantification of adenosyl-related compounds

Various adenosyl-containing metabolites like SAM, SAH, MTA, and dcSAM have been quantified in biological tissues using different chromatographic procedures. The importance of determining levels of these metabolites has been established; specifically decreased SAM concentrations in erythrocytes is a diagnostic marker for clinical depression [160]. Also, SAM levels are monitored in patients who are given additional dietary supplements of SAM to treat alcoholic liver damage and hepatotoxicity [161, 162]. Adenosyl metabolites have not previously been quantified in *P. falciparum*, and little is known of the fluctuating levels of these metabolites during the IDC. The effects of polyamine inhibitors on *P. falciparum* SAM levels are not known and this further emphasized the importance of establishing a quantitative method in our laboratory. Such a method was established which allowed the detection of these adenosyl-related metabolites in the parasites, and this section explains the optimization of a HPLC-UV based detection method for adenosyl-containing compounds.

HPLC-UV detection procedures have prominently been utilised to measure adenosyl-related metabolites and techniques range from ion-exchange to RP separating conditions [161, 163-165]. Fluorescent derivatization techniques have also been applied to detect adenosyl-related metabolites, and offer increased detection sensitivity compared to UV-adsorption analysis [166]. HPLC with MS-based detection procedures, with increased detection sensitivity and selectivity, have also recently become more popular [167, 168]. Due to limited resources a HPLC-UV detection procedure was established in our laboratory. A previously published RP separation technique by Wang *et al.* was adapted for the measurement of five different adenosyl-containing compounds [164]. The procedure involved the employment of an ion-pairing agent which adds additional ionic character to RP separation techniques. In this case octanesulfonic acid (OSA) was used as the ion pairing agent. The lipophilic portions of the molecule are able to interact with the hydrophobic stationary phase. The sulfonate groups of the compound, which have anionic character, promote electrostatic interaction with passing solutes in the mobile phase. Adenosyl-containing compounds were detected using UV monitoring at 254nm.

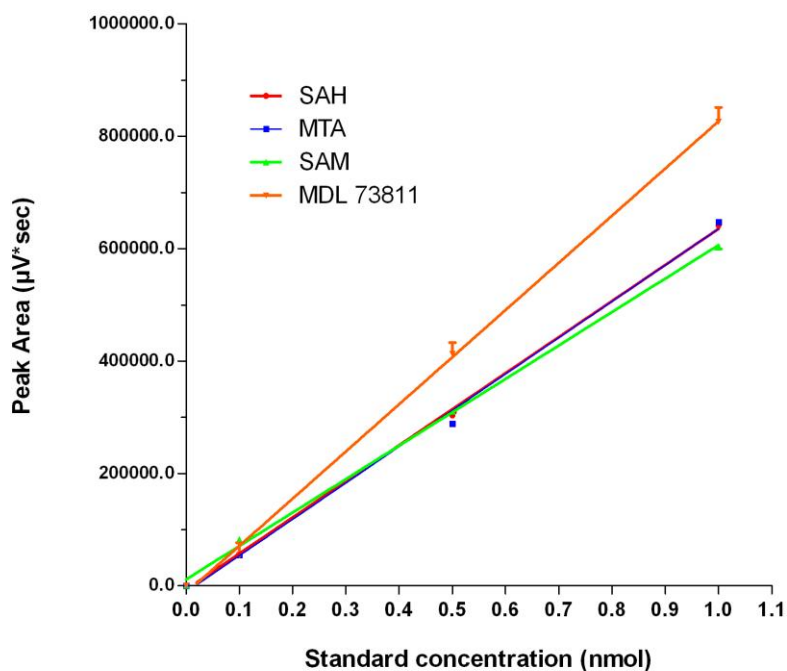
A chromatogram demonstrating the separation of SAM, SAH, MTA, dcSAM and MDL73811 is shown in Fig 2.4. The adenosyl-containing standards were shown to be well resolved in the 50mM phosphate buffered mobile phase. The elution profile of the adenosyl-containing compounds was shown to be related to both the ionic and hydrophobic character of the compounds. SAH eluted before SAM, suggesting that the additional methyl group of SAM delayed its elution, and could be due to additional hydrophobic interaction with the stationary phase. The elution profile also compared to previous accounts by Byers *et al.*, although marginal differences in the retention times could be related to the particular RP columns employed during HPLC [140]. dcSAM peaks were shown to vary in retention time, and accurate detection of these

was not always possible. During quantification of dcSAM, a linear line, generated by plotting peak areas against dcSAM standard concentrations, with  $R^2$  values of above 0.95 could not be generated. This suggested that accurate quantification of dcSAM was not possible. Reasons for this could be related to the sensitivity of the UV-detector. MDL78311 was included as control to determine whether MTA and MDL78311 potentially co-elute, and as discussed in more detail below. MDL78311 was effectively separated from MTA, and eluted close to peaks of dcSAM (Fig 2.4).



**Figure 2.4: Adenosyl-containing standards separated during ion-pairing RP-HPLC.** An overlay chromatogram, representing consecutive triplicate 10  $\mu$ M standard injections, corresponding to 1 nmol of each respective adenosyl-related compound. Reverse-phase ion pairing chromatography was performed according to Wang *et al.* [164].

The LOD and LOQ<sub>t</sub> were established to determine the accurate range in which these molecules can be detected using instrumentation in our laboratory. This was determined by generating a standard series of adenosyl-containing compounds. Standard solutions of these compounds were prepared in 5% PCA, and triplicate injections of increasing concentrations were performed during RP ion-pairing HPLC. Peak integration was performed using the Empower 2 Software package. The representative peak areas generated from the process were plotted against the concentration, and linear lines were fitted to the data (Fig 2.5). The linear lines of SAH, SAM, MTA and MDL78311 were shown to have excellent linearity, with  $R^2$  values above 0.95 (Table 2.2). This suggested that a linear relationship existed, which accounted for 95% of the standard deviation in the peak area observations. Linear lines generated for dcSAM had  $R^2$  values below 0.95 (data not shown), and accurate estimations on the concentration of this metabolite could therefore not be made.



**Figure 2.5: Linear regression of adenosyl-containing standards during ion-pairing RP-HPLC.** SAM, MTA, MDL73811 and SAH linear lines were generated by plotting the peak areas against the standard concentration. The linear regression lines represent data generated from a single experiment in which 1.0, 0.5 and 0.1 nmol standards were injected, in triplicate.

The LOD and LOQt were calculated (Table 2.2) using the formula listed in the method section. The  $S_{y,x}$  parameter was calculated from the linear lines generated from each adenosyl-containing standard. This value represents the sum of the standard deviations for the measured peak areas. Lower  $S_{y,x}$  values are therefore associated with better reproducible peak areas from consecutive injections. By incorporating this value in the LOD and LOQt formula, the error of peak area observation is accounted for, establishing the accuracy of determination. Compared to LOD and LOQt calculations, in which the peak heights are measured, the formula which uses the  $S_{y,x}$  parameter eliminates the possibility of selective manipulation in the peak area observations.

**Table 2.2: Summary of adenosyl-containing compound HPLC LOD and LOQt determinations from standard linear lines.** A standard series of adenosyl-containing compounds, of which triplicate injections at each concentration was used during the HPLC LOD and LOQt establishment.

Experiment		SAH	MTA	SAM	MDL 73811
1	Slope $\pm$ SD	500400 $\pm$ 7814	367700 $\pm$ 14650	571600 $\pm$ 2322	837300 $\pm$ 20660
	$S_{y,x}$	10540	19770	3132	27870
	$R^2$	0.9983	0.989	0.9999	0.9958
	LOD (nmol)	0.070	0.177	0.018	0.110
	LOQt (nmol)	0.211	0.538	0.055	0.333
2	Slope $\pm$ SD	640000 $\pm$ 6100	650000 $\pm$ 12000	590000 $\pm$ 7000	840000 $\pm$ 16000
	$S_{y,x}$	8300	16000	9600	22000
	$R^2$	1.0	1.0	1.0	1.0
	LOD (nmol)	0.043	0.081	0.054	0.086
	LOQt (nmol)	0.130	0.246	0.163	0.262
<b>Average LOD (nmol)</b>		0.056 $\pm$ 0.019	0.129 $\pm$ 0.068	0.036 $\pm$ 0.025	0.098 $\pm$ 0.017
<b>Average LOQt (nmol)</b>		0.170 $\pm$ 0.057	0.392 $\pm$ 0.206	0.109 $\pm$ 0.076	0.297 $\pm$ 0.05



The LOD and LOQt for the adenosyl-containing compounds, as listed in Table 2.2, were marginally higher compared to literature. Wang *et al.* [164] previously calculated the LOD by comparing the signal-to-noise (S/N) ratio of adenosyl-standard peaks to a blank sample, in a region of similar retention time compared to the standard. The LOD and LOQt was the concentration at which the adenosyl-containing standards gave at least 5- and 12.5-times S/N values, respectively. The LOD for SAM and SAH was established at 22 pmol and 20 pmol, and the LOQt values as 55 pmol and 50 pmol, respectively [164]. The higher LOD and LOQt values of the method applied here could have been related to lower UV-detector sensitivity. The method of calculation in this study considers the average deviation in multiple standard injections, compared to single injection analyses performed by Wang *et al.* [164]. The LOD and LOQt are reflective of the accuracy at which adenosyl-containing compounds can be detected and quantified in our laboratory. Although these values do not always compare well, they are indicative of the accuracy which can be achieved, and were applied during the determination of adenosyl-related compounds in *P. falciparum*. During detection and quantification of adenosyl-containing compounds from unknown samples with values below the threshold LOD and LOQt were therefore not considered.

In conclusion, a HPLC-UV based separation procedure was established, that allowed sensitive detection and quantification of three major adenosyl-containing metabolites. Fluorescent techniques are more sensitive; however, due to instrumental constraints, a UV-based detection procedure was only possible in our laboratory. The method was shown to achieve effective separation of five major adenosyl-containing compounds, four of which could be accurately quantified. The procedure was applied for the detection of adenosyl-containing metabolites extracted from *P. falciparum*.

### **2.3.2. Polyamine and adenosyl-related metabolites quantified from *P. falciparum***

#### **2.3.2.1. Polyamine levels during erythrocytic maturation of *P. falciparum***

Polyamine levels were monitored during trophozoite maturation using the optimized benzylation derivatization procedure followed by HPLC-UV detection. One milliliter packed iRBC, and RBC controls, were deproteinized using 5% PCA, and the resulting extracts were benzyolated according to a modified benzyolation procedure. The majority of studies that have measured polyamines in *P. falciparum* have clearly demonstrated the importance of these metabolites during the asexual intraerythrocytic life-cycle [82]. Assaraf *et al.* reported the concomitant increase of polyamines during the IDC of the parasites, with spermidine as the most prominent polyamine during each developmental stage [82]. Reports by Das Gupta *et al.* [1], using dansylation polyamine detection, confirmed increasing levels of polyamines during the IDC (Table 2.3). These levels were, however, marginally lower compared to Assaraf *et al.* [1, 82]. In each case polyamines were extracted using PCA and detected using dansylation derivatization. PCA has recently been shown to achieve the greatest extraction of polyamines in *P. falciparum*, and Teng *et al.* could also confirm that the polyamine represent major metabolites of the parasite [81]. Additional compartmental analysis has also revealed the majority of polyamines are

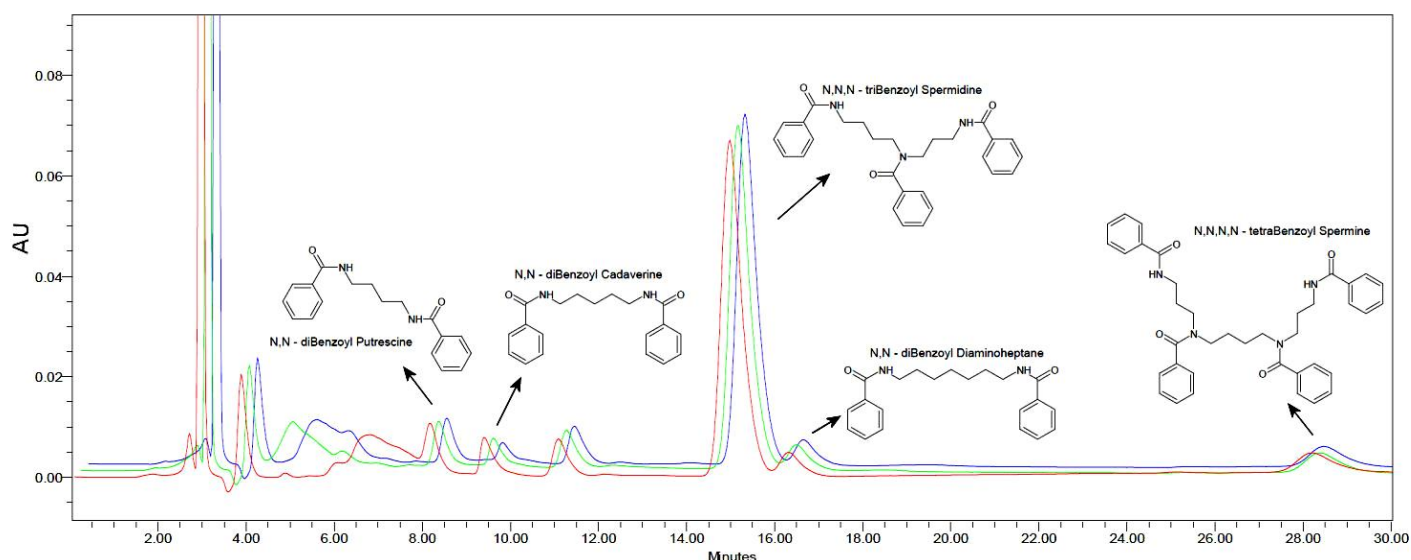
associated with the parasites compared to low levels observed within the erythrocytic compartments [1].

**Table 2.3: Polyamine levels in *P. falciparum* iRBC as determined by Das Gupta *et al.*** Parasites were enriched to 95% parasitemia using discontinuous Percoll-alanine gradient centrifugation, after which the polyamines were extracted with PCA. Polyamine were derivatized using dansylation followed by HPLC detection [1]. Values are given as nmol per  $10^{10}$  cells, from enriched iRBC fractions, together with the SD, as adapted from [1]. These values are also summarised in Fig 1.6 A.

	<b>Putrescine</b>	<b>Spermidine</b>	<b>Spermine</b>
Rings	35.9 ± 24.2	93.4 ± 62.9	5.1 ± 3.3
Trophozoites	454.5 ± 195.8	1079.0 ± 185.0	39.8 ± 17.2
Schizonts	624 ± 227.7	1295.4 ± 398.9	112.5 ± 53.2
Cocultured unRBC	23.1 ± 10.3	43.5 ± 19.6	11.9 ± 8

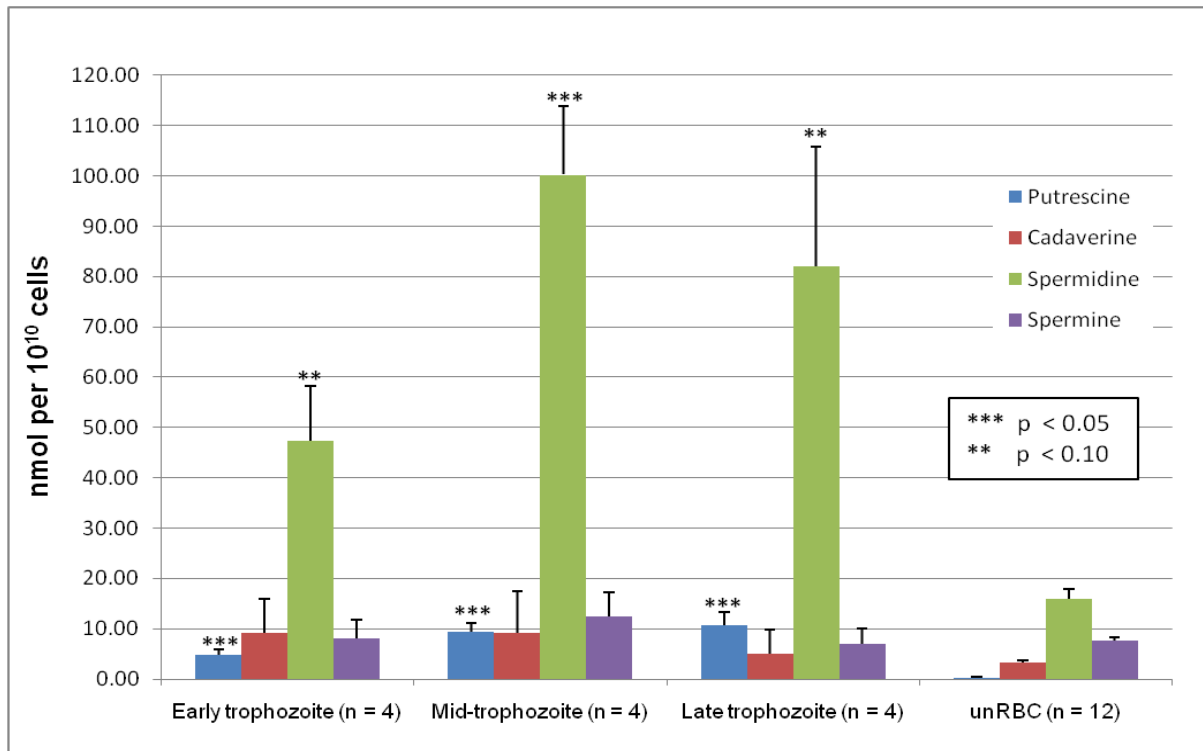
In this study, polyamine metabolites were quantified from *P. falciparum* whole cell extracts using benzoylation, subsequently followed by HPLC-UV detection. This study confirms increased polyamine levels in the IDC of the parasites, however, direct comparisons of the fold change in polyamine levels, to that of Assaraf *et al.* [82] and Das Gupta *et al.* [1] may be misleading. The aforementioned authors determined the polyamine concentrations in enriched parasite fractions, often at 95% parasitemia. Considering the difference in parasitemia, as polyamine measurements from this study were made at 12 – 15% parasitemia, the values are not directly comparable to Assaraf *et al.* [82] and Das Gupta *et al.* [1] (Table 2.3). The lowered levels of parasitemia therefore require that comparisons to consider the difference in parasitemia from the whole cell polyamine measurements. Experimentation also mainly focused on the development of trophozoite forms of the parasite, the phase demonstrated to most significantly require polyamine metabolites, and comparisons are therefore limited to this phase [82].

Polyamines were detected from *P. falciparum* iRBC whole cell lysates. One milliliter washed packed cells, from parasite cultures, was treated with a final 5% PCA and the supernatants obtained after protein precipitation were subjected to benzoylation. Five hundred microliters of the 5% PCA extract was used, and an I.S. of known amount was included before each polyamine benzoylation. A series of standard polyamines, of increasing concentration, was included and were used to generate external calibration lines. Peak areas generated from HPLC separated benzoylated polyamines from the parasite derived samples were correlated to external standard calibration lines, and the representing concentration of polyamine was determined. A chromatogram, in which benzoylated polyamines were detected from the mid-trophozoite parasites, is shown in Fig 2.6. Additional calculations considered the dilution of the samples, and also incorporated the cell count, which was obtained from the original 1 mL packed cell sample. Polyamine concentrations were calculated to obtain values expressed in nmol polyamine per  $10^{10}$  cells, referring to the amount of polyamine in the total cell count, which included both iRBCs at approximately 15% parasitemia and unRBCs (Fig 2.7).



**Figure 2.6: Chromatogram representing benzoylated polyamines extracted from mid-trophozoite parasites.** Benzoylation was performed on 500  $\mu\text{L}$  of PCA iRBC extract. Triplicate 100  $\mu\text{L}$  injections of the benzoylated polyamine mixture were performed. AU was determined at 229 nm and given in units of  $\mu\text{V}\cdot\text{sec}$ . The benzoylated polyamine concentrations were calculated using the peak areas, which were correlated to an external standard calibration curve included in the HPLC run.

Low levels of putrescine were observed in unRBC, agreeing with previous suggestions that unRBC contain trace levels of this metabolite (Fig 2.7) [1, 82, 169]. Putrescine levels were lower in the unRBC compared to Das Gupta *et al.* [1], who reported  $23.1 \pm 10.3$  nmol per  $10^{10}$  cells, with  $0.28 \pm 0.1$  nmol per  $10^{10}$  cells reported here. Similar PCA extraction procedures were performed compared to Das Gupta *et al.*, however, polyamine derivatization and cell-counting methods were markedly different from what was used in this study. This could suggest that benzoylation and detection of putrescine from PCA extracted parasite samples was not as efficient compared to dansylation procedures used by Das Gupta *et al.* [1] PCA extracts were spiked with a known amount of I.S, and the peak areas generated from these aided in correcting for inefficient polyamine benzoylation. Also, a series of external standards, prepared in 5% PCA, was always included in the same HPLC separation procedure. Linear lines fitted to peak area observations of from the standard benzoylated standards had  $R^2$  values above 0.95, accounted for more than 95% of the standard deviation in the observations. This suggested that benzoylation of putrescine standards was accurate, and the differences could have been introduced during polyamine extraction from the parasites. Moreover, cell-counting was also performed using a Neubauer cell counter, which could have contributed to inaccurate measurements, compared to automated methods used by Das Gupta *et al.* [1]. The lower measured values could therefore be attributed to differences in both polyamine detection and cell-counting procedures.



**Figure 2.7: Polyamine concentrations during the IDC of *P. falciparum*.** In each case spermidine was the major polyamine metabolite present, with middle stage trophozoites having the most. Co-cultured unRBC also appeared to have spermine present, with little detectable levels of putrescine. Error bars represent the standard error of the mean (SEM). Statistical significance is indicated by \*\*\* equivalent to 95% ( $p < 0.05$ ) and \*\* to 90% ( $p < 0.10$ ) determined through a heteroscedastic student t-test analysis comparing the infected RBC populations to unRBC, in each case.

Trophozoite maturation was shown to result in significantly increased levels of putrescine production (Fig 2.7). Taking the difference in parasite enrichment into account, the putrescine levels was approximately 75 nmol per 10<sup>10</sup> iRBC cells in mid-stage trophozoites (27HPI), lower compared to Das Gupta *et al.* (Table 2.3) [1]. Polyamine concentrations reported by Das Gupta *et al.* [1] had a considerable standard deviation, as shown in Table 2.3. The differences could be related to the specific polyamine derivatization procedure and cell-counting method used. Assaraf *et al.* also reported the putrescine concentration in enriched trophozoites at 112 nmol per 10<sup>10</sup> cells, and these lowered values are in closer relation compared to measurements from this study [80]. Late trophozoite parasites from this study were shown to have the highest concentrations of putrescine at  $10.66 \pm 2.6$  nmol per 10<sup>10</sup> iRBC, approximately 40-fold greater compared to unRBC. The trend measured in experimentation performed here suggests increasing putrescine production, and correlates with erythrocytic maturation, as previously established [1].

The cadaverine content in normal uninfected red blood cells (unRBC) was previously reported by van den Berg *et al.* with levels ranging from 0.44 – 0.56 nmol per 10<sup>10</sup> cells [170]. Measurements from polyamine benzoylation, observed in this study, are higher at 3.26 nmol per 10<sup>10</sup> unRBC cells (Fig 2.7). Cadaverine was previously included in polyamine determinations from the parasites by Assaraf *et al.*, the cellular levels were, however, not reported [85]. Cadaverine measurements were included in this study as this metabolite was previously reported to

compensate for putrescine depletion, and this is discussed in greater detail below. The cadaverine diamine was shown not to fluctuate during the IDC (Fig 2.7). As mentioned, during HPLC separation, unknown interfering peaks often co-eluted with benzoylated cadaverine. Accurate peak quantification in parasite polyamine extracts was therefore not always possible and is reflected by the large standard error in the observations (Fig 2.7). No statically significant differences could be observed from the iRBC compared to unRBC.

Comparing polyamine levels during the maturation from early to late trophozoite stages, the spermidine metabolite was shown to be the major polyamine. The metabolite increased 3-, 6-, and 5-fold in early, middle, and late trophozoite parasite forms, respectively, compared to unRBC (Fig 2.7). Experimental results here represent the average quantity of polyamine from four independent determinations, sampled during the 16 h trophozoite window period. The observed decreases at the late-trophozoite stage, which was not significantly different from the mid-trophozoites, suggested some permissible biological variation existed in the observations. Assaraf *et al.* previously reported the spermidine content in enriched, early trophozoites at 550nmol per  $10^{10}$  cells [80]. Measurements from this study, considering the enrichment difference, were observed at approximately 684 nmol per  $10^{10}$  cells spermidine in early trophozoites, and are comparable to reports by Assaraf *et al.* [80]. Moreover, Das Gupta *et al.* [1] previously measured spermidine levels in mid-trophozoites at  $1079 \pm 185$  nmol per  $10^{10}$  iRBC. Mid-trophozoites had approximately 793 nmol spermidine per  $10^{10}$  cells, which were marginally less compared to values reported by Das Gupta *et al.* (Table 2.3) [1, 82]. The cell-counting methods, in which case manual counting methods used here, together with the polyamine detection methods, could have introduced a degree of difference in the measurements.

No statistically significant differences in the levels of spermine were observed when unRBC and iRBC were compared. Previous accounts by Assaraf *et al.* suggested at least 10-fold change in the levels of this metabolite when early trophozoites are compared to unRBC [80]. This previous account compared polyamine levels in 80% enriched parasitized RBC to unRBC, making the difference more noticeable. Das Gupta *et al.* [1], however, reported less prominent difference in highly enriched infected cells. The authors suggested only 4-fold differences in the spermine level at mid-trophozoite stage, with levels ranging around  $39.8 \pm 17.2$  nmol per  $10^{10}$  cells. Results from this study are in closer agreement with previously established polyamine levels from Das Gupta *et al.* [1]. Spermine levels determined in mid stage trophozoites were found to be at most approximately 2-fold greater compared to unRBC, at  $12.39 \pm 4.81$  nmol per  $10^{10}$  cells (Fig 2.7). When parasite enrichment differences are considered, a value of approximately 95 nmol per  $10^{10}$  cells is expected at 95% parasitemia, marginally higher compared to Das Gupta *et al.* (Table 2.3) [1]. Moreover, spermine levels reported here are in closer agreement with Whaun *et al.* [132]. The authors also determined polyamine levels in non-enriched iRBC. The fact that spermine was found to be similar in iRBC and unRBC suggests that the process of enrichment is required to reveal the subtle difference in the spermine concentration.

Polyamines are some of the major metabolites observed during erythrocytic maturation of *P. falciparum* [81]. Parasite polyamine production is regulated by *PfA/O* and *PfSpdSyn*. mRNA

transcript of these have been shown to reach maximal levels during the mid- to late-trophozoite parasite stages (24-30HPI) [86, 87]. The polyamine metabolites are also demonstrated to peak in the schizont parasite stages (35 - 40HPI) [1, 82]. The importance of the polyamines have been emphasised through the use of specific inhibitors against both the bifunctional enzyme and *PfSpdSyn*, and results in parasite growth arrest. Spermidine appears to be the major metabolic output of the polyamine pathway, as this metabolite is always present in greater concentrations compared to putrescine and spermine. It is also evident that spermine production is less prominent compared to the other polyamines. A *PfSpmSyn* enzyme has not yet been discovered, however, it has been demonstrated that *PfSpdSyn* accounts for a small percentage of spermine formation [86].

### 2.3.2.2. Adenosyl-related metabolite fluctuations during the IDC of *P. falciparum*

Adenosyl-containing metabolites, like SAM, SAH, MTA, and dcSAM and the fluctuating levels of these have not previously been studied in *P. falciparum*. The maintenance of parasitic SAM levels is vital in two major pathways; during methylation and polyamine production. By-products from these essential cellular processes are recycled to maintain SAM homeostasis. Methylation reactions involved the C<sub>1</sub> transfer of the methyl moiety on the SAM molecule to nucleic acid, protein or lipid receptors [171]. After transfer of the methyl moiety, SAM is converted to SAH (Fig 1.7). The by-products produced from methylation are recycled to ensure cellular maintenance of SAM levels. Moreover, the SAH methylation by-product acts as a potent feedback inhibitor of methyltransferase reactions, and is therefore maintained at low cellular concentrations, rapidly converted into homocysteine (Hcy) and adenosine by S-adenosyl homocysteine hydrolase (SAHH) [171]. Homocysteine is recycled to form part of the methionine regeneration pathway, and adenosine is re-phosphorylated to ATP, both of which are utilised during the *de novo* synthesis of SAM [171, 172]. These regeneration pathways ensure cellular replenishment of SAM after methylation reactions. In this study the SAH levels, together with SAM, was measured during trophozoite erythrocytic maturation (Table 2.4).

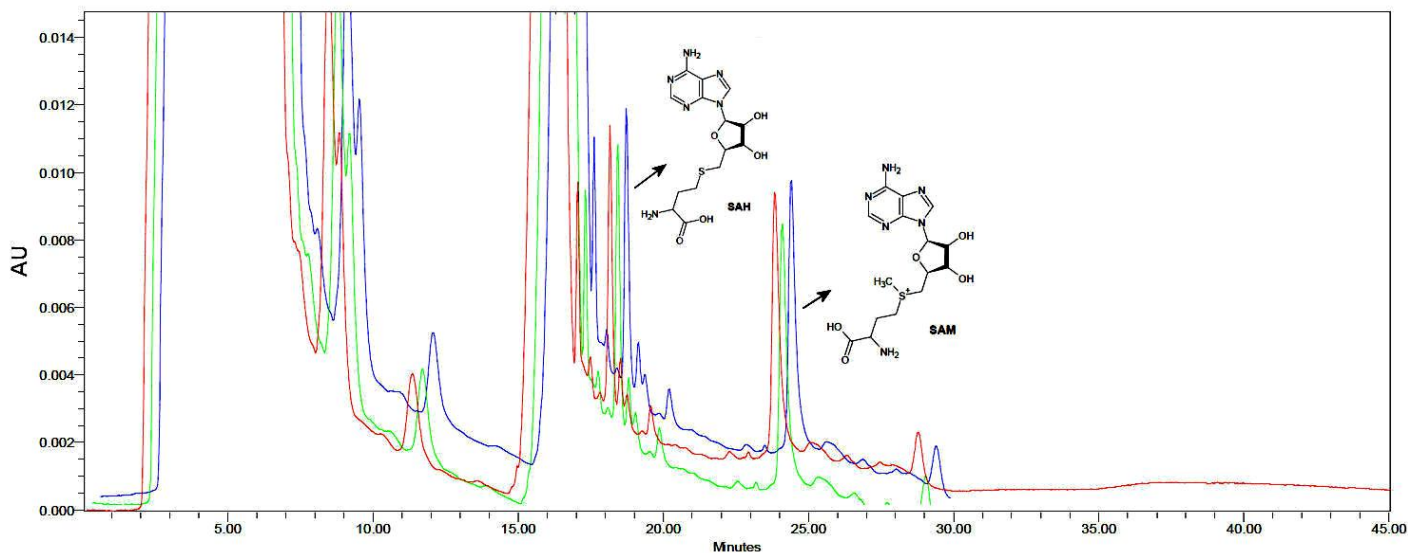
Polyamine biosynthesis is also directly dependent on the SAM cellular concentrations. After decarboxylation of SAM, the newly formed dcSAM serves as an essential aminopropyl donor during the formation of the polyamines, more specifically during production of spermidine and spermine. The equimolar requirement of dcSAM for each spermidine molecule in *P. falciparum* suggests that the cellular levels of dcSAM could be comparable to that of spermidine. The importance of spermidine has been illustrated in the parasites, and this polyamine also occurs in the greatest levels. It is therefore remarkable that dcSAM levels have not yet been measured in the parasites. Moreover, the adenosyl-containing by-product of polyamine aminopropylation, 5'-deoxy-5'-(methylthio)adenosine (MTA), must be produced in equimolar relation to dcSAM utilization. MTA is reportedly catabolised into adenine and L-methionine precursors, which re-enter the SAM biosynthetic pathway [114]. SAM homeostasis is crucial in the parasites, and the fluctuating levels in some of these adenosyl-containing metabolites were studied here.

Adenosyl-containing metabolites were extracted from *P. falciparum* trophozoites. Packed cell pellets, obtained after washing of iRBC, were deproteinated using 5% PCA and the adenosyl-containing compound content in these were determined according to the established HPLC-UV based detection method. A chromatogram representing adenosyl-related metabolites extracted from late trophozoites iRBC is shown in Fig 2.8. Various solvent extraction procedures have previously been employed for effective extraction of these metabolites from tissues, however, no particular technique has been reported to achieve the greatest extraction. In most cases, extraction of adenosyl-containing compounds has been accomplished under acidic conditions and trichloroacetic acid (TCA) and PCA are the most commonly employed extraction and protein precipitating reagents [140, 161, 173, 174]. Acidic conditions are readily employed to limit the degradation and racemization of SAM, which is the most sensitive metabolite readily degraded at high temperatures and in alkaline conditions [175]. In a recent publication by Teng *et al.*, it could be demonstrated that adenosine diphosphate (ADP) and adenosine triphosphate (ATP), which are both adenosyl-containing compounds, were most effectively extracted from *P. falciparum* parasites using 5% PCA [81]. Adenosine monophosphate (AMP) was also demonstrated to be equally well extracted using either 5% PCA or a cold water/methanol extraction mixture [81]. Adenosyl-containing compounds in this study were extracted using 5% PCA, and the extraction technique is thought to offer efficient extraction.

A large number of studies have focused on determining the normal erythrocytic levels of SAM and SAH, as these can be diagnostic markers for various clinical conditions, as mentioned. Wise *et al.* reported SAM to have an average range of 2.41 - 6.76 nmol.mL<sup>-1</sup> of packed RBC in TCA precipitated human blood samples [160]. Similar SAM levels were reported by Castagna *et al.* [173], Perna *et al.* [176, 177] and Oden *et al.* [178] at 2.95 ± 0.66, 2.56 ± 0.46, 3.5 ± 0.5 nmol.mL<sup>-1</sup> packed erythrocytes, respectively. Barber *et al.* [179] and Lagendijk *et al.* [161] reported SAM levels using PCA extraction techniques, although marginally higher at 4.9 and 5.2 ± 0.48 nmol.mL<sup>-1</sup> packed cells, respectively. Recently, Loehrer *et al.* could show that the recovery of SAM and SAH from PCA precipitated samples was 98 and 97% effective [174]. The authors report the measurement of SAM concentrations in fifty healthy patients, the values ranging between 2.70 – 5.34 nmol.mL<sup>-1</sup> packed RBC, with the average recovery of 3.73 nmol.mL<sup>-1</sup> SAM [174]. In each case, different precipitation techniques were employed, including sulfosalicylic acid, TCA and PCA. These studies have illustrated similar recovery of SAM, and therefore suggested these reagents achieve similar extraction efficiencies of SAM from normal human erythrocytes.

The mean recovery of SAM from three independent experiments in this study, with nine erythrocyte extracts (n = 9), revealed normal erythrocytic SAM concentrations to be 4.37 ± 0.73 nmol.mL<sup>-1</sup> packed RBC, as shown in Table 2.4. This is in accordance with previously published concentration ranges of SAM in human erythrocytes. The overnight incubation of the cells with 5% PCA, as performed in this study, therefore offers similar extraction of the polar metabolite and correlate with that reported by Loehrer *et al.* [174]. SAM is a major contributor to methylation reactions that occur in the unRBC. Methylation has been demonstrated on various erythrocyte membrane proteins, including the band 3 anion transport protein and glycophorin

[180]. The specific methylation of D-aspartyl carboxyl groups on cytoskeletal proteins is thought to be part of erythrocyte repair mechanisms that regulate erythrocyte membrane deformability [181]. The regulation of SAM levels in the erythrocytes is accomplished by erythrocytic SAM synthetase (SAMS), which is dramatically affected by product feedback inhibition, with a  $K_i$  of  $2.0 - 2.9 \text{ nmol.mL}^{-1}$  for SAM [178]. The erythrocytic levels of SAM, which are within this concentration range, could therefore be determined through tightly controlled biosynthesis.



**Figure 2.8:** A chromatogram representing adenosyl-containing metabolites identified from late trophozoite iRBC. Adenosyl-containing compounds were extracted from iRBC using 5% PCA, after which triplicate 100  $\mu\text{L}$  injections were performed during RP ion-pairing HPLC. AU is given in units of  $\mu\text{V}\cdot\text{sec}$  measured at 254 nm.

SAH levels are also reported in erythrocytic extracts, and the average established value in normal healthy individuals has been reported to fluctuate between  $0.44 - 1.3 \mu\text{M}$ . Perna *et al.* could show PCA precipitated erythrocyte extracts had  $0.77 \pm 0.05 \text{ nmol.mL}^{-1}$  SAH concentrations [176, 177]. Moreover, Loehrer *et al.* measured SAH concentrations in fifty healthy patients, the average range was shown to fluctuate between  $0.128 - 0.328 \text{ nmol.mL}^{-1}$ , with the mean SAH content at  $0.205 \text{ nmol.mL}^{-1}$  [174]. The observed erythrocytic levels of SAH in this study are marginally higher at  $1.28 \pm 0.20 \text{ nmol.mL}^{-1}$  of packed red blood cells ( $n = 9$ ). These differences could, however, be related to the single source of unRBC in this study. Oden *et al.* established that unRBC had SAH levels of  $1.3 \pm 0.5 \text{ nmol.mL}^{-1}$ , suggesting some degree of permissible biological variation [178].

As shown in Table 2.4, the SAM levels in early, middle and late trophozoite vary between  $2.85 - 2.9 \mu\text{M}$ , which is lower compared to the established baseline values of  $4.37 \mu\text{M}$  for unRBC. The large standard error of the observations however suggested no statistical significance difference in first two time point extract values. Late trophozoite parasites did have significantly less SAM compared to unRBC, however, the biological significance of this 1.5-fold difference could be questioned. In *P. falciparum* the metabolic origin of SAM is still rather speculative, and it is not known if the majority of this metabolite is salvaged from erythrocytic compartments or if this



metabolite is synthesized from methionine and ATP [171]. Evidence exists to support both theories.

**Table 2.4: Adenosyl metabolism in normal and iRBC.** SAM, SAH and other adenosyl containing metabolites were measured during the erythrocytic maturation of *P.falciparum* from three independently performed experiments. Triplicate 100  $\mu$ L injections were performed during RP-ion pairing HPLC. Peak areas from identifiable adenosyl-containing compounds were correlated to an external calibration curve, which was included during the same HPLC procedure. Values are given in nmol per mL packed RBC extract ( $\text{nmol}\cdot\text{mL}^{-1}$ ), with the SEM.

	SAH	SAM
Early Trophozoites (n = 3)	1.25 $\pm$ 0.69	2.9 $\pm$ 0.79
Middle Trophozoites (n = 3)	0.85 $\pm$ 0.61	2.85 $\pm$ 0.9
Late Trophozoites (n = 3)	0.6 $\pm$ 0.42	2.87 $\pm$ 0.15**
unRBC (n = 9)	1.28 $\pm$ 0.21	4.37 $\pm$ 0.73

A heteroscedastic Student t-test analysis was performed comparing the SAH and SAM levels in the respective parasite infected samples to the quantity of metabolite in the red blood cell populations. Statistical significance is indicated by \*\* to 90% ( $p < 0.10$ ).

Salvage of purines requires a specific transporter, *P. falciparum* nucleotide transporter (*PfNT1*) [182]. Downie *et al.* reports that *PfNT1* was able to transport both adenosine, inosine and also the pyrimidine nucleoside thymidine [183]. It was also recently shown that the parasites transport nucleobases, including the *in vitro* experimental prerequisite hypoxanthine, and adenine [184]. Bissati *et al.* recently confirmed the lack of adenosine, inosine and hypoxanthine transport in a *pfnt1* $\Delta$  knock-out and complemented strains, and suggested the parasites have the ability to transport the nucleobases; guanine, xanthine and adenine through *PfNT1* [185]. The relative non-selective properties of nucleoside and nucleobase import process in *P. falciparum* might lead one to speculate that SAM molecules could potentially be transported through the same mechanism. *de novo* synthesis of SAM has also been suggested. Molecular studies have revealed the presence of a *PfSAMS* gene copy in *P. falciparum* cDNA libraries, which has sequence conservation compared to other SAMS proteins [172]. Synthesis of SAM occurs through enzymatic ligation of ATP with methionine [172]. Transcript levels of *PfSAMS* have been shown to peak during mid-trophozoite parasitic phases [89]. This therefore suggests that *de novo* synthesis of SAM is possible in the parasites, however, it could also be possible that the parasites obtain SAM through a combination of *de novo* synthesis and extracellular salvage. The observation of lowered iRBC SAM compared to the unRBC could have suggested that SAM could be potentially utilised from the erythrocytic compartments, however, no definitive conclusions could be made.

The observations from three independently performed experiments suggests that the SAH levels measured from *P. falciparum* iRBC are not significantly different compared to unRBC, as shown in Table 2.4. A decreasing trend of SAH was also observed during the maturation of the parasites in the erythrocytes, with late trophozoites having the least SAH, however, this was not statistically significant. Methylation of the cytosine of CpG dinucleotides is a known gene silencing mechanism in humans and quintessential during regulation of gene expression [186]. The extent of CpG methylation on DNA from *P. falciparum*, and its role during epigenetic gene regulation, is not yet fully appreciated. The compositional A/T bias that exists in the genome of

the parasites, however, does question the role of methylation as a mainstay epigenetic regulatory mechanism [187]. SAH acts a potent feedback inhibitor during methylation reactions and due to irregular methylation caused by accumulation of SAH, is maintained at low cellular concentrations [188]. The parasites were demonstrated to contain *PfSAHH* enzymes involved in the catabolism of SAH [188, 189]. SAHH transcript expression in *P. falciparum* has also been shown to reach maximal levels during middle trophozoite development (PFE1050w, DeRisi Lab). The action of this enzyme is proposed to ensure that lethal SAH accumulation is circumvented through hydrolysis of SAH into adenosine and L-homocysteine [171, 189, 190]. Trophozoite maturation therefore appears not to reflect any dramatic changes in SAH levels, and could indicate efficient activity of SAHH enzymes. The unchanging level of SAH support the notion that this metabolite is effectively removed before appreciable parasitic accumulation occurs.

MTA and dcSAM could not be detected in either unRBC or iRBC PCA lysates. The HPLC-UV based method was established to have LOD for MTA at 50 pmol and 200 pmol for dcSAM. The major source of dcSAM and MTA originates from polyamine biosynthesis, and stoichiometric amounts of MTA are formed during synthesis of both spermidine and spermine [191, 192]. These adenosyl-containing metabolites were therefore expected in concentration ranges similar to polyamines, which were demonstrated to increase during trophozoite maturation. The fact that no dcSAM was detected could have been related to less sensitive UV-detection. Moreover, as already demonstrated, accurate quantification of dcSAM required linear calibration lines, which could not always be created. It is not known whether MTA is efficiently extracted from the parasites, as this compound is proposed to have hydrophobic character, and could therefore have preferential solubility in organic solvent like methanol rather than PCA [191].

In conclusion, various metabolic pathways are interrelated with SAM metabolism and effective recycling of adenosyl-related by-products in these pathways is an important part of parasite metabolism. More specifically this study focuses on the underlying effect of polyamine depletion on SAM and SAH metabolism, and is discussed in section 2.3.3.2.

### **2.3.3. Polyamine and Adenosyl-related metabolite fluctuations during *PfA/O* co-inhibition.**

#### **2.3.3.1. Co-inhibition of *P. falciparum* and reflecting polyamine levels.**

In this study, *P. falciparum* was co-inhibited using both MDL73811 and DFMO, which are established *PfA/O* inhibitors, respectively. Parasites cultured at approximately 12% parasitemia, were treated with 5 mM DFMO and 5  $\mu$ M MDL73811 before parasite erythrocyte invasion. Control cultures, which were not treated with the inhibitors (UT), were also included to allow direct stage-specific comparison. Five millimolar DFMO and 5  $\mu$ M MDL73811 effectively blocked parasite development and growth arrest was evident in early trophozoite parasites stages (19HPI) in the treated cultures. Previous studies, using similar concentrations in DFMO and MDL73811, could confirm complete enzymatic inhibition of both decarboxylases in the parasites [89]. The treated parasites (T) were observed to have morphological characteristics associated

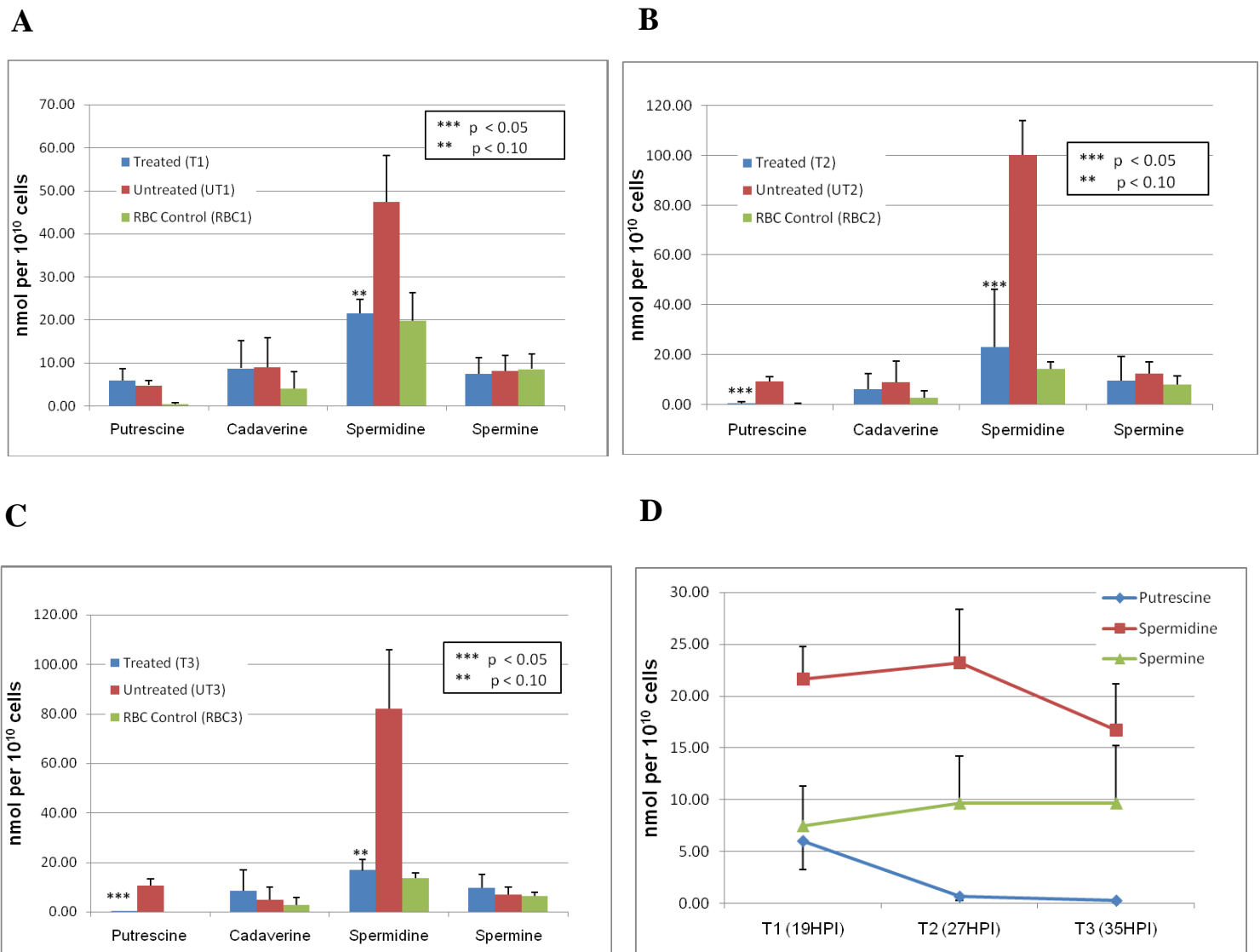
with early trophozoites, and no additional phenotypic changes were further observed during the IDC of T parasites (data not shown). The UT control parasites appeared to have normal erythrocyte maturation. Polyamine extracts were taken at 19HPI, 27HPI and 35HPI time-points and the polyamine levels were measured using benzylation and HPLC-UV detection. The extent of polyamine disruption was determined by comparing *PfA/O* co-inhibited extracts to normal UT parasites.

*PfA/O* co-inhibited *P. falciparum* extracts were observed to have decreased spermidine levels during the period equivalent to normal trophozoite maturation (Fig 2.9, A-C). The extent of spermidine depletion was evident at the early treated ( $T_1$ ) trophozoites stages, and was significantly less compared to untreated cells ( $UT_1$ ) (Fig 2.9A). This trend of significantly decreased spermidine in treated cultures was also observed for mid-trophozoite ( $T_2$ ) (Fig 2.9, B) and late-trophozoite ( $T_3$ ) (Fig 2.9, C) treated parasites. The levels of spermidine in T iRBC were comparable to that of unRBC (Fig 2.9, A-C). Late trophozoite T parasites appeared to have most significantly decreased spermidine levels at  $16.72 \pm 4.47$  nmol per  $10^{10}$  cells (Fig 2.9, D). Control parasite cultures, or untreated (UT) parasites, were observed with increasing spermidine production, which was already established for parasite erythrocyte maturation (Fig 2.9, A-C). Depletion of spermidine in co-inhibited parasite extracts was expected to be caused by the combined action of both DFMO and MDL73811. The lack of substrates; putrescine from *PfODC* and dcSAM from *PfAdoMetDC*, resulted in diminished action of *PfSpdSyn* and was reflected as significantly lowered spermidine formation in *PfA/O* co-inhibited parasites.

*PfA/O* co-inhibited parasites were observed to have significant depletion in putrescine, however, this only occurred during mid- and late-trophozoite parasite stages equivalent stages (Fig 2.9, A-D). As shown in Fig 2.9 D, a trend of decreasing putrescine production was observed with depletion most pronounced at the late-stage  $T_3$  trophozoite phases. The levels of putrescine were significantly decreased in  $T_3$  parasites, and these were approximately 40-fold lower compared to  $UT_3$  parasites (Fig 2.9, C). Depletion in putrescine could be directly related to the action of DFMO, and as previously shown, at 5 mM DFMO almost completely abolishes *PfODC* activity, and is reflected as a depletion in putrescine [85]. Control UT trophozoites were observed to have increasing concentrations of putrescine, corresponding to normal erythrocytic growth conditions (Fig 2.9, A-C).

Previous studies employing solely DFMO, however, have demonstrated that putrescine depletion should be evident at the early trophozoite parasite stages [80]. The observation of normal cellular levels of putrescine in the  $T_1$  parasites from this study was therefore peculiar. The unchanged levels were attributed to the presence of MDL73811. The *PfAdoMetDC* inhibitor was previously shown to deplete only spermidine levels, however, putrescine levels increased 3-fold in mid-trophozoites [1, 133]. This characteristic action of MDL73811, with dramatically increased putrescine formation, may counteract the intended action of DFMO in co-inhibited parasites, as employed in this study. Decreased availability of dcSAM during co-inhibition, caused through the action of MDL73811, therefore resulted in lower metabolic putrescine consumption, and was

also observed as dramatic decreased spermidine formation. This indicates that parasite putrescine levels are dependent on the rate of cellular utilisation of dcSAM at *Pf*SpdSyn.



**Figure 2.9: Polyamine concentrations measured in treated (T) and untreated (UT) trophozoites.**

Polyamines were benzoylated from DFMO/MDL73811 co-inhibited parasite populations together with untreated controls and unRBC. The figures represent the average polyamine concentrations, with error bars indicating the SEM, from four independent experiments in **A)** early trophozoite, **B)** mid-trophozoite, **C)** late trophozoite parasites. The trend of polyamine levels in the co-inhibited iRBC is summarized in **D)**. Statistical significance is indicated by \*\*\* equivalent to 95% ( $p < 0.05$ ) and \*\* to 90% ( $p < 0.10$ ) determined through a heteroscedastic student t-test analysis comparing the T parasite extracts to UT iRBC, in each case. unRBC controls were included for comparative purposes.

Cadaverine levels appeared unaffected by *Pf*A/O co-inhibition (Fig 2.9, A-C). Some difficulty was, however, experienced during peak quantification of cadaverine standards. The linear regression lines generated for benzoylated cadaverine standards often had  $R^2$  values below 0.95 (data not shown). Cadaverine could therefore only be accurately quantified in two experiments from the *P. falciparum* extracts, and this was reflected by the large standard errors of the observations (Fig 2.9, A-C). Assaraf *et al.* previously studied cadaverine levels in DFMO-inhibited parasites [85]. The authors could show that 0.4 mM of exogenously supplied cadaverine

reversed DFMO-induced cytostasis [85]. Altered parasite cadaverine production was therefore thought to alleviate and compensate for putrescine depletion caused by DFMO. A recent publication by van Brummelen *et al.* evaluated the transcriptomic, proteomic and metabolomic effect of *Pf*ODC and *Pf*AdoMetDC co-inhibition [89]. The authors revealed a compensatory response during *Pf*A/O co-inhibition was upregulation of lysine decarboxylase (*Pf*LDC) transcripts [89]. The *Pf*LDC transcripts were shown to be upregulated almost 3-fold, and altered cadaverine metabolite production was thought to alleviate putrescine depletion during *Pf*A/O co-inhibition, agreeing with previous suggestions by Assaraf *et al.* [85]. Increased cadaverine levels in *Pf*A/O inhibited parasites could, however, not be demonstrated here or elsewhere using LC-MS/MS based detection approach [89]. The procedure of cadaverine benzylation and HPLC-UV detection may not be accurate and sensitive enough to observe low level changes expected for the cadaverine metabolite.

Spermine concentrations were not significantly different between T and UT trophozoites (Fig 2.9, A-C). Moreover, *Pf*A/O co-inhibition appeared not to affect the cellular levels of spermine concentration during trophozoite maturation (Fig 2.9, D). Previously, DFMO treatment was shown to increase spermine levels [80]. Studies employing other *Pf*ODC inhibitors have also revealed that both putrescine and spermidine depletion occurs, however marginal increases in spermine have been reported [1, 80, 134]. These increases in spermine could potentially arise as a consequence of dcSAM accumulation, driving the formation of spermine at *Pf*SpdSyn. Spermine biosynthesis was previously postulated to occur as part of *Pf*SpdSyn residual activity, and no native spermine synthase has been identified in *P. falciparum* [86]. The expected increase in dcSAM during DFMO treatment could promote this additional spermine synthase activity of *Pf*SpdSyn.

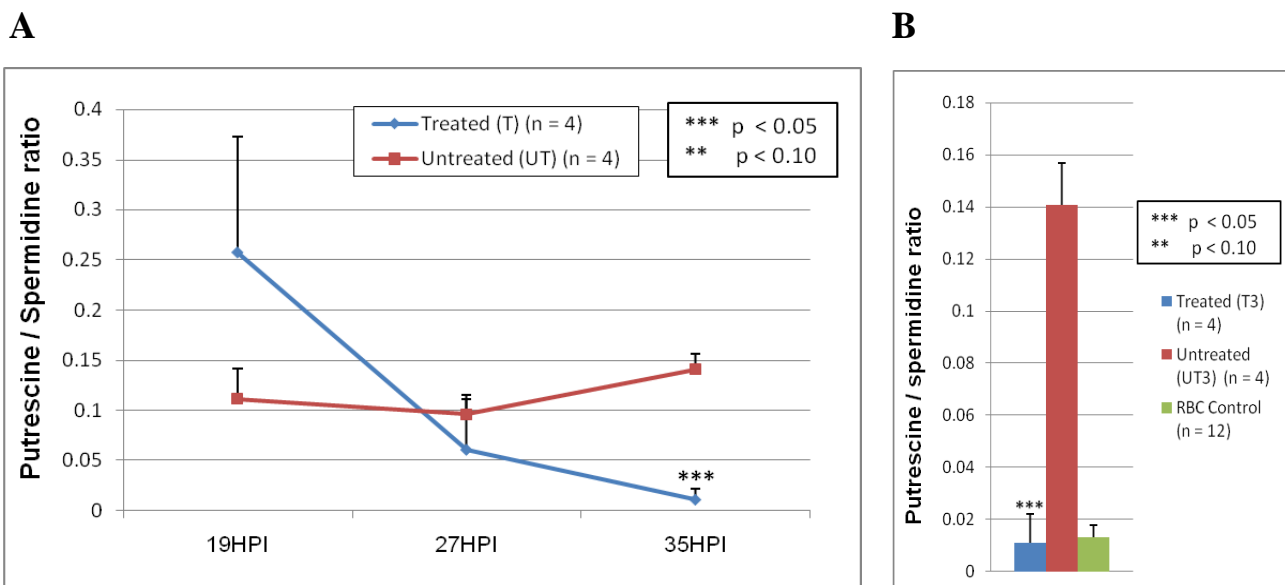
The unchanged levels of spermine in the co-inhibited cultures also showed that depletion of upstream substrates, putrescine and spermidine, are not rapidly communicated downstream. As already mentioned, parasite enrichment was previously employed to reveal the low level differences between erythrocytic and parasite derived spermine [1, 80]. The large volume sampling conditions and separate time-point analysis during the co-inhibition experiment made additional enrichment of the parasite extracts very difficult. Also, it was previously shown that spermine is noticeably more in the schizont phases [1]. Sampling, in experimentation performed here, was from whole cell infected trophozoites at 12% parasitemia and it is possible that any low level changes in the metabolite could not have been observed.

The fact that spermine remains unchanged during DFMO/MDL73811 co-inhibition is peculiar. It can be that the metabolite is only formed as a stress response, induced by a depletion of putrescine, and may partly simulate the function of putrescine. Previous studies have suggested that spermidine is formed within the parasite cytosolic compartments [86]. It can be possible that spermine molecules are differently processed and may be compartmentalized in parasite food vacuoles, as shown for other basic cellular components. Transport of polyamines into vacuolar compartments was demonstrated in yeast and compartmentalization was proposed to facilitate regulation of polyamine homeostasis within the cytosol [193]. Low parasitic utilization of

spermine, together with the disconnective relationship from the other polyamines, could suggest that this metabolite may be compartmentalized.

The ratio of putrescine production compared to that of spermidine formation appears to remain relatively unchanged in untreated parasites, with early trophozoites having  $0.11 \pm 0.03$ , middle trophozoites  $0.10 \pm 0.02$  and late trophozoites  $0.14 \pm 0.02$ , as observed from 4 independent experiments (Fig 2.10, A-B). The abundance of spermidine was stoichiometrically correlated to cellular levels of putrescine, and cellular excess of spermidine was always maintained. The non-equimolar distribution, favouring the formation of spermidine, was also observed in normal parasites elsewhere [1]. Regulation of this tightly controlled ratio is interesting, as this suggests that there could be a concomitant relationship between the activities of both *Pf*ODC and *Pf*SpdSyn, and these proteins may be regulated to ensure higher cellular levels of spermidine; however, the underlying mechanisms require further investigation.

The cellular distribution of polyamine production was disrupted during *PfA/O* co-inhibition. Treated parasites had a decreasing trend of putrescine-to-spermidine ratio (Fig 2.10, A). Early trophozoites were observed to have higher putrescine-to-spermidine ratios compared to UT parasites, reflecting that the cellular levels of putrescine were unchanged, and depletion in spermidine occurred more prominently (Fig 2.10, A). Mid-trophozoite  $T_2$  parasites were observed with putrescine-to-spermidine values comparable to normal UT parasites (Fig 2.10, A). This ratio was most significantly affected in late-stage trophozoites, with a value of  $0.01 \pm 0.01$ . This illustrated that *PfA/O* co-inhibition disrupted the polyamine distribution in trophozoites. Co-inhibition caused parasite cyto-stasis in early trophozoites, and the communicated effects on the polyamine distribution were extended throughout trophozoite maturation.



**Figure 2.10: The ratio of putrescine compared to spermidine production during uninhibited and DFMO / MDL73811 co-inhibition of *P. falciparum*.** The putrescine-to-spermidine ratio was measured in *P. falciparum* *PfA/O* co-inhibited, UT iRBC and unRBC. The putrescine-to-spermidine ratio was calculated and is shown; **A)** during trophozoite maturation, **B)** in late trophozoites. Statistical significance is indicated by \*\*\* equivalent to 95% ( $p < 0.05$ ) determined through a heteroscedastic student t-test analysis comparing the T iRBC ratios to UT iRBC ratios, in each case.

In conclusion, *PfA/O* co-inhibition of *P. falciparum* demonstrated that spermidine depletion occurred more rapidly than putrescine. Parasites may have more rapid spermidine metabolism compared to that of putrescine. The fact that spermidine was observed as the major polyamine metabolite in normal parasites, and in non-equimolar relationship to putrescine, suggests *PfSpdSyn* rapidly consumes putrescine for spermidine production. *PfSpdSyn* could therefore be the flux regulating enzyme in the parasite polyamine pathway. The combined cytostatic effect of DFMO and MDL73811 is therefore metabolic depletion of both putrescine and spermidine. The fact that cytostasis was correlated with depletion in spermidine, rather than putrescine, suggests that spermidine has a more important metabolic function within the parasites. Employment of solely DFMO or MDL73811 against the parasites, which also cause cytostasis, has been demonstrated to cause depletion in spermidine [1, 80, 133]. Moreover, *PfSpdSyn* inhibition results in parasite growth arrest at the early trophozoite parasite stages [86, 194]. The underlying polyamine fluctuations during *PfSpdSyn* inhibition have not yet been established, however, this is expected to result in the depletion of spermidine. Furthermore, exogenous supplied spermidine was also shown to alleviate the effect of DFMO induced cytostasis [85]. Wright *et al.* [133] could also show that spermidine was more effective in elevating MDL73811 induced cytostasis in *P. falciparum*, compared to putrescine. These results therefore suggest that spermidine depletion is directly correlated to polyamine inhibitor-induced growth arrest.

### **2.3.3.2. SAM homeostasis during co-inhibition of *P. falciparum* polyamine enzymes.**

This study focused on measurable metabolite changes during co-inhibition of *PfA/O*. The effects of these inhibitors, evident as growth arrest at early trophozoite stages, were studied in terms of adenosyl-related metabolism during an equivalent trophozoite maturation period. As already mentioned, the adenosyl-related compounds in the parasites originate from various pathways, and also overlap with SAM homeostasis. Effective recycling of the adenosyl-containing compounds replenishes substrates in these pathways, and is of vital importance in parasite metabolism. Previous studies have, however, not intently focused on *in vitro* fluctuation in adenosyl-related metabolites in *P. falciparum*. Moreover, levels of SAM, SAH, MTA, and dcSAM have not been established during inhibition of polyamine biosynthesis. The underlying effect on SAM metabolism is an important consideration during polyamine depletion, as the parasites were proposed to have compensatory response mechanisms, that intricately regulate homeostasis of this metabolite [89]. Various adenosyl-related metabolites were therefore extracted from *PfA/O* co-inhibited *P. falciparum*, and quantified using an established HPLC-UV based detection procedure.

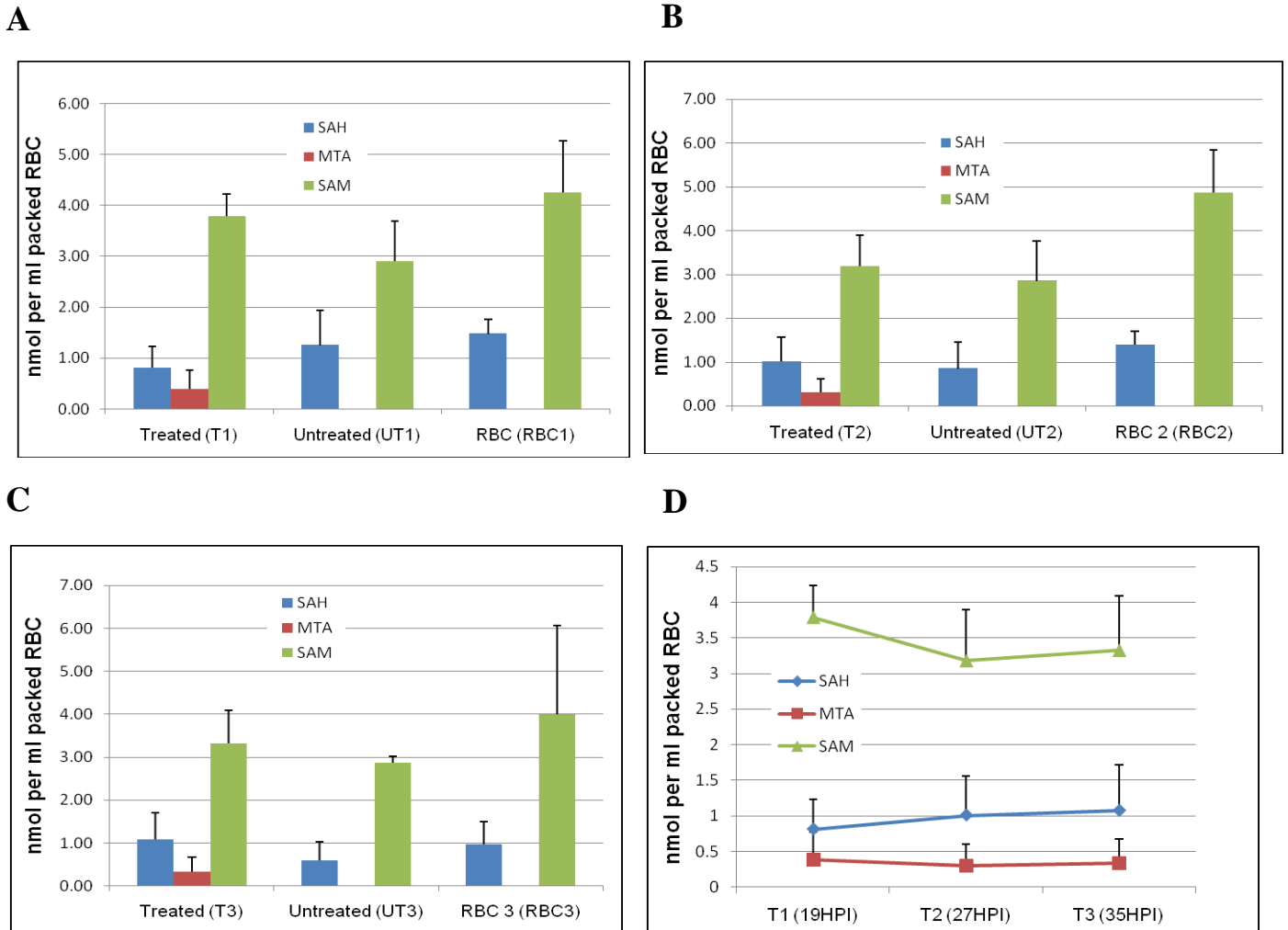
The importance of dcSAM, and flux of this adenosyl-compound through the polyamine pathway, has been demonstrated in *T. brucei*. Byers *et al.* illustrated that dramatic increases in SAM and dcSAM occur in *T. brucei brucei*, treated with either DFMO or MDL73811 [140]. *Trypanosoma brucei* was suspected of having unregulated SAM production and inhibition of polyamine flux resulted in dramatic accumulation of SAM. The authors concluded that both DFMO and MDL73811 had similar trypanocidal effects, causing increased SAM-to-SAH methylation ratios in the parasites, and this resulted in toxic hypermethylation status [140, 171].

The measurement of SAM levels, from three independent experiments in this study, revealed that T and UT iRBC had comparable SAM levels. The SAM concentration in early stage trophozoites, treated, parasites extracts was  $3.78 \pm 0.44 \text{ nmol.mL}^{-1}$  packed cells, compared to UT parasites having  $2.90 \pm 0.79 \text{ nmol.mL}^{-1}$  (Fig 2.11, A). These concentrations were not significantly different. SAM levels in mid- and late-trophozoites were also shown not to differ significantly between the T and UT iRBCs (Fig 2.11, B-C). Moreover, the trend in SAM levels was shown not to dramatically change during the course of trophozoite maturation (Fig 2.11, D). As revealed in early trophozoite polyamine extracts, the effect of co-inhibition was already evident as decreased spermidine production. It was therefore expected that decreased dcSAM consumption in the polyamine pathway could have had an accumulative effect on parasite SAM levels. Results from adenosyl-related metabolite extracts suggests that prolonged co-inhibition of *PfA/O* does not affect SAM homeostasis.

This could suggest that utilization of SAM during the production of dcSAM through the polyamine pathway is insignificant, and inhibition of polyamine flux does not dramatically alter SAM levels. The stoichiometric requirement of a dcSAM molecule for each spermidine and spermine formed, however, does suggest otherwise. Equivalent untreated early trophozoites had spermidine levels of  $189.26 \pm 63.73 \text{ nmol.mL}^{-1}$  iRBC, which was at least four times more than unRBC with  $39.71 \pm 8.86 \text{ nmol.mL}^{-1}$  (data not shown). If equimolar concentrations of dcSAM are utilised for this dramatic polyamine requirement, it suggests that *PfAdoMetDC* plays a significant part in SAM flux utilization. Van Brummelen *et al.* showed that DFMO / MDL73811 co-inhibited parasites exhibited decreased *PfSAMS* transcript and protein expression [89]. The compensatory response, also measured as decreased SAM metabolite levels, suggested that SAM homeostasis is maintained through decreased *de novo* production [89]. Data from this study therefore provides metabolomic evidence for SAM homeostasis during polyamine depletion.

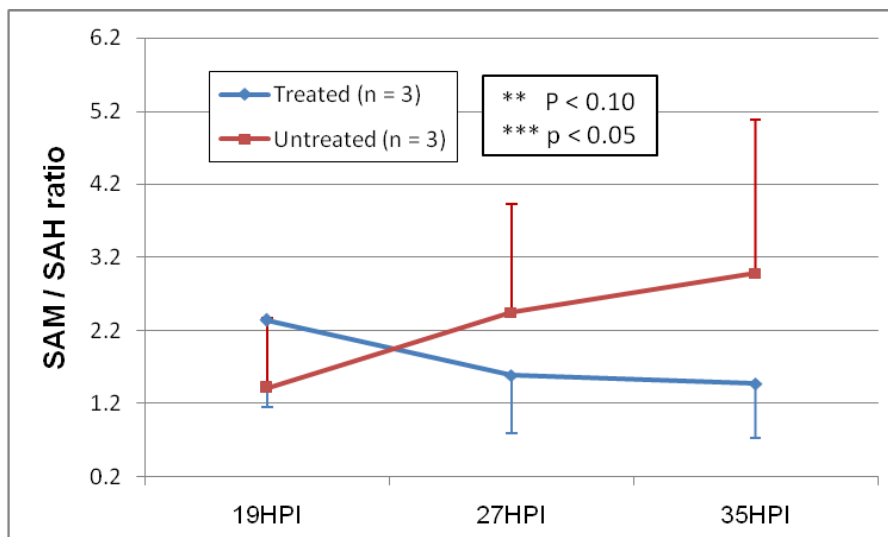
SAH levels were not significantly different between the co-inhibited early trophozoites compared to UT iRBC. T iRBC parasites had  $0.81 \pm 0.42 \text{ nmol.mL}^{-1}$  packed cells, compared to  $1.25 \pm 0.69 \text{ nmol.mL}^{-1}$  packed cells in UT iRBC (Fig 2.11, A). This observation was also made for the mid- and late-trophozoites, and these were shown not to have significantly different SAH levels (Fig 2.11, B and C). The *PfA/O* co-inhibited iRBC SAH levels were shown to remain relatively constant throughout the 16h window period of trophozoite maturation (Fig 2.11, D). The effects of polyamine depletion were suggested not to affect the metabolism of SAH. Parasitic concentrations of SAH are regulated through the actions of *PfSAHH*. Secondary effects caused by disruption of SAM levels could have been communicated in SAH levels, however, these were not observed either.





**Figure 2.11: Adenosyl metabolites extracted from *P. falciparum* T and UT trophozoites.** The levels of adenosyl metabolites were determined in treated, untreated trophozoites and RBC control populations. The figures represent the average adenosyl-related metabolites, together with the SEM, from three independent experiments extracted from **A**) early trophozoites, **B**) mid-trophozoites, and **C**) late-trophozoites. Figure **D**) summarizes the cellular levels of SAM, SAH and MTA in T parasites during trophozoite maturation. Statistical significance is indicated by \*\*\* equivalent to 95% ( $p < 0.05$ ) and \*\* to 90% ( $p < 0.10$ ) determined through a heteroscedastic student t-test analysis comparing the T iRBC populations to UT iRBC, in each case.

The polyamine inhibitors, DFMO and MDL73811, have previously been shown to disrupt the SAM/SAH ratio in *T. brucei* [138, 140]. The ratio of SAM/SAH, often referred to as the methylation potential in a biological organism, was caused by the accumulation of SAM in *T. brucei* [140]. Increased SAM results in aberrant methylation and was thought to promote the toxic effects of polyamine inhibitors [140]. Considering that no noticeable changes in the measurable SAM and SAH levels were observed in *P. falciparum* PfA/O co-inhibited parasites, the methylation potential was expected to be comparable amongst the extracts. Early T trophozoite parasites had a SAM/SAH ratio of  $2.34 \pm 1.19$ , and was not statistically significantly different compared to UT iRBC at  $1.41 \pm 0.94$  (Fig 2.12). Comparing the SAM/SAH ratio in the second and third time-point extracts also revealed that there was no statistical significant difference between T and UT iRBC (Fig 2.12). This suggested that prolonged exposure to DFMO and MDL73811 had little impact on the methylation potential during trophozoite growth arrest.



**Figure 2.12: The methylation potential of DFMO / MDL73811 co-inhibited *P. falciparum*.** The SAM / SAH ratio of *P. falciparum* PfA/O co-inhibited iRBC and UT iRBC were determined throughout trophozoite maturation. Statistical significance is indicated by \*\*\* equivalent to 95% ( $p < 0.05$ ) and \*\* to 90% ( $p < 0.10$ ) determined through a heteroscedastic student t-test analysis comparing the T iRBC populations to UT iRBC, in each case.

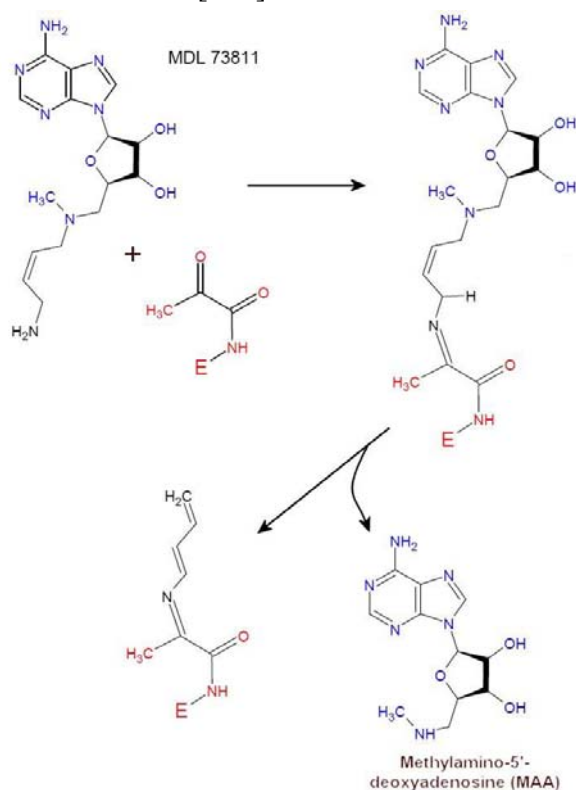
Polyamine levels in the equivalent early trophozoite phases, treated with DFMO and MDL73811, were shown to have decreased levels of spermidine. This was postulated to be related to the action of MDL73811, which effectively inhibited *PfAdoMetDC*, decreasing cellular dcSAM levels. Accurate HPLC quantification of dcSAM, however, could not be achieved, as demonstrated earlier, and determining the levels of the metabolite in *P. falciparum* was not possible. The presence of dcSAM could be confirmed using LC-MS detection methods (Appendix, Fig A.1.3), however, considering that this was only a qualitative analysis, little could be concluded on the fluctuations of this metabolite.

MTA, a stoichiometric by-product of *PfSpdSyn* enzymatic activity, was observed in treated parasite extracts for the first time point (Fig 2.11, A-C). The large standard error of the value reflects that these MTA peaks were only observed in one of three independently performed experiments. As shown in polyamine determinations for early trophozoites, spermidine was significantly depleted compared to untreated cells. Questions to the metabolic source of MTA arose, as this was not readily expected in the co-inhibited cultures. In the Appendix section further investigations to determine the metabolic source of MTA in treated extracts is given. In retrospect, it was later established that MTA peaks in these extracts were unknown contaminants, as second and third independent determinations did not reveal any significant levels of MTA in T iRBC.

Further investigations enquiring the metabolic source of MTA, formed during co-inhibition, prompted the inclusion of MDL73811 during HPLC separation. This aimed to establish that this non-physiological compound does not interfere or co-elute with MTA. If co-elution was possible, the measured MTA in the first experiments could therefore be accounted for. The retention time of MDL73811 at 33.87 min was found to clearly separate from MTA at 22.87 min, as already shown in Fig 2.4, and therefore eliminated the possible co-elution of these compounds. SAM

decomposition has also been shown to result in the formation of MTA, and these were thought to have been observed in the samples [175]. However, samples were processed exactly the same in each case, and MTA formation would have been observed in UT, as well as RBC controls, if any appreciable SAM degradation had occurred. The presence of MTA was therefore speculated to either to be of parasite origin or a by-product formed after MDL73811 inhibitory action.

Differences in *E. coli* and human AdoMetDC proteins have been observed relating to the mode of action of MDL73811 [122, 195, 196]. Irreversible inactivation in both enzymes was observed, however, in *E. coli* the process of MDL73811 inhibition is followed by  $\beta$ -elimination of 5'-(methylamino)-5'-deoxyadenosine (MAA), an MTA analogue, having an amino-group in the position of the sulphur atom (Fig 2.13) [122, 195]. This suggested that part of the butenyl chain remains bound to the pyruvoyl catalytic residue and a mechanism of irreversible inactivation was subsequently postulated by Casara *et al.* (Fig 2.13) [122]. In the human enzyme this process does not occur; Lysine-C protease digestion of human AdoMetDC-MDL73811 bound complexes followed by HPLC analysis confirmed that transamination and pyruvoyl-inactivation is favoured, and the MAA by-product could not be detected [195]. Shantz *et al.* concluded that human, and mammalian AdoMetDC proteins are inhibited through a different reaction mechanisms than that of bacterial origin, and that this observation holds some selective advantage when designing “species specific” AdoMetDC inhibitors [195].



**Figure 2.13: MDL73811 inhibitory action.** The proposed reaction mechanism for the inhibitory action of MDL73811 [122].

Casara *et al.* [122] reported the formation of MAA during the incubation of *E. coli* AdoMetDC with MDL73811. The by-product MAA, also known as MDL74281, resembles MTA structurally, except the sulphur atom has been replaced by an amine group [122]. It could be possible that

MAA was formed in the *PfA/O* co-inhibited parasites and may have overlapped with MTA peaks, as these were observed only in the treated parasite extracts. In the acidic pH conditions maintained during chromatographic separation of adenosyl compounds, both sulphur containing groups of MTA and MAA would be protonated and these compounds, with similar charge distribution, could therefore have similar retention times. The initial observation of trace MTA levels in only treated parasites was therefore thought to be MAA by-products, with similar retention time as MTA. As this compound was not commercially available, a qualitative MS based separation technique was established to confirm whether MDL73811 is potentially converted into the MAA by-product after enzymatic inhibition of *PfAdoMetDC*. This is discussed in the Appendix section. Later observations in *PfA/O* co-inhibited parasites did not show the MTA peaks, and this was therefore thought to be contaminant material of unknown origin.

## 2.4. Conclusions

Various studies have focused on the inhibition of the bifunctional protein, and the functional consequence on the transcriptome, proteome and the metabolome [1, 85, 89, 133, 134, 197]. Recently, van Brummelen *et al.* could demonstrate the compensatory responses towards polyamine depletion at mRNA, protein and metabolite level [89]. This therefore prompted further investigations into the underlying fluctuations of polyamine and adenosyl related metabolite levels during inhibition of the bifunctional enzyme.

In this report an account is given, on the fluctuations of polyamine and adenosyl metabolites during polyamine inhibition. The approach followed was a downscaled target-analysis form of metabolomic investigations, and future studies will undoubtedly try to encompass a wider scope of metabolites. In this dissertation it was demonstrated that *PfAdoMetDC*-ODC inhibition results in a condition of cytostasis, which was strongly correlated to the depletion of spermidine. Both putrescine and spermidine depletion, which was evident at a later stage, was not communicated in spermine concentrations. This could indicate slow metabolic turnover of the spermine metabolite. The co-inhibition of *PfODC* and *PfAdoMetDC* holds promise as potential therapeutic strategy. The cytostatic induced conditions, *in vitro*, may suggest polyamine depletion can be combined with other effective therapeutics, including artemisinins. The advantage of such an early trophozoite cytostatic drug is that reduced parasite cytoadherence may also occur.

The skewed non-equimolar production of spermidine compared to cellular levels of putrescine, together with the observation of coinciding conditions of cytostasis and spermidine depletion, suggests that *PfSpdSyn* is the focal point of polyamine production in the parasites. Spermidine has been shown to be involved in various essential reactions. Moreover, previous accounts of cytostasis, employing both *PfODC* and *PfAdoMetDC* inhibitors, were shown to correlate with depletion in spermidine [1]. It may be that this specific depletion in this specific metabolite results in conditions of cytostasis, rather than putrescine or spermine. Future experimentation will focus on the inhibition of *PfSpdSyn*, and the metabolic implications of inhibition.

The regulation of SAM, SAH, dcSAM and MTA levels within the parasite was also studied during co-inhibition of *PfA/O*. The SAM levels were shown to remain unchanged, thus corroborating with results by van Brummelen *et al.* [89]. SAM accumulation was previously shown in polyamine inhibited *T. brucei*, and Byers *et al.* [140] suggested that these parasites have unregulated SAM homeostasis. They also suggested that this could lead to toxic side effects which make polyamine inhibitors effective in the treatment of these parasitic infections. The absence of SAM accumulation in *P. falciparum* could suggest that the concentrations of SAM are more efficiently regulated. This metabolite is central and required for an array of essential processes, and intricate homeostasis could ensure decreased perturbations in response to polyamine flux alterations. SAM homeostasis could therefore have potential in the design of antimalarial therapeutics.

## Chapter 3: Evaluation of novel identified *PfSpdSyn* inhibitors *in vitro*

### 3.1. Introduction to *PfSpdSyn*

#### 3.1.1. The functional importance of spermidine biosynthesis

One of the most important enzymes in the polyamine pathway of the parasite is *P. falciparum* spermidine synthase (*PfSpdSyn*). As mentioned, the enzyme catalyzes a reaction which requires two substrates, and results in the addition of an aminopropyl moiety, derived from dcAdoMet, unto a putrescine molecule. Remarkably, the malarial enzyme has additional catalytic activity, allowing a second aminopropyl moiety to be added onto the spermidine molecule and this extended substrate accommodation may have evolved to compensate for the lack of spermine synthesis [86]. These features are considered as parasite-specific properties and are potential leverage points for selective inhibitor or lead design.

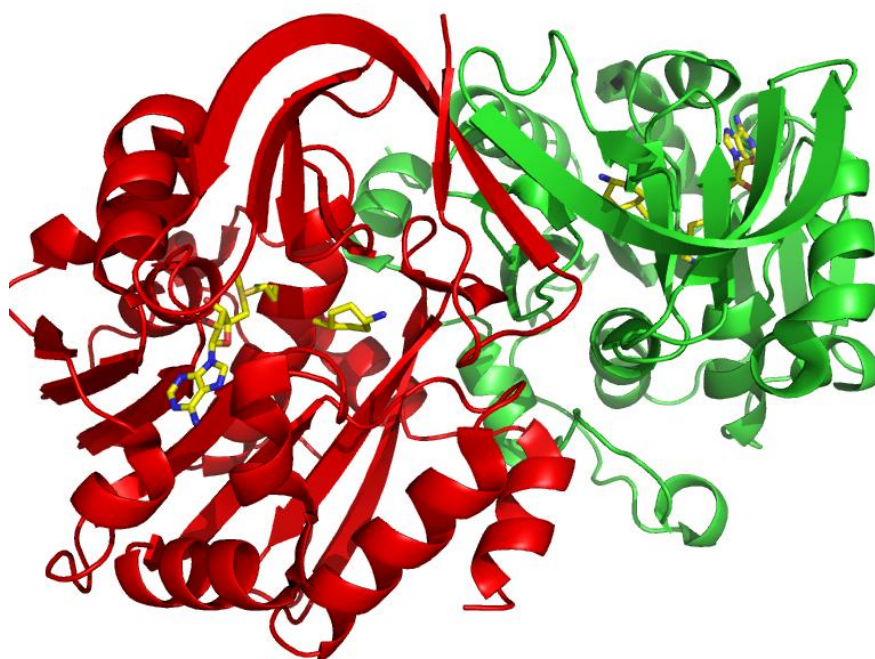
Spermidine seems to have greater metabolic importance compared to the other polyamines and is shown to be a prerequisite for activation of protein translational machinery in the parasites. The eukaryotic translation initiation factor (eIF5a) is a protein involved in RNA trafficking and ribosomal protein synthesis; however the exact role is still somewhat speculative [198, 199]. The activity of this essential protein is dependent on a post-translational modification in which spermidine is involved. The malarial equivalent eIF5a is proposed to be a 17.3 kDa protein product [198]. *PfeIF5a* is post-translationally modified on the  $\epsilon$ -amino group of a *PfK*<sub>50</sub> residue and the process involves the transfer of the aminobutyl chain of spermidine forming a deoxyhypusine moiety on the eIF5a protein [198]. This process is followed by the hydrolysis of the deoxyhypusine modified residue at the  $\gamma$ -carbon, thereby forming active eIF5a protein [199, 200].

It was suggested that the depletion of active eIF5A results in growth arrest in mammalian cells [199], and this is a peculiar trademark effect in polyamine depleted malaria parasites [85]. It can therefore be speculated that spermidine disruption results in more inactive forms of eIF5A, and this is directly reflected as cytostatics in treated parasite cultures [1, 86]. Moreover, especially in cases where ODC is inhibited; the exogenous addition of putrescine is often able to release the cells from cellular arrest. Additionally supplied putrescine could therefore be utilised by *PfSpdSyn* to replenish spermidine reserves and re-initiate *PfeIF5a* hypusine formation. The importance of spermidine is also further stressed by the observation of dramatically increased *PfDNA*-polymerase activity in the presence of spermidine [201].

#### 3.1.2. General characteristics

SpdSyn proteins share sequence similarity to SAM binding methyltransferases and the resulting proteins form a similar Rossmann-like fold protein [115]. SpdSyn have larger C-terminal regions with Rossmann fold character, resembling a division sign ( $\div$ ), where a central  $\beta$ -sheet region is flanked on either side by regions consisting of  $\alpha$ -helices [115]. Several crystal structures of SpdSyn from different organisms have recently become available; *Thermotoga maritima*

(*TmSpdSyn*) [202], *P. falciparum* (*PfSpdSyn*) [203, 204] and *Homo sapiens* (*HsSpdSyn*) [205] resulting in a detailed understanding of the mechanism of these proteins. *PfSpdSyn* proteins were shown to have a five-stranded  $\beta$ -sheet domain, with the larger C-terminal Rossmann fold consisting of seven  $\beta$ -sheets with a total of nine  $\alpha$ -helices arranged around the central  $\beta$ -sheet [203]. The *PfSpdSyn* illustrates the conservation of the Rossmann-fold SAM-binding motif (G<sub>124</sub>-X-G-X-G<sub>128</sub>) normally associated with SAM methyltransferases. A homology model generated by Burger *et al.* compared well with crystallized forms of *PfSpdSyn*, and from the modelled structure mechanistic properties of the enzyme were elucidated [206]. More importantly, pharmacophore features extracted from *PfSpdSyn* crystals structures, performed by Burger *et al.* aided in structure based drug design (SBDD), and successful low energy binding inhibitors were identified [207].

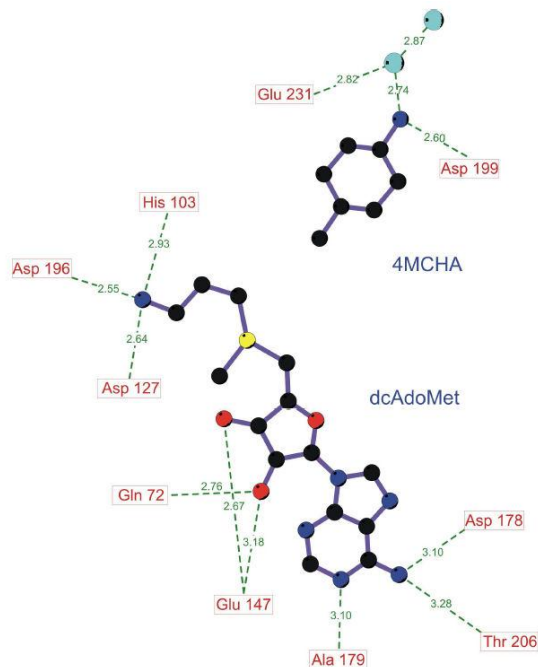


**Figure 3.1:** *PfSpdSyn* dimer in complex with dcSAM and *trans*-4-methylcyclohexylamine (4MCHA). *PfSpdSyn*, which contains a Rossmann-fold, forms a dimer. The two substrate binding sites of the enzyme are shown here, occupied by dcSAM, and the potent 4MCHA which are coloured in yellow (PDB 2PT9 [203]).

### 3.1.3. Active site properties

*PfSpdSyn* contains two binding sites, in which putrescine and dcSAM are aligned, to allow the catalytic transfer of aminopropyl groups onto putrescine to form spermidine. The dcSAM binding site of *PfSpdSyn* was shown to have features that ensure selective binding of dcSAM. A distinguishing *PfD*<sub>127</sub> residue located in-between the conserved G-residues of the SAM binding motif determines the selectivity of most SpdSyn enzymes, and confers specificity for dcSAM molecules, rather than allow competitive binding of SAM [113, 115]. Electrostatic repulsion from this residue towards carboxyl groups of SAM was thought to promote selective binding of only dcSAM in this site (Fig 3.2). The dcSAM binding pocket of *PfSpdSyn* contains *PfE*<sub>147</sub> and *PfQ*<sub>72</sub> residues which impart hydrogen stabilization onto the ribose hydroxyl components of dcSAM (Fig 3.2). These residues were shown to be well conserved in most SpdSyn proteins from other

organisms [203, 206]. Adenine ring primary amine groups of dcSAM were shown to be stabilized by *PfD*<sub>178</sub> and conformationally restricted *PfP*<sub>203</sub> residues in a crystal structure of *PfSpdSyn* [203]. As previously predicted, H<sub>2</sub>O solvent molecules were not involved in this stabilization [203, 204, 206]. Additionally cationic amine groups on the aminopropyl chain of dcSAM were also shown to be stabilized through interactions with, most notably *PfD*<sub>127</sub> and *PfD*<sub>196</sub>, which are required to align aminopropyl groups for nucleophilic attack [203, 206].



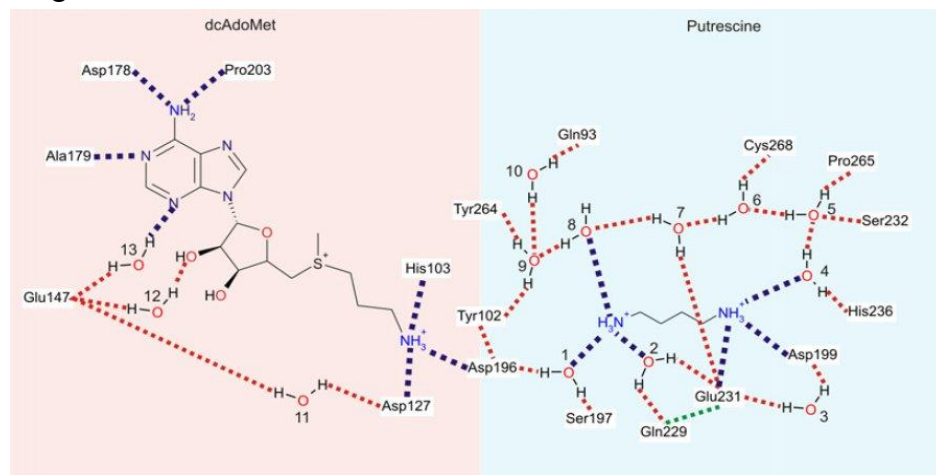
**Figure 3.2: Interactions of *PfSpdSyn* with dcSAM and 4MCHA.** dcSAM aminopropyl groups are stabilized through hydrogen bond interactions with aspartic acid residues, *PfD*<sub>196</sub> being 2.5Å from the amino groups of the aminopropyl chain. Also, 4MCHA is shown in the putrescine binding pockets, with amine groups stabilized by *PfE*<sub>231</sub> and *PfD*<sub>199</sub>. The figure was obtained from [207].

The putrescine binding cavity of *PfSpdSyn* localizes the bound putrescine in close proximity to the dcSAM aminopropyl chains. A reaction mechanism has been proposed by various authors, and it is suggested that nucleophilic attack takes place on the sulphur group of the dcSAM by deprotonated amine groups of putrescine (Fig 3.3) [202, 206]. The result is inversion of configuration on the sulphur atom, characteristic of a S<sub>N</sub>2 reaction, with in the transfer of the aminopropyl moiety to the amino group of putrescine. MTA is formed as the reaction by-product. The putrescine binding cavity is therefore suggested to maintain conditions that favour neutral state binding of the putrescine molecule, or at least of the attacking amino groups [206].

Evidence for neutral putrescine binding is found in both *TmSpdSyn* and *PfSpdSyn*, where the putrescine binding site was shown to contain a central hydrophobic region, with flanking negatively charged residues [202, 203]. Korolev *et al.* proposed that a conserved aspartic acid (*TmD*<sub>170</sub>, *PfD*<sub>196</sub>, *HsD*<sub>173</sub>) is involved in deprotonation of the putrescine attacking amino group [202]. A similar residue, *PfD*<sub>196</sub>, was predicted to be the most likely candidate in the *P. falciparum* homology model generated by Burger *et al.* [206]. This residue also plays a role in putrescine cavity binding inhibitors, as discussed below. Other interactions with the attacking amino group of putrescine molecule also involve invariant Y-residues (*TmY*<sub>239</sub>, *PfY*<sub>264</sub>, *HsY*<sub>241</sub>),



where the hydroxyl groups of the residue have hydrogen bonding capability with the terminal amine groups [203]. Aromatic stacked orientation of this residue is also observed in human and malarial SpdSyn, where the residue has parallel orientation to the central methylene chains of putrescine [203, 205]. The roles of these residues are not yet fully appreciated, and inhibitor binding has also implicated that favourable interactions with these are required for effective inhibitor binding.



**Figure 3.3:** The catalytic interacting residues of *PfSpdSyn* active sites. Predicted active site interactions with the dcSAM and putrescine, with prominent residues in the dcSAM binding being Glu<sub>147</sub>, Asp<sub>178</sub> and Pro<sub>203</sub> [206].

*PfSpdSyn* was also reported to have low spermine synthase activity (SpmSyn), in which an additional aminopropyl moiety could be catalyzed into the spermidine molecule [86]. It was concluded that the putrescine hydrophobic cavity had less sterical hindrance, compared to other SpdSyn, and was able to accommodate or maintain bound spermidine with the attacking amine group orientated in the correct fashion [86]. Other examples where this has been reported include the *T. brucei brucei* SpdSyn (*TbSpdSyn*), reported to be able to utilize spermidine and cadaverine as aminopropyl acceptors [208]. A remarkable feature of SpmSyn proteins is orientation of spermidine molecule in the active site. The putrescine aliphatic carbon chain, rather than the aminopropyl moiety, is orientated to receive additional aminopropyl moiety to form spermine. How this selectivity is achieved for SpmSyn enzymes is not yet known, however, the process is thought to involve electrostatic repulsion of C<sub>3</sub>-chain length amine groups. *PfSpdSyn*, with residual SpmSyn activity, may have definite selectivity for C<sub>4</sub> diamines in the putrescine binding pockets. This definite atomic length preference was demonstrated by Shirahata *et al.* during identification of novel inhibitors against pig SpdSyn, as discussed below [209]. These features are important considerations during identification and optimization of inhibitors directed to *PfSpdSyn*.

### 3.1.4. Direct enzyme inhibitors

Shirahata *et al.* synthesized a range of different SpdSyn and SpmSyn inhibitors which also led to some novel discoveries about the aminopropyltransferase active site [209]. The authors tested various cyclohexylamine (CHA) analogues for their inhibition efficacy against purified pig SpdSyn, as at the time it was known that these molecules can competitively bind to the putrescine

binding pockets of SpdSyn. These were proposed to be putrescine binding site inhibitors, and the authors reflected that CHA molecules shared characteristics to putrescine, including atomic length. Shirahata *et al.* also proposed that the conformational flexibility of CHA was important [209]. This was supported by the observation that aniline (1-aminobenzene) was far less efficient than the CHA counterpart. Conformational isomerism is possible in the non-aromatic CHA, whereas the benzene rings are planar molecules. This suggested that flexibility is an important consideration, and additional steric clash from the electron rich  $\pi$ -orbitals of the benzene rings may result in less favourable putrescine binding action in the pig SpdSyn.




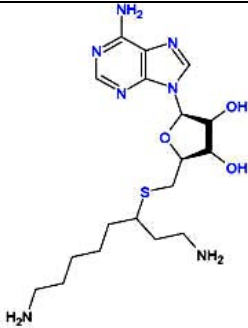
Shirahata *et al.* [209] demonstrated that a *trans-meta*-methylated form of cyclohexylamine (*trans*-1,4-methylcyclohexylamine, *trans*-4-MCHA, Table 3.1) was almost 5 times as potent as the parent compound. This suggested that favourable hydrophobic docking with the methyl group occurred within the active site. Obvious differences between the *cis*- and *trans*- isomers also suggested a stringent stereo-selective interaction with this alkyl component of the compound [209]. In a separate study using rat SpdSyn experiments a similar pattern was observed in which the *cis*-isomer of 4-MCHA was 400 times less effective in inhibiting the aminopropyl transferases than the *trans* counterpart [210].

*Pf*SpdSyn proteins have been demonstrated to have similar sensitivity to CHA and 4MCHA [86]. The additional methyl group of 4MCHA, compared to CHA, has been shown to provide additional interactions that favour low energy binding compared to non-methylated counterparts [203, 209]. 4MCHA was identified as a more potent inhibitor, with an  $IC_{50} = 1.4 \mu M$  and  $K_i$  at  $0.18 \mu M$  (Table 3.1) [86]. The crystal structure of *Pf*SpdSyn in complex with 4MCHA revealed that these molecules are in reverse expected orientation, and rather have amine groups orientated away from the attacking amino group positioning normally associated with putrescine binding [203]. Binding of the non-attacking amine portion of 4MCHA is also thought to involve an active site *PfD*<sub>199</sub>, and hydrophobic interactions are thought to be promoted through interactions with a *PfY*<sub>264</sub>. The methyl groups of 4MCHA, corresponding to the attacking amino groups of putrescine, are believed not to occupy the entire putrescine binding site [203]. Interactions with the catalytic components *PfD*<sub>196</sub> were not expected to occur, and additional hydrophobic stabilization from the *PfY*<sub>264</sub> appears to have significant stacking influence [203]. This therefore suggested that hydrophobic contacts in the putrescine binding site play a significant role, also especially reflected in the efficacy of uncomplexed, C<sub>4</sub> chain aliphatic inhibitors, like 5-amino-1-pentene (APE) and other alkylamines [86, 209].

Goda *et al.* reported the synthesis of APE, the compound was subsequently found to be as potent SpdSyn inhibitor as *trans*-4MCHA [210]. They suggested that the inter-atomic distance of between the proximal-amino and distal-carbon groups of APE and *trans*-4MCHA correlate at 0.59 nm, and suggested that this may be an important property for effective binding in the putrescine binding site of SpdSyn. Furthermore, the double bond in APE was shown to influence the inhibitor activity quite significantly, as the corresponding alkyne substituent resulted in 12-fold decreased inhibitory activity [210]. Considering that *trans*-4MCHA occupies the putrescine binding site with amine groups orientated away from the dcSAM molecule, a similar binding

action can potentially be ascribed to the APE compound. *Pf*SpdSyn is also strongly inhibited by APE, with a  $IC_{50}$  of 6.5  $\mu$ M (Table 3.1), close to that of 4-MCHA [86]. The  $K_i$  values of APE against *Pf*SpdSyn have not yet been determined.

**Table 3.1: Inhibitors of *Pf*SpdSyn.** These are shown with enzyme inhibitory activity ( $IC_{50}$ ) and *in vitro* determined growth inhibitory efficiency ( $IC_{50}$ ) as reported by [86] and [203].

Inhibitor name	Chemical structure	Enzyme $IC_{50}$ ( $\mu$ M)	$IC_{50}$ ( $\mu$ M) against cultured <i>P. falciparum</i> <i>in vitro</i>	Mechanism
Cyclohexylamine (CHA)		$19.7 \pm 3.1$	198	Reversibly binds in the putrescine binding cavity of <i>Pf</i> SpdSyn [86].
4-Methyl cyclohexylamine (4MCHA)		$1.4 \pm 0.1$	34.2	
5-Amino-1-pentene (APE)		$6.5 \pm 2.1$	83.3	
(AdoDATO)		$8.5 \pm 0.3$	8.5	Occupies the dcAdoMet binding site of <i>Pf</i> SpdSyn, reversible binding is expected [203].

Another interesting compound, a putrescine analogue, which potentially binds in the putrescine binding cavity, is 3-aminooxy-1-propanamine (APA, also called 1-aminooxy-3-aminopropane). Previous inhibitor studies against purified *Pf*SpdSyn showed that APA effectively inhibits the aminopropyltransferase with an enzyme  $IC_{50}$  of  $84 \pm 21$   $\mu$ M (no  $K_i$  available) [86]. It was also established that APA has an *in vitro* efficacy, however, this was attributed to *Pf*ODC inhibition, as discussed in Chapter 2 [1].

Other inhibitors of SpdSyn include those that bind in the adenosyl binding cavity of the enzyme. dcAdoMet analogues have been shown to have effective inhibitory action against SpdSyn. The synthesis of multi-substrate analogues, which resemble both the dcAdoMet and putrescine transition state, have remarkably good binding character. The compound S-adenosyl-1,8-diamino-3-thiooctane (AdoDATO), is such a multi-substrate analogue, and was reported to have potent inhibitory activity against *Pf*SpdSyn and an  $IC_{50}$  of 8.5  $\mu$ M [203]. Elucidation of *T.*

*maritima* SpdSyn in complex with AdoDATO by Korolev *et al.* has significantly improved our understanding of inhibitor binding [202]. The molecule is proposed to have ribose hydroxyl groups stabilized through interaction by *TmE*<sub>121</sub> and additional adenine ring amine group H-bonding with *TmQ*<sub>178</sub> (corresponding residue in alignment of *P. falciparum*, HsP<sub>203</sub>) and also *TmN*<sub>152</sub>[202]. The involvement of tyrosine residues (*TmY*<sub>76</sub> and *TmY*<sub>239</sub>) in aliphatic stabilization of the thiooctane chain of AdoDATO could also be observed. Recent crystallization of *Pf*SpdSyn with AdoDATO has revealed that the inhibitor interactions are quite similar. Two tyrosine residues (*PfY*<sub>264</sub> and *PfY*<sub>102</sub>), equivalent to those found in *Tm*SpdSyn, were also shown to be involved in close proximity to hydrophobic portions of AdoDATO [203].

### 3.1.5. Implications of inhibition

*Pf*SpdSyn inhibition and the resulting effects on parasite polyamine levels have not intensively been studied compared to *Pf*ODC and *Pf*AdoMetDC inhibition. Some researchers have observed that *in vitro* administration of 4MCHA and other *Pf*SpdSyn inhibitors results in decreased spermidine levels, however, the effect on the other polyamines in the pathway have not been established [86, 211]. The extent of spermine formation in the parasites during *Pf*SpdSyn inhibition is also not known. Considering that residual spermine formation has been attributed to the enzymatic action by *Pf*SpdSyn, little of this metabolite is expected to form during inhibition of *Pf*SpdSyn [86]. Becker *et al.* recently demonstrated that the effect of 2 mM CHA on the parasites results in compensatory decreases in *Pf*SAMS transcripts, and increases in *Pf*LDC gene expression [194]. *Pf*SpdSyn transcript levels were, however, shown not to be affected by CHA, questioning the degree of transcriptional gene regulation of this protein [194].

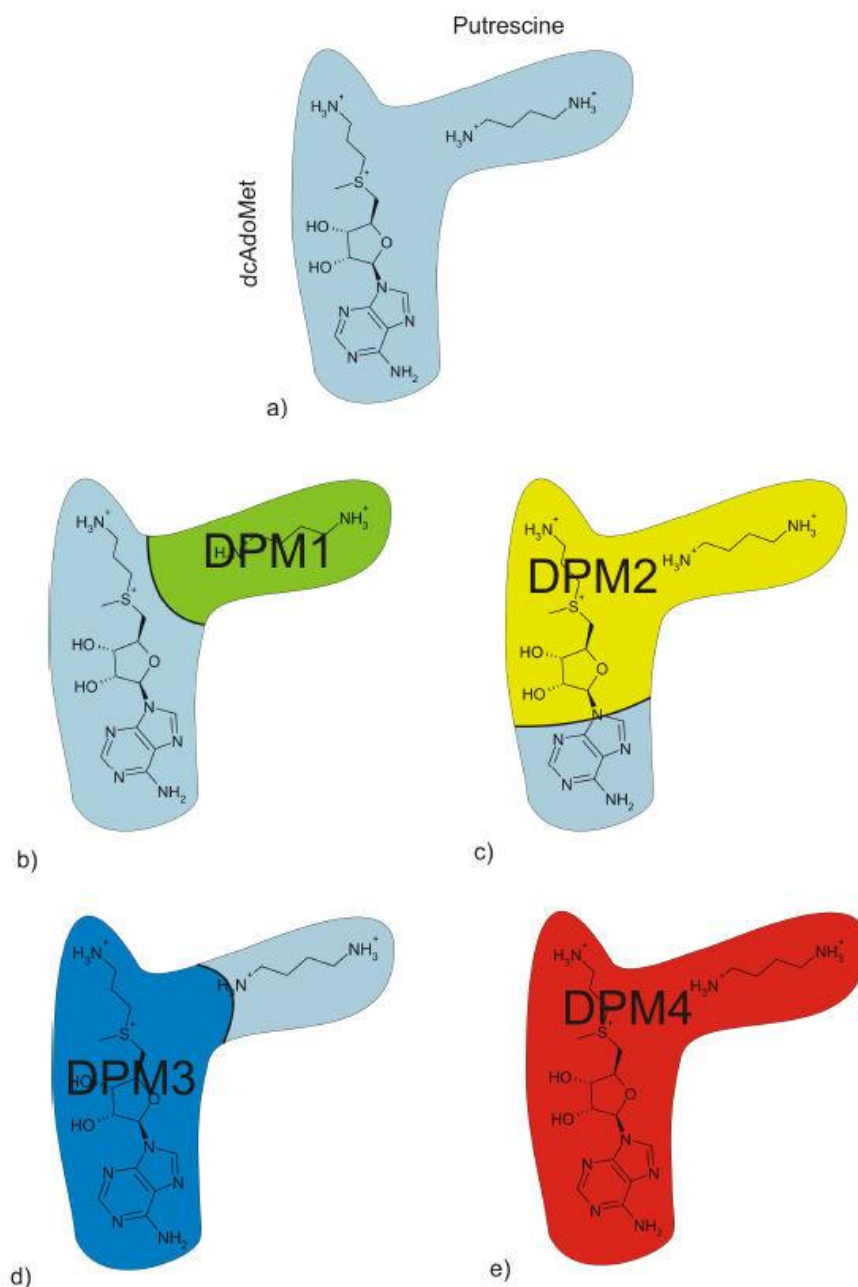
4MCHA has been shown to arrest parasitic development *in vitro*, with an IC<sub>50</sub> value against cultured parasites of 34.2 μM reported. Haider *et al.* also reports the addition of exogenous spermidine to 4MCHA treated *P. falciparum* is not able to alleviate the therapeutic effect of inhibition, and some suggest that this is in part due to the parasite lacking the ability to salvage the spermidine metabolite as efficiently as putrescine [1, 86]. In a recent review by Müller *et al.* it was stated that administration of 25 mg/kg of 4MCHA to mice infected with *P. berghei* had an indifferent effect on both the parasitic proliferation and survival of the mice [212]. 4MCHA was suggested to be assimilated rapidly by the host organism, and the lack of therapeutic effect was attributed to sub-optimal doses of the compound.

### 3.1.6. Pharmacophore modelling of *Pf*SpdSyn

A pharmacophore was originally coined by Paul Ehrlich as the “molecular framework that carries the essential features responsible for a drug’s biological activity”. Considering the enormous range of biological and synthetic molecules that have interactions within a biological system as an inhibitor, activator, or substrate; the pharmacophore was recently broadly restated as the 3D arrangement of chemical features responsible for a molecule to exhibit a specific biological activity [213]. A recent publication by Jacobsson *et al.* also demonstrated the usefulness of pharmacophore identification, and this was specifically applied to identify potential active site binders in *Pf*SpdSyn [214]. Their approach followed the virtual docking of a library of 2.8

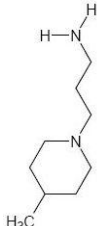
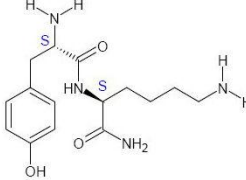
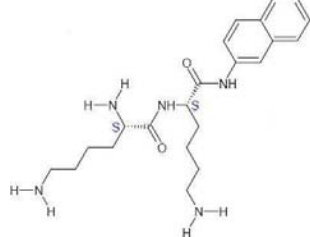
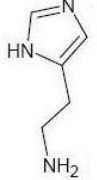
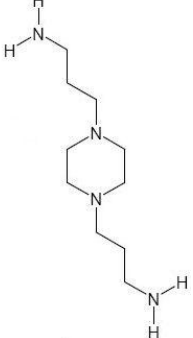
million compounds in the representing pharmacophore of *Pf*SpdSyn. Their results report that 28 novel inhibitors for *Pf*SpdSyn were identified. These inhibitors were then further tested using NMR binding analyses, in which the degree of competitive binding with MTA was reflective of inhibitor strength. MTA is known to inhibit *Pf*SpdSyn at 159  $\mu$ M; therefore any appreciable competition with MTA could therefore have been equivalent to a moderately effective inhibitor. Their approach identified a single compound that was suggested to strongly compete with MTA for the *Pf*SpdSyn dcSAM active site [214]. However, no direct enzyme inhibition, or effect on parasite growth could be demonstrated *in vitro*.

A similar approach was followed by Pieter Burger of the Bioinformatics and Computational Biology Unit, based at the University of Pretoria. A dynamic receptor-based pharmacophore model (DPM) of *Pf*SpdSyn was constructed by using two recently published crystal structures of *Pf*SpdSyn with PDBid; 2I7C and 2PT9 [203]. The former *Pf*SpdSyn crystal structure represented the protein in complex with AdoDATO, and the latter with PDBid 2PT9 was shown with 4MCHA and dcSAM. The *Pf*SpdSyn active site in each structure was subdivided into four distinct binding cavities, DPM1 to DPM4 (Fig 3.4). Pharmacophoral features were extracted from the individual DPM cavities. Virtual docking was performed, by searching for correlating favourable interactions in the DPM pharmacophores, using 2 million unique compounds of the ZINC chemical database (Bioinformatics and Chemical Informatics Research Center, California, USA). Favourable interacting compounds with low *in silico* docking energy values, in each of the distinctive DPM cavities, were identified [207]. Nine of these compounds, given in Table 3.2, were then selected for *in vitro* evaluation against purified *Pf*SpdSyn. This work was performed in collaboration with Dr. I. B. Müller, Dr. C. Wrenger and Prof. R. D. Walter at the BNI in Hamburg, Germany.



**Figure 3.4: The DPM cavities of *PfSpdSyn*.** During the generation of the DPM of *PfSpdSyn*, the binding cavities were subdivided into DPM sites. **a)** Represents the DPM1 putrescine binding cavity, **b)** DPM2 was a region encompassing the putrescine and part of the dcSAM binding cavity. **c)** DPM3 represented the dcSAM binding cavity and **d)** DPM4 the entire *PfSpdSyn* binding cavity. Each DPM cavity was identified with a unique set of pharmacophoral components, and *in silico* docking experiments determined favourable DPM-site binding compounds from the ZINC chemical database [207].

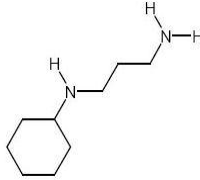
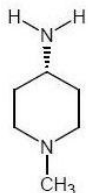
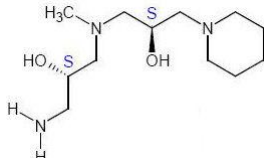
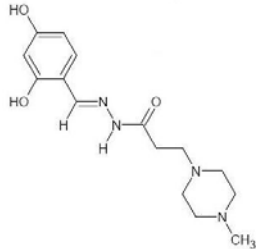

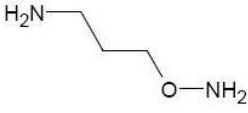
**Table 3.2: Pharmacophore identified inhibitors of *Pf*SpdSyn.** Favourable binding interactions were probed against a pharmacophore-receptor generated from *Pf*SpdSyn and the following compounds were selected for additional *in vitro* kinetic evaluation. The Figure was adapted from [207].

Compound Name and ZINC database ID	Chemical structure	Proposed binding cavity	<i>In silico</i> predicted docking energy (kcal / mol)	
			PDBid 2I7C	PDBid 2PT9
Compound 1 (ZINC02582060)		DPM1	-9.2	-9.4
Compound 3 (ZINC02561129)		DPM2	-13.1	-11.8
Compound 4 (ZINC04899780)		DPM4	-11.6	N.R.D
Compound 5 (Histamine dihydrochloride)		DPM1	N.B.P	N.R.D
Compound 6 (ZINC01683322)		DPM2	-14.0	-12.3

N.R.D. - Could not be realistically docked.

N.D. - Not determined

**Table 3.2 Continued.**

Compound Name and ZINC id	Chemical structure	Proposed binding cavity	Docking energy (kcal / mol)	
			PDBid 2I7C	PDBid 2PT9
Compound 7 (N-(3-aminopropyl)-cyclohexylamine) (NAC)		DPM2	-9.4	-10.5
Compound 8 ( <i>trans</i> -4-amino-1-methylpiperidine)		DPM1	-7.6	-7.7
Compound 9 (ZINC04955838)		DPM3	-13.2	-9.8
Compound 10 (ZINC05030866)		DPM3	-12.0	-10.5
<i>trans</i> -4MCHA		Previously identified (positive control) [86]	-7.2	-7.2
1-aminoxy-3-aminopropane (APA)		Previously identified (positive control) [86]	N.D.	N.D.

N.R.D. - Could not be realistically docked.

N.D. - Not determined



## 3.2. Methods

### 3.2.1. Expression of Spermidine Synthase

#### 3.2.1.1. Heat shock transformation of *E. coli*

Constructs containing *P. falciparum* spermidine synthase were obtained from Dr. I. B. Müller from the Bernard-Nocht Institute for Tropical Medicine (BNI, Hamburg, Germany). The pTRCHisB construct containing a 87bp 5'-deletion mutant of *PfSpdSyn* was previously shown to achieve greater protein expression levels in *E. coli* BLR (DE3) [86]. The construct was transformed into *E. coli* BLR (DE3) protein expression cell line using heat shock transformation. Briefly, approximately 50 ng of plasmid DNA was incubated with 100 µL heat shock competent *E. coli* (BLR) cells for 30 min on ice. Heat shock transformation was performed at 42°C for 60sec after which the cells were directly transferred to ice for an additional 2 min. 800 µL of preheated Luria-Bertani (LB) broth (1% w/v Tryptone, 0.5% w/v Yeast Extract, 1% w/v NaCl, pH 7.2) was added and the cells were incubated on a benchtop shaking incubator at 37°C for 30 min. The cells were pelleted by centrifugation at 10000 x g for 3 min (Eppendorf, Hamburg, Germany) after which the remaining pellets were plated out on LB-agar plates containing 50 µg/mL ampicillin antibiotic (Sigma-Aldrich, St. Louis, USA). The agar plates were incubated overnight (16 h) at 37°C, and single colonies were selected and used to inoculate 10 mL LB-broth, containing 50 µg/mL ampicillin, for large scale protein expression. This 10 mL culture was grown overnight at 37°C in a shaking incubator at 200 revolutions per minute (rpm).

#### 3.2.1.2. Protein expression

The 10 mL LB culture was diluted 1:100 into 1 L of LB broth, containing 50 µg/mL ampicillin. The solution was grown at 37°C in a waterbath shaking incubator until an optical density of 0.6 at 600 nm was reached. Protein expression was initiated through the introduction of 1 mM isopropyl β-D-1-thiogalactopyranoside (IPTG), and expression was continued for 4 h at 37°C. The bacterial solution was pelleted using centrifugation for 10 min at 3500 x g (Sorvall, Thermo Fisher Scientific). Resulting pellets were re-suspended using 10 mL Lysis buffer (50 mM NaH<sub>2</sub>PO<sub>4</sub>, 300 mM NaCl, 20 mM imidazole, pH 8.0) per milliliter equivalent bacterial pellet. At this stage pellets were subjected to protein isolation procedure or alternatively stored at -20°C for later use.

#### 3.2.1.3. Protein isolation

Re-suspended bacterial pellets were placed in a 50 mL glass beaker, ensuring this is kept cool by working on ice (4°C). PMSF (phenylmethanesulphonyl fluoride), a serine protease inhibitor in isopropyl alcohol, was diluted 1:1000 into the bacterial pellets to achieve a final concentration of 0.1 mM, by adding 10 µL of 0.1M PMSF per 10mL equivalent bacterial pellet. The pellets were sonified continuously at 100% duty cycle, output 3, for 1 min (Branson, Branson Ultrasonics). Sonification was repeated 8 times, with 1 min resting on ice between each sonification interval. The lysed bacterial cells were cleared by high-speed centrifugation at 47000 x g for 1 h (Sorvall Evolution, RC, with SS-34 Rotor, Thermo Fisher Scientific). The clear supernatant from the

centrifugation process was applied to nickel-nitrilo triacetic acid (Ni-NTA) coupled Sepharose CL-6B (Qiagen, Hilden, Germany) affinity resin for further protein isolation of the C-terminal hexahistidine tagged *PfSpdSyn*. One milliliter of the Ni-NTA resin was used per 10 mL of equivalent supernatant. The Ni-NTA resin was initially washed in 50 mL wash buffer (50 mM NaH<sub>2</sub>PO<sub>4</sub>, 300 mM NaCl, pH 8.0) by rotating the mixture at 4°C for 1 h. After packing of the resin in supplied sintered columns, the supernatant was eluted through the columns three or more times. Non-specific proteins were washed from the columns through applying 30 mL of Wash buffer containing imidazole (50 mM NaH<sub>2</sub>PO<sub>4</sub>, pH 8.0, 300 mM NaCl, 20 mM imidazole). Hexahistidine tagged proteins were eluted from the columns using elution buffer (50 mM NaH<sub>2</sub>PO<sub>4</sub>, 300 mM NaCl, pH 8.0, and 1 M imidazole). The imidazole groups effectively out-compete the hexahistidine tags for interactions with the Ni-NTA resin. Additional overnight dialysis was performed using Slide-A-lyzer<sup>®</sup> dialysis cassettes (Thermo Scientific) with 10 kDa molecular weight cut-off. The dialysis buffer consisted of 50 mM KH<sub>2</sub>PO<sub>4</sub>, 1.25 mM EDTA, 1 mM DTT at pH 7.0. Protein dialysis was performed overnight at 4°C, using 2L dialysis buffer per protein-loaded cassette.

#### **3.2.1.4. Protein concentration determination**

The protein concentration of the purified proteins from the Ni-NTA purification process was determined using Bradford reagent, consisting of Coomassie Brilliant Blue G-250. One hundred microliters of diluted protein was added to 1 mL of Bradford reagent (Bio-Rad, Germany). The samples were briefly vortexed and the absorbance was determined using a UV spectrophotometric analysis at 595 nm. A previous standard curve generated from known standards was programmed directly on the UV spectrophotometer, and was used to determine the concentration of protein.

#### **3.2.1.5. Polyacrylamide gel electrophoresis**

Sodium dodecyl sulphate (SDS) polyacrylamide gel electrophoresis (PAGE) was performed as previously established by Laemmli *et al.* [215]. Electrophoresis was performed in Biometra Minigel protein electrophoresis housings (Biometra, Göttingen, Germany) with plastic gel cassettes of sizes of 8.6 x 7.7 cm (Invitrogen, California, USA). Protein samples were denatured in sample loading buffer (200 mM Tris-HCl, pH 6.8, 8% SDS, 40% glycerine, β-mercaptoethanol, 0.1% bromophenol blue) by adding 2 μL to 18μL of sample loading dye and boiling samples for 5 min. A 10% separating gel was prepared by adding 1.5 M Tris-HCl pH 8.7, bis-acrylamide (29.1% acrylamide, 0.9% bis-acrylamide), 0.1% SDS, 10% APS, and 33.5 nM (5μL) TEMED. The stacking gel component at 5% consisted of Tris-HCl, pH 6.7, Bis-acrylamide, 0.1% SDS, 10% APS, 33.5 nM (5μL) TEMED. Electrophoresis buffer consisted of 25 mM Tris-HCl, 192 mM Glycine, 0.1% SDS (w/v). Loaded protein samples were run at 120V. SDS-PAGE gels were stained with Coomassie, containing 0.3 mM Coomassie R-250, 40% v/v MeOH, 7% v/v glacial acetic acid. Destaining was performed using a solution containing 40% v/v MeOH and 7% v/v glacial acetic acid.

### 3.2.2. Kinetic determinations

#### 3.2.2.1. 100 $\mu$ M inhibitor assays

Initially, the computationally identified inhibitors were assayed to determine the inhibitory activity against *PfSpdSyn*. Due to time-constraints, inhibitors were tested at 100  $\mu$ M to determine the most active inhibitors, which were selected for further kinetic analyses against *PfSpdSyn*. Inhibitors were supplied by the following manufacturers; compound 1 (Matrix Scientific, Columbia, South Carolina, USA) Compound 2, compound 3, compound 4, compound 5, compound 6, and compound 7 were purchased from TCI Europe, Antwerp, Belgium. Compound 8 was supplied by CHEM IMPEX International, Inc, Wooddale IL, USA. Compound 9 and compound 10 was purchased from Chembridge Ltd., CA, USA. Stock solutions of the inhibitors were prepared in dddH<sub>2</sub>O, with exception to Compound 10, which was prepared in dddH<sub>2</sub>O containing 5% v/v DMSO (Sigma-Aldrich, St. Louis, USA). APA was kindly provided by Alex Khomutov (Russian Academy of Sciences, Moscow, Russia). 4MCHA was a kind gift from Keijiro Samejima (Josia University, Saitama, Japan). 4MCHA and APA were also prepared in dddH<sub>2</sub>O.

*PfSpdSyn*, together with the inhibitors, was assayed according to the procedure followed by Haider *et al.* [86]. The reaction assay measured the <sup>3</sup>H-labelled production of spermidine in the presence of purified *PfSpdSyn* together with *RS*-dcAdoMet and [1,4-<sup>3</sup>H] putrescine dihydrochloride. The assays were performed in reaction conditions containing 50 mM KH<sub>2</sub>PO<sub>4</sub> (pH 7.0), 1 mM EDTA (pH 8.0), and 1 mM DDT. Additionally, 50  $\mu$ M *RS*-dcAdoMet and 50  $\mu$ M unlabelled putrescine dihydrochloride (Merck, Darmstadt, Germany) was added to each reaction. Inhibitors were added to a final concentration of 100  $\mu$ M and dddH<sub>2</sub>O was used to fill the reaction to 100 $\mu$ L final volume. To each reaction tube 100 nCi [1,4-<sup>3</sup>H] putrescine dihydrochloride (GE Healthcare, Amersham, UK) was added and the process initiated by adding 1 $\mu$ g of purified *PfSpdSyn*. The tubes containing the reaction mixture were incubated at 37°C for 30 min, after which the enzyme was deactivated at 95°C for 5 min. The <sup>3</sup>H-labelled products from the reaction was determined using TLC separation and liquid scintillation counting as described in section 3.2.2.3.

#### 3.2.2.2. K<sub>i</sub> determinations

Compound 7 was selected for further kinetic analysis. Conditions containing 100  $\mu$ M *RS*-dcAdoMet was maintained in a 50  $\mu$ L reaction volume. Putrescine concentrations were varied at 20, 80, 160, and 300  $\mu$ M, and a blank reaction was also included. The inhibitor was tested at varying concentrations of 0 or blank, 20 and 40  $\mu$ M. 50 mM KH<sub>2</sub>PO<sub>4</sub> (pH 7.0), 1 mM EDTA (pH 8.0), 1mM DTT together with 100 nCi/ $\mu$ L [1,4-<sup>3</sup>H] putrescine dihydrochloride (GE Healthcare, Amersham, England) was added to the reaction tubes. The final volume was adjusted to 50  $\mu$ L using dddH<sub>2</sub>O. The reactions were initiated by adding 0.5  $\mu$ g of purified *PfSpdSyn*. The reactions were incubated and processed according to the method described in section 3.2.2.1

### 3.2.2.3. TLC Separation of polyamines formed in SpdSyn reaction

For reaction assay analysis 10  $\mu$ L of the *PfSpdSyn* reaction mixtures, together with 5  $\mu$ L of a mixture containing 25 mM putrescine and spermidine was loaded on Silica Gel 60 TLC plates (Merck, Darmstadt, Germany). The putrescine / spermidine tracer cocktail, which did not contain any radioactive material, was only used to visually identify the elution of putrescine and spermidine equivalent molecules. TLC mobile phase consisted of ethylene-glycol monomethyl ether (Merck, Darmstadt, Germany), propionic acid (Merck, Darmstadt, Germany) and a saturated solution of NaCl (Merck, Darmstadt, Germany). The loaded TLC plates were equilibrated in TLC mobile phase, consisting of ethylene-glycol monomethyl ether, propionic acid, saturated NaCl (70 : 15 : 15) at RT. TLC separation was terminated once the mobile phase solvent front reached the upper portion of the TLC plate, which took approximately 3 h. The plates were allowed to air dry, sprayed using 15% v/v ninhydrin, prepared by adding 1.5 g of ninhydrin to 10mL of Acetone (Merck, Darmstadt, Germany). The plates were developed for 10 min at 60°C. Spots from the TLC plates were subsequently cut-out and placed in 5 mL Ultima-Gold Scintillation fluid XR (Packard Technologies). The samples were left overnight, in a cool dark place, and counted the following day using an United Technologies Packard 2000CA Tri-Carb® Scintillation counter (Packard Technologies, Perkin-Elmer, Massachusetts, USA), with preset tritium CPM determinations (Lower Limit : 0.05mV and Upper Limit: 0.19mV). Samples were counted for at least 10 min, during which at least 10000 counts were accumulated.

The enzyme activity was calculated by the following formula, according to Haider *et al.* [86];

$$\begin{aligned}
 PfSpdSyn \text{ specific activity} &= \frac{\text{Spd}}{(\text{Put} + \text{Spd})} \times \frac{\text{unlabelled Put}}{\text{Enzyme (mg)} \times 30\text{min}} \\
 &= \text{nmol.min}^{-1}.\text{mg protein}^{-1}
 \end{aligned}$$

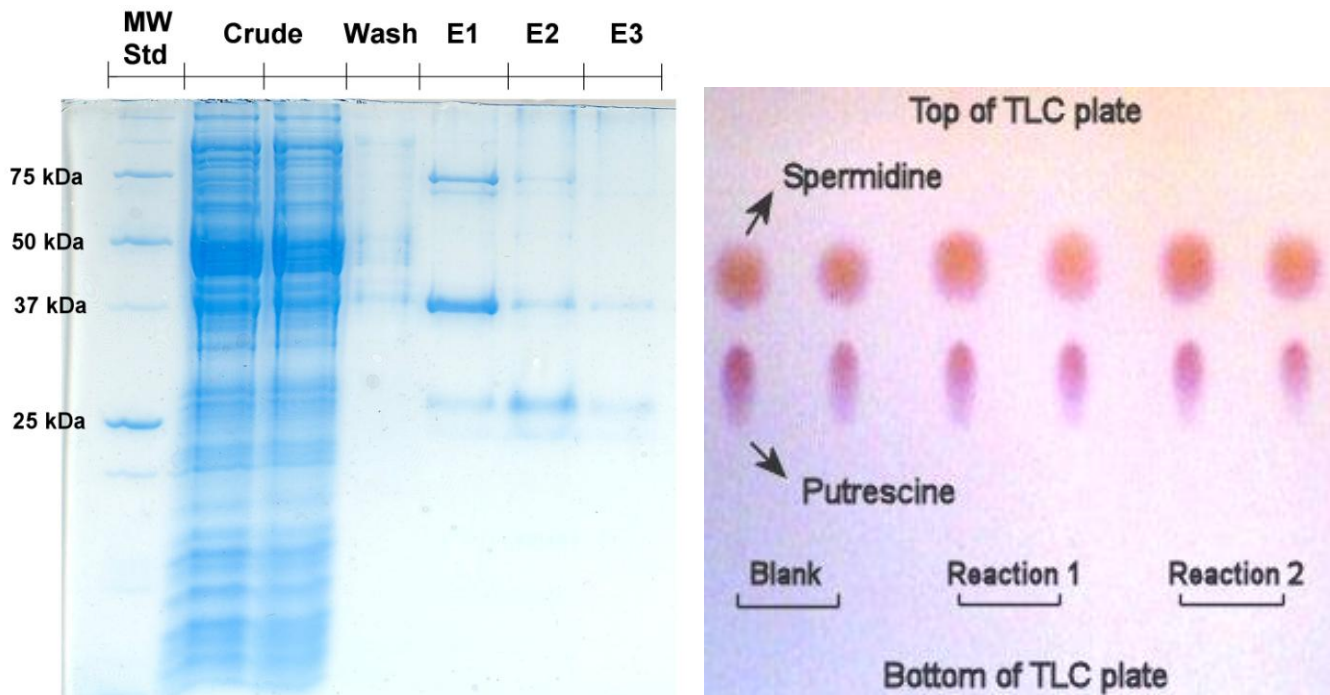
Spd and Put represents the amount of  $^3\text{H}$ -labelled spermidine and putrescine counted from the excised TLC eluted spots, respectively. The activity was determined from the ratio of  $^3\text{H}$ -spermidine formed compared to the total amount of  $^3\text{H}$ -putrescine and  $^3\text{H}$ -spermidine present. This fractional activity considered the potential losses in  $^3\text{H}$ -labelled material, as occurs when low levels of spermine is produced. The fraction activity was related to the amount of unlabelled putrescine present (nmol), and expressed as enzyme specific activity, incorporating the amount of purified *PfSpdSyn* enzyme and the reaction incubation time at 37°C.

## 3.3. Results and Discussion

### 3.3.1. SpdSyn protein expression and isolation

Expression of N-terminally truncated *PfSpdSyn* was verified using SDS-PAGE, which revealed the expected 37 kDa protein band (Fig 3.5). After repetitive elution of crude extracts through the Ni-NTA affinity resins, non-specific proteins were washed from the column using a solution containing 20 mM imidazole. The resulting liquid from the washing step, shown in Fig 3.5, was shown to contain little or no non-specific protein. His-tagged *PfSpdSyn* proteins were

incrementally eluted from the resins using 1 mL of elution buffer which contained 1 M of imidazole. The majority of the protein, corresponding to 37 kDa protein, was detected within the first millilitre of applied elution buffer, and subsequently purification procedures only involved the isolation of the first 1 mL fraction during protein elution from Ni-NTA affinity resins.



**Figure 3.5: *PfSpdSyn* protein expression and TLC kinetic analysis.** **A)** The figure represents individual steps and the eluted protein products at each stage during *PfSpdSyn* protein isolation. “Crude” protein sample was from the original supernatants obtained after centrifugation of *E. coli* lysates. “Wash” represents the proteins eluted from the Ni-NTA resin after washing with buffer, containing 20 mM imidazole. “E1, E2 and E3” represents the eluted fractions after 3 x 1 mL incremental addition of elution buffer containing 1M imidazole. **B)** Representative TLC of separated *PfSpdSyn* reaction mixtures. The TLC was stained with ninhydrin to reveal putrescine and spermidine tracers, which allowed visual identification of the localization of radioactively labelled polyamine products. These spots were cut out and placed in liquid scintillation fluid to determine the radioactive products from the reaction assays.

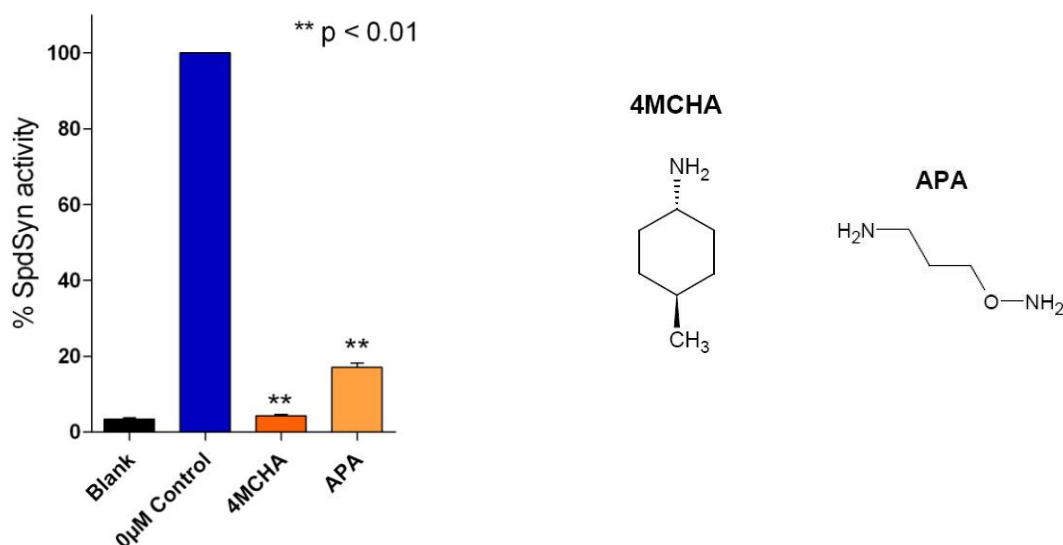
The 37 kDa band, shown in lane E1 in Fig 3.5, corresponded to monomeric N-terminally truncated forms of *PfSpdSyn*, as previously shown by Haider *et al.* [86]. Protein determination according to Bradford revealed protein expression levels in the range of 1-5 mg/mL, although from SDS-PAGE contaminating bands of 75 and 27 kDa also appear to be present and may have influenced this estimation. Also, initial kinetic investigations prompted the removal of the high concentrations of imidazole using overnight dialysis. Increased enzyme activity could be confirmed in the dialyzed samples (results not shown). Purified *PfSpdSyn* appeared to be quite stable, and enzyme activity could be successfully detected in samples stored at 4°C a week later (results not shown). The enzyme activity of purified *PfSpdSyn* was verified through TLC analysis of <sup>3</sup>H-labelled production of spermidine from <sup>3</sup>H-putrescine (Fig 3.5 B). As shown in section 3.3.3, Michaelis-Menten kinetic plots could confirm the reaction specificity of purified *PfSpdSyn*, and is discussed later.

### 3.3.2. Evaluation of pharmacophore-identified inhibitors

The initial evaluation of novel pharmacophore-identified inhibitors against *PfSpdSyn* occurred at 100  $\mu\text{M}$ . The compounds were tested together with substrate concentrations of 50  $\mu\text{M}$  putrescine and 50  $\mu\text{M}$  dcSAM concentrations. Also, only an isomeric mixture *RS*-dcSAM was available, and previously it was suggested that only *S*-dcSAM forms can be utilised by *PfSpdSyn*, as discussed below. Hence, the effective working concentration of *S*-dcSAM was 25  $\mu\text{M}$  from the 50  $\mu\text{M}$  *RS*-dcSAM mixture. The  $K_m$  values for putrescine and dcSAM of *PfSpdSyn* was previously reported at  $52.0 \pm 0.6 \mu\text{M}$  and  $35.3 \pm 4.1 \mu\text{M}$ , respectively [86]. Previous reaction assay conditions, in which 4MCHA, APA, APE and CHA were evaluated, were performed at 200  $\mu\text{M}$  putrescine and 100  $\mu\text{M}$  *S*-dcSAM. This study therefore evaluated inhibitors in substrate conditions close to the  $K_m$  reported for *PfSpdSyn*. Excess inhibitor conditions at 100  $\mu\text{M}$  would have made any observable inhibitory activity more noticeable.

Enzyme inhibitory activity was expressed as the specific activity of the inhibited enzyme normalized to the uninhibited control enzyme activity at 100%. 4MCHA was included as a positive control. At 100  $\mu\text{M}$  4MCHA almost complete enzyme inhibition was evident with  $4.2 \pm 0.3\%$  activity remaining (Fig 3.6). As previously shown, the non-aromatic compound had appreciable inhibitory activity against *PfSpdSyn* and an  $\text{IC}_{50}$  of  $1.4 \pm 0.1 \mu\text{M}$ , and  $K_i$  value of 0.18  $\mu\text{M}$  has been reported [86].

APA was previously tested against *PfSpdSyn*. APA was shown to inhibit the enzyme with  $\text{IC}_{50}$  reported as  $84 \pm 21 \mu\text{M}$  [86]. The compound is thought to occupy a position to the diamine putrescine in the *PfSpdSyn* active site. Moreover, efficient binding of compounds in the putrescine cavity which is flanked with negatively charged residues on either side, is proposed to require complementary positive ionisable groups [207]. During  $\text{S}_{\text{N}}2$  reaction displacement of aminopropyl chains from dcSAM, the attacking amino groups of putrescine are required to be deprotonated [206]. The aminoxy groups of APA are known to be deprotonated at physiological conditions, and these molecules could potentially act as competitive inhibitors during the aminopropyl transfer reaction. Shared amine characteristics between APA and putrescine also suggested that the former could act as an aminopropyl acceptor. It is not uncommon for inhibitor to act as aminopropyl acceptor, and previously Shirahata *et al.* could show that various diaminocyclohexane analogues were substrates in the pig liver SpdSyn [209]. During the course of TLC product analysis of APA-inhibited *PfSpdSyn* additional spots of greater polar character, similar to spermine, could be identified (data not shown). This suggested that APA can in fact act as an aminopropyl acceptor, however further HPLC investigations would however be required to confirm this. At 100  $\mu\text{M}$  APA inhibited 80% of the purified *PfSpdSyn* activity, correlating with previous  $\text{IC}_{50}$  suggestions (Fig 3.6) [86].

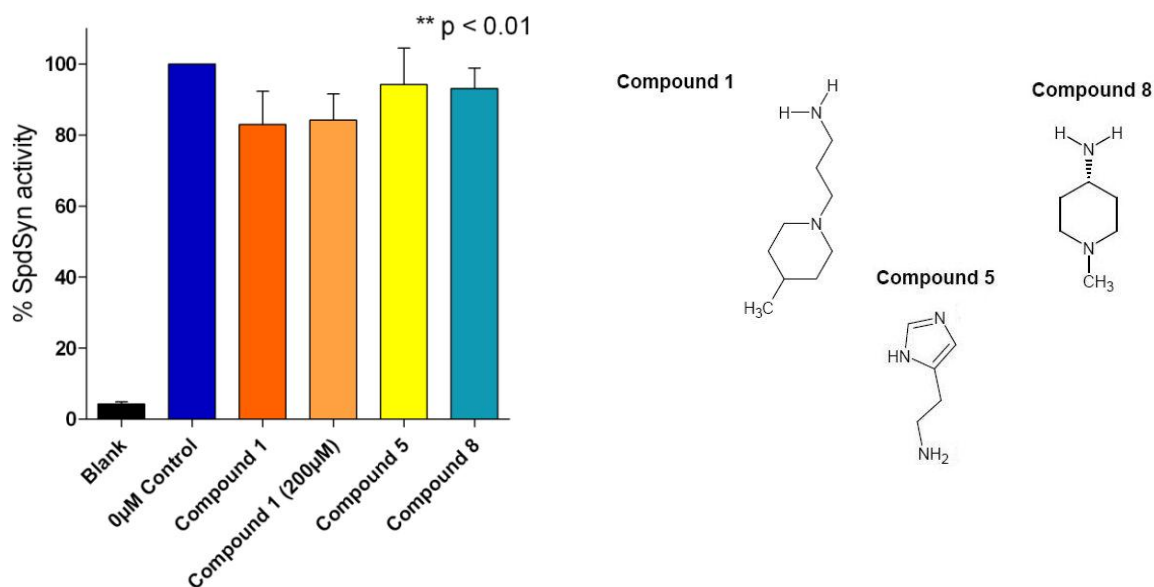


**Figure 3.6: Inhibitor assay of 4MCHA and APA at 100 µM against PfSpdSyn.** Results represent the % PfSpdSyn activity compared to uninhibited enzyme of three independent experiments performed in duplicate, error bars represent the standard error of the mean (SEM). Statistical analysis using paired Students t-test was performed with GraphPad Prism®, Where \*\* represented 99% significance with p-values below 0.01.

Compound 1 was identified as a putrescine cavity or DPM1 cavity binding inhibitor. The compound contained a piperidine ring, with *para*-orientated methyl- and aminopropyl groups. The piperidine ring was proposed to occupy the same position as the cyclohexane ring of 4MCHA [207]. Docking of the compound, *in silico*, predicted that the methyl group was orientated toward the active center in the DPM1 binding cavity and located close to the position the dcSAM amino substrate amino groups would occupy. The aminopropyl chain of the molecule was predicted to hydrogen bond to PfD<sub>199</sub> and PfE<sub>231</sub>. The former invariant residue was strictly shown to have interactions with the amine groups of the 4MCHA inhibitor [203]. The latter residue was also predicted to aid in solvation of the 4MCHA amine groups through interactions with a closely located H<sub>2</sub>O molecule [203]. *In vitro* kinetics established that the compound had some inhibitory activity; however at 100 µM it was noted that 82.9 ± 8.0% of PfSpdSyn activity remained (Fig 3.7). At 200 µM concentration, as shown in Fig 3.9, 84.1 ± 6.0% PfSpdSyn remained, suggesting that the equivalent IC<sub>50</sub> of the compound was expected well above 200µM. The relatively low activity was thought to be related to the piperidine ring, and similar piperidine containing compounds were shown not to have favourable binding in the DPM1 cavity, as explained below.

Additional compounds that were tested included compound 5, also known as histamine; a biological molecule involved in allergic reactions (Fig 3.7). The imidazole moiety of histamine was observed, *in silico*, to have favourable interactions with PfY<sub>102</sub> and PfS<sub>197</sub> in the DPM2 spanning site of PfSpdSyn. These residues were also implicated for binding of the attacking amine groups of putrescine [203]. The aminoethyl chain of histamine was also suggested to span across the DPM2 cavity towards the active center of the enzyme, and docked with amine groups in the dcSAM cavity. Residues PfD<sub>127</sub> and PfD<sub>196</sub>, were involved in hydrogen bonds with

aminopropyl chains of dcSAM, and these residues were subsequently predicted to hydrogen bond to the primary amine groups of histamine during *in silico* docking [207]. The compound did not show any appreciable inhibitor activity at 100  $\mu$ M, with  $94.2 \pm 8.8$  % *PfSpdSyn* activity remaining.



**Figure 3.7: The inhibition of *PfSpdSyn* DPM1 active site using 100  $\mu$ M of compound 1, 5, and 8.** The inhibitory activity of the inhibitors was determined against purified *PfSpdSyn* at 100  $\mu$ M. Error bars indicating the standard error of the mean (SEM) from four independent experiments performed in duplicate. Compound 1 was additionally tested at 200  $\mu$ M ( $n = 3$ ). Statistical analysis using paired Students t-test was performed with GraphPad Prism®, where \*\* represented 99% significance with  $p$ -values below 0.01.

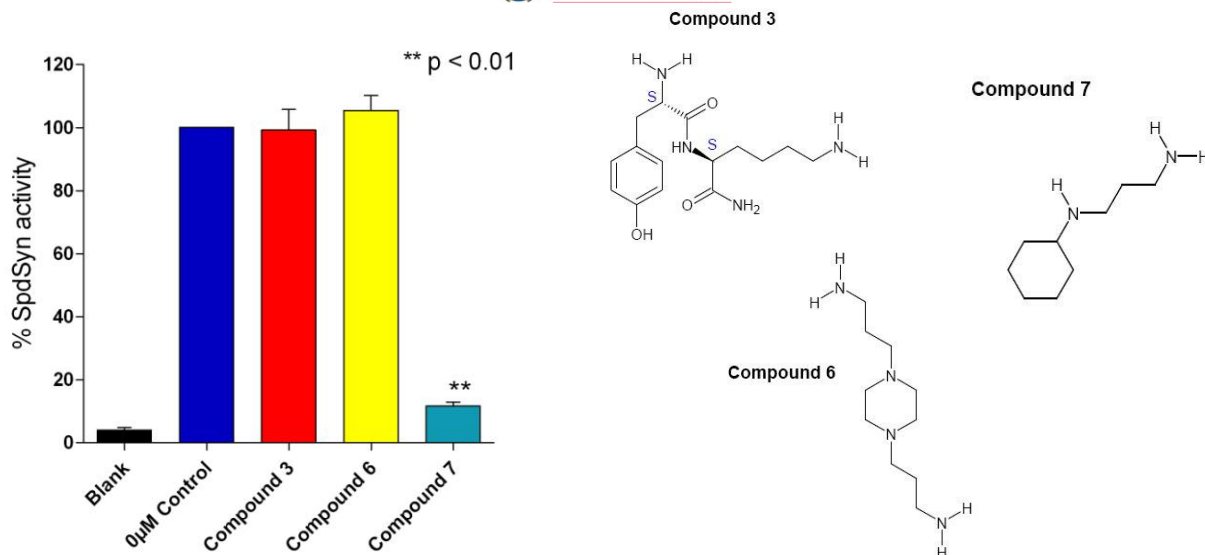
Compound 8, an 4MCHA equivalent molecule with an additional nitrogen atom which forms a piperidine ring, was also identified during the *in silico* pharmacophore modelling as performed by Burger *et al.* [207]. The piperidine component of the compound, also identified in other structure-based virtual screening approaches [214], was predicted to bind in the putrescine or DPM1 cavity [207]. It is not known whether piperidine ring containing compounds, like compounds 1 and 8, are well accommodated in the putrescine binding site. Compound 1 was predicted to have hydrogen bonds between the piperidine nitrogen and the  $PfD_{199}$  residue [207], also shown to hydrogen bond with amine groups of 4MCHA [203]. The piperidine groups are expected to be conformationally flexible, a proven requirement for putrescine binding site inhibitors, elegantly shown by Shirahata *et al.* in pig liver SpdSyn [209]. Piperidine compounds had unfavourable binding, and this was shown by the same author. Nitrogen atoms of piperidine rings have additional electron density from unbounded  $\pi$ -orbitals. In tertiary bonded state the nitrogen atoms in a piperidine structure are also thought to have a trigonal pyramidal shape, and are therefore stereochemically flexible as required. These considerations cannot therefore warrant the inefficacy of the piperidine like compounds. Another possibility is the charged character of piperidine compounds, the  $pK_a$  of piperidine nitrogen is established at 11.20, and therefore charged at physiological pH conditions [216]. Essential hydrophobic contacts made to cyclohexane rings as shown for 4MCHA and CHA could possibly be disrupted by the electron rich character of the positively ionized group in piperidine compounds. The lack of *in vitro*



efficacy of compound 8, identical to 4MCHA except for the piperidine moiety, also supports this notion (Fig 3.7).

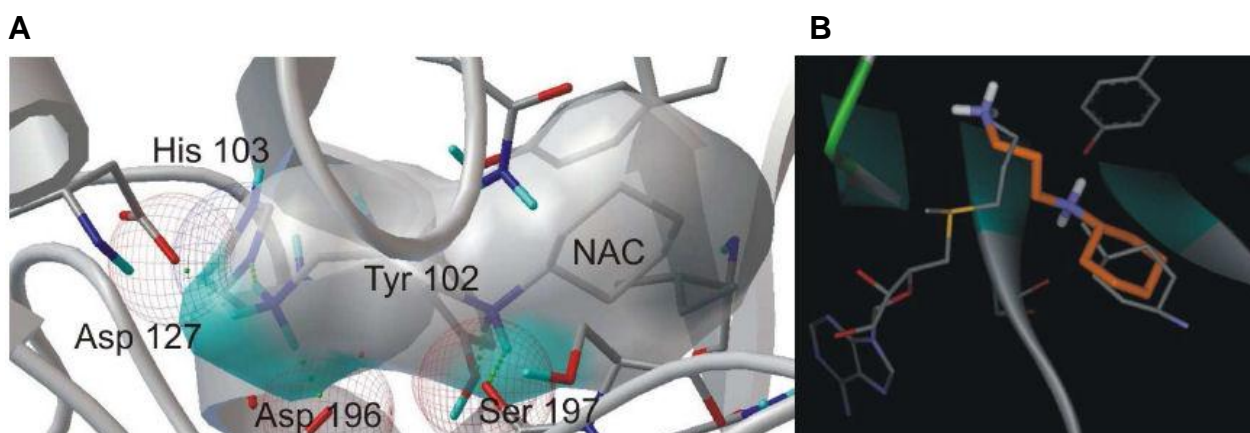
Compound 3 appeared not to affect the *PfSpdSyn* activity, and at 100  $\mu\text{M}$  concentrations  $99.2 \pm 5.3\%$  activity was still evident (Fig 3.8). Compound 3 was initially identified to have potential DPM2 cavity binding interactions and a low docking energy [207]. The benzene ring of the compound was predicted to hydrogen bond with PfQ<sub>72</sub> and PfE<sub>147</sub> in the *PfSpdSyn* model (PDBid 2I7C). These residues are also known to be associated with the hydroxyl groups of the dcSAM substrate shown in the *PfSpdSyn* crystal structure [203]. Also, favourable hydrogen bonds were predicted for the terminal amines of the aminobutenyl chain of compound 3, and these were suggested to have favourable interactions with the pharmacophoral equivalent position occupied by the non-attacking putrescine groups [207]. The lack of inhibitory action at 100  $\mu\text{M}$  does suggest this compound is a weak inhibitor, but does not exclude the possibility of further chemical optimization and potentiation.

Compound 6, a piperazine with terminal aminopropyl groups attached to the secondary amine groups, was proposed to be a DPM2 binding site inhibitor. The compound was predicted to have four pharmacophoral features which interact both in the putrescine and dcSAM binding cavity [207]. Moreover, *in silico* docking suggested that the piperazine component of the compound simulated the cyclohexane ring of 4MCHA and similar binding orientations were also shown [207]. Favourable hydrogen bonds were also shown for aminopropyl groups of the compound with PfH<sub>102</sub>, PfD<sub>196</sub> and PfD<sub>127</sub>, located in the dcSAM binding pocket. Remaining aminopropyl groups of the compound were also predicted to protrude into the non-attacking putrescine binding cavity with hydrogen bonds with PfD<sub>199</sub> and PfE<sub>231</sub> [207]. At 100  $\mu\text{M}$  concentrations *in vitro* the compound showed that  $105.4 \pm 4.0\%$  of the *PfSpdSyn* activity was still present (Fig 3.8). The lack of effective inhibition could be related to the piperazine ring components which disrupt hydrophobic contacts, as explained below from piperidine rings.



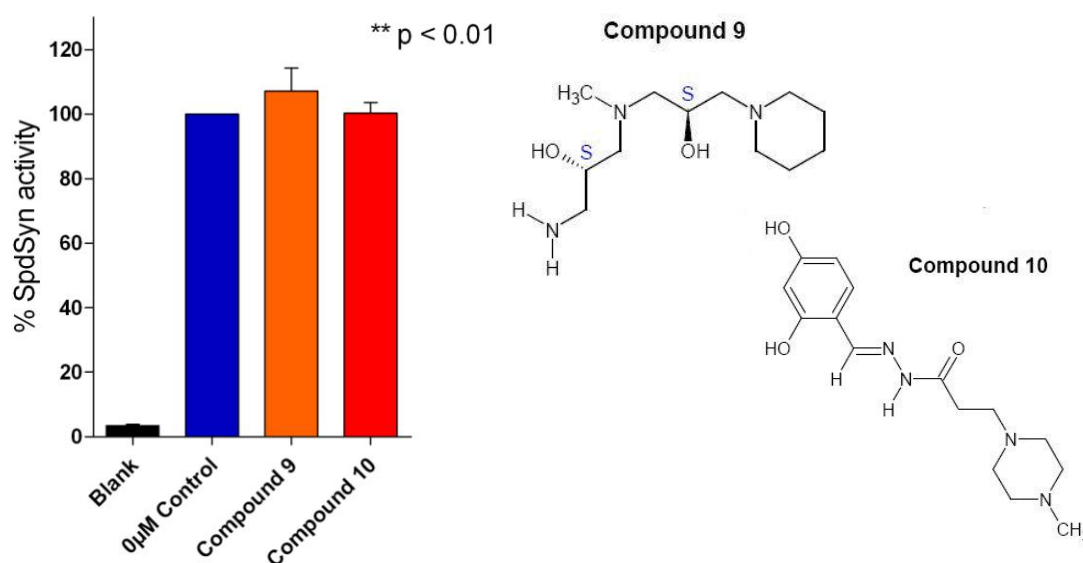
**Figure 3.8:** The activity of inhibitors targeted at the DPM 2 cavity of *PfSpdSyn* at 100 µM. The pharmacophorally identified inhibitors; compound 3, 6, 7 were tested against purified *PfSpdSyn*. Results are expressed as the percentage *PfSpdSyn* activity compared to uninhibited enzyme from at least three independent experiments performed in duplicate. Error bars represent the standard error of the mean (SEM). Statistical analysis, using paired Students t-test, was performed with GraphPad Prism®, where \*\* represented 99% significance with p-values below 0.01.

Compound 7, an aminopropyl CHA molecule, was also identified as a potential inhibitor in the *PfSpdSyn* DPM2 pharmacophore sites [207]. The compound was proposed to bind in the DPM2 cavity, with the aminopropyl moiety protruding into the dcSAM equivalent aminopropyl binding site (Fig 3.9, B). Hydrogen bonds were also predicted from *PfY*<sub>102</sub> of the *PfSpdSyn* model (PDBid 2I7C) towards the cyclohexyl nitrogen group, and *PfD*<sub>127</sub> and *PfD*<sub>196</sub> residue were involved in aminopropyl group hydrogen bonding (Fig 3.9, A) [207]. Through the selection of compound 7 the accommodative nature of the active site, shown to allow spermine formation, was also probed [207]. The compound was shown to have appreciable inhibition, able to decrease *PfSpdSyn* activity to  $11.6 \pm 1.0\%$  at 100 µM (Fig 3.8). This also prompted additional  $K_i$  determinations to be performed, in which the inhibitory action of the compound was further elucidated. This is discussed below.



**Figure 3.9:** *In silico* docked Compound 7 in *PfSpdSyn* (PDBid 2PT9) as determined by P. Burger [207]. **A)** Compound 7, also called NAC, was predicted to have hydrogen bond interactions with *PfY*<sub>102</sub> and *PfD*<sub>127</sub>. **B)** Compound 7, overlaid with dcSAM and 4MCHA, was proposed to orientate with aminopropyl groups protruding into the dcSAM binding cavity. Figure obtained from [207].

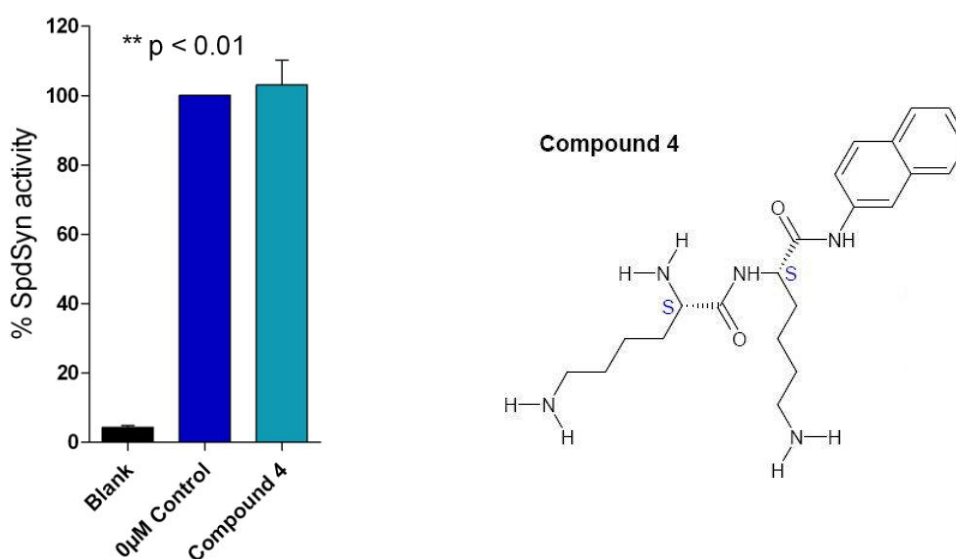
Compound 9, together with compound 10, were originally selected to determine the possible occupation of piperidine, piperazine and phenol chemical moieties in the dcSAM binding cavity [207]. Compound 9 was predicted to bind in the DPM3 cavity, the equivalent binding site of dcSAM, also spanning across the catalytic center of the enzyme. The docked molecule was proposed to have the piperidine rings orientated to dcSAM adenine ring equivalent positions. The terminal hydroxyl aminopropyl chain of compound 9 was proposed to have hydrogen binding interactions with *PfG*<sub>124</sub>, *PfD*<sub>127</sub> and *PfD*<sub>196</sub>. The latter residues were implicated to interact with the aminopropyl chain of dcSAM [203, 207]. *In vitro* kinetics revealed marginal increased enzyme activity at  $107.1 \pm 5.7\%$  compared to uninhibited enzyme from the same isolation procedure (Fig 3.10). This suggested that Compound 9 does not have appreciable inhibitor activity and that the piperidine rings may not be well accommodated in the dcSAM binding site of *PfSpdSyn*.



**Figure 3.10: Compounds proposed to bind in the DPM3 active site tested against *PfSpdSyn* at 100 µM concentrations.** The inhibition, expressed as the percentage remaining *PfSpdSyn* represented data from four experiments performed in duplicate, with the error bars indicating the SEM. Statistical analysis using paired Students t-test was performed with GraphPad Prism®, where \*\* represented 99% significance with p-values below 0.01.

Compound 10 was suggested to bind in the DPM3, dcSAM equivalent cavity, with low energy [207]. The compound was included in kinetic studies to probe the possible interactions phenol groups have with equivalent dcSAM adenosyl moiety positions. A proline residue, *PfP*<sub>203</sub>, part of the gatekeeper loop (residues 197-205), was previously shown to be involved in adenosyl group stabilization through hydrogen bonding with primary amine groups of the adenine substituent [203]. The terminal phenolic hydroxyl groups of Compound 10 were predicted to have similar hydrogen bonds with *PfP*<sub>203</sub> in the *PfSpdSyn* pharmacophore model [207]. The lack of *in vitro* inhibitory activity of the compound, as shown at 100 µM with  $100.3 \pm 2.7\%$  of SpdSyn activity remaining, suggested that the phenolic groups are not well accommodated in the DPM3 site (Fig 3.10) [207].

Compound 4, which contained two aminobutenyl chains and a naphthalene moiety, was also proposed to bind in the DPM4 cavity together with DPM2 binding [207]. The compound was predicted to interact with *PfD*<sub>127</sub> and *PfQ*<sub>93</sub>, the former residue implicated in close association with aminopropyl groups of dcSAM [203]. The compound was shown to orientate with the naphthalene aromatic group in a position equivalent to ribosyl components of AdoDATO. Burger *et al.* [207] suggested that interactions with residues *PfE*<sub>147</sub> and *PfQ*<sub>72</sub> are required for binding in the large DPM4 cavity. These contacts are involved in hydrogen bond stabilization of ribosyl hydroxyl groups of both dcSAM and AdoDATO [203, 207]. Similar interactions were, however, not predicted for compound 4 and from the low inhibitor activity at 100  $\mu$ M, shown in Fig. 3.11, it was postulated that equivalent ribosyl stabilization on synthetic molecules should be maintained for efficient binding in the dcSAM site.



**Figure 3.11: Compound 4 was predicted to bind in the large DPM4 cavity of *PfSpdSyn* at 100  $\mu$ M concentrations.** The inhibition, expressed as the percentage remaining *PfSpdSyn* represented data from four experiments performed in duplicate, in which the error bars represent the SEM. Statistical analysis using paired Students t-test was performed with GraphPad Prism®, where \*\* represented 99% significance with p-values below 0.01.

### 3.3.3. Kinetics of Compound 7

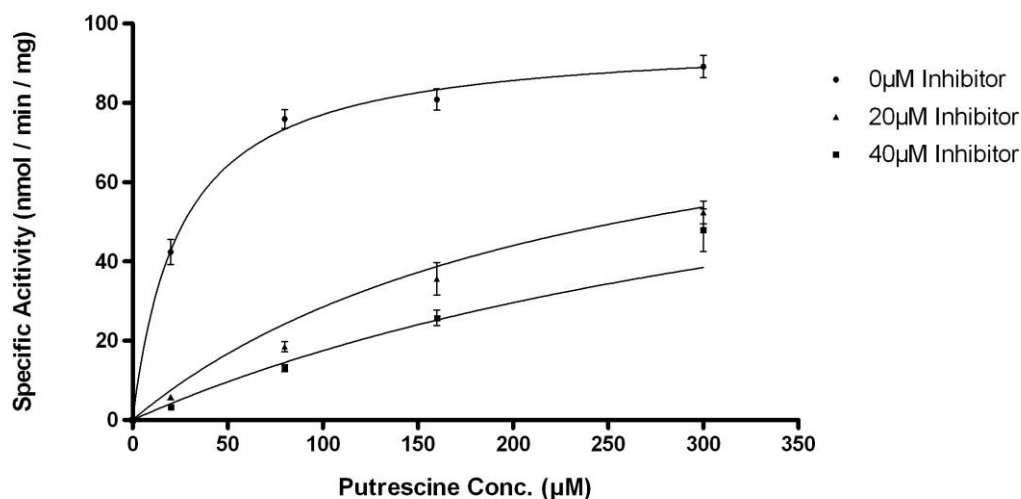
The efficacy of compound 7 in inhibitor assays at 100  $\mu$ M warranted further investigation and  $K_i$  determinations. Previously  $IC_{50}$  values of active inhibitors were reported for *PfSpdSyn* [86]. In this study, enzyme kinetics focussed on  $K_i$  value determination. The  $IC_{50}$  value represents the concentration of inhibitor required to diminish the enzyme activity to half of the original activity. Experiments that aim to determine the  $IC_{50}$  are often performed at a fixed substrate concentration, whilst the effect of increasing amounts of inhibitor is measured on the enzyme velocity.  $IC_{50}$  values cannot explain the mode of inhibitory action within the binding site, be it competitive, non-competitive or uncompetitive. The  $K_i$  is, however, a more accurate parameter when binding analysis is questioned. The  $K_i$  is assigned to the equilibrium reaction that exists when a competitive inhibitor competes for an equivalent binding substrate site within an enzyme active center. For competitive inhibition, in which ideally  $V_{max}$  parameters remain unaltered, the  $K_i$

represents the concentration of inhibitor that doubles the value of the enzyme  $K_m$  [217].  $K_i$  determinations can therefore reveal the extent of binding interactions that may occur for a particular inhibitor.

Previous kinetic determinations on *PfSpdSyn*, performed at the BNI laboratory in Hamburg, suggested that the enzyme had  $K_m$  values of  $52.0 \pm 0.6 \mu\text{M}$  for putrescine and  $35.3 \pm 4.1 \mu\text{M}$  for dcSAM [86]. It was, however, stipulated that in the case of the latter, isomerically pure *S*-dcSAM was used to determine the  $K_m$ . In experimentation performed here the only obtainable source of dcSAM contained both *R* and *S* isomers. Only *S*-dcSAM could be shown to bind in the dcSAM binding site in crystal structures generated from *T. maritima* SpdSyn [205]. This suggested that only *S*-dcSAM isomers are enzymatically active and the use of an isomeric mixture of dcSAM during *PfSpdSyn* inhibitor kinetic experiments required this discrepancy to be considered [86].

Initial kinetic determinations were performed at a fixed concentration of  $100 \mu\text{M}$  dcSAM and increasing levels of putrescine. This probed the activity on the putrescine binding site. The Michaelis-Menten plots generated are shown (Fig 3.12,  $0 \mu\text{M}$  conditions), with the  $K_m$  values for putrescine determined to be  $25.1 \pm 3.2 \mu\text{M}$ . The  $V_{\text{max}}$  of *PfSpdSyn*, under saturating dcSAM conditions, was estimated at  $96.4 \pm 2.7 \text{ nmol}\cdot\text{min}^{-1}\cdot\text{mg protein}^{-1}$ . These values were lower than previously reported. These lowered parameters could have been related to the source of *RS*-dcSAM used here compared to *S*-dcSAM in previous kinetic determinations as performed by Haider *et al.* [86].

Compound 7 was identified as a putrescine binding site inhibitor through the *in silico* SBDD approach performed by Burger *et al.* [207]. Kinetic experimentation therefore only focused on the competitive binding interactions of the compound for the putrescine binding site in *PfSpdSyn*. dcSAM was also in limited supply, and the competitive interactions between Compound 7 and dcSAM was not performed, however forms part of a future planned study. Due to time constraints initial Michaelis-Menten kinetics was performed using  $20$  and  $40 \mu\text{M}$  of compound 7. Michaelis-Menten graphs obtained from kinetic data revealed the extent of inhibition by Compound 7 (Fig 3.12).

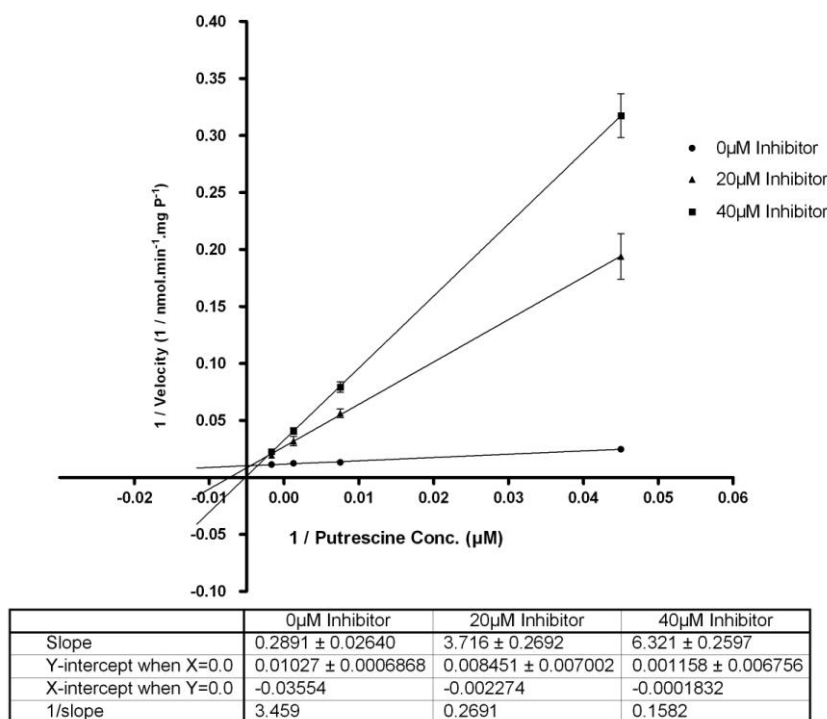


**Figure 3.12: Michaelis-Menten enzyme kinetics of *PfSpdSyn*.** The assays were also performed with increasing concentrations of compound 7 as shown in representative 20  $\mu\text{M}$  and 40  $\mu\text{M}$  curves. Error bars represent the SEM from five independent determinations performed in duplicate.

The inhibitor had more noticeable decline in maximal specific activity,  $V_{\text{max}}$ , at 40  $\mu\text{M}$  (Fig 3.12). For true competitive inhibition, the maximal velocity or  $V_{\text{max}}$  of the enzyme can be restored by increasing the substrate concentrations. This stipulates that at high concentrations the substrates effectively out-compete the inhibitor for binding site interactions. This was found not to be the case for compound 7. As shown in Michaelis-Menten plots (Fig 3.12), the  $V_{\text{max}}$  of the enzyme could not be restored, even at ten times  $K_m$  concentrations of putrescine. This suggested that the inhibitor had additional binding qualities not easily disrupted by putrescine. As elegantly shown by Burger *et al.*, compound 7 assumed a conformation that occupied both the putrescine as well as dcSAM binding cavities [207]. As already discussed, the compound was proposed to have aminopropyl chains protruding into the dcSAM site. *In vitro* generated kinetic data also support the notion that the compound is situated in the dcSAM binding cavity, and mixed inhibition was evident. Non-linear regression analysis was performed on the Michaelis-Menten plots, with constraints on a shared  $V_{\text{max}}$  parameter for competitive inhibition, using the GraphPad Prism<sup>®</sup> software package, version 5.00. The  $K_i$  value determined from the curve-fitted Michaelis-Menten data was  $2.35 \pm 0.28 \mu\text{M}$ . Additional experimentation is, however, required and should consider the activity of the inhibitor within lower concentration ranges, as this study focussed at concentrations of inhibitor well above the  $K_i$ -value determined for the compound.

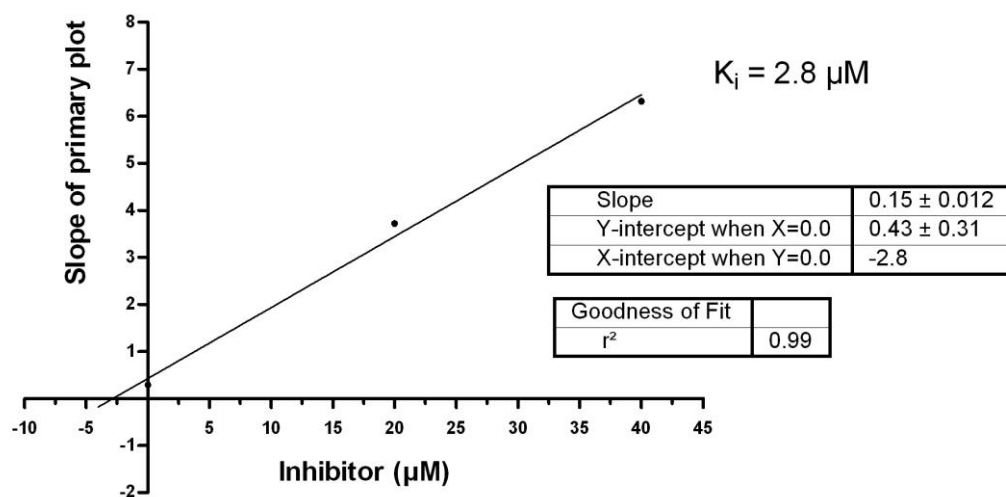
Linearization of Michaelis-Menten *PfSpdSyn* kinetic data into Lineweaver-Burk extrapolations also revealed that the compound 7 had characteristic mixed competitive inhibitory action (Fig 3.13). Uninhibited *PfSpdSyn* was shown with a y-intercept value, representing the  $1/V_{\text{max}}$  parameter, equivalent to  $97.37 \text{ nmol} \cdot \text{min}^{-1} \cdot \text{mg protein}^{-1}$ . Incrementally higher concentrations of compound 7 also revealed that the apparent  $V_{\text{max}}$  parameter increased to 125 and 869  $\text{nmol} \cdot \text{min} \cdot \text{mg protein}^{-1}$  in conditions of 20 $\mu\text{M}$  and 40 $\mu\text{M}$ , respectively. The reflective changes in the x-intercept value also suggested that the  $K_m$  was influenced, and changed from uninhibited conditions with 28.1  $\mu\text{M}$  to 454  $\mu\text{M}$  at 20  $\mu\text{M}$  concentrations of compound 7. This alteration in both the  $V_{\text{max}}$  and  $K_m$  values is a phenomenon associated with mixed inhibition [217]. These observations could support the view that compound 7, whilst competitively binding with

putrescine, has additional mixed competitive interactions that interfere with dcSAM binding. In future, the inhibitory mechanism of compound 7 will be confirmed using both dcSAM and putrescine. If increasing concentrations of dcSAM restores the enzyme  $V_{max}$  it would confirm the extended occupation of aminopropyl groups of compound 7, as proposed by Burger *et al.* [207].



**Figure 3.13: Lineweaver-Burk enzyme kinetic of *PfSpdSyn* inhibited by Compound 7.** These extrapolations were made from Michaelis-Menten data as determined from *PfSpdSyn* inhibition by Compound 7. Error bars represent the standard error of the mean from five experiments performed in duplicate.

A secondary plot, created using the slope at each incremental inhibitor concentration from the Lineweaver-Burk plot, was also used to confirm the  $K_i$  value of the inhibitor (Fig 3.14). The  $K_i$  value, reflected as the x-intercept of the slope, was calculated to be 2.8  $\mu$ M, in agreement with the calculations performed using the GraphPad Prism<sup>®</sup> Software package. Compound 7 therefore is a putrescine binding-site *PfSpdSyn* inhibitor and compares in potency to 4MCHA. Future studies will focus on additional kinetic determinations.



**Figure 3.14:** Secondary plot of *PfSpdSyn* inhibited by compound 7. The plots were generated using the slope generated from the respective inhibitor concentrations obtained from Lineweaver-Burk plots (x;y coordinates are as follows; (0  $\mu\text{M}$ ; 0.28), (20  $\mu\text{M}$ ; 3.71), (40  $\mu\text{M}$ ; 6.32).

### 3.4. Conclusions

With the release of several crystal structures, *PfSpdSyn* is becoming an increasingly attractive therapeutic target, and various SBDD approaches have already been followed [206, 214]. A limited number of studies, however, report the metabolic effect of spermidine depletion through inhibition of this enzyme. The parasitic importance *PfSpdSyn* is stressed by the levels of production of spermidine, which represents the major polyamine formed in the parasites. The functional requirement of the metabolite for the activation of *PfeIF5a* was also previously demonstrated. The inhibition of *PfODC* and *PfAdoMetDC* has been demonstrated to result in the depletion of spermidine, and cytostasis caused by this may be related to the lack of active *PfeIF5a*. Future investigations using *PfSpdSyn* inhibitors may still reveal other cellular components affected by polyamine depletion, and could aid in pinpointing the cause of cytostasis.

The computational approach followed by Mr. P. Burger allowed individual pharmacophore sites to be probed using distinctly different chemical moieties, which displayed favourable binding. Successful expression of *PfSpdSyn* protein was achieved and the various inhibitors were tested against the purified enzyme. It was established that piperidine and piperazine containing compounds are not well accommodated in the DPM1 putrescine binding cavity. As previously explained, there is a definite  $\text{C}_4$  aliphatic preference in the putrescine binding site and groups with electro-negative or -positive character may have repulsive effects if situated in this region. This therefore eliminated piperidine-like compounds as potential *PfSpdSyn* inhibitor candidates.

It was also shown that APA had inhibitory action against *PfSpdSyn*, also correlating with the previously established  $\text{IC}_{50}$  value of  $84\mu\text{M}$  for *PfSpdSyn* [86]. The fact that this molecule is able to inhibit both *PfODC* ( $K_i = 2.7 \text{ nM}$ ) and *PfSpdSyn* suggest that aminoxy compounds have further potential for optimization. The aminoxy groups are thought to be deprotonated at physiological pH, and this could therefore allow efficient binding in the putrescine binding site of *PfSpdSyn*. The requirement of  $\text{C}_4$  aliphatic chains is prominent in this site, and by potentially



increasing the length of APA to 4-aminooxy-1-butanamine (ABA) may increase inhibitor activity specifically for *PfSpdSyn*.

Compound 7 was identified as a favourable putrescine binding site inhibitor of *PfSpdSyn*. The compound was an analogue of CHA with an additional aminopropyl chain. Additional kinetic determinations also revealed mixed competitive kinetic binding, and this suggested that the interaction not only involves the competitive interactions with putrescine. As elegantly demonstrated by virtual docking of compound 7, the aminopropyl groups protrude into the dcSAM active site, and these embedded groups therefore ensure less out-competition by putrescine. The  $K_i$  of the compound was calculated to be 2.8  $\mu\text{M}$ , comparable to that of 4MCHA. Additional kinetic studies are required to confirm the mixed competitive inhibitory action, as observed for this compound. The *in vitro* activity of compound 7 still needs to be established against *P. falciparum* parasites, and with concomitant polyamine determinations, could confirm the *in vitro* selective inhibitory action the compound.

Pharmacophore modelling is a powerful tool for extracting representative biologically active components from both inhibitor ligands and their intended protein target receptors. The extraction of the pharmacophore from *PfSpdSyn*, performed by Mr. P. Burger, allowed the identification of novel inhibitors through virtual docking. The chemical validation of these occurred in Hamburg, Germany under the kind supervision of Dr. I. B. Müller at the BNI. The successful identification of a single inhibitor out of the ten compounds revealed the supportive function computational methods have. SBDD reduces the intensity at which *in vitro* testing needs to be performed for successful validation of inhibitory compounds. The selection of groups of molecules with a particular scaffold also allowed rational deductions as to the properties of ideal SpdSyn inhibitors, and these structure-function relationships will be exploited in future for optimization of *PfSpdSyn* inhibitors.

## Chapter 4: Concluding Discussion

Malaria, caused by *P. falciparum*, is a persistent disease that has plagued the world for centuries. The parasites are thought to have originated from the African continent almost 50 million years ago [218]. Still today the high mortality rates in Africa account for 90% of all malaria associated deaths [5]. In fact, the longevity of malaria on the African continent is also reflected by the severity of some naturally acquired resistance mechanisms, like sickle cell anaemia [25]. The disease is also associated with poverty and economic burden, and ineffective eradication sustains the vicious cycle of further economic downfall. Various efforts of the WHO are aimed at reducing the high mortality rates associated with this disease. In 2006 it was reported that almost 36 million ITN were distributed to African countries, and the employment of ACT antimalarials has increased almost 8-fold [5]. The rigorous employment of ITN and IRS has, however, not impacted in the number of reported malaria deaths in the last five years [5].

Malaria can successfully be treated using various artemisinin combinations, although at a higher cost compared to other available regimens [59]. Initial reports, however, indicate that parasites have the ability to develop resistance against artemisinin therapeutics, and the spread of these resistant parasites are being urgently addressed [63]. An approach followed here considers the parasite polyamine metabolism for prospective antimalarial drug-design. The safety and efficacy of polyamine enzyme-specific inhibitors has been established for the treatment of African human sleeping sickness caused by *T. brucei* [92]. The trypanosomes have, however, been shown to have alternative metabolic processes that require polyamines, compared to *P. falciparum*, and disruption of these during polyamine depletion could promote cytotoxic effects. The efficiency of DFMO, shown in *T. brucei gambiense*, was proposed to be due to depletion of parasitic polyamine levels, which in turn depletes the availability of dihydrotrypanothione, as mentioned. Moreover, the lack of SAM regulation has been proposed to result in toxic aberrant methylation [140]. Also, the trypanosomes lack an efficient mechanisms involved in polyamine transport, and the exogenous presence of polyamines was found not to reverse the effects of polyamine depletion [90, 219]. The presence of polyamine-dependent processes, and lack of effective salvaging, could therefore hold a selective advantage during application of polyamine inhibitors against the trypanosomes.

The lack of similar polyamine-dependent processes in *P. falciparum* may give reason for the observed *in vitro* cytostasis, rather than cytotoxicity. As demonstrated here and elsewhere [89], the parasites have compensatory mechanisms that may serve to reduce the toxic effects of these inhibitors. Previous studies have also demonstrated that polyamine depletion is not easily achieved in *P. falciparum*. DFMO treatment results in increased spermine formation, and MDL73811 treatment reveals higher levels of putrescine, and co-inhibition has an indifferent effect on spermine metabolism [1, 80, 133]. This could therefore suggest that the polyamine pathway is intricately regulated and, although mammalian equivalent back-conversion enzymes are not present, a mechanism exists to ensure cellular homeostasis of polyamines. The bifunctional *PfA/O* protein, and the advantage of the bifunctional cellular arrangement, is not yet clear under conditions of polyamine depletion. Transcript production of *pfa/o* has been

demonstrated to decrease during conditions of polyamine depletion [89]. This response does suggest that underlying metabolic regulatory mechanisms involve this parasitic protein, however, may be more complex.

Both inhibition of either domains of bifunctional *PfA/O*, and also *PfSpdSyn*, results in cytostasis, and this growth-arrest is commonly reflected as depletion in spermidine [1, 211]. The metabolite is involved in the activation of *PfεIF5a* and demonstrated to be important for the activity of parasite DNA-polymerases [198, 201]. Rapid parasite biosynthesis of spermidine was also suggested from this study. Spermidine biosynthesis in the parasites may therefore hold selective potential for abrogative strategies. The fact that this can be achieved through targeting of three different enzyme entities of the parasitic polyamine pathway further confirms the potential of these proteins as potential drug targets.

Polyamine transport in the parasites is thought to be a major contributing factor that circumvents polyamine depletion during the application of polyamine inhibitors [84]. On several occasions the exogenous addition of putrescine and spermidine has been shown to revive cellular arrested parasites [1, 85]. This indicates that extracellular transport mechanisms present may serve to antagonise the effects of polyamine inhibitors. A combination of polyamine inhibitors, both direct-enzyme inhibitors and transport inhibitors, is therefore proposed to have potential as a parasite eliminating strategy. A bis(benzyl)polyamine analogue, MDL27695, (N,N'-bis[3-[(phenylmethyl)amino]propyl]-1,7-diaminoheptane), has been reported to have potential as a transport inhibitor of *P. falciparum*. The compound was shown to effectively arrest parasite growth *in vitro* with IC<sub>50</sub> of 3.0μM [220]. Moreover, the administration of MDL27695 in combination with DFMO cured 87% of mice infected with *P. berghei* [221]. MDL27695 was shown not to have additive effects in combination with DFMO, and the effects on cultured parasites was similar to SpdSyn inhibition, where putrescine levels remained unchanged and spermidine levels decreased [134]. MDL 27695 was therefore not considered as a polyamine enzyme specific inhibitor, as the exogenous addition of polyamines could not reverse the cytostatic effects of MDL27695 treated parasites [221]. Moreover, it was shown that MDL27695 alone did not disrupt the polyamine levels; this is therefore evidence to suggest that this inhibitor is of a mimetic type, either disrupting normal polyamine influx / efflux or acts to displace natural polyamine function [134].

In conclusion, the polyamine pathway of *P. falciparum* holds potential for the development of antimalarials. The pathway contains three chemically validated drug targets that have a central function in the regulation of parasite polyamine metabolism. Strategies aimed at these parasitic drug targets should consider combination employment of polyamine transport inhibitors.

## Appendix

### A.1. Qualitative assessment of MDL73811 by-products from *P. falciparum*.

#### A.1.1. LC-MS method establishment

For the qualitative analysis of adenosyl-related compounds from *P. falciparum* extracts, as well as in purified *PfAdoMetDC* enzyme preparations, a LC-MS method was developed. This was performed to establish the identity of MTA-like peaks observed in *PfA/O* co-inhibited *P. falciparum*. MDL73811 was thought to cause by-product formation, which led to MTA-like peak formation during HPLC-UV separation of adenosyl-related metabolites. The LC-MS method allowed the analysis and separation of four major adenosyl containing metabolites, SAM, SAH, MTA, dcSAM and the non-physiological compound MDL73811 using isocratic mobile phase conditions in a 20 min run. The technique was used to verify the presence of the adenosyl containing metabolites in *P. falciparum* extracts, however quantitative procedures were not performed using this analysis.

Standards consisted of SAM, SAH, MTA, MDL73811 and dcSAM. The standards were dissolved in 5% PCA at 1 mM concentrations. A combination standard, consisting of the five compounds above, was prepared in 5% PCA and serially diluted to obtain 100  $\mu$ M, 10  $\mu$ M and 1  $\mu$ M samples. Ten microliters of each standard preparation was injected during the LC-MS based separation technique, corresponding to 1nmol, 100pmol and 10pmol of each adenosyl-containing standard.

HPLC, coupled with MS, was performed on an Agilent 1100 Binary pump system (Agilent, Waldbronn, Germany). Isocratic conditions were maintained at 1 mL/min using 20% v/v MeOH: dddH<sub>2</sub>O with 0.8 mL/L Heptafluorobutyric acid (HFBA, Fluka Steinheim, Germany) as ion-pairing agent. Solvent were degassed and filtered using 0.22  $\mu$ m filters (Sartorius, Goettingen, Germany) prior to use. Separation occurred on a Prodigy ODS (3), 100 x 4.6 mm, 3  $\mu$ m RP column (Phenomenex, Chesire, UK), equilibrated in Agilent heating block conditions of 45°C. Automated injections were performed using Agilent 1100 Series Autosampler unit (Agilent, Waldbronn, Germany). Solvent flow was directly connected to a 4000 Q Trap® LC/MS/MS system (Applied Biosystems, California, USA) operated in positive ion mode. The temperature of the electrospray was 450°C, with the turbo spray capillary voltage at 4200 V. The primary ion-source gas was at 30 psi, and secondary ion-source gas at 40 psi. The curtain gas was set at 23 L/min. The declustering potential was set to 23, with the entrance potential set to 10.0. Collision cell potential was set at 11. Multiple reaction monitoring (MRM) was performed, monitoring the fragment ions generated from SAH: 385.3  $\rightarrow$  136.0; SAM: 400.1  $\rightarrow$  251.0; MTA: 298.0  $\rightarrow$  136.0; dcSAM: 356.3  $\rightarrow$  356.0 and MDL73811: 350.2  $\rightarrow$  350.2. Data was acquired using the Analyst 1.4.2 Software package, Build 1228 (Applied Biosystems, Sierra Analytics LLC).

### **A.1.2. Adenosyl metabolite extraction from *P. falciparum*.**

Adenosyl metabolite extracts were taken from co-inhibited, untreated and red blood cell samples as described in Section 2.2.2.3. A single time-point corresponding to early trophozoite parasites (19HPI) was only used in this case. 5 mM DFMO / 5  $\mu$ M MDL73811 treatment occurred as described in section 2.2.2.2. 5% PCA protein precipitation was performed as previously described in section 2.2.2.3. The precipitated material was centrifuged at 16000 x g for 10 min (Eppendorf, Hamburg, Germany), and the remaining supernatants were filtered through 0.22  $\mu$ m Minisart RC4 filters (Sartorius, Goettingen, Germany). Ten microliters of the 5% PCA extracts was injected during LC-MS separation and detection of adenosyl-related compounds, described in section A.1.1.

Methanol metabolite extraction was performed according to a protocol obtained from T. van Brummelen (personal communication). PBS-washed cell pellets, not treated with PCA, from section 2.2.2.3 were used. Two milliliters of cold (-70°C) HPLC-grade methanol (Merck, Darmstadt, Germany) was added to 500  $\mu$ L of the washed cell pellets. This mixture was vigorously vortexed. The samples were placed at -70°C for 15 min, with vigorous vortexing at 5min intervals. The cell lysates were centrifuged at 500 x g for 5 min at 4°C (Eppendorf, Hamburg, Germany). The supernatant was removed to another tube stored at -70°C, and the pellets were subjected to another methanol extraction using cold (4°C) MeOH. Five hundred microliters of the 80% v/v MeOH : dddH<sub>2</sub>O was added to the pellets, and the pipette tip used to agitate any hardened material. The extracts were placed in a Sonifier waterbath (MRC, Holon, Israel), containing ice cold water, and were sonicated at 40KHz for 15 min. The samples were briefly centrifuged at 500 x g for 5 min at 4°C, and the supernatants pooled with the remaining 100% MeOH extracts. The pellets were subjected to another 80% MeOH extraction, as before, only the final centrifugation occurred at 16000 x g for 10 min (Eppendorf, Hamburg, Germany). The supernatants were again pooled with the 100% MeOH extracts. The methanol extracts were centrifuged at 16000 x g at 4°C for 10 min, and the supernatants were filtered through 0.22  $\mu$ m Minisart RC4 filters (Sartorius, Goettingen, Germany). Ten microliter injections were performed during LC/MS separation as explained in section A.1.1

### **A.1.3. *PfAdoMetDC* expression and MDL73811 by-product formation**

Recombinant protein expression of the single *PfAdoMetDC* domain of the bifunctional *PfAdoMetDC*-ODC (*PfA/O*), cloned in pASK-IBA3 (IBA GmbH, Germany), was performed in *E. coli* (Star cells) by E. Human (personal communication). Recombinant expression was induced using anhydrotetracycline (AHT) induction, and proteins were subsequently purified using StrepTactin® Affinity columns (IBA GmbH, Germany). The procedure is described elsewhere [88]. Purified *PfAdoMetDC* was used to assess the by-product formation upon enzyme incubation with increasing concentrations of MDL73811. By-products were detected using the MS-based detection procedure according to section 2.2.3.1. *PfAdoMetDC* was incubated in 1mM ethylenediaminetetraacetic acid (EDTA) (pH 7.5), 1mM dithiothreitol (DTT), 50 mM KH<sub>2</sub>PO<sub>4</sub> (pH 7.5) and 100  $\mu$ M SAM chloride (Sigma-Aldrich, St. Louis, USA). MDL73811 of increasing

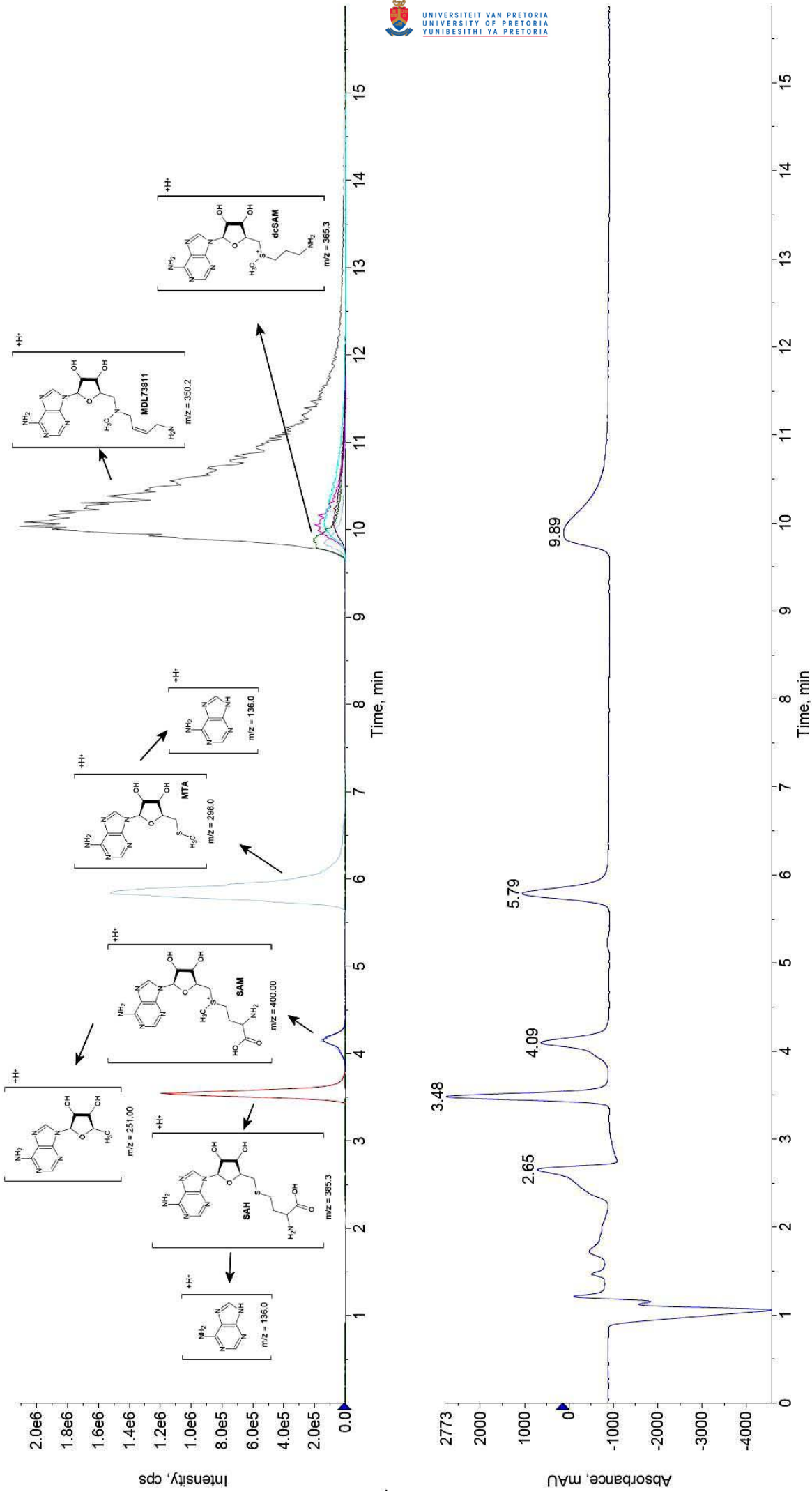
concentrations at 1  $\mu\text{M}$ , 5  $\mu\text{M}$ , 10  $\mu\text{M}$ , and 20  $\mu\text{M}$  was added to the reaction tubes. Blank tubes contained no MDL73811. Reactions were initiated through the addition of 50  $\mu\text{g}$  of purified *PfAdoMetDC* in a final volume of 500  $\mu\text{L}$ . The tubes were incubated at 37°C for 30 min, after which the tubes were immediately transferred to -70°C. Prior to MS qualitative by-product analysis, the samples were filtered through 0.22  $\mu\text{M}$  Minisart RC4 filters (Sartorius, Goettingen, Germany). Ten microliter injections were performed on the MS Autosampler system with conditions identical to those described in Section A.1.1.

## A.2. Results

### A.2.1 LC-MS method establishment

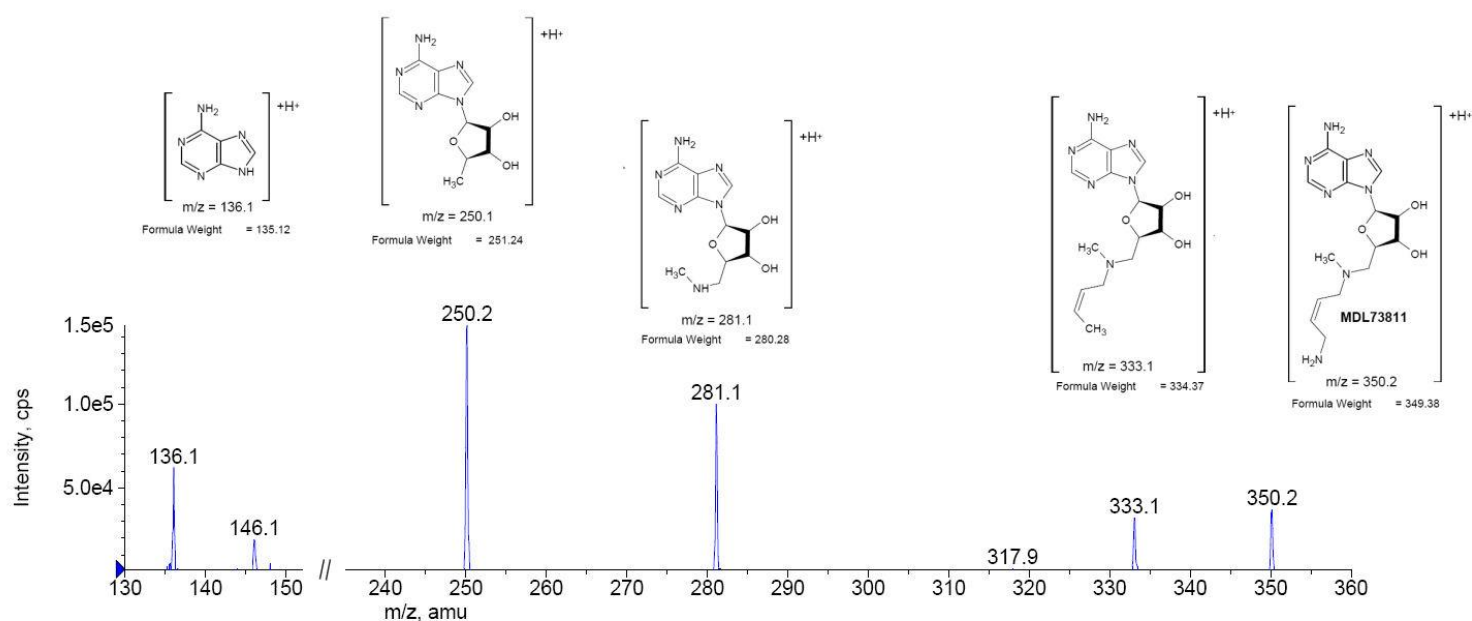
Further investigations as to the identity of the MTA peaks, observed during co-inhibition of *P. falciparum* using DFMO and MDL73811, required the establishment of a qualitative MS-based detection procedure. HPLC separation of adenosyl compounds in the LC-MS procedure occurred through ion-pairing RP chromatography [167]. For LC-MS detection of these metabolites an alternative more volatile ion-pairing agent, heptafluorobutyric acid (HFBA), was used. RP separation conditions were optimized using isocratic conditions of 20% MeOH, supplemented with 0.8 mL/L HFBA. These conditions were found to achieve sufficient separation of most of the adenosyl containing standards (Fig A.1.1). dcSAM and MDL73811 peaks were found to co-elute at 9.89 min, however considering the high-selectivity of multiple reaction monitoring (MRM) fragment monitoring in MS, the individual fragments of dcSAM and MDL73811 were easily identified from each other (Fig A.1.1).

The precursor ions generated for the adenosyl containing standards, and their respective product ions, were found to be in accordance with published literature [168]. The adenine substituent of adenosyl containing compounds was often generated as a characteristic secondary ion fragment, and the positive ion of 136.0  $m/z$  was a fingerprint fragment generated from both SAH and MTA (Fig A.1.1). Simultaneous UV monitoring at 254 nm also revealed that SAH elutes at 3.48 min and MTA at 5.79 min. SAM, which eluted at 4.09 min, was often overlaid with fragments corresponding to MTA (298.0  $m/z$ ), suggesting that this compound is easily fragmented during initial electrospray ionization conditions before passage through the collision gas. Other fragments generated through ionization of SAM include ion fragments of 251.0  $m/z$ . This could represent the adenosine components in which the methionine group has been lost (Fig A.1.1), a known fragment of SAM [168]. dcSAM precursor ions were identified with fragment masses of 356.3  $m/z$ , and high abundance fragment ions were found to exist at the same mass-to-charge ratio of 356.0. The dcSAM molecules, which eluted at approximately 10 min, were also shown to fragment into minor peaks of mass corresponding to MTA with 298  $m/z$ . As mentioned, MDL73811 was found to co-elute with dcSAM, however MDL73811 fragmented into product ions of 350.2  $m/z$  units and was easily distinguishable from dcSAM fragments using MRM. A 250.1  $m/z$  ion was also a fragment of MDL73811, and the fragmentation pathway to this ion is discussed below.



**Figure A.1.1: LC-MS separation of adenosyl compounds containing standards.** The bottom graph represents the total wavelength chromatogram (TWC) at 254 nm, representing 1 nmol of each SAH, SAM, MTA, dcSAM and MDL73811. Fragments generated from the MRM process are shown in the top part of the figure, with corresponding retention times for the respective fragments shown in the bottom part. The bottom part therefore represents peaks monitored through UV absorbance monitoring at 254 nm.

Enhanced product ion (EPI) monitoring was performed for a standard solution containing MDL73811 in 5% PCA. This allowed the select monitoring of single precursor ions generated during the fragmentation of MDL73811. Some product ions generated in the process suggested that the compound could fragment into a 333.1 m/z product, which suggested the loss of an amino group on the butenyl chain. Other fragments generated were a 281.1 m/z product, suggesting the loss of the aminobutenyl chain on the molecule (Fig A.1.2). The 136.1 m/z product was again characteristic of an adenosyl compound of which the adenine is fragmented from the ribosyl group.



**Figure A.1.2: MDL73811 fragmentation.** Enhanced product ion (EPI) monitoring was performed for the 350.2 m/z MDL73811 precursor.

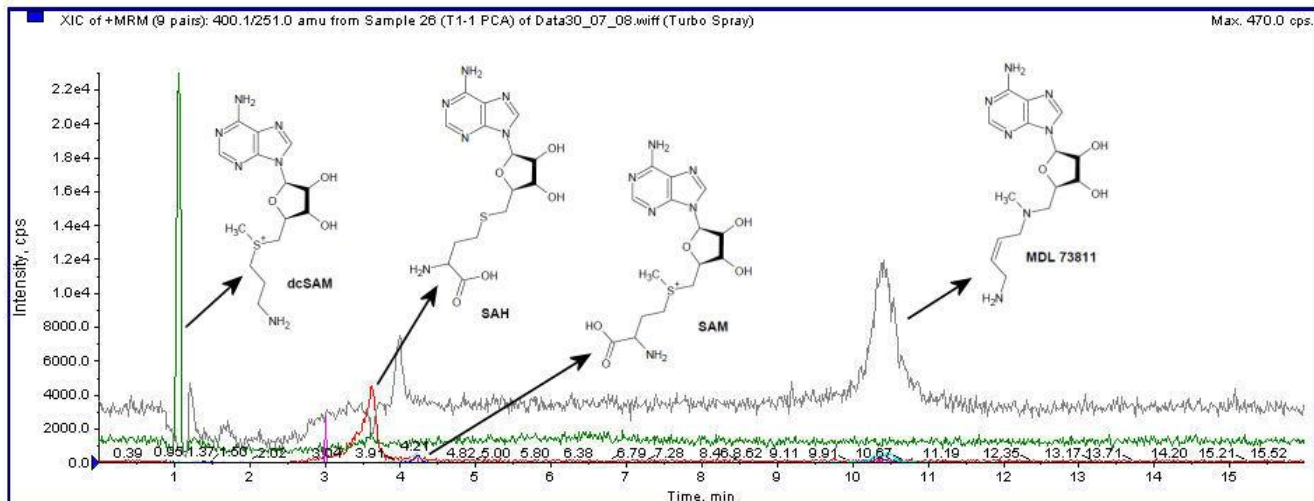
Of the fragment ions generated in the process, a 281.1 m/z species, suggested that MDL73811 is capable of fragmenting into methylaminoadenosine (MAA). Previously Casara *et al.* [122] demonstrated that inhibition of *E. coli* AdoMetDC with MDL73811 resulted in the stoichiometric MAA product. The MAA species detected during the fragmentation of MDL73811 allowed further investigation as to whether MAA does in fact form during *Pf*AdoMetDC inhibition by MDL73811. MDL73811 by-product formation was therefore studied *in vitro* upon co-inhibition of *P. falciparum* using 5 mM DFMO and 5  $\mu$ M MDL73811, and also during inhibition of purified *Pf*AdoMetDC.

## A.2.2 MS of *P. falciparum* extracts after co-inhibition

The MS-based qualitative procedure was used to detect MDL73811 inhibition by-products during co-inhibition of *P. falciparum*. Metabolite extracts were made for treated and untreated early trophozoites. Two different extraction procedures were used to compare the efficiency of adenosyl related metabolite extraction and detection. PCA, which is a known ion-suppressing agent, was often visible in the early part of run, and caused an overall suppression in the MS-spectra (data not shown). The alternative cold methanol extraction procedure overcame this

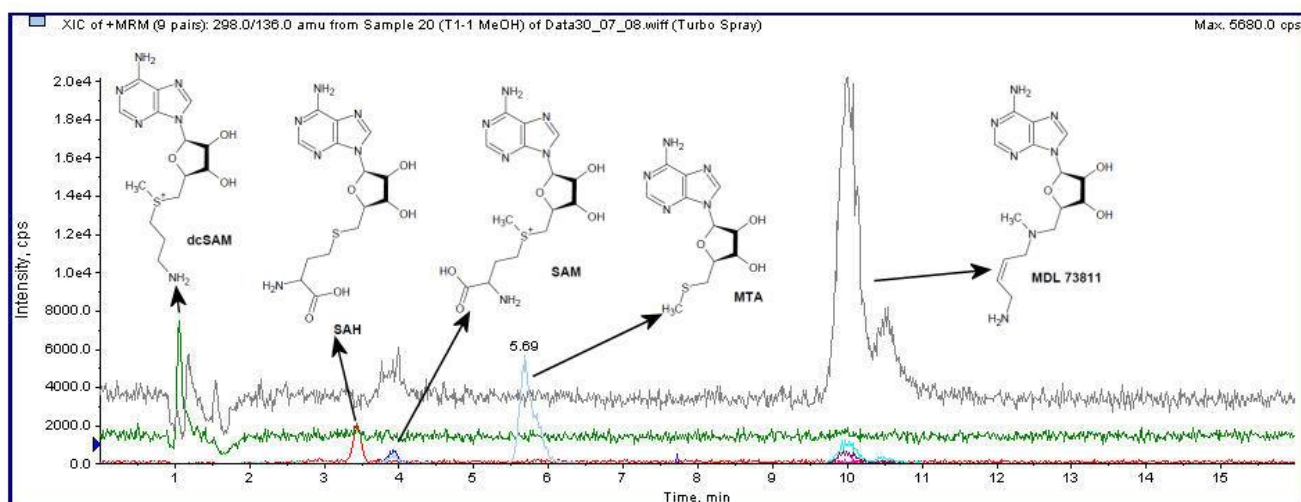


pitfall, and had less severe ion-suppressing impact. In 10  $\mu$ L 5% PCA extracts made from early treated *P. falciparum* trophozoites the major adenosyl related metabolites; SAM, SAH and dcSAM could easily be detected (Fig A.1.3). Simultaneous UV absorbance monitoring also suggested that these compounds were in very low concentrations, as the UV absorbance could not readily be detected in this 10  $\mu$ L injection volume (data not shown). The presence of MDL73811 could also be confirmed in the treated samples (Fig A.1.3).



**Figure A.1.3** MS-spectra generated from treated *P. falciparum* early trophozoites. 5% PCA extract were made to determine the potential MDL73811 by-products formed during co-inhibition. dcSAM is represented by dark green peaks, SAH by red peaks, SAM by dark blue and MDL73811 by grey peaks. MTA, not visible here, was shown as light blue peaks.

*P. falciparum* extracts made using a cold methanol procedure appeared to have less negative ion-suppression effect compared to PCA extraction. Fragment ions characteristic of SAM, SAH, dcSAM and MDL73811 were successfully identified in the methanol extracts (Fig A.1.4). Also, MTA was also more readily detectable in these samples compared to PCA extracts (Fig A.1.4). No ion fragments corresponding to the MAA, with fragment masses of 381.1 m/z, were observed in cold methanol extracts. As already discussed, this initial observation was not reproduced in subsequent PCA extracts during HPLC/UV detection and could have been a co-eluting unidentifiable substance.

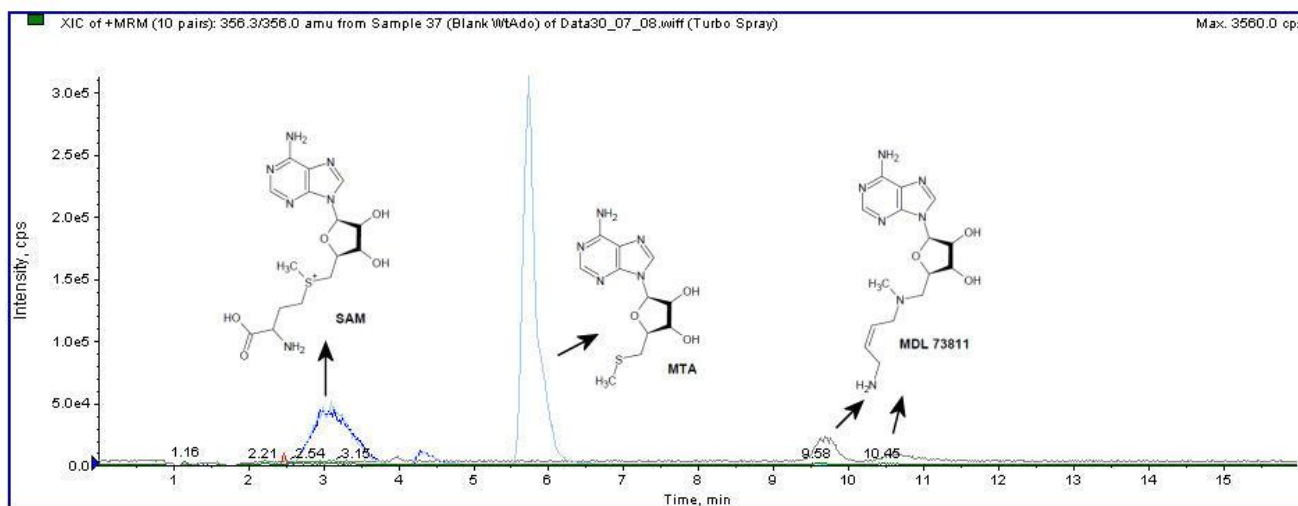


**Figure A.1.4: MS-spectra generated from treated *P. falciparum* early trophozoites.** Cold methanol extraction procedure was used to determine the extent of MDL73811 by-product formation. The samples were from the same procedure as Fig A.1.3. dcSAM is represented by dark green peaks, SAH by red peaks, SAM by dark blue and MDL73811 by grey peaks. MTA was shown as light blue peaks.

### A.2.2. MS of recombinant *PfAdoMetDC* upon MDL73811 treatment

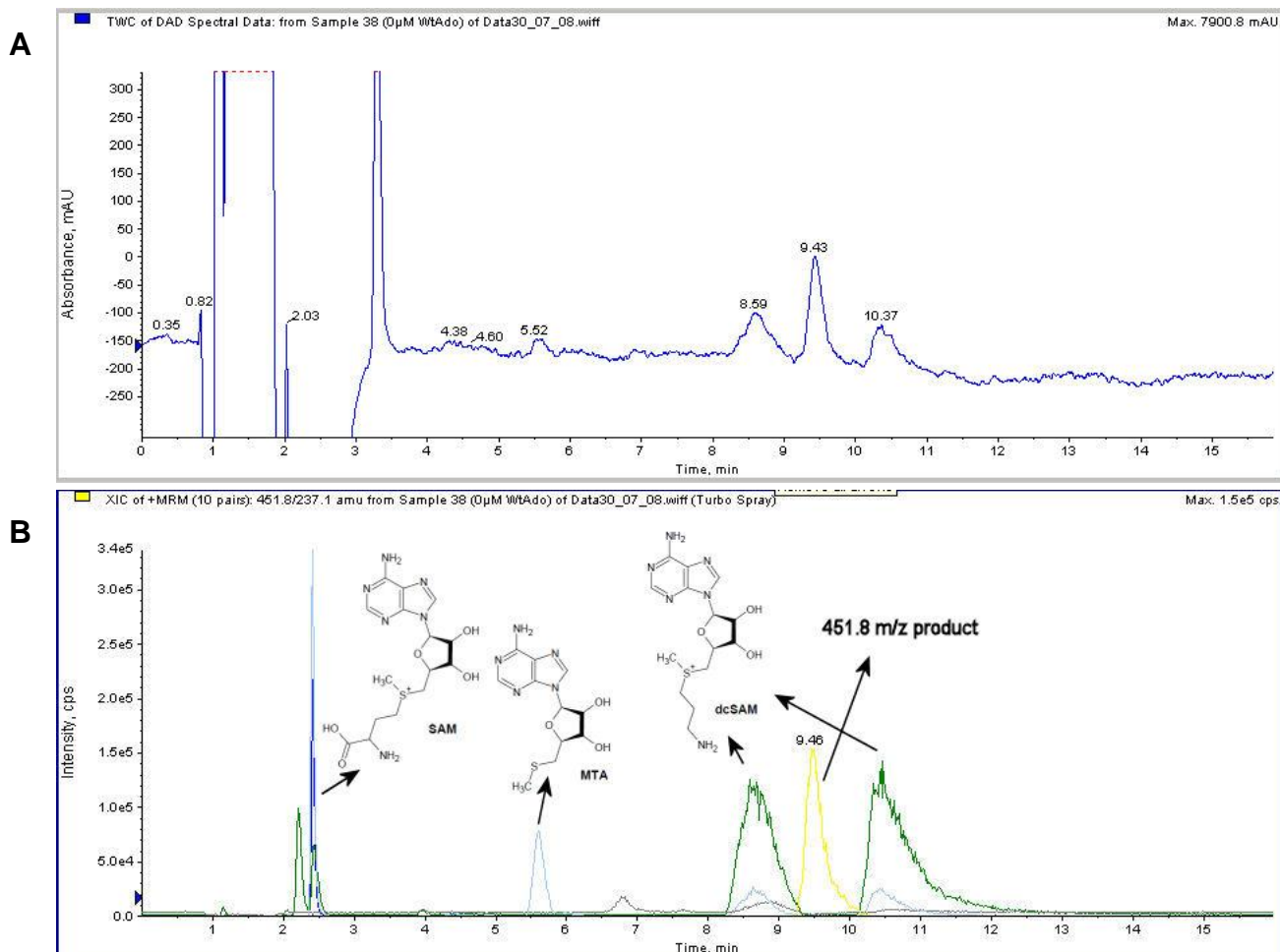
The lack of any observable MTA-like peaks, using the qualitative MS-based detection approach, in *P. falciparum* extracts prompted further investigation. Successful recombinant expression of *PfAdoMetDC* has been achieved in our laboratory [88]. To determine the extent of MDL73811 by-product formation, purified *PfAdoMetDC* was incubated with increasing concentrations of MDL73811. The enzyme incubation mixtures consisted of EDTA,  $\text{KH}_2\text{PO}_4$ , DTT and 100  $\mu\text{M}$  SAM as previously reported [88].

Initial control assays were set-up and contained neither MDL73811 nor purified *PfAdoMetDC*. This control was included to determine the extent of MTA formation during the incubation of SAM in reaction conditions at 37°C for 30 min. As shown in MS-spectra obtained from the control reactions, in Fig A.1.5, peaks corresponding to SAM at 3.0 min and MTA at 5.9 min were visible in the chromatograms. Freshly prepared standards of SAM were observed not to have any MTA eluting peaks (data not shown). The incubation of SAM, in the conditions suitable for *PfAdoMetDC* assay, therefore resulted in residual formation of MTA. SAM, as previously mentioned, is unstable at conditions above room temperature and the MTA degradation by-product in the reaction assay conditions could be accounted for [175]. Residual carry-over of MDL73811, visible as grey peaks at 9.58 and 10.45 min, was also observed in the control reactions (Fig A.1.5). This, as mentioned, was result from the autosampler unit, and could not be eliminated.



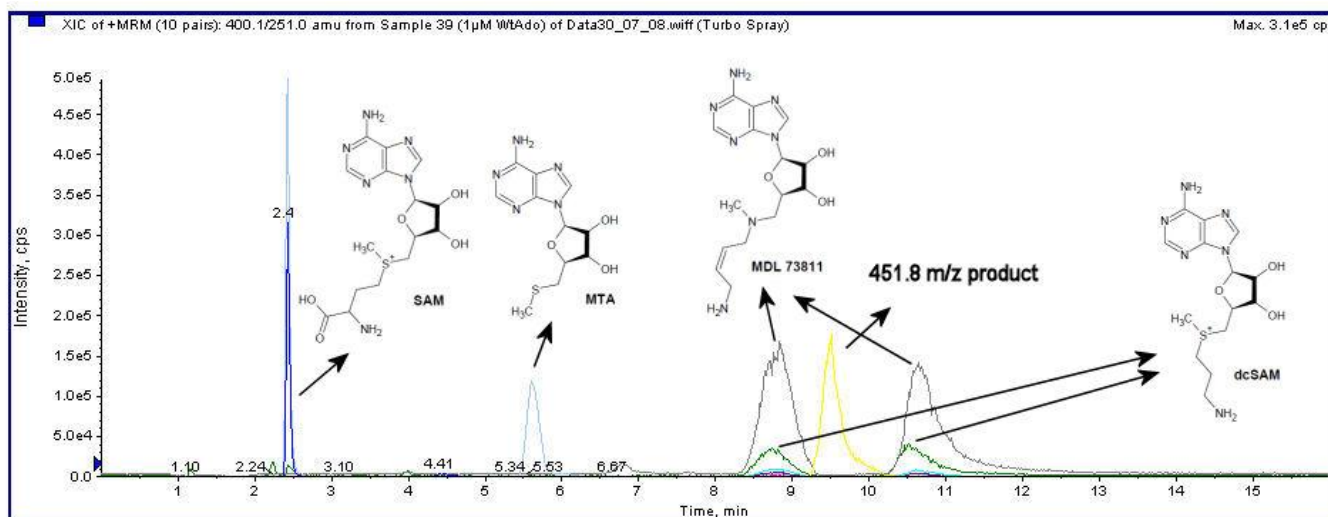
**Figure A.1.5: MS-spectra generated from blank reaction conditions in the absence of recombinant *PfAdoMetDC* and MDL73811.** The figure represents the MS fragment profile obtained during the separation of the adenosyl related compounds from a blank reaction containing neither *PfAdoMetDC* nor MDL73811. Blue peaks represent SAM, light blue peaks are MTA, grey indicates MDL73811 and dark green indicates dcSAM.

In assay conditions containing 50  $\mu\text{g}$  of purified *PfAdoMetDC*, with no MDL73811, clear formation of dcSAM was visible (Fig A.1.6). Also, two separate dcSAM fragment peaks were observed, one eluted at 8.8 min, the other eluted at 10.6 min. The chromatographic separation of dcSAM under RP, ion-paired, conditions has not previously been studied. However, the longer retained dcSAM molecules could have been chemical forms that may have additional interaction with the HFBA ion-pairing agent. MTA and SAM were also visible in the *PfAdoMetDC* incubation mixture (Fig A.1.6). Another unidentifiable peak of 451.8 m/z ratio was also detected, and the peak was also more prominent in the UV-chromatograms (Fig A.1.6, A). This relatively large fragment ion, which was found to further fragment into 238.1 m/z fragments, could have been a reaction intermediate. The fragment was not formed in equimolar concentrations with either dcSAM or MDL73811, and was considered to be related to the fixed presence of *PfAdoMetDC* enzyme, as shown below.



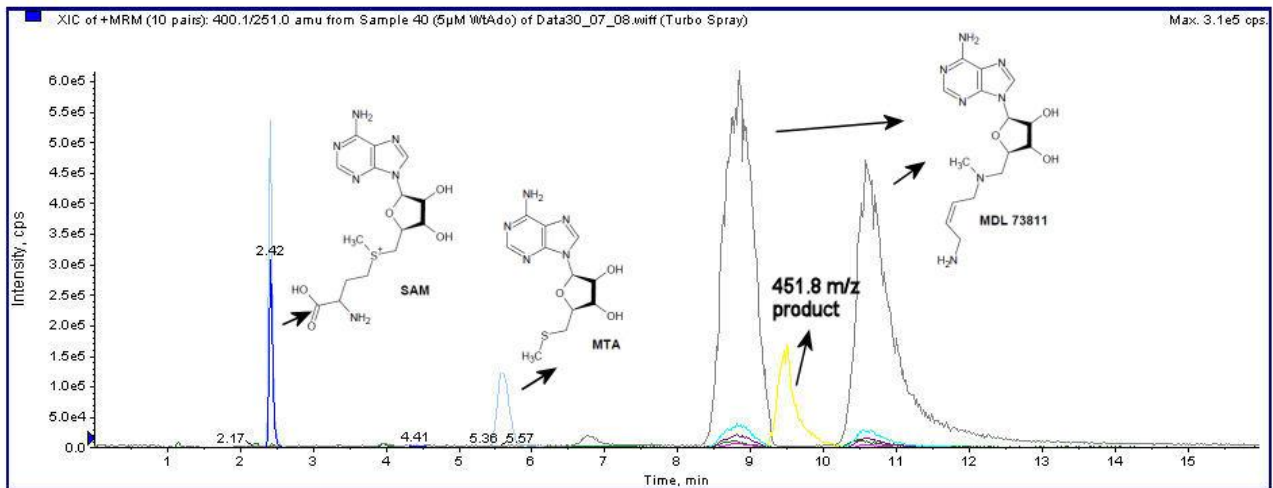
**Figure A.1.6: The MS-spectra generated from *PfAdoMetDC* during normal reaction conditions.** The MS fragments produced from reaction conditions in which *PfAdoMetDC* was incubated with in 100  $\mu$ M SAM, 1 mM EDTA, 1 mM DTT, 50 mM KH<sub>2</sub>PO<sub>4</sub> with no MDL73811. **A)** Total wavelength chromatogram (TWC) at 254 nm of the UV absorbing species eluted during the separation of *PfAdoMetDC* reaction products. **B)** MS-spectral chromatogram of product ions eluted during the separation of *PfAdoMetDC* reaction products. Fragments correspond to peaks from TWC. Blue lines represent SAM, light blue lines correspond to MTA, grey lines indicated MDL73811 and dark green lines represented dcSAM. Yellow lines represented an unknown ion of 451.8 m/z with secondary ions of 238.1 m/z.

Incubation of 50  $\mu$ g of *PfAdoMetDC* with 1  $\mu$ M MDL73811 could confirm the direct decarboxylase inhibition activity. Chromatographic separation of the assay mixture revealed less prominent dcSAM fragment peaks compared to conditions without MDL73811 (Fig A.1.7). Also, two separate MDL73811 fragment peaks were visible on the MS-spectra eluting at 8.8 min and 10.7 min, overlapping with dcSAM. Again, additional chromatographic interactions could have resulted in two observed MDL73811 eluting peaks. The comparatively large 451.8 m/z product was also observed. The area of the corresponding 451.8 ion peak, determined from the total wavelength chromatograms (TWC), was found to be similar to that of found in uninhibited reaction mixtures (data not shown). This therefore suggested that the same amount of 451.8 m/z fragment was present, and could be related to the enzyme concentration.



**Figure A.1.7: MS-spectra of reaction product from *Pf*AdoMetDC incubation with 1  $\mu$ M MDL73811.** Recombinant *Pf*AdoMetDC was incubated with 100  $\mu$ M SAM, also containing 1  $\mu$ M MDL73811. Blue lines represent SAM, light blue lines correspond to MTA, grey lines indicated MDL73811 and dark green lines represented dcSAM. Yellow lines represented an unknown ion of 451.8 m/z with secondary ions of 238.1 m/z.

Incubation of *Pf*AdoMetDC with 5  $\mu$ M MDL73811 revealed more dramatic reduction in dcSAM production compared to conditions containing 1  $\mu$ M MDL73811, as expected (Fig A.1.8). The MDL73811 ion fragments were also more prominent and the late eluting species could again be identified. Fragment ions of 451.8 m/z were also identified, and levels of these ions were comparable to that of previous incubations of *Pf*AdoMetDC containing less MDL73811. Unchanged intensities of the 451.8 m/z corresponding UV peaks suggested that the compound remains in equimolar concentration (data not shown). In each assay a fixed amount, 50  $\mu$ g, of purified *Pf*AdoMetDC was used. The large fragment ion could be observed in reaction conditions that lacked MDL73811. It was therefore speculated that these species were associated with the enzyme and potentially a reaction intermediate maintained during decarboxylation. The lack of any observable MAA-like fragments also confirmed that the MTA peaks observed in co-inhibited *P. falciparum* extracts may have been contaminants.



**Figure A.1.8: MS-spectra of reaction product from *PfAdoMetDC* incubation with 5 µM MDL73811.** MS fragments from recombinantly expressed *PfAdoMetDC* incubated with 100 µM SAM, also containing 5 µM MDL73811. Blue lines represent SAM, light blue lines correspond to MTA, grey lines indicated MDL73811 and dark green lines represented dcSAM. Yellow lines represented an unknown ion of 451.8 m/z with secondary ions of 238.1 m/z.

## References

1. Das Gupta, R., T. Krause-Ihle, B. Bergmann, I.B. Müller, A.R. Khomutov, S. Müller, R.D. Walter, and K. Lüersen (2005), 3-Aminooxy-1-aminopropane and derivatives have an antiproliferative effect on cultured *Plasmodium falciparum* by decreasing intracellular polyamine concentrations. *Antimicrobial Agents and Chemotherapy*. **49**(7): p. 2857-2864.
2. *10 Facts on Malaria*. <http://www.who.int/features/factfiles/malaria/en/index.html> World Health Organization [cited 2007-11-18].
3. Sachs, J., and P. Malaney (2002), The economic and social burden of malaria. *Nature*. **415**: p. 680-685.
4. Hay, S.I., C.A. Guerra, A.J. Tatem, A.M. Noor, and R.W. Snow (2004), The global distribution and population at risk of Malaria: Past, Present, and Future. *The Lancet, Infectious Diseases*. **4**: p. 327-336.
5. World Health Organization - World malaria report 2008 (ISBN 978 92 4 156369 7): p. 99-101.
6. *Malaria Fact sheet*. <http://www.who.int/features/factsheets/fs094/en/index.html> World Health Organization [cited 2007-11-18].
7. Yarney, G. (2004), Roll Back Malaria: a failing global health campaign. *British Medical Journal* **328**: p. 1086-1087.
8. *Roll back malaria* <http://www.rbm.who.int/gmap/2-1.html> Roll Back Malaria [cited 2009-03-07].
9. *The Global Fund* <http://www.theglobalfund.org/en/malaria/> [cited 2009-03-08].
10. Mota, M.M., and A. Rodriguez (2001), Migration through host cells by apicomplexan parasites. *Microbes and Infection*. **3**: p. 1123-1128.
11. Koella, J.C. (1999), An evolutionary view of interactions between anopheline mosquitoes and malaria parasites *Microbes and Infection*. **1**(4): p. 303-308.
12. Barnwell, J.W. (2001), Hepatic Kupffer Cells: The portal that permits infection of hepatocytes by malarial sporozoites? *Hepatology*. **33**(5): p. 1331-1333.
13. Baum, J., T.W. Gilberger, F. Frischknecht, and M. Meissner (2008), Host-cell invasion by malaria parasites: insights from *Plasmodium* and *Toxoplasma*. *Trends in Parasitology*. **24**(12): p. 557-563.
14. Ishino, T., Y. Chinzei, and M. Yuda (2005), A Plasmodium sporozoite protein with a membrane attack complex domain is required for breaching the liver sinusoidal cell layer prior to hepatocyte infection. *Cellular Microbiology*. **7**(2): p. 199-208.
15. Greenwood, B.M., D.A. Fidock, D.E. Kyle, S.H.I. Kappe, P.L. Alonso, F.H. Collins, and P.E. Duffy (2008), Malaria: progress, perils, and prospects for eradication. *The Journal of Clinical Investigations*. **118**(4): p. 1266-1276.
16. Cowman, A.F., and B.S. Crabb (2006), Invasion of Red Blood Cells by Malaria Parasites *Cell*. **124**: p. 755-766.
17. Chitnis, C.E., and M.J. Blackman (2000), Host cell invasion by malaria parasites. *Parasitology Today*. **16**(10): p. 411-415.
18. *Malaria life-cycle*. [http://www.dpd.cdc.gov/dpdx/hTML/ImageLibrary/Malaria\\_il.htm](http://www.dpd.cdc.gov/dpdx/hTML/ImageLibrary/Malaria_il.htm) Centre for Disease Control [cited 2009-02-25].

19. Bozdech, Z., M. Llinas, B.L. Pulliam, E.D. Wong, J. Zhu, and J.L. DeRisi (2003), The Transcriptome of the Intraerythrocytic developmental cycle of *Plasmodium falciparum*. *Plos Biology*. **1**(1): p. 85-100.
20. Mamoun, C.B., I.Y. Gluzman, C. Hott, S.K. MacMillian, A.S. Amarakone, D.L. Anderson, J.M.R. Carlton, J.B. Dame, D. Chakrabarti, R.K. Martin, B.H. Brownstein, and D.E. Goldberg (2001), Co-ordinated programme of gene expression during asexual intraerythrocytic development of the human malaria parasite *Plasmodium falciparum* revealed by microarray analysis. *Molecular Microbiology*. **39**(1): p. 26-36.
21. Alano, P. (2007), Plasmodium falciparum gametocytes: still many secrets of a hidden life. *Molecular Microbiology*. **66**(2): p. 291-302.
22. Scherf, A., J.J. Lopez-Rubio, and L. Riviere (2008), Antigenic variation in *Plasmodium falciparum*. *Annual Reviews in Microbiology*. **62**: p. 445-470.
23. Sherman, I.W., S. Eda, and E. Winograd (2003), Cytoadherence and sequestration in *Plasmodium falciparum*: defining the ties that bind. *Microbes and Infection*. **5**: p. 897-909.
24. Mackintosh, C.L., J.G. Beeson, and K. Marsh (2004), Clinical features and pathogenesis of severe malaria. *Trends in Parasitology*. **20**(12): p. 597-603.
25. Williams, T.N. (2006), Human red blood cell polymorphisms and malaria. *Current Opinion in Microbiology*. **9**: p. 388-394.
26. Kirchgatter, K., and H.A. Del Portillo (2005), Clinical and molecular aspects of severe malaria. *Annals of the Brazilian Academy of Sciences*. **77**(3): p. 455-475.
27. Lell, B., J. May, R. Schmidt-Ott, L.G. Lehman, D. Luckner, B. Greve, P. Matousek, D. Schmid, K. Herbich, F.P. Mockenhaupt, C.G. Meyer, U. Bienzle, and P.G. Kremsner (1999), The role of red blood cells polymorphisms in resistance and susceptibility to malaria. *Clinical Infectious Diseases*. **28**: p. 794-799.
28. Carter, R., and K.N. Mendis (2002), Evolutionary and Historical Aspects of the Burden of Malaria. *Clinical Microbiology Reviews*. **15**(4): p. 564-594.
29. Maitland, K., and C.R.J.C. Newton (2005), Acidosis of severe falciparum malaria: heading for a shock? *Trends in Parasitology*. **21**(1): p. 11-16.
30. Merck, Diagnostica Merck - Hematological Laboratory Methods. Third ed, ed. D. Merck. 1984, Darmstadt,
31. Voet, D., and J.G. Voet, Biochemistry. Third ed. Wiley International 2004: John Wiley and sons, Inc. 1026-1027, 0-471-19350-x
32. Stacpoole, P.W., C.L. Barnes, M.D. Hurbanis, S.L. Cannon, and D.S. Kerr (1997), Treatment of congenital lactic acidosis with dichloroacetate. *Archives of Disease in Childhood*. **77**: p. 535-541.
33. Day, N., and A.M. Dondorp (2007), The management of patients with severe malaria. *The American Journal of Tropical Medicine and Hygiene*. **77**(Suppl 6): p. 29-35.
34. Francis, S.E., D.J.J. Sullivan, and D.E. Goldberg (1997), Hemoglobin metabolism in the malaria parasite *Plasmodium falciparum*. *Annual Reviews in Microbiology*. **51**: p. 97-123.
35. Hyde, J.E. (2005), Exploring the folate pathway in *Plasmodium falciparum*. *Acta Tropica*. **95**: p. 191-206.



36. Bongfen, S.E., P.M. Ntsama, S. Offner, T. Smith, I. Felger, M. Tanner, P. Alonso, I. Nebie, J.F. Romero, O. Silvie, R. Torgler, and G. Corradin (2009), The N-terminal domain of *Plasmodium falciparum* circumsporozoite protein represents a target of protective immunity. *Vaccine*. **27**: p. 328-335.
37. Tsuji, M., and F. Zavala (2001), Peptide-based subunit vaccines against pre-erythrocytic stages of malaria parasites. *Molecular Immunology*. **38**: p. 433-442.
38. Ménard, R., V. Heussler, M. Yuda, and V. Nussenzweig (2008), Plasmodium pre-erythrocytic stages: what's new? *Trends in Parasitology*. **24**(12): p. 564-569.
39. Sharma, S., and S. Sulabha (2008), Malaria vaccine: a current perspective. *Journal of Vector Borne Diseases*. **45**: p. 1-20.
40. World Health Organization, Malaria vector control and personal protection: report of a WHO study group. *WHO technical report series; No 936 - ISBN 92 4 120936 4 (ISBN 978 92 4 120936 6)*.
41. Walker, K. (2000), Cost-comparison of DDT and alternative insecticides for malaria control. *Medical and Veterinary Entomology*. **14**: p. 345-354.
42. Takken, W. (2002), Do insecticide-treated bednets have an effect on malaria vectors? *Tropical Medicine and International Health*. **7**(12): p. 1022-1030.
43. Gregson, A., and C.V. Plowe (2005), Mechanisms of Resistance of Malaria Parasites to Antifolates. *Pharmacological Reviews*. **57**(1): p. 117-145.
44. Wongsrichanalai, C., A.L. Pickard, W.H. Wernsdorfer, and S.R. Meshnick (2002), Epidemiology of drug-resistant malaria. *Infectious Diseases*. **2**: p. 209-218.
45. AlKadi, H.O. (2007), Antimalarial drug toxicity: A review. *Chemotherapy*. **53**: p. 385-391.
46. Flanagan, K.L., M. Buckley-Sharp, T. Doherty, and C.J.M. Whitty (2006), Quinine levels revisited: the value of routine drug level monitoring for those on parenteral therapy. *Acta Tropica*. **97**: p. 233-237.
47. Rosenthal, P.J. (2003), Antimalarial drug discovery: old and new approaches. *The Journal of Experimental Biology*. **206**: p. 3735-3744.
48. Snyman, P.J.R., MIMS Monthly index of medical specialities. Nov / Dec 2005 ed, ed. P.J.R. Snyman. Vol. 45 (No. 11). 2005, Pinegowrie, Johannesburg: Johnic Publishing Limited,
49. Hayton, K., and X. Su (2008), Drug resistance and genetic mapping in *Plasmodium falciparum*. *Current Genetics*. **54**: p. 223-239.
50. Advanced Chemistry Development, I., *Advanced Chemistry Development, Inc. (ACD/Labs)*, O. Toronto, Canada, Editor. ACD/Labs Release: 10.00 Product Version 10.02 (Build 14890, 09 Nov 2006).
51. Egan, T.J. (2008), Haemozoin formation. *Molecular and Biochemical Parasitology*. **157**(2): p. 127-136.
52. Pisciotta, J.M., and D. Sullivan (2008), Hemozoin: Oil versus water. *Parasitology International*. **57**: p. 89-96.
53. Bell, A. (2005), Antimalarial drug synergism and antagonism: mechanistic and clinical significance. *FEMS Microbiology Letters*. **253**: p. 171-184.

54. Henry, M., S. Alibert, C. Rogier, J. Barbe, and B. Pradines (2008), Inhibition of efflux of quinolines as new therapeutic strategy in malaria. *Current Topics in Medicinal Chemistry*. **8**: p. 563-578.
55. Yeung, S., W. Pongtavornpinyo, I.M. Hastings, A.J. Mills, and N.J. White (2004), Antimalarial drug resistance, artemisinin-based combination therapy, and the contribution of modellin to elucidating policy choices. *The American Journal of Tropical Medicine and Hygiene*. **71**: p. 179-186.
56. Woodrow, C.J., and S. Krishna (2006), Antimalarial drugs: recent advances in molecular determinants of resistance and their clinical significance. *Cellular and Molecular Life Sciences*. **63**: p. 1586-1596.
57. Anderson, A.C. (2005), Targeting DHFR in parasitic protozoa. *Drug Discovery Today*. **10**(2): p. 121-128.
58. Yuvaniyama, J., P. Chitnumsub, S. Kamchonwongpaisan, J. Vanichtanankul, W. Sirawaraporn, P. Taylor, M.D. Walkinshaw, and Y. Yuthavong (2003), Insights into antifolate resistance from malarial DHFR-TS structures. *Nature Structural Biology*. **10**(5): p. 357-365.
59. White, N.J. (2008), Qinghaosu (Artemisinin): The price of success. *Science*. **320**: p. 330-334.
60. Ashley, E.A., and N.J. White (2005), Artemisinin-based combinations. *Current Opinion in Infectious Diseases*. **18**: p. 531-536.
61. Ezzet, F., M. van Vugt, F. Nosten, S. Looareesuwan, and N.J. White (2000), Pharmacokinetics and pharmacodynamics of lumefantrine (benflumetol) in acute falciparum malaria. *Antimicrobial Agents and Chemotherapy*. **44**(3): p. 697-704.
62. Golenser, J., J.H. Wainwright, M. Krugliak, N.H. Hunt, and G.E. Grau (2006), Current perspectives on the mechanism of action of artemisinins. *International Journal of Parasitology*. **36**: p. 1427-1441.
63. Maude, R.J., W. Pongtavornpinyo, S. Saralamba, R. Aguas, S. Yeung, A.M. Dondorp, N.P.J. Day, N.J. White, and L.J. White (2009), The last man standing is the most resistant: eliminating artemisinin-resistant malaria in Cambodia. *Malaria Journal*. **8**(1): p. (In press).
64. Bloland, P.B., M. Ettling, and S. Meek (2000), Combination therapy for malaria in Africa: hype or hope? *Bulletin of the World Health Organization*. **78**(12): p. 1378-1388.
65. de Beer, T., G. Wells, P.B. Burger, F. Joubert, E. Marechal, L. Birkholtz, and A.I. Louw (Ahead of publication), Antimalarial drug discovery: *in silico* structural biology and rational drug design. *Unpublished*.
66. Blundell, T.L., B.L. Sibanda, R.W. Montalvão, S. Brewerton, V. Chelliah, C.L. Worth, N.J. Harmer, O. Davies, and D. Burke (2005), Structural biology and bioinformatics in drug design: opportunities and challenges for target identification and lead discovery. *Philosophical Transactions of the Royal Society of Britain*. **10**: p. 1-11.
67. Bozdech, Z., J. Zhu, M.P. Joachimiak, F.E. Cohen, B.L. Pulliam, and J.L. DeRisi (2003), Expression profiling of the schizont and trophozoite stages of *Plasmodium falciparum* with a long-oligonucleotide microarray. *Genome Biology*. **4**(2): p. R9.0 - R9.15.

68. Florens, L., M.P. Washburn, J.D. Raine, R.M. Anthony, M. Grainger, J.D. Haynes, J.M. Moch, N. Muster, J.B. Sacci, D.L. Tabb, A.A. Witney, D. Wolters, M.J. Gardner, A.A. Holder, R.E. Sinden, J.R. Yates, and D.J. Carucci (2002), A proteomic view of the *Plasmodium falciparum* life cycle. *Nature*. **419**: p. 520-526.
69. Birkholtz, L., A.C. van Brummelen, K. Clark, J. Niemand, E. Maréchal, M. Llinás, and A.I. Louw (2008), Exploring functional genomics for drug target and therapeutics discovery in Plasmodia. *Acta Tropica*. **105**(2): p. 113-123.
70. Birkholtz, L., O. Bastien, G. Wells, D. Grando, F. Joubert, V. Kasam, M. Zimmermann, P. Ortet, N. Jacq, N. Saïdani, S. Roy, M. Hofmann-Apitius, V. Breton, A.I. Louw, and E. Maréchal (2006), Integration and mining of malaria molecular, functional and pharmacological data: How far are we from a chemogenomic knowledge space? *Malaria Journal*. **5**: p. 110.
71. Wallace, H.M., A.V. Fraser, and A. Hughes (2003), A perspective of polyamine metabolism. *Biochemical Journal*. **376**: p. 1-14.
72. D'Agostino, L., M. di Pietro, and A.D. Luccia (2005), Nuclear aggregates of polyamines are supramolecular structures that play a crucial role in genomic DNA protection and conformation. *FEBS Journal*. **272**: p. 3777-3787.
73. D'Agostino, L., M. di Pietro, and A.D. Luccia (2006), Nuclear aggregates of Polyamines. *IUBMB Life*. **58**(2): p. 75-82.
74. Williams, K. (1997), Interactions of polyamines with ion channels. *Biochemical Journal*. **325**: p. 289-297.
75. Sato, N., Y. Ohtake, H. Kato, S. Abe, H. Kohno, and Y. Ohkubo (2003), Effects of polyamines on histone polymerization. *Journal of Protein Chemistry*. **22**(3): p. 303-307.
76. Thomas, T., and T.J. Thomas (2001), Polyamines in cell growth and cell death: Molecular mechanisms and therapeutic applications. *Cellular and Molecular Life Sciences*. **58**(2): p. 244-258.
77. Mather, M., and H. Rottenberg (2001), Polycations induce the release of soluble intermembrane mitochondrial proteins. *Biochimica et Biophysica Acta*. **1503**: p. 357-368.
78. Seiler, N., and F. Raul (2005), Polyamine and apoptosis. *Journal of Cellular and Molecular Medicine*. **9**(3): p. 623-642.
79. Bitonti, A.J., P.P. McCann, and A. Sjoerdsma (1987), *Plasmodium falciparum* and *Plasmodium berghei*: effects of ornithine decarboxylase inhibitors on erythrocytic schizogony. *Experimental Parasitology*. **64**(2): p. 237-243.
80. Assaraf, Y.G., L. Abu-Elheiga, and D.T. Spira (1987), Effect of polyamine depletion on macromolecular synthesis of the malarial parasite, *Plasmodium falciparum*, cultured in human erythrocytes. *Biochemical Journal*. **242**(1): p. 221-226.
81. Teng, R., P.R. Junankar, W.A. Bubb, C. Rae, P. Mercier, and K. Kirk (2009), Metabolite profiling of the intraerythrocytic malaria parasite *Plasmodium falciparum* by <sup>1</sup>H NMR spectroscopy. *NMR in Biomedicine*. **22**(3): p. 292-302.
82. Assaraf, Y.G., J. Golenser, D.T. Spira, and U. Bachrach (1984), Polyamine levels and the activity of their biosynthetic enzymes in human erythrocytes infected with the malarial parasite, *Plasmodium falciparum*. *Biochemical Journal*. **222**(3): p. 815-819.

83. Moulinoux, J.P., M.L. Calve, V. Quemener, and G. Quash (1984), In vitro studies on the entry of polyamines into normal red blood cells. *Biochimie*. **66**(5): p. 385-393.
84. Ramya, T.N.C., N. Surolia, and A. Surolia (2006), Polyamine synthesis and salvage pathways in the malaria parasite *Plasmodium falciparum*. *Biochemical and Biophysical Research Communications*. **348**(2): p. 579-584.
85. Assaraf, Y.G., J. Golenser, D.T. Spira, G. Messer, and U. Bachrach (1987), Cytostatic effect of DL-alpha-difluoromethylornithine against *Plasmodium falciparum* and its reversal by diamines and spermidine. *Parasitology Research*. **73**(4): p. 313-318.
86. Haider, N., M.L. Eschbach, S. De Souza Dias, T.W. Gilberger, R.D. Walter, and K. Lüersen (2005), The spermidine synthase of the malaria parasite *Plasmodium falciparum*: Molecular and biochemical characterisation of the polyamine synthesis enzyme. *Molecular and Biochemical Parasitology*. **142**(2): p. 224-236.
87. Müller, S., A. Da'dara, K. Lüersen, C. Wrenger, R. Das Gupta, R. Madhubala, and R.D. Walter (2000), In the human malaria parasite *Plasmodium falciparum*, polyamines are synthesized by a bifunctional ornithine decarboxylase, S-adenosylmethionine decarboxylase. *Journal of Biological Chemistry*. **275**(11): p. 8097-8102.
88. Birkholtz, L.M., C. Wrenger, F. Joubert, G.A. Wells, R.D. Walter, and A.I. Louw (2004), Parasite-specific inserts in the bifunctional S-adenosylmethionine decarboxylase/ornithine decarboxylase of *Plasmodium falciparum* modulate catalytic activities and domain interactions. *Biochemical Journal*. **377**(2): p. 439-448.
89. van Brummelen, A.C., K.L. Olszewski, D. Wilinski, M. Llinas, A.I. Louw, and L. Birkholtz (2008), Co-inhibition of *Plasmodium falciparum* S-adenosylmethionine decarboxylase/ornithine decarboxylase reveals perturbation-specific compensatory mechanisms by transcriptome, proteome and metabolome analyses. *Journal of Biological Chemistry*. **284**(7): p. 4635-4646.
90. Bacchi, C.J., and N. Yarlett (2002), Polyamine metabolism as chemotherapeutic target in protozoan parasites. *Mini Reviews in Medicinal Chemistry*. **2**: p. 553-563.
91. Heby, O., S.C. Roberts, and B. Ullman (2003), Polyamine biosynthetic enzymes as drug targets in parasitic protozoa. *Biochemical Society Transactions*. **31**(2): p. 415-419.
92. Burri, C., and R. Brun (2002), Eflornithine for the treatment of human African trypanosomiasis. *Parasitology Research*. **90**: p. S49-S52.
93. Schneider, G., H. Käck, and Y. Lindqvist (2000), The manifold of vitamin B<sub>6</sub> dependent enzymes. *Structure*. **8**: p. R1-R6.
94. Toney, M.D. (2005), Reaction specificity in pyridoxal phosphate enzymes. *Archives of Biochemistry and Biophysics*. **433**: p. 279-287.
95. Christen, P., and P.K. Mehta (2001), From cofactor to enzymes. The molecular evolution of pyridoxal-5'-phosphate-dependent enzymes. *The Chemical Record*. **1**: p. 436-447.
96. Kern, A.D., M.A. Oliveira, P. Coffino, and M.L. Hackert (1999), Structure of mammalian ornithine decarboxylase at 1.6Å resolution: stereochemical implications of PLP-dependent amino acid decarboxylase. *Structure*. **7**(5): p. 567-581.
97. Jansonius, J.N. (1998), Structure, evolution and action of vitamin B<sub>6</sub>-dependent enzymes. *Current Opinion in Structural Biology*. **8**: p. 759-769.

98. Birkholtz, L., F. Joubert, A.W.H. Neitz, and A.I. Louw (2003), Comparative properties of a three-dimensional model of *Plasmodium falciparum* ornithine decarboxylase. *Proteins: Structure, Function and Genetics*. **50**(3): p. 464-473.
99. Osterman, A.L., L.N. Kinch, N.V. Grishin, and M.A. Phillips (1995), Acidic residues important for the substrate binding and cofactor reactivity in eukaryotic ornithine decarboxylase identified by alanine scanning mutagenesis. *The Journal of Biological Chemistry*. **270**(20): p. 11797-11802.
100. Almrud, J.J., M.A. Oliveira, A.D. Kern, N.V. Grishin, M.A. Phillips, and M.L. Hackert (2000), Crystal structure of human ornithine decarboxylase at 2.1 Å resolution: structural insights to antizyme binding. *Journal of Molecular Biology*. **295**: p. 7-16.
101. Jackson, L.K., H.B. Brooks, A.L. Osterman, E.J. Goldsmith, and M.A. Phillips (2000), Altering the reaction specificity of eukaryotic ornithine decarboxylase. *Biochemistry*. **39**: p. 11247-11257.
102. Grishin, N.V., A.L. Osterman, H.B. Brooks, M.A. Phillips, and E.J. Goldsmith (1999), X-ray structure of ornithine decarboxylase from *Trypanosoma brucei*: The native structure and the structure in complex with  $\alpha$ -difluoromethylornithine *Biochemistry*. **38**(46): p. 15174-15184.
103. Bey, P., C. Danzin, V. Van Dorsselaer, P. Mamont, M. Jung, and C. Tardif (1978), Analogues of ornithine as inhibitors of ornithine decarboxylase. New deductions concerning the topography of the enzyme's active site. *Journal of Medicinal Chemistry*. **21**(1): p. 50-55.
104. Adbel-Monem, M.M., N.E. Newton, and C.E. Weeks (1974), Inhibitors of polyamine biosynthesis. 1- $\alpha$ -methyl-( $\pm$ )-ornithine, an inhibitor of ornithine decarboxylase *Journal of Medicinal Chemistry*. **17**(4): p. 447-451.
105. Metcalf, B.W., P. Bey, C. Danzin, M.J. Jug, P. Casara, and J.P. Vever (1978), Catalytic irreversible inhibition of mammalian ornithine decarboxylase (E.C. 4.1.1.17) by substrate and product analogues. *Journal of the American Chemical Society*. **100**(8): p. 2551-2553.
106. Dufe, V.T., D. Inger, O. Heby, A.R. Khomutov, L. Persson, and S. Al-Karadaghi (2007), A structural insight into the inhibition of human and *Leishmania donovani* ornithine decarboxylase by 1-amino-oxy-3-aminopropane. *Biochemical Journal*. **405**: p. 261-268.
107. McKay, A.F., D.L. Garmaise, G.Y. Paris, and S. Gelbum (1960), Bacteriostats III: Oxyamines and their derivatives. *Canadian Journal of Chemistry*. **38**(3): p. 343-358.
108. Khomutov, R.M., T. Hyvonen, E. Karvonen, L. Kauppinen, T. Paalanen, L. Paulin, T. Eloranta, R. Pajula, L.C. Andersson, and H. Poso (1985), 1-aminooxy-3-aminopropane, a new potent inhibitor of polyamine biosynthesis that inhibits ornithine decarboxylase, adenosylmethionine decarboxylase and spermidine synthase. *Biochemical and Biophysical Research Communications*. **130**(2): p. 596-602.
109. Stanek, J., J. Frei, M. Helmut, P. Schneider, and U. Regenass (1991), 2-Substituted 3-(aminoxy)propanamines as inhibitors of ornithine decarboxylase: Synthesis and biological activity. *Journal of Medicinal Chemistry*. **35**: p. 1339-1344.
110. Berger, B.J. (2000), Antimalarial activities of aminoxy compounds. *Antimicrobial Agents and Chemotherapy*. **44**(9): p. 2540-2542.

111. Krause, T., K. Luersen, C. Wrenger, T.W. Gilberger, S. Müller, and R.D. Walter (2000), The ornithine decarboxylase domain of the bifunctional ornithine decarboxylase/S-adenosylmethionine decarboxylase of *Plasmodium falciparum*: Recombinant expression and catalytic properties of two different constructs. *Biochemical Journal*. **352**(2): p. 287-292.
112. Fontecave, M., M. Atta, and E. Mulliez (2004), S-Adenosylmethionine: nothing goes to waste. *Trends in Biochemical Sciences*. **29**(5): p. 243-249.
113. Martin, J.L., and F.M. McMillan (2002), SAM (dependent) I AM: the S-Adenosylmethionine-dependent methyltransferase fold. *Current Opinion in Structural Biology*. **12**: p. 783-793.
114. Walker, J., and J. Barret (1997), Parasite sulphur amino acid metabolism. *International Journal of Parasitology*. **27**(8): p. 883-897.
115. Kozbial, P.Z., and A.R. Mushergian (2005), Natural history of S-adenosylmethionine-binding proteins. *BMC Structural Biology*. **5**: p. 19.
116. Ekstrom, J.L., M.I. I., B.A. Stanley, A.E. Pegg, and S.E. Ealick (1999), The crystal structure of human S-adenosylmethionine decarboxylase at 2.25 Å resolution reveals novel fold. *Structure*. **7**(5): p. 583-595.
117. Tolbert, W.D., J.L. Ekstrom, I.M. Irimpan, J.A. Secrist, P. Kapoor, A.E. Pegg, and S.E. Ealick (2001), The structural basis for substrate specificity and inhibition of human S-adenosylmethionine decarboxylase. *Biochemistry*. **40**(32): p. 9484-9494.
118. Bennett, E.M., J.L. Ekstrom, A.E. Pegg, and S.E. Ealick (2002), Monomeric S-adenosylmethionine decarboxylase from plants provides an alternative putrescine stimulation. *Biochemistry*. **41**: p. 14509-14517.
119. Xiong, H., B.A. Stanley, and A.E. Pegg (1999), Role of cysteine-82 in the catalytic mechanism of human S-adenosylmethionine decarboxylase *Biochemistry*. **38**: p. 2462-2470.
120. Wells, G.A., L.M. Birkholtz, F. Joubert, R.D. Walter, and A.I. Louw (2006), Novel properties of malarial S-adenosylmethionine decarboxylase as revealed by structural modelling. *Journal of Molecular Graphics and Modelling*. **24**(4): p. 307-318.
121. Wrenger, C., K. Lüersen, T. Krause, S. Müller, and R.D. Walter (2001), The *Plasmodium falciparum* Bifunctional Ornithine Decarboxylase, S-Adenosyl-L-methionine Decarboxylase, Enables a Well Balanced Polyamine Synthesis without Domain-Domain Interaction. *Journal of Biological Chemistry*. **276**(32): p. 29651-29656.
122. Casara, P., P. Marchal, J. Wagner, and C. Danzin (1989), 5'-{[(Z)-4-Amino-2-butenyl]methylamino}-5'-deoxy-adenosine: A potent enzyme-activated irreversible inhibitor of S-adenosyl-L-methionine decarboxylase from *Escherichia coli*. *Journal of American Chemical Society*. **111**: p. 9111-9113.
123. Hillary, R.A., and A.E. Pegg (2003), Decarboxylases involved in polyamine biosynthesis and their inactivation by nitric oxide. *Biochemica et Biophysica Acta*. **1647**: p. 161-166.
124. Seiler, N. (2003), Thirty years of polyamine-related approaches to cancer therapy. retrospect and prospect. Part 1. Selective enzyme inhibitors. . *Current Drug Targets*. **4**: p. 537-564.

125. Regenass, U., H. Mett, J. Stanek, M. Mueller, D. Kramer, and C.W. Porter (1994), CGP 48664, a New S-Adenosylmethionine decarboxylase inhibitor with broad spectrum antiproliferative and antitumor activity. *Cancer Research*. **54**: p. 3210-3217.
126. Stanek, J., G. Caravatti, H. Capraro, P. Furet, H. Mett, P. Schneider, and U. Regenass (1993), S-Adenosylmethionine decarboxylase inhibitors: New aryl and heteroaryl analogues of methylglyoxal bis(guanylhydrazone). *Journal of Medicinal Chemistry*. **36**: p. 46-54.
127. Eskens, F.A.M., G.A. Greim, C. van Zuylen, I. Wolff, L.J. Denis, A.S.T. Planting, and N.C. Barbet (2000), Phase I and pharmacological study of weekly administration of the polyamine synthesis inhibitor SAM 486A (CGP 48 664) in patients with solid tumours. *Clinical Cancer Research*. **6**: p. 1736-1743.
128. Dorhout, B., M.F.G. Odink, E. de Hoog, and A.W. Kingma (1997), 4-Amidiodindan-1-one 2'-amidinohydrazone (CGP 48664A) exerts in vitro growth inhibitory effects that are not only related to S-adenosylmethionine decarboxylase (SAMdc) inhibition. *Biochimica et Biophysica Acta*. **1335**: p. 144-152.
129. Crick, F.H.C. (1970), Central dogma of molecular biology. *Nature*. **227**: p. 561-563.
130. Villas-Bôas, S., S. Mas, M. Åkesson, J. Smedsgaard, and J. Nielsen (2005), Mass spectrometry in metabolome analysis. *Mass Spectrometry Reviews*. **24**: p. 613-646.
131. Hollywood, K., D.R. Brison, and R. Goodacre (2006), Metabolomics: Current technologies and future trends. *Proteomics*. **6**: p. 4716-4723.
132. Whaun, J.M., and N.D. Brown (1985), Ornithine decarboxylase inhibition and the malaria-infected red cell: A model for polyamine metabolism and growth. *Journal of Pharmacology and Experimental Therapeutics*. **233**(2): p. 507-511.
133. Wright, P.S., T.L. Byers, D.E. Cross-Doersen, P.P. McCann, and A.J. Bitonti (1991), Irreversible inhibition of S-adenosylmethionine decarboxylase in *Plasmodium falciparum*-infected erythrocytes: Growth inhibition *in vitro*. *Biochemical Pharmacology*. **41**(11): p. 1713-1718.
134. Das, B., R. Gupta, and R. Madhubala (1995), Combined action of inhibitors of polyamine biosynthetic pathway with a known antimalarial drug chloroquine on *Plasmodium falciparum*. *Pharmacological Research*. **31**(3-4): p. 189-193.
135. Hollingdale, M.R., P.P. McCann, and A. Sjoerdsma (1985), *Plasmodium berghei*: Inhibitors of ornithine decarboxylase block exoerythrocytic schizogony. *Experimental Parasitology*. **60**(1): p. 111-117.
136. Gillet, J.M., G. Boné, and F. Herman (1982), Inhibitory action of  $\alpha$ -difluoromethylornithine on rodent malaria (*Plasmodium berghei*). *Transactions of the Royal Society of Tropical Medicine and Hygiene*. **76**(6): p. 776-777.
137. Bacchi, C.J., and N. Yarlett (1993), Effects of antagonists of polyamine metabolism on African trypanosomes. *Acta Tropica*. **54**: p. 225-236.
138. Fairlamb, A.H., G.B. Henderson, C.J. Bacchi, and A. Cerami (1987), *In vivo* effects of difluoromethylornithine on trypanothione and polyamine levels in bloodstream forms of *Trypanosoma brucei*. *Molecular and Biochemical Parasitology*. **24**: p. 185-191.

139. Bacchi, C.J., B. Goldberg, J. Garofalo-Hannan, D. Rattendi, P. Lyte, and N. Yarlett (1995), Fate of soluble methionine in African trypanosomes: effects of metabolic inhibitors. *Biochemical Journal*. **309**: p. 737-743.
140. Byers, T.L., T.L. Bush, P.P. McCann, and A.J. Bitonti (1991), Antitrypanosomal effects of polyamine biosynthesis inhibitors correlate with increases in *Trypanosoma brucei* *brucei* S-adenosyl-L-methionine. *Biochemical Journal*. **274**: p. 527-533.
141. Sufrin, J.R., S.R. Meshnick, A.J. Spiess, J. Garofalo-Hannan, X.Q. Pan, and C.J. Bacchi (1995), Methionine recycling pathways and antimalarial drug design. *Antimicrobial Agents and Chemotherapy*. **39**(11): p. 2511-2515.
142. Stjernborg, L., O. Heby, P. Mamont, and L. Persson (1993), Polyamine-mediated regulation of S-adenosylmethionine decarboxylase expression in mammalian cells. *European Journal of Biochemistry*. **214**: p. 671-676.
143. Pegg, A.E., H. Poso, K. Shuttleworth, and R.A. Bennett (1982), Effect of inhibition of polyamine synthesis in the content of decarboxylated S-Adenosylmethionine. *Biochemical Journal*. **202**: p. 519-526.
144. Taibi, G., M.R. Schiavo, M.C. Gueli, P. Calanni Rindina, R. Muratore, and C.M.A. Nicotra (2000), Rapid and simultaneous high-performance liquid chromatography assay of polyamines and monacetylpolyamines in biological specimens. *Journal of Chromatography B*. **745**: p. 431-437.
145. Schenkel, E., V. Berlaimont, J. Dubois, M. Helson-Cambier, and M. Hanocq (1995), Improved high-performance liquid chromatography method for the determination of polyamines as their benzoylated derivatives: application to P388 cells. *Journal of Chromatography B*. **668**: p. 189-197.
146. Trager, W., and J.B. Jensen (1976), Human malaria parasites in continuous culture. *Science*. **193**: p. 673-675.
147. Lambros, C., and J.P. Vanderberg (1979), Synchronization of *Plasmodium falciparum* erythrocytic stages in culture *The Journal of Parasitology*. **3**(65): p. 418-420.
148. Verkoelen, C.F., J.C. Romijn, and F.H. Schroeder (1988), Quantitation of polyamines in cultured cells and tissue homogenates by reversed-phase high-performance liquid chromatography of their benzoyl derivatives. *Journal of Chromatography: Biomedical Applications*. **426**: p. 41-54.
149. Häkkinen, M.R., T.A. Keinänen, J. Vesäläinen, A.R. Khomutov, L. Alhonen, J. Jänne, and S. Auriola (2007), Analysis of underivatized polyamines by reversed phase liquid chromatography with electrospray tandem mass spectrometry. *Journal of Pharmaceutical and Biomedical Analysis*. **45**(4): p. 625-634.
150. Redmond, J.W., and A. Tseng (1979), High-pressure liquid chromatography determination of putrescine, cadaverine, spermidine and spermine. *Journal of Chromatography*. **170**: p. 479-481.
151. Mei, Y. (1994), A sensitive and fast method for the determination of polyamines in biological samples. Benzoyl chloride pre-column derivatization high-performance liquid chromatography. *Journal of Liquid Chromatography*. **17**(11): p. 2413-2418.



152. Sugiura, T., T. Hayashi, S. Kawai, and T. Ohno (1975), High-speed liquid chromatography determination of putrescine, spermidine and spermine. *Journal of Chromatography*. **110**: p. 385-388.
153. Seiler, N. (1986), Polyamines. *Journal of Chromatography*. **379**: p. 157-176.
154. Minocha, S.C., R. Minocha, and C.A. Robie (1990), High-performance liquid chromatographic method for the determination of dansyl-polyamines. *Journal of Chromatography*. **511**: p. 177-183.
155. Bardelmeijer, H.A., H. Lingeman, C. de Ruiter, and W.J.M. Underberg (1998), Derivatization in capillary electrophoresis. *Journal of Chromatography A*. **807**(1): p. 3-26.
156. Coppex, L. *Derivatives for HPLC analysis*.  
[http://www.sigmaaldrich.com/img/assests/22084/HPLC\\_Derivatization\\_Literature.pdf](http://www.sigmaaldrich.com/img/assests/22084/HPLC_Derivatization_Literature.pdf)  
[cited 27-03-2007].
157. Watanabe, S., T. Saito, S. Sato, S. Nagase, S. Ueda, and M. Tomita (1990), Investigation of interfering products in the high-performance liquid chromatographic determination of polyamines as benzoyl derivatives. *Journal of Chromatography*. **518**: p. 264-267.
158. *Validation of Analytical Procedures: Methodology*, in *Eudralex 1998, Volume 3A - 3AQ13A*, T.G. Administration, Editor. p. 107-117.
159. Hockl, P.F., S.M. Thyssen, and C. Libertun (2000), An improved HPLC method for identification and quantitation of polyamines and related compounds as benzoylated derivatives. *Journal of Liquid Chromatography & Related Technologies* **23**(5): p. 693-703.
160. Wise, C.K., C.A. Cooney, S.F. Ali, and L.A. Poirier (1997), Measuring S-adenosylmethionine in whole blood, red blood cells and cultured cells using a fast preparation method and high-performance liquid chromatography. *Journal of Chromatography B*. **696**(1): p. 145-152.
161. Lagendjik, J., J.B. Ubbink, and W.J. Hayward Vermaak (1992), Quantification of erythrocyte S-adenosyl-L-methionine levels and its application in enzyme studies. *Journal of Chromatography B: Biomedical Sciences and Applications*. **576**: p. 95-101.
162. Lieber, C.S. (1999), Role of S-adenosyl-L-methionine in the treatment of liver diseases. *Journal of Hepatology*. **30**: p. 1155-1159.
163. Miura, G.A., J.R. Santangelo, and R.K. Gordon (1984), Analysis of S-adenosylmethionine and related sulfur metabolites in animal tissues. *Analytical Biochemistry*. **141**: p. 161-167.
164. Wang, W., P.M. Kramer, S. Yang, M.A. Pereira, and L. Tao (2001), Reversed-phase high performance liquid chromatography procedure for the simultaneous determination of S-adenosyl-L-methionine and S-adenosyl-L-homocysteine in mouse liver and the effect of methionine on their concentrations. *Journal of Chromatography B: Biomedical Sciences and Applications*. **762**(1): p. 59-65.
165. Hamedani, M.P., K. Valko, X. Qi, K.J. Welham, and W.A. Gibbons (1993), Two-dimensional high-performance liquid chromatographic method for assaying S-adenosyl-L-methionine and its related metabolites in tissues. *Journal of Chromatography*. **619**: p. 191-198.

166. Wagner, J., Y. Hirth, N. Claverie, and C. Danzin (1986), A sensitive high-performance liquid chromatography procedure with fluorometric detection for the analysis of decarboxylated S-adenosylmethionine and analogs in urine samples. *Analytical Biochemistry*. **154**(2): p. 604-617.
167. Burren, K.A., K. Mills, A.J. Copp, and N.D.E. Greene (2006), Quantitative analysis of S-adenosylmethionine and S-adenosylhomocysteine in neurulation-stage mouse embryos by liquid chromatography tandem mass spectrometry. *Journal of Chromatography B*. **844**: p. 112-118.
168. Wang, Y., H.Y. Zhang, Q.L. Liang, H. Yang, Y.M. Wang, Q.F. Liu, P. Hu, X.Y. Zheng, X.M. Song, G. Chen, T. Zhang, J.X. Wu, and G.A. Luo (2008), Simultaneous quantification of 11 pivotal metabolites in neural tube defects by HPLC-electrospray tandem mass spectrometry. *Journal of Chromatography B*. **863**: p. 94-100.
169. Gerbaut, L. (1991), Determination of erythrocytic polyamines by reversed-phase liquid chromatography. *Clinical Chemistry*. **37**(12): p. 2117-2120.
170. van den Berg, G., G.H. Munneke, A.W. Kingma, J.W. Smit, and F.A.J. Muskiet (1987), Method for isolating erythrocytes influences their measured polyamine content. *Clinical Chemistry*. **37**(6): p. 1081-1082.
171. Reguera, R.M., C.M. Redondo, Y. Pérez-Pertejo, and R. Balaña-Fouce (2007), S-adenosylmethionine in protozoan parasites: functions, synthesis and regulation. *Molecular and Biochemical Parasitology*. **152**: p. 1-10.
172. Chaing, P.K., M.E. Chamberlin, D. Nicholson, S. Soubes, X. Su, G. Subramanian, D.E. Lanar, S.T. Prigge, J.P. Scovill, L.H. Miller, and J.Y. Chou (1999), Molecular characterization of *Plasmodium falciparum* S-adenosylmethionine synthetase. *Biochemical Journal*. **344**: p. 571-576.
173. Castagna, A., C. Le Grazie, A. Accordini, P. Guilidori, G. Cavalli, T. Bottiglieri, and A. Lazzarin (1995), Cerebrospinal fluid S-adenosylmethionine (SAME) and glutathione concentrations in HIV infection: effect of parenteral treatment with SAME. *Neurology*. **45**: p. 1678-1683.
174. Loehrer, F.M.T., M. Tschöpl, C.P. Angst, L. P., K. Jäger, B. Fowler, and W.E. Haefeli (2001), Disturbed ratio of erythrocyte and plasma S-adenosylmethionine:S-adenosylhomocysteine in peripheral arterial occlusive disease. *Atherosclerosis*. **154**: p. 147-154.
175. Parks, L.W., and F. Schlenk (1957), The stability and hydrolysis of S-adenosyl-L-methionine; isolation of S-ribosylmethionine. *Journal of Biological Chemistry*. **230**(1): p. 295-305.
176. Perna, A.F., D. Ingrosso, V. Zappia, P. Galletti, G. Capasso, and N.G. De Santo (1993), Enzymatic methyl esterification of erythrocyte membrane proteins is impaired in chronic renal failure. *Journal of Clinical Investigation*. **91**: p. 2497-2503.
177. Perna, A.F., D. Ingrosso, N. De Santo, P. Galletti, and V. Zappia (1995), Mechanism of erythrocytic accumulation of methylation inhibitor S-adenosylhomocysteine in uremia. *Kidney International*. **47**: p. 247-253.

178. Oden, K.L., and S. Clarke (1983), S-adenosyl-L-methionine synthetase from human erythrocytes: role in the regulation of cellular S-adenosylmethionine levels. *Biochemistry*. **22**(12): p. 2978-2986.
179. Barber, J.R., B.H. Morimoto, L.S. Brunauer, and S. Clark (1986), Metabolism of S-adenosyl-l-methionine in intact human erythrocytes. *Biochemica et Biophysica Acta*. **887**: p. 361-372.
180. Terwilliger, T.C., and S. Clark (1981), Methylation of membrane proteins in human erythrocytes. *The Journal of Biological Chemistry*. **256**(6): p. 3067-3076.
181. Barber, J.R., and S. Clarke (1984), Inhibition of protein carboxyl methylation by S-adenosyl-L-homocysteine in intact erythrocytes. *The Journal of Biological Chemistry*. **259**(11): p. 7115-7122.
182. Bissati, K.E., R. Zufferey, W.H. Witola, N.S. Carter, B. Ullman, and C.B. Mamoun (2006), The plasma membrane permease PfNT1 is essential for purine salvage in the human malaria parasite *Plasmodium falciparum*. *Proceedings of the National Academy of Sciences of the United States of America*. **103**(24): p. 9286-9291.
183. Downie, M.J., K.J. Saliba, S.M. Howitt, S. Broër, and K. Kirk (2006), Transport of nucleosides across the *Plasmodium falciparum* parasite plasma membrane has characteristics of PfENT1. *Molecular Microbiology*. **60**(3): p. 738-748.
184. Downie, M.J., K.J. Saliba, S. Broër, S.M. Howitt, and K. Kirk (2008), Purine nucleobase transport in the intraerythrocytic malaria parasite. *International Journal of Parasitology*. **38**: p. 203-209.
185. Bissati, K.E., M.J. Downie, S.K. Kim, M. Horowitz, N. Carter, B. Ullman, and C.B. Mamoun (2008), Genetic evidence for the essential role of PfNT1 in the transport and utilization of xanthine, guanine, guanosine and adenine by *Plasmodium falciparum*. *Molecular and Biochemical Parasitology*. **161**: p. 130-139.
186. Delcuve, G.P., M. Rastegar, and J.R. Davie (2009), Epigenetic control. *Journal of Cellular Physiology*. **219**(2): p. 243-250.
187. Musto, H., H. Rodriguez-Maseda, and G. Bernardi (1995), Compositional properties of nuclear genes from *Plasmodium falciparum*. *Gene*. **152**: p. 127-132.
188. Nakanishi, M., A. Iwata, C. Yatome, and Y. Kitade (2001), Purification and properties of recombinant *Plasmodium falciparum* S-adenosyl-L-homocysteine hydrolase. *Journal of Biochemistry*. **129**(1): p. 101-105.
189. Tanaka, N., M. Nakanishi, Y. Kusakabe, K. Shiraiwa, S. Yabe, Y. Ito, Y. Kitade, and K.T. Nakamura (2004), Three-dimensional structure of S-adenosyl-L-homocysteine hydrolase from *Plasmodium falciparum*. *Nucleic Acids Symposium Series*. **48**: p. 281-282.
190. Tanaka, N., M. Nakanishi, Y. Kusakabe, K. Shiraiwa, S. Yabe, Y. Ito, Y. Kitade, and K.T. Nakamura (2004), Crystal structure of S-adenosyl-L-homocysteine hydrolase from the human malaria parasite *Plasmodium falciparum*. *Journal of Molecular Biology*. **343**(4): p. 1007-1017.
191. Avila, M.A., E.R. Garcia-Trevijano, S.C. Lu, F.J. Corrales, and J.M. Mato (2004), Methylthioadenosine. *The International Journal of Biochemistry and Cell Biology* **36**: p. 2123-2130.

192. Carteni-Farina, M., F.D. Ragione, G. Cacciapuoti, M. Porcelli, and V. Zappia (1983), Transport and metabolism of 5'-methylthioadenosine in human erythrocytes. *Biochimica et Biophysica Acta*. **727**: p. 221-229.
193. Tomitori, H., K. Kashiwagi, T. Asakawa, Y. Kakinuma, A.J. Michael, and K. Igarashi (2001), Multiple polyamine transport systems on the vacuolar membrane of yeast. *Biochemical Journal*. **353**: p. 681-688.
194. Becker, J., L. Mtwisha, B. Crampton, S. Stoychev, A.C. van Brummelen, L. Birkholtz, and D. Mancama (2009), Spermidine synthase inhibition of *Plasmodium falciparum* indicates perturbation-specific effects in the transcriptome and the proteome. *In Press (CSIR Biosciences, Pretoria, South-Africa)*.
195. Shantz, L.M., B.A. Stanley, J.A. Secrist, and A.E. Pegg (1992), Purification of human S-Adenosylmethionine decarboxylase expressed in *Eschericia coli* and the use of this protein to investigate the mechanism of inhibition by the irreversible inhibitors, 5'-deoxy-5'-[(3-hydrazinopropyl)methylamino] adenosine and 5'-{[(Z)-4-amino-2-butenyl]methylamino}-5'-deoxyadenosine. *Biochemistry*. **31**(29): p. 6848-6855.
196. Danzin, C., P. Marchal, and P. Casara (1990), Irreversible inhibition of rat S-adenosylmethionine decarboxylase by 5'-((Z)-4-amino-2-butenyl)methylamino)-5'-deoxyadenosine. *Biochemical Pharmacology*. **40**(7): p. 1499-1503.
197. Clark, K., M. Dhoogra, A.I. Louw, and L. Birkholtz (2008), Transcriptional responses of *Plasmodium falciparum* to alpha-difluoromethylornithine-induced polyamine depletion. *Biological Chemistry* **389**(2): p. 111-125.
198. Molitor, I.M., S. Knöbel, C. Dang, T. Spielmann, A. Alléra, and G.M. König (2004), Translation initiation factor eIF-5A from *Plasmodium falciparum*. *Molecular and Biochemical Parasitology*. **137**(1): p. 65-74.
199. Park, M.H. (2006), The post-translational synthesis of a polyamine-derived amino acid, hypusine, in the eukaryotic translation initiation factor 5A (eIF5A). *Journal of Biochemistry* **139**(2): p. 161-169.
200. Park, M.H., E.C. Wolff, and J.E. Folk (1993), Hypusine: its post-translational formation in eukaryotic initiation factor 5A and its potential role in cellular regulation. *Biofactors*. **4**(2): p. 95-104.
201. Bachrach, U., and L. Abu-Elheiga (1990), Effect of polyamines on the activity of malarial  $\alpha$ -like DNA polymerase. *European Journal of Biochemistry*. **191**(3): p. 633-637.
202. Korolev, S., Y. Ikeguchi, T. Skarina, S. Beasley, C. Arrowsmith, A. Edwards, A. Joachimiak, A.E. Pegg, and A. Savchenko (2002), The crystal structure of spermidine synthase with a multisubstrate adduct inhibitor. *Nature Structural Biology*. **9**(1): p. 27-31.
203. Dufe, V.T., W. Qiu, I.B. Müller, R. Hui, R.D. Walter, and S. Al-Karadaghi (2007), Crystal structure of *Plasmodium falciparum* spermidine synthase in complex with the substrate decarboxylated S-adenosylmethionine and the potent inhibitors 4MCHA and AdoDATO. *Journal of Molecular Biology*. **373**: p. 167-177.
204. Vedadi, M., J. Lew, J. Artz, M. Amani, Y. Zhao, A. Dong, G.A. Wasney, M. Gao, T. Hills, S. Brokx, W. Qiu, S. Sharma, A. Diassiti, Z. Alam, M. Melone, A. Mulichak, A. Wernimont, J. Bray, P. Loppnau, A.N. Plotnikov, K. Newberry, E. Sundararajan, S. Houston, J. Walker, W. Tempel, A. Bochkarev, I. Kozieradzki, A. Edwards, C.

- Arrowsmith, D. Roos, K. Kain, and R. Hui (2007), Genome-scale protein expression and structural biology of *Plasmodium falciparum* and related apicomplexan organisms. *Molecular and Biochemical Parasitology*. **151**: p. 100-110.
205. Wu, H., J. Min, Y. Ikeguchi, H. Zeng, A. Dong, P. Loppnau, A.E. Pegg, and A.N. Plotnikov (2007), Structure and mechanism of spermidine synthases. *Biochemistry*. **46**(28): p. 8331-8339.
206. Burger, P.B., L.M. Birkholtz, J. Fourie, N. Haider, R.D. Walter, and A.I. Louw (2007), Structural and mechanistic insights into the action of *Plasmodium falciparum* spermidine synthase. *Bioorganic and Medicinal Chemistry*. **15**: p. 1628-1637.
207. Burger, P.B., *Development of a dynamic receptor-based pharmacophore model of Plasmodium falciparum spermidine synthase for selective inhibitor identification*, in *Faculty of Natural and Agricultural Science, Bioinformatics and Computational Biology Unit, Department of Biochemistry*. 2008, University of Pretoria: Pretoria. p. 176.
208. Bitonti, A.J., S.E. Kelly, and P.P. McCann (1984), Characterization of spermidine synthase from *Trypanosoma brucei brucei*. *Molecular and Biochemical Parasitology*. **13**(1): p. 21-28.
209. Shirahata, A., T. Morohohi, M. Fukai, S. Akatsu, and K. Samejima (1991), Putrescine or spermidine binding site of aminopropyltransferases and competitive inhibitors. *Biochemical Pharmacology*. **41**(2): p. 205-212.
210. Goda, H., T. Watanabe, N. Takeda, M. Kobayashi, M. Wada, H. Hosoda, A. Shirahata, and K. Samejima (2004), Mammalian spermidine synthase - identification of cysteine residues and investigation of the putrescine binding site. *Biological Pharmacological Bulletin*. **27**(9): p. 1327-1332.
211. Kaiser, A., A. Gottwald, C. Wiersch, B. Lindenthal, W. Maier, and H. Seitz (2001), Effect of drugs inhibiting spermidine biosynthesis and metabolism on the in vitro development of *Plasmodium falciparum*. *Parasitology Research*. **87**(11): p. 963-972.
212. Müller, I.B., R. Das Gupta, K. Lüersen, C. Wrenger, and R.D. Walter (2008), Assessing the polyamine metabolism of *Plasmodium falciparum* as chemotherapeutics target. *Molecular and Biochemical Parasitology*. **160**: p. 1-7.
213. Dror, O., A. Shulman-Peleg, R. Nussinov, and H.J. Wolfson (2004), Predicting molecular interactions *in silico*: I. A guide to pharmacophore identification and its applications to drug design. *Current Medicinal Chemistry*. **11**(1): p. 71-90.
214. Jacobsson, M., M. Gäredal, J. Schultz, and A. Karlén (2008), Identification of *Plasmodium falciparum* spermidine synthase active site binders through structure-based virtual screening. *Journal of Medicinal Chemistry*. (Ahead of publication).
215. Laemmli, U.K. (1970), Cleavage of structural proteins during the assembly of the head of bacteriophage T4. *Nature*. **117**: p. 680-685.
216. Solomons, T.W.G., and C.B. Fryhle, Organic Chemistry. Eight ed, ed. D. Brennan. 2004: Wiley International Edition, 0-471-41799-8
217. Palmer, T., Enzymes: Biochemistry, Biotechnology and Clinical Chemistry First ed. Vol. 2. 2001: Horwood Publishing limited. 390, 1-898563-78-0
218. Conway, D.J., C. Fanello, J.M. Lloyd, B.M.A.-S. Al-Joubori, A.H. Baloch, S.D. Somanath, C. Roper, A.M.J. Oduala, B. Mulder, M.M. Pova, B. Singh, and A.W.

- Thomas (2000), Origin of *Plasmodium falciparum* malaria is traced by mitochondrial DNA. *Molecular and Biochemical Parasitology*. **111**: p. 163-171.
219. Reguera, R.M., B.L. Tekwani, and R. Balaña-Fouce (2005), Polyamine transport in parasites: A potential target for new antiparasitic drug development. *Comparative Biochemistry and Physiology - C Toxicology and Pharmacology*. **140**(2): p. 151-164.
220. Edwards, M.L., D.M. Stemerick, A.J. Bitonti, J.A. Dumont, P.P. McCann, P. Bey, and A. Sjoerdsma (1991), Antimalarial polyamine analogues. *Journal of Medicinal Chemistry*. **34**(2): p. 569-574.
221. Bitonti, A.J., J.A. Dumont, T.L. Bush, L. Edwards, D.M. Stemerick, P.P. McCann, and A. Sjoerdsma (1989), Bis(benzyl)polyamine analogs inhibit the growth of chloroquine-resistant human malaria parasites (*Plasmodium falciparum*) *in vitro* and in combination with DL- $\alpha$ -difluoromethylornithine cure murine malaria. *Proceedings of the National Academy of Sciences of the United States of America*. **86**(2): p. 651-655.